Bulletin 37
Part 5
(of 7 Parts)

THE
SHOCK AND VIBRATION
BULLETIN

JANUARY 1968

A Publication of
THE SHOCK AND VIBRATION
INFORMATION CENTER
Naval Research Laboratory, Washington, D.C.

Office of
The Director of Defense
Research and Engineering

This document has been approved for public release and sale; its distribution is unlimited.

SYMPOSIUM MANAGEMENT

THE SHOCK AND VIBRATION INFORMATION CENTER

William W. Mutch, Director
Henry C. Pusey, Coordinator
Rudolph H. Volin, Coordinator
Katherine G. Jahnel, Administrative Secretary

37th Program Committee

David Askin, U.S. Army Frankford Arsenal
Jerry Sullivan, Naval Ship Systems Command Hdq.
Robert F. Wilkus, Systems Engineering Group, W-PAFB
Dennis J. Martin, NASA Langley Research Center

Navy Liaison

Naval Training Device Center
William Powell
Allan Collier

Bulletin Production

Graphic Arts Branch, Technical Information Division,
Naval Research Laboratory

THE
SHOCK AND VIBRATION
BULLETIN

JANUARY 1968

A Publication of
THE SHOCK AND VIBRATION
INFORMATION CENTER
Naval Research Laboratory, Washington, D.C.

The 37th Symposium on Shock and Vibration was
held in Orlando, Florida, on 24-26 October 1967.
The U.S. Navy was host.

Office of
The Director of Defense
Research and Engineering

CONTENTS

PART 5

Large Vibroacoustic Test Facilities

---

*This paper appears in Shock and Vibration Bulletin 37, Supplement.

PAPERS APPEARING IN PART 1
Part 1 - Classified
(Titles Unclassified)

PAPERS APPEARING IN PART 2

Instrumentation and Analysis

---

*This paper appears in Shock and Vibration Bulletin 37, Supplement.

PAPERS APPEARING IN PART 4

Shock Analysis and Simulation

---

*This paper appears in Shock and Vibration Bulletin 37, Supplement.

HYBRID VIBRATION-ISOLATION SYSTEM FOR HELICOPTERS
    D. A Bies and T. M. Yang, Bolt Beranek and Newman Inc., Los Angeles, California

RECENT ADVANCES IN THE STUDY OF SYNCHRONOUS VIBRATION ABSORBERS
    A. V. Srinivasan, Kaman Corporation, Bloomfield, Connecticut

OPTIMIZING THE DYNAMIC ABSORBER TO INCREASE SYSTEM DAMPING
    G. K. Jones, NASA Goddard Space Flight Center, Greenbelt, Maryland

APPLICATION OF THE DYNAMIC ANTIRESONANT VIBRATION ISOLATOR TO HELICOPTER
VIBRATION CONTROL
    R. Jones and W. G. Flannelly, Kaman Corporation, Bloomfield, Connecticut

PAPERS APPEARING IN PART 7

Environmental Data

SURVEY OF THE CARGO-HANDLING SHOCK AND VIBRATION ENVIRONMENT
    F. E. Ostrem, General American Research Division, Niles, Illinois

A NEW LOOK AT TRANSPORTATION VIBRATION STATISTICS
    J. W. Schlue and W. D. Phelps, Jet Propulsion Laboratory, Pasadena, California

RECENT SHOCK AND VIBRATION MEASUREMENTS ON THE M-151 (JEEP) VEHICLE
    R. D. Brunnemer and G. M. Pomonik, Hughes Aircraft Company, Canoga Park, California

LATERAL IMPACT SHOCK DURING SHIP LOADING OF THE A3 POLARIS MISSILE
    E. G. Fischer, C. R. Brown, and A. J. Molnar, Westinghouse Electric Corporation, Pittsburgh,
    Pennsylvania

*RF-4C VIBRATION AND ACOUSTIC ENVIRONMENT STUDY
    J. F. Dreher, Air Force Flight Dynamics Laboratory, and W. D. Hinegardner, Systems Engi-
    neering Group, Wright-Patterson AFB, Ohio

EMPIRICAL CORRELATION OF FLIGHT VEHICLE VIBRATION RESPONSE
    W. H. Roberts, Martin-Marietta Corporation, Orlando, Florida

VIBRATION DATA SUMMARY OF MINUTEMAN WING VI FLIGHT TEST MISSILES
    R. R. Burnett and R. E. Morse, TRW Systems, Redondo Beach, California

SPACECRAFT VIBRATION: COMPARISON OF FLIGHT DATA AND GROUND TEST DATA
    G. Kachadourian, General Electric Company, Philadelphia, Pennsylvania

MEASUREMENT AND ANALYSIS OF GUN FIRING AND VIBRATION ENVIRONMENTS OF THE
RIVER PATROL BOAT
    R. S. Reed, Naval Ordnance Laboratory, Silver Spring, Maryland

*RESPONSE OF THE AIM-9D (SIDEWINDER) MISSILE TO CAPTIVE-FLIGHT VIBRATION
    W. W. Parmenter, Naval Weapons Center, China Lake, California

SCALE-MODEL WIND-TUNNEL ACOUSTIC DATA
    J. R. Baratono and F. A. Smith, Martin-Marietta Corporation, Denver, Colorado

---

*This paper appears in Shock and Vibration Bulletin 37, Supplement.

LARGE VIBROACOUSTIC TEST FACILITIES

VIBROACOUSTIC ENVIRONMENTAL SIMULATION
FOR AEROSPACE VEHICLES

Kenneth McK. Eldred
Wyle Laboratories
El Segundo, California

Requirements for vibroacoustic simulation in the laboratory in support of vehicle reliability goals are discussed. The qualitative nature of the vibration environment for a typical space payload mission is discussed, and the concept of the vibration field within the vehicle as a description of the vibration environment for both flight and simulation is developed. Problems in conventional laboratory vibration testing, the notion of structural sufficiency, and comments on the possible requirement for combined load testing are presented. The simulation potential of the new vibroacoustic test facilities is related to these simulation requirements.

INTRODUCTION

Vibration and acoustic testing methodology has advanced during the past two years to the point where it has become practical to test large sections of space vehicles with realistic simulation of launch dynamic environments. This advance has accrued from the development and activation of acoustic test facilities, such as those at Manned Spacecraft Center, Wright-Patterson Air Force Base, and Wyle Laboratories, together with the development of high-force vibration test capabilities, such as those at Wyle Laboratories in Huntsville, Alabama, and Norco, California. The utilization of these facilities in the past year has amply demonstrated their capability and represents a major step in environmental simulation.

The conventional approach to the assurance of system reliability under dynamic loading has usually involved accomplishing extensive component and subsystem dynamic tests during vehicle development and construction. These test programs often have resulted in subjecting all the components to the maximum anticipated environment, since it has been impossible to predict the exact environment for any one component location. Characteristically, specifications for such tests are based on an envelope of vibration data measured in current vehicles,

and scaled appropriately to the future vehicle's size and mission profile. To the extent that those test levels are excessive in crucial frequency regions, they may lead to overdesign with the accompanying possible weight penalties.

The development of large-scale vibroacoustic facilities, accommodating major sections of space vehicles, offers the possibility of an entirely new approach to qualification, placing maximum emphasis on the system environment, which can be more accurately simulated. Through this approach, it may be possible to screen components at nominal vibration levels and then check the adequacy of their performance in a total systems test. In many programs, it may be possible to follow a procedure which begins with an engineering and developmental test with simulated components, followed by a systems qualification test with all subsystems operational, and then, finally, acceptance tests at an appropriately lower level for each flight article. In this manner, it will be possible to take advantage of the real vibration environment for each component, singling out only those components in extremely high environments for additional testing, or perhaps vibration isolation. Further, the inclusion of accurate environmental simulation should make the standard acceptance tests more meaningful and thereby significantly reduce the possibility of catastrophic failure for each individual vehicle.

Therefore, the advent of large-scale facilities which can accommodate major sections of vehicles opens an entirely new door to the vibroacoustic test procedure. In the future, it will not be necessary at all times to qualify components for a maximum conceivable environment; rather it may only be necessary to qualify a component to an average environment, checking its qualifications when installed in the vehicle system and the entire system is subjected to an appropriate vibroacoustic test. Further component testing, when required, could then be tailored to the "real" environment of the component, perhaps even utilizing recordings from the systems test. This change in test philosophy, which may result from the validation of programs currently underway in the new facilities, has the potential of reducing component weight and hence increasing the mission capability of future vehicles.

This paper briefly reviews the vibration phases and accompanying sources for a space vehicle payload during flight. It then develops the concept of a vibration field as a tool for obtaining criteria for the accuracy of simulation. The problems related to component testing are then discussed and followed by a development of an approach for determining the amount of structure required for a test, and the application of the new vibroacoustic facilities to testing.

SOURCE OF THE VIBRATION ENVIRONMENT

The vibration environment within any aerospace vehicle varies as a function of position, structural and propulsion configuration, and mission parameters. The first two of these variables are specific to each individual vehicle. However, the effect of various mission parameters on the vibration environment may be qualitatively generalized for each class of vehicles. As an example of these effects, the environment of a space vehicle payload is summarized below, together with comments on the appropriate methods of simulation. There are six principal phases of the vibration environment of a space vehicle payload. These are:

1. Liftoff

2. Transonic flight

3. Maximum dynamic pressure flight

4. Stage separation in space

5. Space maneuvers

6. Reentry

The vibration of the payload at liftoff results primarily from the noise field produced by the rocket exhaust flows. The actual characteristics of this environment depend on the size of the rocket engines, the deflector configuration, and the distance between the payload and the base of the vehicle. In addition to the vibration resulting from noise directly impinging on the payload (or its shroud), there are some additional low-frequency vibration components resulting from acoustic excitation of the basic modes of the entire launch vehicle. This vibration is transmitted to the payload by the vehicle structure. Simulation of this environment is best achieved by a combination of acoustic noise and low-frequency vibration excitation.

The second phase of the payload's vibration occurs during the transonic flight, as the shock waves generated at various points on the vehicle move toward the nose, prior to their eventual stabilization in supersonic flight. In addition to their gross motion, the shocks may oscillate and be coupled with, or supplemented by, possible severe buffeting. The magnitudes of these external pressure fluctuations are highly dependent on vehicle geometry and presently are most accurately estimated from the results of wind tunnel tests. Examination of flight vehicle records obtained during this flight regime typically show transient vibration response. Exact duplication of the environment in the laboratory is beyond the current state of the art, and vibroacoustic simulation must be carefully tailored to specific vehicle requirements.

The third phase of vibration response occurs when the vehicle accelerates through the maximum dynamic pressure (q), where the excitation results primarily from turbulent fluctuations in the aerodynamic flow over the payload. The exact nature of these turbulent fluctuations, including the phenomena of buffeting, oscillating shock, and separated flow, can be currently estimated only through the use of wind tunnel models. Laboratory simulation is best produced by acoustic configurations which are tailored to the requirements of each specific vehicle design.

The fourth phase involves stage separation when the vehicle is leaving, or has left, the atmosphere, where the vibratory loads result from explosive stage separation and starting transients of the upper stage engines which put longitudinal shock forces into the payload. This response is best simulated by longitudinal vibration excitation, acting at the stage interface or through the engines, as appropriate.

2

The fifth phase is similar in nature to the fourth phase. However, the exact form of the environment is dependent on the starting characteristics, absolute forces, and locations of the various control and maneuvering engines. In general, the vibration resulting from control engines, and other onboard vibration sources, has a much lower level than that which occurs during the flight profile. However, on occasion the vibration resulting from the use of larger propulsion systems can be severe. This environment is best simulated by vibration excitation applied at the individual engine mounts.

The sixth phase occurs during reentry and is extremely dependent on the vehicle configuration and reentry parameters. Again, this phase has generally not been found to produce the most severe environment. Optimum simulation techniques, as necessary for a particular vehicle, will depend on the portion of the flight regime to be simulated.

Thus, the most severe vibration environments in the vehicle generally occur as a result of:

1. External pressure fluctuations

2. Mechanical vibration from onboard propulsion and auxiliary systems

3. Stage separation shocks

The latter two types can be readily identified with specific mechanical components in the vehicle, and the vibratory source characteristics of these components may be directly defined by analysis and laboratory measurement. Some of the external pressure fluctuations are much more difficult to identify and quantify; hence, extensive use of scale-model devices is warranted throughout any development program to improve environmental definition.

SIMULATION CRITERIA

The simulation should be adequate for the purpose of qualification testing if it results in a distribution of vibration within the test specimen which is nearly identical in all characteristics to that which occurs in flight. This assumption rests on the fact that any failures expected in vibroacoustic qualification testing result from the local vibration environment of the failing element. Implicit in the above reasoning is the certainty of a one-to-one relationship between vehicle vibration and vibration induced failure statistics.

It also can be assumed that ground simulation which reproduces all flight loads should result in a correct reproduction of flight vibration throughout the vehicle. However, in practice, ground simulation generally involves some compromise in the reproduction of flight loads, resulting in an increase of the uncertainty of the degree to which the vibration environment is simulated. Consequently, it is necessary to define a quantitative measure of the vehicle's vibration which can be used as a standard of compromise between ground simulation and flight. This measure should account for the vibration at all points throughout the vehicle. The distribution of vibration throughout the vehicle can be qualitatively described as a vibration field (V). A convenient physical motivation for the concept can be attained by defining the vibration field as the distribution of vibratory kinetic energy throughout the vehicle. With this definition, the functional form of V is

$$V = f \left(m_{ki} \overline{v_{ki}^2}, \, k, \, i, \, \omega \right)$$

where

m_{ki} is the mass in the vicinity associated with point k,

$\overline{v_{ki}^2}$ is the average mean square vibratory kinetic energy,

$k = 1, 2, 3, \ldots$ denotes the different points on the structure,

$i = 1, 2, 3$ direction of motion, and

$\omega = $ frequency.

With this definition, the accuracy of an experiment in simulating a flight vibration field may be related to the sum of the differences between the simulated and flight energy spectra at each point k for each of three orthogonal axes.

One convenient measure of the accuracy of the simulation is obtained by dividing the energy spectrum obtained in the laboratory by that obtained in flight at corresponding points and directions, to give the relative simulation spectra. The mean and variance for the relative spectra can then be computed by summing over all points. These mean relative spectra can then be used to adjust the frequency and amplitude characteristics of the laboratory forcing functions, to reduce the mean error toward zero. A measure of the overall resulting accuracy can then be obtained by integrating

the variances about the mean energy spectra over frequency.

This method was utilized in an elementary fashion in the design of the test of the Apollo LEM described in Ref. 1. In that test, flight vibration data were available at a few points, so that the ground acoustic simulation could be adjusted to match. However, for future vehicles tested before flight, the actual flight vibration will be unknown at the time of test. Consequently, engineering methods must be developed which enable adjustment of the simulation parameters relative to predicted flight loads and vehicle characteristics. Again, the proof of adequacy of these methods must be derived from extensive comparisons of data for both flight and ground simulation.

SIMULATION PROBLEMS IN CON-VENTIONAL COMPONENT TESTING

There are several types of tests conducted during vehicle development which are directed toward achieving reliability in a vibration environment. Generally, the tests are conducted at component and subsystem level prior to flight of the first prototype vehicle. The test purposes range from exploratory, engineering investigation of the nature of the component's dynamic characteristics, to qualification of operating components in a vibration environment.

The development of the large vibroacoustic test facility capability has led to the test of even larger sections of vehicles, and to suggestions of "all systems qualification in a vibration environment," followed by acceptance tests in a vibration environment. These new concepts have considerable technical merit in that their implementation can remove some of the major deficiencies of the "component level testing only" state of the art which has, of necessity, existed for many years.

The two principal difficulties of the component vibration test are:

1. Specification of the environment to be simulated, and

2. Provision of realistic dynamic boundary conditions for the component during test.

The specifications for component vibration tests are developed first in the preliminary design stage, and are often incorporated into the basic contract requirements. At this stage of vehicle development, very little is known about the actual vehicle in terms of detailed

design, so the estimates of the vibration environment must be based on simple prediction methods which enable extrapolation of typical vibration data from previous vehicles to the new design. Often the specifications are stated in terms of vehicle zone, taking account of both structural type within the zone and the estimated pressure fluctuations over the zone.

The accuracy of such estimates is admittedly poor, because of the enormous variation in the amplitudes of the frequency spectra within a zone, often even on somewhat similar structures. This variation in amplitude can typically range between a factor of 10 to 100, or one to two orders of magnitude. Such variation is not easily understood by engineers who specialize in other areas of the design and who are working towards typical accuracies of 0.1 to 10 percent.

The only practical method to account for this variation in developing a specification which insures high reliability is to give heavy weight to the maximum amplitude in the baseline vibration data. This weighting usually results in an envelope approach, or a statistical approach at the 95 percent (or higher) confidence level. The resulting test specifications, after simplifying the data curve to a series of straight lines, guarantee that almost every component will have an overtest, except for those components whose resonant frequencies tend to coincide with frequency regions of maximum response at the attachment points to the new vehicle.

As the design of the vehicle evolves, more information is available from which calculations of its probable dynamic response behavior can be made. However, because of the infinite complexity of a real vehicle, it is still not possible to compute even quasi-realistic vibration spectra for any arbitrary point and direction in the vehicle. Consequently, the principal application of the more sophisticated calculations is limited to low-frequency basic vehicle and shell modes, providing little guidance for the revision of component vibration specifications.

As a result, the vibration specifications usually are not significantly changed from those developed at preliminary design until data from a static firing or other major experiment become available. Further changes can be made to those specifications after the flight of the first prototype. However, by this time in the vehicle's development, most components have been qualified to the preliminary specifications and their design has of necessity accounted for

4

any overtest load factors resulting from the original specifications.

The second principal difficulty in component testing arises in the design of the experimental test setup. Considerable effort is expended to design a resonant-free stiff fixture which will enable accurate achievement of the specified motion spectrum at the component's mount points. As a result, in many cases the attainment of a motion specification at a mount point requires far greater force and vibratory power input to the component than the vehicle is capable of supplying, thus clearly giving an overtest.

Conversely, when the fixture is not sufficiently stiff, the coupling between the component and the fixture may induce spurious dynamic characteristics in the component itself. One of the classic examples of this situation arises in testing a complex cryogenic piping system by conventional means. After observing such a test, one quickly recognizes that the dynamic characteristics of the piping system measured during a test probably bear little resemblance to the characteristics of the system when mounted in the vehicle on the tanks. This change in dynamic characteristics results from the impossibility of duplicating in the test setup the coupling between the components and the tank and vehicle structure. Clearly, the only real solution to the inadequacy of this type of test setup is to generate the vibration environment in the tank and vehicle structure associated with the piping system, so that the vibration response of the piping system is realistic.

Therefore, the design of the test setup for the mounted component must consider methods for reproducing a reasonable facsimile of the probable service environment, together with the essential characteristics of the local dynamics of the mounted components. For this purpose, there are three basic variables which can be controlled:

1. The number and position of vibration/acoustic sources and control data points.

2. The characteristics of the source forcing functions, impedances, and the relationships between sources.

3. The amount of structure to be tested together with the mounted component and the edge fixity of such structure.

The utilization of either or both of the first two approaches involves an electronic and system control sophistication which is now becoming possible. However, use of this sophistication effectively during test requires knowledge of the vehicle impedances at and between the various attachment points in each of the directions to be simulated in the test. Such information may be available for components which are attached in a simple manner.

Unless this detailed information is available, the principal use of multiple sources and control points (other than to provide added force, control accuracy, stability, etc.) can be to provide additional statistical degrees of freedom in the test input. Theoretically, the increase of the number of input degrees of freedom should increase the probability that whatever is going to happen in flight will also happen in the test. However, this addition of degrees of freedom also increases the number of things which happen in test which will never happen in flight, leading again to overtest.

Therefore, the preferred method is to mount the component in a section of vehicle structure, reproduce the estimated vibration field in the structural section, and find out the nature of the component's response amplitude and spectra. If the structure is properly chosen, all important interactions between the component and structure will occur naturally, and the test can be conducted at realistic levels for qualification.

STRUCTURAL SUFFICIENCY
  FOR TESTING

The preceding section discussed the deficiencies of conventional component testing and suggested that they might be overcome if the component or subsystem were mounted properly in real vehicle structure. The next question that arises is: "How much of the vehicle is required to enable adequate simulation of the vibration field?" In this section, several possible dynamic situations are discussed, leading to the development of qualitative criteria for structural sufficiency for test.

The assessment of the amount of structure which is sufficient to reproduce the essential local dynamic characteristics of a mounted component is sometimes relatively simple. An appropriate example is given by a masslike component attached through relatively flexible mounts to a major frame which is both massive and stiff relative to the component. In this case, it is clear that the motion of the frame in the vehicle is little affected by the presence of the component and that a reasonable reproduction of the vibration of a segment of the frame

mounted on a shake table will service as an adequate test input to the mounted component.

Unfortunately, real structure and real components offer many counterexamples where the component mass and stiffness are on the same order, or greater, than those of the surrounding structure, or the extensive nature of the subsystem interacts with many structural elements. In these latter cases, the definition of sufficient structure may become exceedingly difficult because present engineering criteria are generally ill defined.

The development of a logic for a structural sufficiency criteria can be approached through the examination of a simplified concept of the vehicle as a vibratory system, and considering the effects of adding a component to a small region of this vibratory system. The vibratory motion experienced in this region on the actual vehicle is a result of mechanically induced vibration from the engine and other mechanical auxiliaries, and vibration induced by fluctuating pressures over the surface of the vehicle.

In examining the motion of this small region when the component is not present as a function of frequency, one finds that the primary responses in the low frequencies are dictated by the location of the region relative to the fundamental vehicle modes. As the frequency is increased, the bending wavelengths decrease, and the various shell modes make their appearance. Often in this second frequency regime, the vehicle can be considered as a group of relatively loosely coupled cylinders each having its own distinct, equivalent shell mode. As one examines the motion at even higher frequencies, the major local structural elements such as frames and longerons begin to distort the actual motion from that predicted by equivalent shell theory, and the dynamic response becomes more closely associated with the local characteristics of the structure mounted between these heavier boundaries.

Thus, it may be seen that the motion of the region is determined to a large extent in each of these three frequency ranges by the amount of associated structure which comprises a fully coupled system. Further, the extent of the fully coupled system decreases with increasing frequency from an entire vehicle at the lowest frequencies to a relatively localized structure at the highest frequencies.

Now consider the problems which result in attempting to reproduce the flight vibration in this region by shaking an arbitrarily chosen partitioned section of the structure which includes the region of concern. It is clear that in the low-frequency modes, where the bending wavelength is very long compared with the dimensions of the partitioned structural specimen, all points of the specimen vibrate essentially in phase. Therefore, by utilizing a suitable input function and edge fixity in the test, it is possible to produce a motion throughout the region that simulates the flight vibration field. Reasonable accuracy of simulation will extend up to a frequency where the bending wavelength decreases to approximately two to four times the typical dimensions of the specimen.

However, at higher frequencies, the specimen will exhibit specific resonances which will depend on its own dynamic characteristics. These characteristics are directly related to the arbitrary dimensions originally selected for partitioning, and to the boundary conditions which are imposed on the specimen during tests. Hence, in this frequency range the dynamic characteristics of the specimen may differ significantly from the dynamic characteristics which it would exhibit when truly mounted on the vehicle. Thus, simulation may be rather poor in this frequency region.

At still higher frequencies, the typical dimensions of the specimen become many times the bending wavelength, and the modal density and damping of the specimen increases sufficiently to deemphasize the effect of exact specimen dimensions. Thus, at a sufficiently high frequency, the motion of the component mounting point region may be essentially independent of the exact choice of partition dimensions and the choice of fixture design. Here again, it becomes possible to simulate the vibration in the component mounting region.

In many practical cases where the structure is not uniform, heavy primary structural members will act as the decoupling boundaries between adjacent lighter weight surface structures. In these cases, the motion of the decoupled structure will become increasingly independent of the motion of neighboring elements at all frequencies above the decoupling frequency. Consequently, above the decoupling frequency, a satisfactory simulation can generally be obtained for the decoupled structure by vibrating it through its bounding frames. This decoupling of structure may often be of primary importance to reduce the size of structure required for satisfactory simulation.

The preceding discussion leads to several useful alternative possibilities which are illustrated in Fig. 1 and summarized below:

6
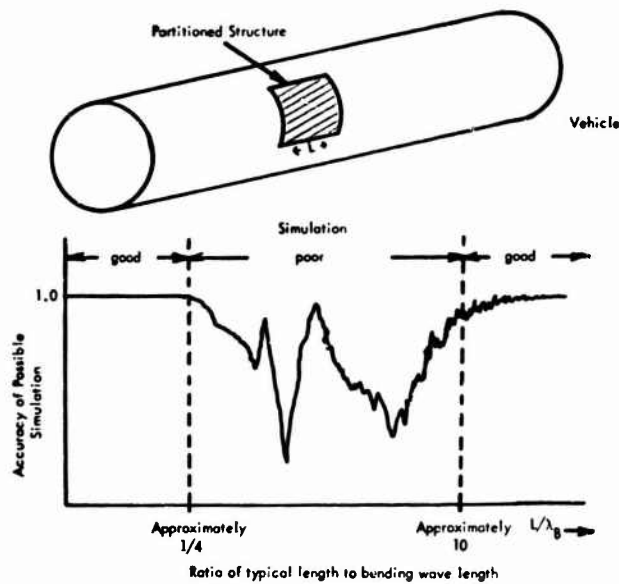
Fig. 1. Conceptualization of frequency
range in which simulation is possible
(values of L/λ_B are very approximate)

1. If the entire vehicle is vibrated with appropriate sources (vibratory and acoustic), the simulation can be good at all frequencies above the frequency at which the vehicle supporting fixtures affect the basic fundamental modes of the vehicle.

2. If a small structural partition surrounding the region is selected for vibration test, the simulation can be accurate up to a frequency at which the typical dimension of the specimen becomes approximately a quarter of the bending wavelength.

3. If simulation is only required above a particular frequency, then a fully coupled partitioned section can be chosen such that its typical dimension is at least 5 to 10 bending wavelengths at the lowest test frequency.

4. If the structural boundaries decouple the partitioned structure from adjoining structures, then the decoupled specimen, vibrated through the decoupling structural members, can give good simulation for the frequency region above the frequency at which decoupling occurs.

The final step in the development of the simplified logic is to examine the effect of mounting a component on the mounting region. For simplicity, first assume that the component behaves dynamically as a simple mass.

Clearly, if the structure in the region has a surface mass density considerably larger than the equivalent surface mass density represented by the component, the actual motion of the region in flight will not be altered by the addition of the component. Hence, the amount of structure required to simulate the vibration of the component is precisely the same as required above for the simulation of the vibration in the region in the absence of the component.

If the component's equivalent surface density is of the same order of magnitude as that of the structure, then the presence of the mass component may be expected to alter the in-flight motion in the mounting region from that which would occur without the presence of the component. Furthermore, it is probable that the motion of structure adjoining the mounting region will also be altered. Thus, to reproduce in a partitioned structure a reasonable facsimile of the flight environment in the mounting region, it would appear necessary to include all of the structure whose motion, when mounted in the actual vehicle, is affected by the addition of the component. For the simple example of a mass-like component, the structure required would have to have a generalized mass several times greater than the mass of the added component.

One method for determining the dimensions of the affected structure is the measurement of point input impedance as a function of distance

7

from the mounting region with and without the mass present. For the frequency range of interest and for the typical cases in real structure with simulated component masses, there will generally exist a distance in all directions from the component mounting region, beyond which no significant change in input impedance is observed. In general, it may be argued that the change in the input impedance observed at various points on the zone of structure within the envelope of these distances indicates that this zone of structure forms part of a vibrating system with the component mass. Therefore, to ensure that the size of the partitioned test structure is sufficient to exhibit the local dynamic characteristics of the component-structure system, it would be necessary that the specimen include the structure within the component influence zone. This conclusion can be generalized to include a component of arbitrary impedance characteristics.

When the mass or impedance of the component becomes much greater than that of the structure in the mounting region, it may be anticipated that the component influence zone will extend to a greater distance from the component than in the previous cases above. Further, the addition of a high impedance component may serve to alter the coupling between the local structure supporting this component and adjoining structures. Clearly, if decoupling boundaries already existed in the frequency range of interest, then the decoupling may be further enhanced by the addition of high impedance equipment.

Finally, in many cases where the structure without the component was highly coupled, the impedance discontinuity presented by the addition of the component to the structure will effectively decouple its supporting structure from adjacent structures, thus minimizing the amount of structure required for a test specimen.

These concepts are summarized in Fig. 2, which contains a simple logic diagram illustrating the types of engineering steps to be followed to determine the amount of structure which is sufficient for a given test purpose. Although engineering methods are not adequate to fully implement these concepts, this logic can be very helpful in deducing the amount of structure required for a specific test objective.

APPLICATION OF THE LARGE VIBROACOUSTIC FACILITY TO TESTING

The preceding sections have established a framework for the definition of simulation criteria, and amount of structure sufficient for a specific test objective and frequency range. Until recently, however, it was not possible to apply these concepts in other than abstract terms to large components, extended subsystems such as piping, and interconnected instrumentation systems. The maximum specimen weights for vibration tests were limited primarily by the capabilities of vibration shakers operating singly, and the maximum specimen sizes for acoustic tests were governed by the small size of acoustic test facilities.

The improvement in the state of the art of multiple shaker installations is perhaps best exemplified by the system of eight shakers utilized by Wyle Laboratories to produce a total force of 400,000 force lb on various segments of the S-II structure, as discussed in Refs. 2 and 3. This development has been made possible both by improvements in shaker technology and by considerable advances in the design of the electronic control systems which now enable considerably greater control over the face and amplitude relations among the shakers than was previously possible.

Similarly, the development of large acoustic facilities such as those at USAF, Wright-Patterson Air Force Base [4], the NASA Manned Spacecraft Center in Houston [5], and Wyle, Huntsville [6], makes it possible for the first time to subject a large section of a vehicle to reasonably realistic external pressure fluctuations. The obvious combination of the enhanced vibration capability with this new acoustic capability makes combined vibroacoustic testing of large sections of vehicles a near reality.

The use of these facilities makes it possible to meet the structural sufficiency criteria for almost all vehicle components and subsystems, as well as its external structure. Thus, for most cases, the vehicle dynamics will be inherently correct over a wide frequency range and, consequently, it should be possible to obtain a good simulation of the vibration field during test.

The application of multiple-shaker high-force systems for simulation of the low-frequency environment is relatively straightforward. However, the definition of "low frequency" must be made for each class and size of vehicle, and the effect of finite impedance and boundary conditions must be considered to avoid overtest at low frequencies.

The rules for application of the acoustic facilities to the remainder of the frequency range are much less exact. Some of the problems are illustrated by theoretical effects of

8

Define frequency range of concern $(f_1 \rightarrow f_2)$ → ②

② **Determine dimensions of component influence zone for frequency range of concern** ③ **Select nearest Logical Structural Boundaries which include influence zone for definition of partitioned structure.** → ④

④ **Compare typical dimension** $(\mathcal{L})$ **between selected boundaries to bending wavelength in** (f_1, f_2) — or / or / — ⑤ **If** $\mathcal{L} < \lambda_{B/4}$ **for all** $f_1 - f_2$, **then partitioned structure is usable for test.** → ⑪

⑥ **If** $\mathcal{L} > 5\lambda_B$ **for all** $f_1 - f_2$, **structure may be considered reverberant and is usable for test** → ⑪

⑦ **If not 5 or 6** — coupled structure — ⑧ **Chose structural dimensions** $\mathcal{L}$, **to be greater than required by** ② **o o sufficient to satisfy** ⑥ , **then structure is usable** → ⑪

decoupled structure — or — ⑨ **If partition Boundaries** ③ **are decoupling boundaries for all** $f > f_1$, **then structure is usable** → ⑪

⑩ **If not** ⑨ , **then increase size of partition until either** ⑥ **or** ⑨ **is satisfied, then structure is usable** → ⑪

⑪ **Determine edge fixity such that** ② **and either** ⑤ , ⑥ , **or** ⑨ **is satisfied on test specimen as well as on the original equivalent structure mounted in the Vehicle** ⑫ **Determine Source configuration, control data points and source forcing functions to achieve a realistic environmental simulation**

note: Values of $\mathcal{L}/\lambda_B$ are only very approximate and are included for orientation only.

Fig. 2. Summary flow diagram for structural sufficiency concept

9

vibroacoustic coupling parameters given in Ref. 7. It is fairly clear that both pure forms of laboratory acoustic simulation, reverberant field and progressive wave, have utility for simulating rocket noise at launch. Furthermore, the work described in Ref. 1 demonstrated that the acoustic levels required to reproduce actual liftoff vibration are essentially equal to those measured at liftoff. This augurs well for accurate simulation of the vibration field at liftoff.

The simulation of the vibration field resulting from unsteady aerodynamic pressure fluctuations is more difficult. Both theory and practice (Refs. 1 and 7) indicate that the vibration field resulting from uniform boundary-layer turbulence can be simulated. However, the exact relationship between point spectra in flight and test is not completely understood or verified. Trends found in Apollo [8] and theory [7] indicate that the test levels should be of the order of 10 db below the flight pressure fluctuation levels. However, this appears true only at frequencies below coincidence. Here considerable work is required to obtain accurate engineering methods for the design of tests.

The most difficult simulation requirement is imposed by separated flows, wakes, shocks, etc., associated with protuberances and geometrical discontinuities. Here simulation can be achieved in principle by local acoustic excitation through closely coupled horn-duct configurations or direct radiation. However, practical cases are only now being attempted, and neither theory nor flight data are sufficient to provide useful guides to engineering methods for test design.

All of the preceding discussion has related to the vibration field of a structure which has no other loads imposed. However, in some cases other loads will be present which affect either the dynamic response characteristics or the failure mode of the specimen. These include static pressure and thermal loads. Work to date illustrates that each may alter the transfer function between environment and failure under certain conditions. However, insufficient knowledge exists to serve as a basis for engineering methods for their evaluation relative to test design.

Despite the problems yet to be solved, the new large facility capabilities offer an order of magnitude improvement in simulating the vibration field in a vehicle throughout launch than that previously attainable. This improvement enables the testing of large vehicle segments with operational systems for both qualification and acceptance testing.

Further, this capability offers a unique method to qualify extended subsystems such as piping systems which interact dynamically with many elements of primary and secondary structure. Full development of the concept should enable some relaxation on component qualification specifications and overtest, particularly where redesign of the component involves significant weight or cost penalties. Here, reliability of the marginal component could be assessed in a realistic environment prior to launch and minor specific fixes with minimum penalties could be proven in the laboratory to ensure sufficient reliability in flight.

Continued work with these facilities in the development of engineering methods for improved test design, and in the comparison of laboratory and flight data, should result in increased confidence in the results of this ground simulation technique. With this confidence, some safety factors can be reduced eventually and enable attainment of the required reliability for less weight.

REFERENCES

1. W. D. Dorland, R. J. Wren, and K. McK. Eldred, Development of Acoustic Test Conditions for Apollo Lunar Module Flight Qualification, Shock and Vibration Bull., 37 (Part 5) (1968)

2. D. R. Reese, A 400,000 Force-Pound, Eight-Exciter Electrohydraulic Vibration System for Space Vehicle Testing, paper presented to Institute of Environmental Sciences, Apr. 1967

3. R. W. Schock and J. M. Everitt, Saturn S-II, S-IVB, and Instrument Unit Subassembly and Assembly Vibration and Acoustic Evaluation Programs. Parts 1 and 2, Shock and Vibration Bull., 37 (Part 5) (1968)

4. A. W. Kolb and H. A. Magrath, RTD Sonic Fatigue Facility, Design and Performance Characteristics, Shock and Vibration Bull., 37 (Supplement) (1968)

5. R. J. Wren, W. D. Dorland, K. McK. Eldred, and J. D. Johnston, Concept, Design, and Performance of the Spacecraft Acoustic Laboratory, Shock and Vibration Bull., 37 (Part 5) (1968)

6. F. M. Murray and L. C. Sutherland, Operational Characteristics of a 100,000 Cu Ft Acoustic Reverberation Chamber, Shock and Vibration Bull., 37 (Part 5) (1968)

7. R. W. White, Theoretical Study of Acoustic Simulation of In-Flight Environments, Shock and Vibration Bull., 37 (Part 5) (1968)

8. J. R. West, D. C. Newbrough, and R. A. Colonna, Development and Verification of the Apollo Command and Service Module Vibration Test Requirements, Shock and Vibration Bull., 37 (Part 5) (1968)

*   *   *

OPERATIONAL CHARACTERISTICS OF A 100,000-CUBIC-FOOT
ACOUSTIC REVERBERATION CHAMBER

Fancher M. Murray
Wyle Laboratories
Huntsville, Alabama

Use of a 100,000-cu-ft reverberation room at the Huntsville facility of Wyle Laboratories has resulted in a significant mass of data relating to large reverberation rooms in general. Overall sound pressure levels of 152-154 db may be generated away from the walls, while the classic 6-db and 9-db increases are seen at the walls and in the corners, respectively.

Tests performed with large specimens show that good spectral and spatial sound distribution may be generated and controlled. The room exhibits a reverberation time of 18 sec at frequencies below 200-300 Hz, while classic air absorption controls damping above this range. The room is driven by one, two, or four airstream modulators of the vibrating vane type. These modulators, rated at 30,000 watts each, were developed by the Huntsville facility specifically for this application. Instrumentation available in the room includes direct cable connection to 160 channels of charge amplifiers in a central instrumentation complex. Switching capability allows acquisition of a total of 480 data channels. The charge amplifiers are connected to multiplexers and an A-D converter for on-line data acquisition by a high-speed digital computer. Computer programs have been developed to accept these data, store it, and then produce final plots of power spectral density, auto- and crosscorrelation, amplitude distribution, and other pertinent parameters related to the acoustic driving forces and the specimen responses. Theoretical and experimental data will be presented to show the operational characteristics of this large reverberation chamber.

INTRODUCTION

As acoustic testing of structural components comes of age, numerous questions arise as to the validity of the tests performed. Many investigators have felt that this is particularly true of reverberation rooms since there are great numbers of "holes" in the low-frequency end of a sound field, in both the frequency and spatial domains. It is claimed that this condition results in overtest in some locations at some frequencies, and undertest in other locations at other frequencies. This turns out to be an unfortunate fact of life; but it can be alleviated considerably by building bigger reverberation rooms.

Another problem associated with acoustic testing concerns the boundary conditions imposed by mounting fixtures used to support a component during the test. The only way that the investigator can assure himself that a given substructure will be mounted in the proper way is to mount it on the actual service structure. This practice can, of course, be carried on until a whole vehicle is used to mount the critical substructure. At this point the worker again finds the need for bigger reverberation rooms.

The free field conditions under which most vehicles travel do not establish a situation where sound approaches with equal probability from all directions. In fact, the sound from a rocket plume can be quite one-sided during initial launch phases, but in a given narrow band of frequencies the probability of there being energy at a given frequency is the same for all frequencies, even though that probability is zero. A reverberation room operated several octaves above its first resonance will approach this same zero probability for energy at a given frequency, but it will also approach omnidirectionality in the sound field. Thus, it is necessary to give up some of the directional characteristics of the sound field in order that the smooth frequency response may be approached. The alternative is a free field test wherein the acoustic power generated is comparable with that generated by the vehicle in

13

its various stages of travel. Since this is of the order of 10 million watts, again, the bigger reverberation room becomes desirable.

There are two schools of thought which permeate all environmental testing. One school insists that the environment must be exactly simulated if the response is to be meaningful in predicting service conditions. This is a "seat-of-the-pants" type of testing and is probably always valid. However, when test programs become large and cost several millions of dollars, it is necessary to use a different philosophy in testing. Thus, there is a second school which states that it is more important that the response of the vehicle be simulated rather than the environment. This philosophy requires that some analysis be combined with simple tests to determine which parameters associated with the environment are important in generating structural response and which ones are not. A greatly simplified example of this would show the futility of generating high acoustic levels at 10,000 Hz for testing heavy structures not capable of responding to such frequencies. From this the investigator may conclude that it is necessary only to match the low-frequency portion of the natural acoustic environment expected for this case.

Consideration of the above arguments prompted Wyle Laboratories to start construction on this room in late 1964. The room has been used for testing various components of the Saturn, and some other vehicles will be tested in the near future. The forward skirt and instrument unit are being tested in this facility at the present time.

ROOM DESIGN

Design considerations for the Wyle reverberation chamber were simple -- make it adequate and make it inexpensive. This latter consideration was imposed by good sense since the structure was paid for from company money. The first consideration was broken down into greater detail so that the room could be designed on paper. Of primary consideration was the frequency distribution of the eigenmodes. A cubical room will have just as many modes as any other shape; but great numbers of modes will occur at the same frequency, and then there will be large gaps between modes. This question is discussed further in the next section.

Another consideration was the high sound pressure levels (SPL's) expected on the walls and the resulting dynamic loading of these walls. A level of 160 db in the room results in 163 db

at the walls, 166 db where two walls meet, and 169 db in the corners. These levels generate significant dynamic pressures and, when integrated over the surface area of the room, large forces are developed which tend to cause cracks and other lossy conditions in the walls. Thus, as is seen in Fig. 1, a large amount of steel work was included in the walls to maintain integrity. Figure 2 is a sketch of the room and shows some dimensions of the plan view. It is seen that the interior surface contains splays to enhance the sound diffusion. Dynamic analysis of the wall showed that the thick portions of the splays would act as sufficient reinforcement of the walls to reduce requirements on the mean thickness. The thick portions are then about 3 ft thick, and the thin sections are about 18 in. thick. The north end of the room consists of a modular construction with blocks 1 ft thick forming this wall. The west half of this wall is supported by large box beams which may be removed for entrance of specimens larger than allowed by the main door. The main door is the east half of the north wall and is power operated for the full height of the room. A specimen 20 ft in diameter and 35 ft high can be moved through this door in a few minutes. Specimens much larger than this would require a couple of days' work by a large crane for removal of the rest of the north wall. Figure 3 shows this conception as it is actually used.

A LITTLE THEORY

The allowed frequencies for any rectangular reverberation room have been derived by several investigators in the past and may be found in any text such as Kinsler and Frey [1]. This equation consists essentially of a three-dimensional version of the Pythagorean theorem in that it is the square root of the sum of three squares:

$$f = \frac{c}{2} \sqrt{\left(\frac{n_x}{\ell_x}\right)^2 + \left(\frac{n_y}{\ell_y}\right)^2 + \left(\frac{n_z}{\ell_z}\right)^2}$$

where c is the speed of sound, ℓ_x, ℓ_y, and ℓ_z are the three dimensions of the room, rank ordered by length, and n_x, n_y, and n_z are positive integers defining the wave number existing in each direction in the room. Since these integers may be varied independently over the range of zero to infinity, it may be seen that a large number of allowed frequencies or eigenmodes may be accumulated within the first decade above the first such frequency. Solution of this equation for a great number of different values of the integers will give the frequencies of a given room. Then these

14
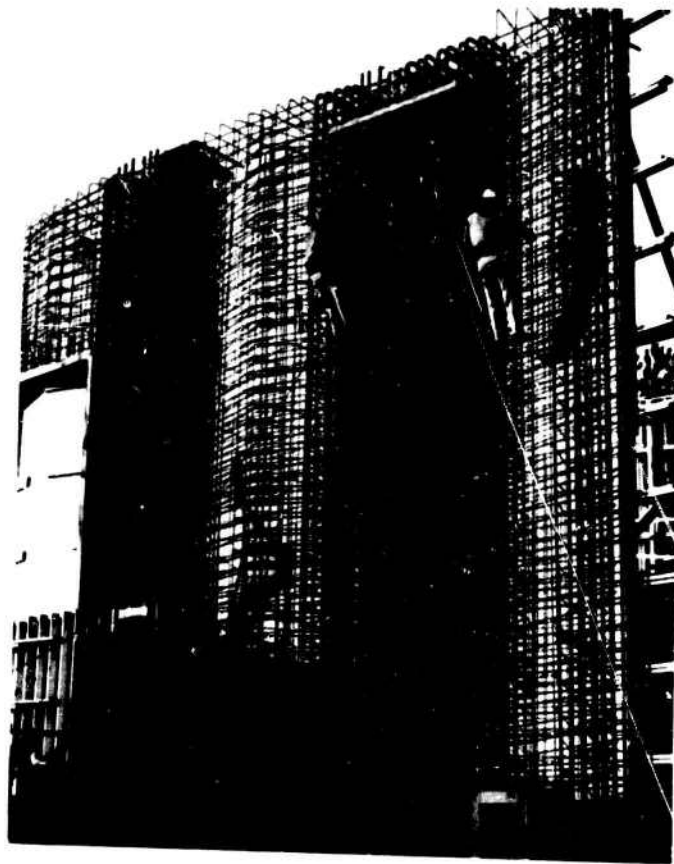
Fig. 1. Steelwork used in the 100,000-cu-ft room
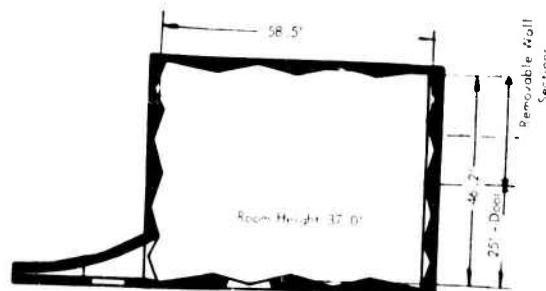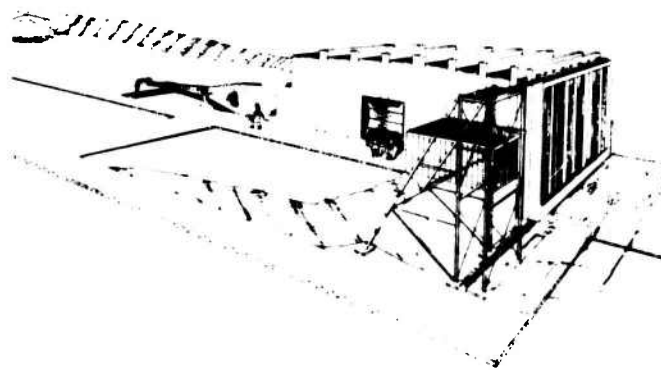
Fig. 2. Completed structure with dimensions

15
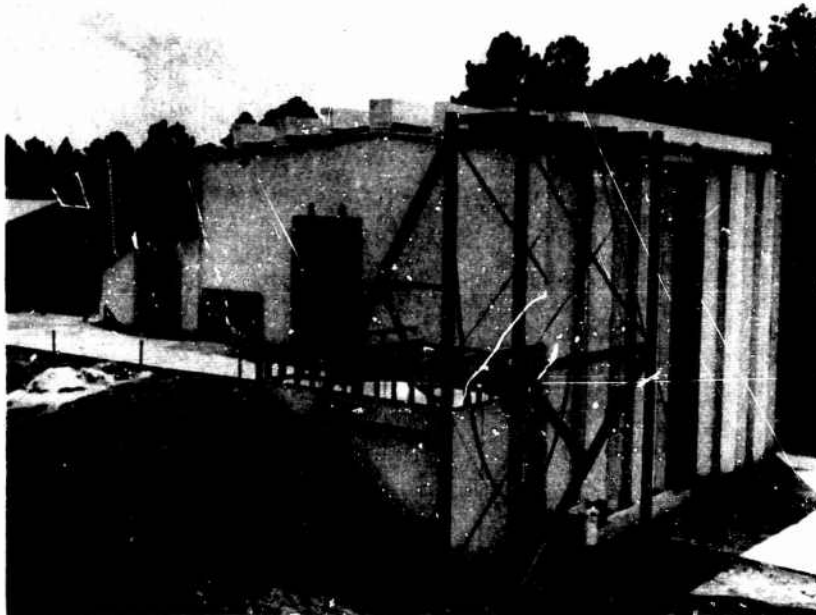
Fig. 3. Completed room from northeast end

frequencies can be plotted as tick marks on a frequency scale to show where gaps occur and where large numbers of modes pile up together. It has long been known that a cubical room, or a room having definite integral relations between the lengths of its walls, will show a tendency for the modes to congregate, leaving large gaps. However, it has been left to the computer to solve the equations quickly enough to produce results which could search for a room shape that spreads the modes in a uniform manner. Sepmeyer [2] has done a monumental work in this field. He used a computer to compare the number of modes theoretically appearing in a given band of frequencies with the number predicted on a statistical basis. His criteria required that the ratio of these two numbers be as close to unity as possible for as many different bands as possible. Since a given modal distribution is independent of the actual size of the room, it is convenient to normalize the equation by dividing through by the length of the longest dimension of the room. Dividing by ℓ_x, and ignoring the $c/2$ factor, gives:

$$\nu = \left[(n_x)^2 + \left(\frac{n_y}{\ell_y / \ell_x} \right)^2 + \left(\frac{n_z}{\ell_z / \ell_x} \right)^2 \right]^{1/2}$$

Thus, a shape may be defined by unity plus two fractions which show the relationship between the length of the longest wall to the next longest wall and to the shortest wall, respectively. A shape of 1, 1, 1 would define any perfect cube,

and a shape of 1, 0.5, 0.5 would indicate that two of the walls were half of the length of the longest wall. The first number is always unity.

Sepmeyer used this form and evaluated rooms from 1, 1, 1 to 1, 0.3, 0.3 in increments of 0.01 for each of the two varying parameters. One of the better rooms he found had the ratio 1, 0.79, 0.63. This ratio has the further advantage that it will reproduce itself if the long dimension of the room is cut in half. Then the ratio for the two resulting rooms is still 1, 0.79, 0.63. The frequency responses of the two rooms will be at a higher range, but the distribution is the same. This ratio was used for the mold lines of the Wyle reverberation room.

Sepmeyer's work does not allow comparisons of small increments taken on the dimensions, and Wyle Laboratories has developed a computer program for presenting this same information in a form more suitable for direct comparison of the "gaposis" of a given room shape. This program determines all the eigenmodes in the first decade of a given room's response range and actually plots them as vertical lines on a horizontal frequency scale. Since these lines tend to get very close together, the program also makes the height of the vertical line proportional to the distance (on the frequency scale) between its two neighbors. Thus, if a line is standing between two widely separated lines it will be taller than its neighbors. Figure 4 is a graph produced by the

16

Reverberation Room Modes

The horizontal scale is a normalized linear frequency scale starting at 0 Hz. Each division is a harmonic of the first room mode.

The height of each line is proportional to the sum of the distances to its two neighbors.

L2= .513000   L3= .513000
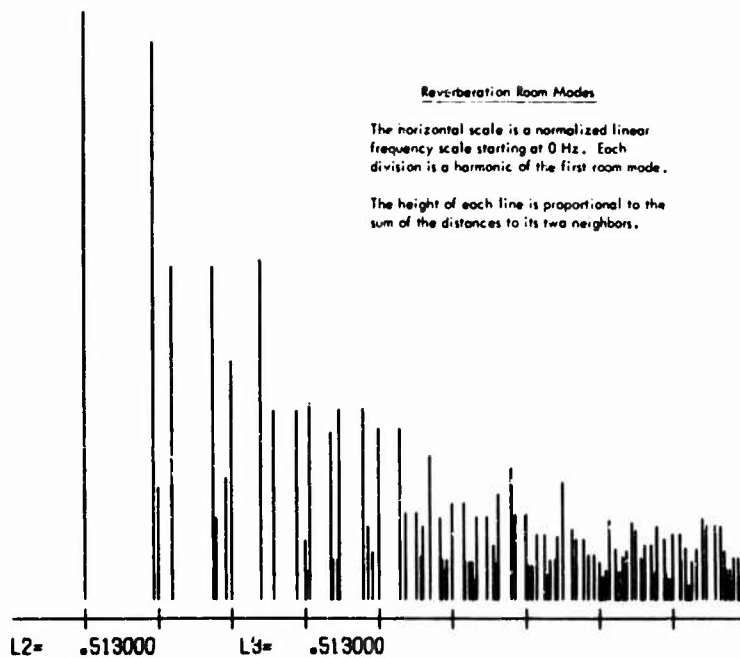
Fig. 4. Graph using a poor room design

Wyle computer to show the frequency distribution of a room having the shape 1, 0.513, 0.513. The gaps are readily apparent, as is the resulting grouping of modes at other frequencies. Since two of the walls of this room would have equal lengths, it is easy to surmise that this would be the result. Figure 5 is a similar graph, using the shape of the Wyle room. Here, the gaps are well filled in, and it is necessary to look for tall vertical lines to see any evidence of some of the gaps.

It may be obvious that an ideal room shape would produce a graph having one tall line on the left and progressively shorter lines toward the right. This would indicate maximum uniformity in spacing and minimum redundancy of modes. Figure 6 is a graph closely approximating such a situation: three definite lines progress toward short lines. This shape requires considerably more than two-place accuracy in definition, and some points are still not understood about its characteristics. Everything that has been learned about it has been encouraging, though, and this may be the closest thing to an ideal room yet. This particular shape was developed by K. McK. Eldred of the Wyle staff.

The acoustic power developed in a reverberant enclosure is given by Kinsler and Frey [1]:

For a diffuse sound field,

$$I = \frac{W}{a} = \frac{p^2}{4 \rho c a}$$

where

I = intensity,

W = acoustic power input,

a = total absorption,

p = acoustic pressure, and

ρc = acoustic impedance of air.

In the English system this may be converted to a logarithmic form

$$PWL = SPL - 6.5 \text{ db} + 10 \log a$$

where

PWL = sound power level re: 10^{-13} watts,

SPL = sound pressure level re: 0.0002 microbar.

Since

$$a = \frac{0.049V}{T}$$

where

17

Reverberation Room Modes

The horizontal scale is a normalized linear
frequency scale starting at 0 Hz. Each
division is a harmonic of the first room mode.

The height of each line is proportional to the
sum of the distances to its two neighbors.
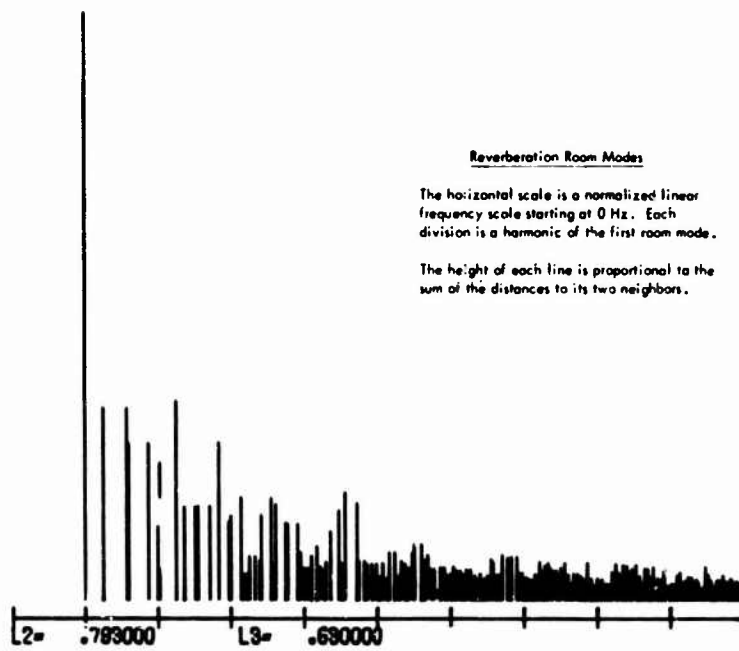
Fig. 5. Graph using a good room design

Reverberation Room Modes

The horizontal scale is a normalized linear
frequency scale starting at 0 Hz. Each
division is a harmonic of the first room mode.

The height of each line is proportional to the
sum of the distances to its two neighbors.
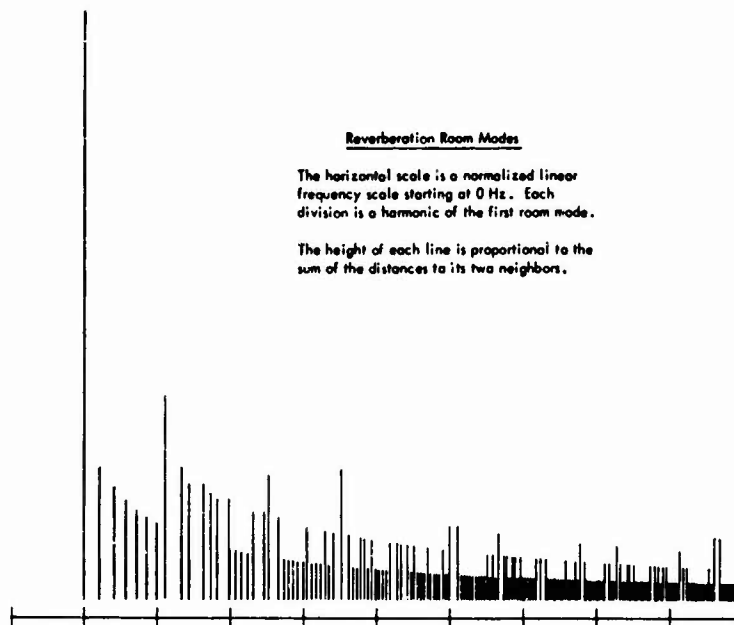
Fig. 6. Graph using a better room design

18

V = room volume,

T = reverberation time, and

$$PWL = SPL - 6.5 \text{ db} + 10 \log \frac{0.049V}{T} .$$

For the Wyle room this becomes

$$PWL = SPL + 17.8 \text{ db} .$$

This equation is the only one that is theoretically defensible and is therefore the only one used for measurements by Wyle Laboratories. There are several variations of this equation that have become popular in recent years because of the large deviations between power measured in a reverberation room by this equation and power measured in an anechoic progressive wave tube by integration of the sound pressure over the cross-sectional area of the tube. Some investigators have experienced as much as 11-db discrepancy, although 4 to 6 db is more common. These discrepancies can be attributed only to poor coupling between the acoustic source and the room. Wyle has made some progress toward better coupling, and some model experiments have shown as little as 0.3-db difference between the two methods of measuring acoustic energy.

Figure 7 shows the energy decay parameters measured in the Wyle room. Two

experimental curves show the reverberation time against the right margin and the absorption in square feet against the left margin. The measured absorption is also compared with computed values of air absorption. It is seen that the measured data compare well with the computed data. It may also be seen that acoustic energy above 1000 cps in the large room is severely discriminated against by the air absorption.

INSTRUMENTATION

The 100,000-cu-ft room is adequately supplied with instrumentation lines to provide response data for large component testing. Figure 8 shows a bank of charge amplifiers used to accept signals from all types of piezoelectric transducers. A total of 160 channels are immediately available to an on-line computer through two high-speed multiplexers. In addition, these may be switched manually by a three-position switch to increase this to 480 channels when needed. During large tests microphone and accelerometer data are directly stored by the computer for analysis.

For smaller tests where a few microphones are sufficient, five carrier-type condenser microphones may be connected to coaxial lines in the room. These provide for research and for tests of components not
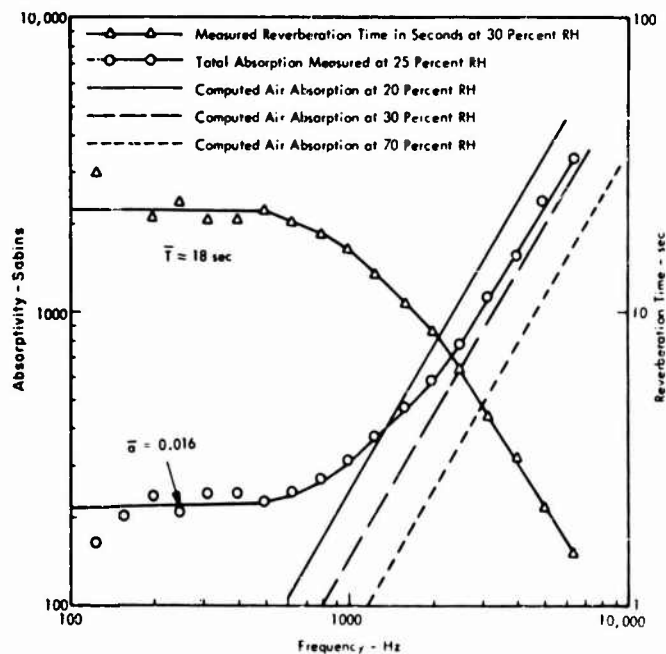
Fig. 7. Air graph, room absorption vs frequency, 100,000-cu-ft reverberation room

19

Fig. 8. Charge amplifiers in instrumentation room

requiring response measurements. This instrumentation is normally analyzed with analog equipment in either one third octaves or narrow band.

DATA DEVELOPED

This section covers some of the data generated in the large room during tests and during room evaluation. Figure 9 is a sine sweep generated in this room with a normal loudspeaker. The frequency scale of this sweep covers the first decade of operations and is intended to match the frequency scale of the computer plot of Fig. 5. Many of the low-frequency modes match quite well with the computer plot, but large numbers of modes in the higher frequencies did not appear. This problem is not as serious at high levels, because nonlinear driving of the modes causes them to exchange energy even if they do not couple with the primary excitation. However, the sweep is instructive in pointing the way for further investigations; it also explains some of the discrepancies between the two methods of measuring acoustic power.
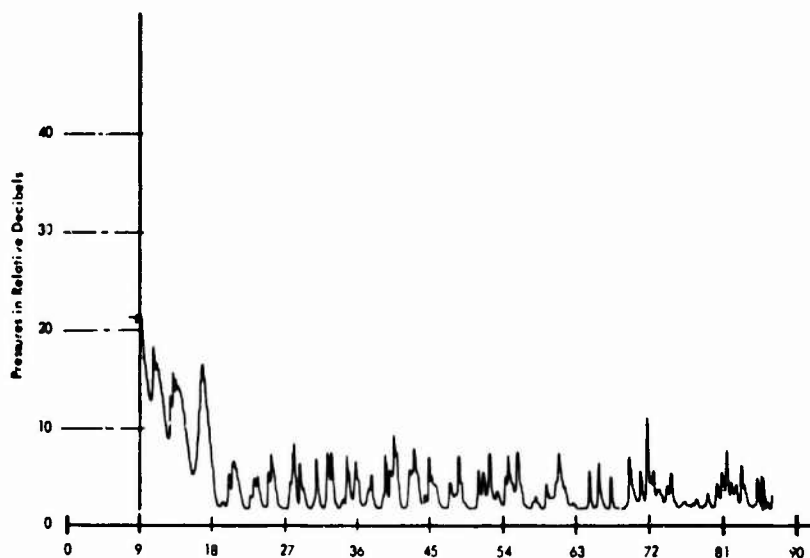
Fig. 9. Sine sweep, 0-90 Hz in room

20

Figure 10 is a sine sweep taken with a B and K oscillator using the Wyle-developed acoustic source model WAS-3000 airstream modulator at low pressure. Figure 10 shows an almost solid mass of modes from 60 to about 700 Hz where the transducer starts cutting off.

Figure 11 shows the broad-band response of the room at three different locations. The top curve was measured in the southwest corner of the room, and, as expected, it is approximately 9 db above the other two curves taken in the normal field of the room. These two other curves were taken approximately 21 ft
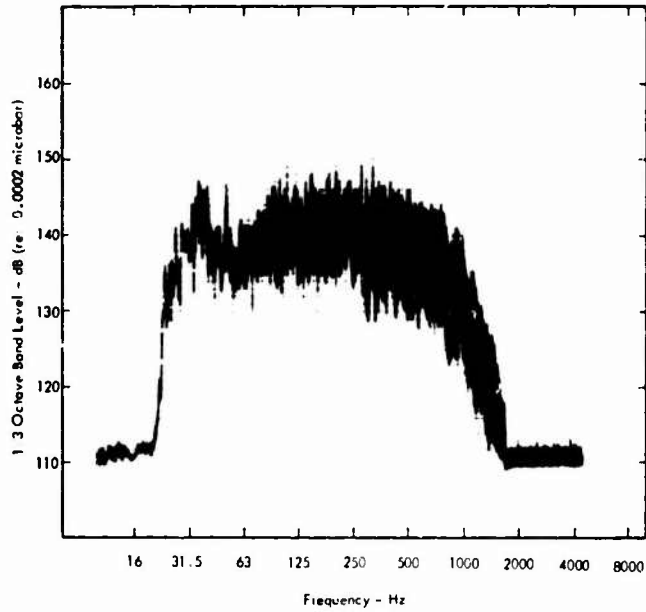
Fig. 10. Log sine sweep, 20-2000 Hz
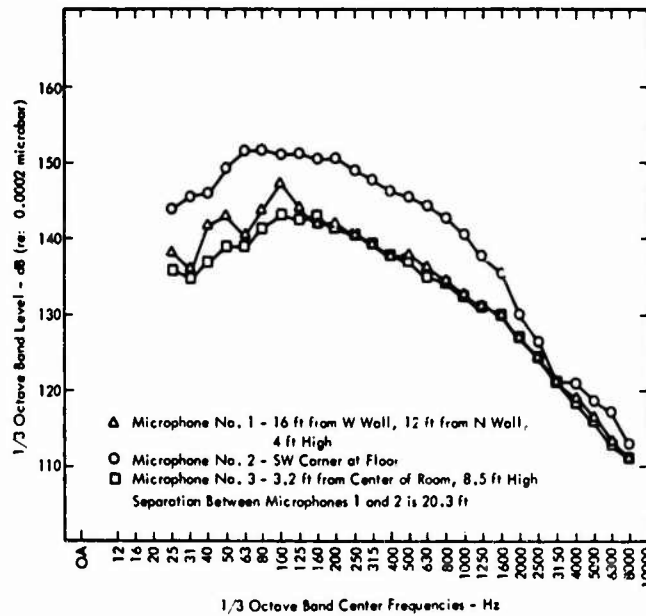
Fig. 11. Broad-band random response
at three locations in room

21

apart in the room at two different heights. It may be seen that they merge very well above 100 cps and that there are no great differences below that frequency.

An interesting way of looking at the frequency response of the room and the high-frequency distortion caused by nonlinear finite amplitude acoustic effects in the air is to put a single one third octave of electrical signal into the drive transducer and determine the resulting spectrum. Figure 12 is one presentation of such data. The actual data are shown in solid lines; there is a strong response at the input frequency and also at the first two harmonics of the input frequency. A narrower band analysis would show other harmonics too, but this one third octave analysis is sufficient for our purposes. For reasons which are apparent in Fig. 13, it
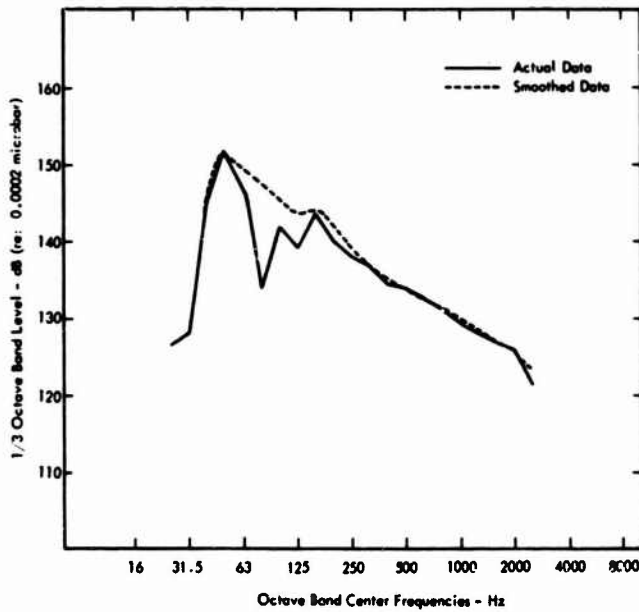
Fig. 12. Single one third octave input to room with actual and smoothed spectra developed
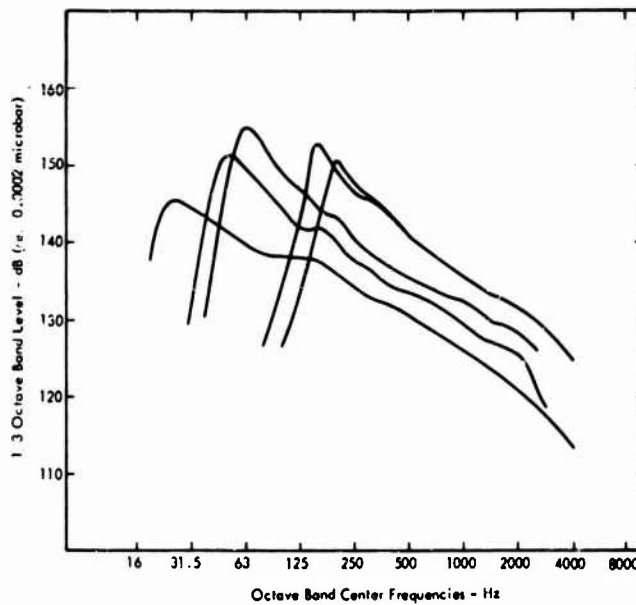
Fig. 13. Several one third octave spectra through 25-Hz horn

22

is convenient to smooth the data to form the dashed curve also shown in Fig. 12. If the input signal was one octave wide, then this is what would actually happen.

Now look at Fig. 13, where the responses to several different one third octave inputs have been plotted. In each case the sound energy rises very sharply to a peak at the input frequency and then tapers off more slowly. This is the result of nonlinear air response generating harmonics. The data of Fig. 13 show the response using a 25-Hz coupling horn between the transducer and the room. Figure 14 shows the effects of using a 50-Hz cutoff horn to drive the room. The lowest input frequency is a one third octave band centered on 25 Hz, but Fig. 14 shows that the maximum response does not occur until the second harmonic of this frequency. The strong discrimination of the 50-Hz horn against the low frequencies is seen in this response. Even an input at 50 Hz is seen to respond only weakly at 50 Hz compared with the response at 100 Hz. It is not until the input frequency reaches 63 Hz that the maximum response occurs at the input frequency.

Figure 15 is some actual working data taken from a large structure under test in the reverberation room at 154 db (re. 0.0002 μbar) and shows the form produced by the Wyle computer facility. This is a normal PSD analysis in g^2/cps and shows a good broad-band response. The analysis used a digital filter of 10-Hz bandwidth and the autocorrelation curve is presented just below the PSD plot. Various statistical characteristics are enumerated below from the variance to the kurtosis. The overall level of vibration is also given as 23.58 g rms.

CONCLUSIONS

From the above discussion several conclusions may be drawn:

1. The facility generates and contains reasonably high SPL's. Proper acoustic coupling between the transducer and the room will be required before the design limitation of 165 db can be reached, but respectable levels are available at the present time.

2. At a frequency approximately one decade above the first resonance, the spatial distribution of energy is very uniform and the facility can be expected to give realistic tests from 100 Hz and up.

3. Testing at frequencies above 1000 Hz is limited by sound absorption, but data presented show a reasonable amount of energy to 10,000 Hz. The levels at these frequencies are not sufficient to cause damage, but they are sufficient to evaluate the possibility of damage by noting the response of structures to the levels that are attained.
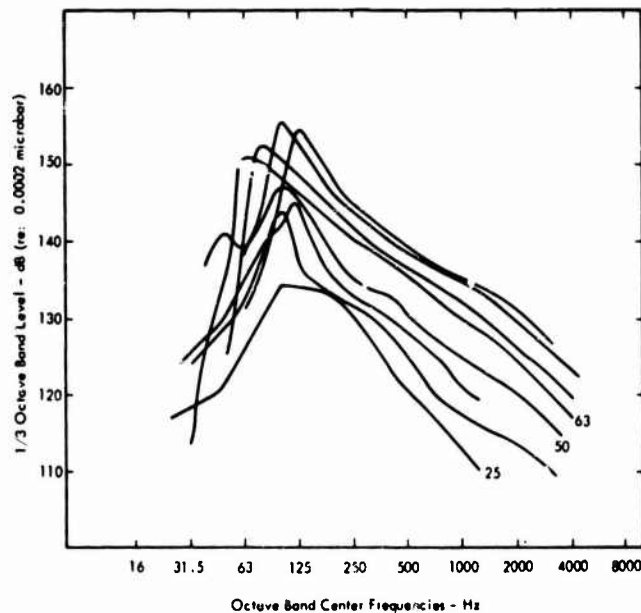
Fig. 14. Several one third octave spectra through 50-Hz horn

23
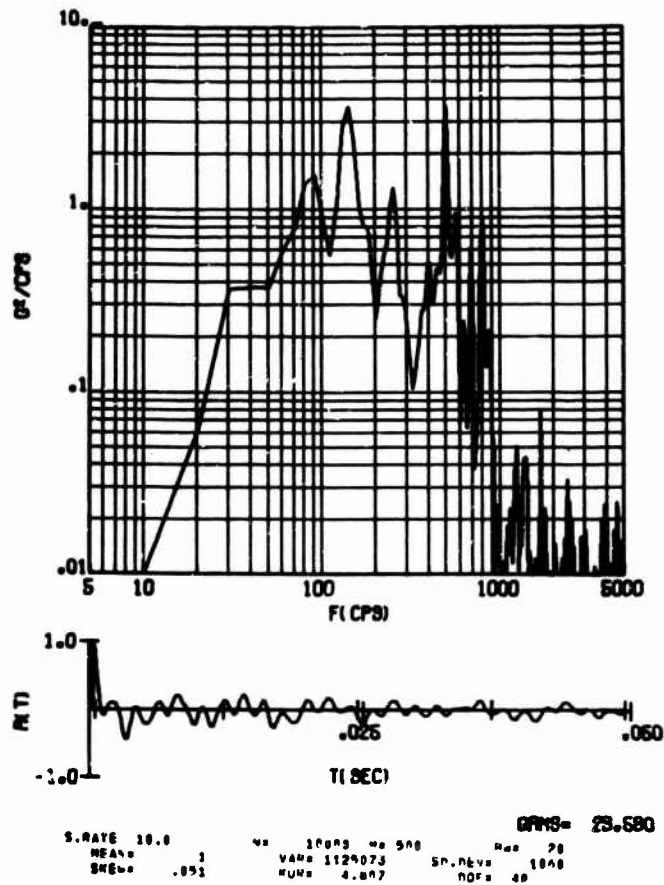
Fig. 15. Acceleration data measured on a typical
vehicle structure under test at 154 db

REFERENCES

1. Lawrence E. Kinsler and Austin R. Frey,
   Fundamentals of Acoustics (2nd ed.) (Wiley,
   New York), 1962, pp. 420-430

2. L. W. Sepmeyer, "Computed Frequency
   and Angular Distribution of the Normal
   Modes of Vibration in Rectangular Rooms,"
   J. Acoust. Soc. of Amer., 37(3):413 (1965)

*   *   *

24

CONCEPT, DESIGN, AND PERFORMANCE OF THE
SPACECRAFT ACOUSTIC LABORATORY

Robert J. Wren, Wade D. Dorland,
and James D. Johnston, Jr.
NASA Manned Spacecraft Center
Houston, Texas

and

Kenneth McK. Eldred
Wyle Laboratories
El Segundo, California

To obtain the best possible ground test verification of the flightworthiness of the Apollo spacecraft to launch and boost fluctuating pressure environments, the NASA Manned Spacecraft Center conceived, designed, and constructed the Spacecraft Acoustic Laboratory which embodies a unique vibratory simulation technique and capability. Apollo acoustic levels and spectra were used to develop acoustic test energy requirements and frequency considerations in the design of the sources, horns, and ducts. The test configuration includes 16 horn/duct channels, each driven by an independently controllable acoustic noise source, which completely envelop the vehicle and control the propagation of high-energy acoustic waves downward over the vehicle. Evaluation of the performance characteristics of the facility was oriented toward verification of acoustic test hardware design and, more importantly, toward comparison of Apollo vehicle vibration responses achieved in the ground test vs flight measurements. With minor exceptions (which were corrected), all acoustic parameters designed into the hardware have been met or exceeded. The shell response of the service module as measured at eight locations on an Apollo flight has been duplicated satisfactorily in the laboratory.

INTRODUCTION

The random fluctuating pressure (acoustic) excitation of the Apollo spacecraft during earth launch and boost is not only severe but also varies as a function of both flight mission time and location on the vehicle. To obtain the best possible verification of the flightworthiness of the spacecraft, evaluation was required of the vibration behavior of the Apollo spacecraft under severe acoustic conditions of flight in a ground test. A review of existing fluctuating pressure simulation techniques and capabilities for full-scale spacecraft led to a concept, design, and development program which has produced an unusual simulation technique and capability. The evolution and embodiment of the simulation technique, which resulted in the Spacecraft Acoustic Laboratory (SAL), are described in this paper. Many simulation and facility hardware design problems were encountered, and both the problems and the solutions are discussed. Actual laboratory performance data are presented, and comparisons with flight measurements are made.

The Apollo spacecraft (Fig. 1) consists of the command module (CM), the service module (SM), and the lunar module (LM). During earth launch and boost, a rocket-propelled launch escape system (LES) is attached to the forward bulkhead of the CM, and a spacecraft lunar module adapter (SLA) surrounds and protects the LM and also serves as the mechanical connection of the SM with the Saturn booster. In addition to the LES on the CM, many other aerodynamic protuberances, such as the reaction control system housing and nozzles on the SM, are located on the surface. The total acoustic excitation of the Apollo spacecraft during earth launch and boost reaches three peaks as a function of flight profile: (a) booster engine noise from the first stage of the Saturn at liftoff; (b) aerodynamic turbulence at transonic velocities; and (c) aerodynamic turbulence during maximum dynamic pressure (Q) conditions at supersonic velocities.

The first acoustic peak can be described as a composite of progressive waves propagating from the base of the Saturn booster forward

25
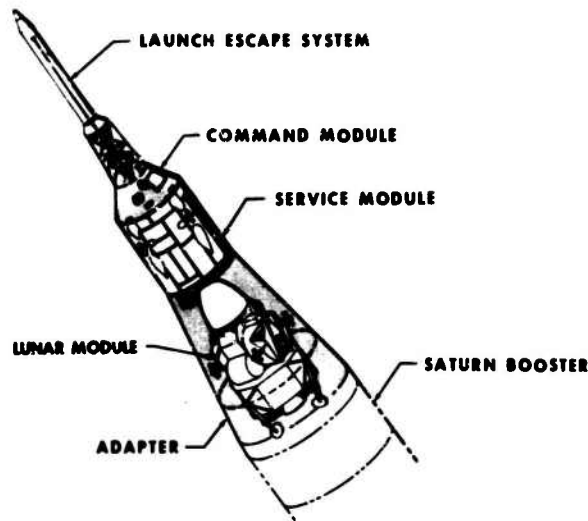
Fig. 1. Apollo spacecraft vehicle in launch
and boost configuration

to the Apollo spacecraft. The second and third acoustic peaks represent the combined actions of several separate aerodynamic mechanisms which are either generated or intensified by the many vehicle protuberances projecting into the airstream and by abrupt changes in the vehicle mold line. These mechanisms include boundary-layer turbulence, separated flow, wake turbulence, and oscillating shocks. The varied nature of the acoustic loadings with respect to magnitude, spectral content, and correlation parameters dictated a ground test tool which would provide as much control over these parameters as possible. In addition, since the flight acoustic loadings are characterized by a spatial distribution of forces over the surface of the vehicle which is of a continuous nature (in lieu of several point forces, for example), a ground test technique was required that would provide spatial continuity of the forcing function.

During the concept studies in 1963 [1], the existing state of the art for simulation of launch and boost acoustic loading or other means of inducing flight-like vibration of spacecraft structures was surveyed and reviewed. The use of electromechanical or hydromechanical shakers, either singly or in multiples, was investigated. The potential use of acoustic waves led to the consideration of reverberation rooms, single-source progressive waves, and multiple-source progressive waves. A multiple-source, multiple-channel (or multiple-duct) approach was chosen with each source channel to be acoustically separated from adjacent channels circumferentially around the vehicle. The sources were located forward of the vehicle to

satisfy spatial profile requirements of the Apollo acoustic levels. The Apollo acoustic levels and spectra were used to develop acoustic test energy requirements and frequency considerations in the design of the sources and channels (horns and ducts). During the concept study, the selected approach was technically verified for practicality through the use of scale models.

The acoustic levels increased aftward on the CM (an uncommon condition since the acoustic levels decrease aftward on all other portions of the Apollo vehicle), which presented an unusually challenging acoustic test hardware design problem [2]. The solution was found in the application of a technique using split horns with one horn reversed. The initial horn, reverse horn, and duct designs were verified with detailed scale models of the Apollo vehicle and acoustic test hardware.

The resulting test setup consists of 16 horn/duct channels each driven by an independently controllable acoustic noise source. Each source is rated at 10,000 watts output. The channels completely envelop the vehicle and control the propagation of high-energy acoustic waves downward over the vehicle. The horns are constructed of fiber glass and steel, and the ducts and duct supports are constructed of wood and steel. Viscoelastic damping compound is used to reduce vibration of steel components. The ducts are adjustable inward or outward so that the cross section of the area through which the progressive waves propagate can be varied. Anechoic wedge terminators are used at the end

26

of each wave propagation channel. Acoustic energy is produced by 16 pneumoacoustic sources, or air modulators. Air is supplied to these devices by a large constant-flow air compressor. Modulation of air valves in the devices is both controlled and powered by electrical control equipment located in a control room adjacent to the test area.

The acoustic hardware was checked out, evaluated, and adjusted during a step-by-step series of checkout test programs. Included in the objective of each checkout experiment was simplicity of operations, including rapid feedback of results. The experiments proceeded in an orderly progression from single horns to multiple horns and from single Apollo modules to multiple modules; this was done for simplicity and to assure isolation of hardware components and dynamic parameters under evaluation. Potential physical interference of the ducts with the vibration response of the shells of test vehicles was investigated in a series of shaker tests. During these tests, the characteristic response was first measured at selected points on the bare checkout test article; then the vehicle response was measured at the same points after the horn and duct system had been mated with the test article.

Evaluation of the performance characteristics of the facility was oriented toward verification of acoustic test hardware design and, of more importance, toward comparison of Apollo vehicle vibration responses achieved in the ground test vs flight measurements. With minor exceptions (which were subsequently corrected), all acoustic parameters designed into the hardware were met or exceeded.

Effects on the vehicle-shell response of physical contact with the ducts are negligible. The SM-shell-vibration data from the laboratory tests compare quite favorably with flight data. The shell response of the SLA as measured at three locations on two separate flights has been duplicated satisfactorily in the laboratory.

In this paper, the facility design requirements are described first, and the discussion includes the philosophy of environmental simulation, the sources of vibration in space vehicles during flight, the aerodynamic pressure fluctuations around the Apollo vehicle, and the simulation of such pressure fluctuations. The next section describes the final facility design, including test configuration and equipment for the Apollo vehicle. Finally, the performance of the facility (for the Apollo configuration) is reported and analyzed. Comparisons are made between intended and actual performance.

FACILITY DESIGN REQUIREMENTS

Philosophy of Environmental Simulation

The purpose of the Apollo acoustic tests as established by the NASA Manned Spacecraft Center (MSC) was to evaluate probable spacecraft vehicle structure and equipment response, failure, or malfunction in the flight environment. Therefore, the criteria applied to the method of laboratory simulation were based on the need to reproduce probable flight responses.

To obtain the maximum information from the complete system test, it was deemed desirable to have the capability for all systems, including astronauts, to be functioning fully during testing. To achieve this requirement, it was necessary for the vehicle axis to be vertical so that the direction of the gravitational vector during flight would be duplicated for fuel tanks, personnel, etc.

Since the purpose of the tests was to produce responses similar to flight responses, the ideal test would have included (a) external pressure fluctuations with correct time and spatial relationships, (b) inertial forces (from body acceleration of spacecraft/booster vehicles), (c) separation and ignition shocks, (d) engine vibration, (e) vibration introduced via structural interfaces into upper stages (spacecraft) from lower stages (booster) that are associated with low-frequency body-bending modes of a complete spacecraft/booster vehicle, (f) external temperatures with time and spatial relationships, (g) quasi-static wind loads, and (h) external static pressure loads with time and spatial relationships.

This is a most formidable list of environmental considerations; the simultaneous accomplishment, or even partial accomplishment, of which far exceeded the existing state of the art in 1963. Further, the concept of combined loadings was only beginning to be explored in the simultaneous application of two forcing functions. The acoustic laboratory was designed to allow simultaneous accommodation of all these loads except external temperatures and static pressures.

Accomplishment of acceleration and quasi-static loads is generally achieved by attaching tension members to various hard points on the vehicle (interstage rings, etc.). These tension members can then transmit the forces of hydraulic jacks which may be programmed. The facility structure was designed to enable installation of attach points for both vertical and horizontal load applications.

27

Accomplishment of shock, engine vibration, and interstage vibration would require placement of vibration generators at appropriate locations on the test vehicle, including the base of the stage under test. Exact simulation of structural interface impedance between stages is beyond the state of the art. However, the interface stiffness between the spacecraft and booster stages can be simulated. The assumption is made that structural impedances at the interfaces between spacecraft modules under test are simulated for all frequencies above the basic body resonances of the complete spacecraft/booster vehicle.

As previously implied, a major source of vibratory energy for the upper stages, including the spacecraft, is the external aerodynamically induced pressure fluctuations. The responses to these fluctuations depend upon the pressure spectrum at a point, the size of the area over which the pressures are correlated, and the natural response characteristics of the structure. The size of the area is generally related to the scale of the turbulent phenomena causing the pressure fluctuations. Unfortunately, the area over which an acoustic wave is correlated, either in time or space, exceeds that over which the aerodynamic phenomena are correlated. Consequently, in many cases, the matching of an aerodynamic pressure spectrum at a point results in a greater generalized force on the vehicle structure. This effect is usually most apparent at low frequencies. Relationships between frequency, boundary-layer thickness, correlation, etc., have been obtained for the normal boundary layer, both experimentally and theoretically. However, there was no information available which would give the space and time correlations for separated flow and oscillating shock phenomena.

Sources of Vibration in Spacecraft
Vehicles During Flight

The four primary sources of spacecraft vibration (at frequencies above the basic body resonances of a complete spacecraft/booster vehicle) during flight are (a) vibrational energy transmitted from propulsion systems or other onboard machinery; (b) vibration induced by ignition, stage separation, and docking impact transients; (c) vibration resulting from rocket noise impinging on the spacecraft shell during launch; and (d) vibration resulting from excitation of the spacecraft shell by aerodynamically derived external pressure fluctuations.

Motions associated with low-frequency body-bending modes of a complete spacecraft/

booster vehicle usually are lower in level, and are not considered to be a primary source of high-level structural vibration, especially at high frequencies (above the basic body resonances of the complete spacecraft/booster vehicle).

In general, the vibration of propulsion systems dominates the vibration levels adjacent to the engines. However, little of this vibrational power is received by forward or remote areas of the spacecraft vehicle because of the attenuation within the damped structural path. This is especially the case for mechanical-borne vibration reaching the spacecraft from the propulsion engines of the lower booster stages.

Shock energy created by ignition, stage separation, and docking impact transients excites the fundamental vehicle vibratory modes and sometimes presents a very severe environment for structure and equipment mounted close to the source of the shock. However, little of the shock energy, particularly at the higher frequencies, is propagated to remote locations.

For much of a spacecraft vehicle, therefore, external pressure fluctuations, whether acoustic wave noise or aerodynamically induced, are responsible for the majority of internal vibration, structural fatigue failure, and equipment malfunction. Generally, the aerodynamic sources are more important in the forward areas of a spacecraft vehicle, whereas the rocket-generated acoustic wave noise is dominant on the aft end. Since simulation of fluctuating pressures associated with aerodynamic sources, or the structural vibration resulting thereof, is less straightforward than simulation of rocket-generated acoustic wave noise, the characteristics of the aerodynamic environment are discussed in detail in the next section.

Aerodynamic Pressure Fluctuations
Around the Apollo Spacecraft Vehicle

The flow field around the Apollo spacecraft is rather complex (Fig. 2) because of the many abrupt geometrical changes. The wake from the rocket tower of the LES covers the entire CM conical face during the launch phase. The presence of the wake makes it impossible for the bow shock formed during supersonic flight in front of the blunt forebody (CM) to remain stationary. The abrupt transition at the shoulder of the CM creates a region of locally separated flow over the surface of the SM which results in high-level excitation throughout the atmospheric portion of the flight. In addition, the entire SM is subjected to a forward-moving

28
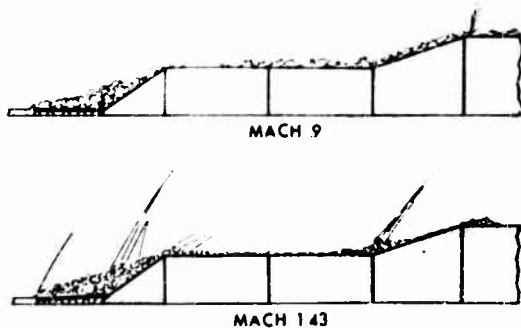
Fig. 2. Two flow regimes over the Apollo vehicle from Marshall Space Flight Center wind-tunnel tests (original SLA configuration)

shock wave as the vehicle accelerates through the transonic region. Evidence of separated flow also exists over the SLA, and another flow separation occurs on the Saturn IVB (S-IVB) shoulder.

Several measurements of the surface pressure fluctuations have been made on models of typical spacecraft configurations [3]. Considerable wind-tunnel tests using various scale models were also performed by North American Aviation (NAA) for NASA MSC at several wind-tunnel facilities, as noted in Fig. 3. (These latter data, although unpublished, were used for the Apollo program environmental definition.) The maximum overall pressure fluctuation levels for several typical stations around the Apollo vehicle at various Mach numbers are given in Fig. 3. The effect

of the violent separation aft of the CM shoulder is clearly evident. The maximum overall level at this point, 173 db (all fluctuating pressure and sound pressure levels are in decibels, referenced to 2×10^{-4} μbar), was obtained by NAA at the Douglas Aircraft Company wind-tunnel facilities on a very small model. More controlled tests gave values of 166 to 168 db. The average of all values was 169 db.

Typical relative one-third octave band spectra in the shoulder area are given in Fig. 4. The results show a constant increase of 10 db/decade from the lowest frequency to the spectral maximum in the vicinity of 80 Hz. This slope is independent of Mach number; however, the spectral levels above 80 Hz are influenced by Mach number with a considerable increase in the supersonic region. Absolute values of typical maximum spectra, without regard to Mach number or station, are given in Fig. 5. The peak in the vicinity of 80 Hz is well defined for all subsonic and transonic regions. The characteristic low-frequency slope of 10 db/decade is also consistent, as is the tendency for the high-frequency noise to increase in supersonic flight.

The clear upper bound of the data in Fig. 5 and the similarity of the spectra enabled the selection of the design acoustic-performance curve shown in Fig. 6. The design curve was selected to have an overall SPL of 171 db at the shoulder position and to give a margin of 2 db. The margin allowed for uncertainties in the capabilities of the yet-to-be-developed noise-source system and allowed the possibility of attaining higher levels, if warranted for specific test objectives.
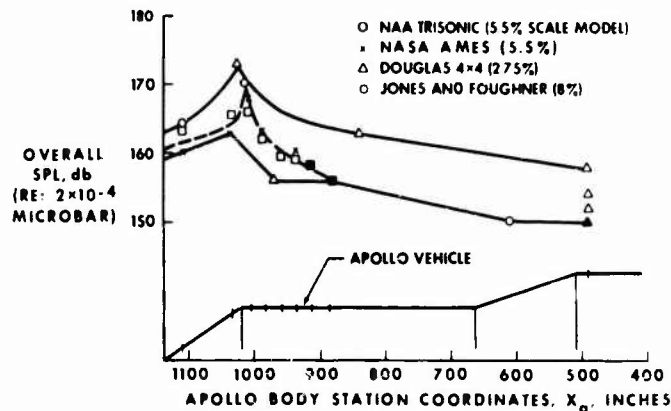
Fig. 3. Comparison of maximum overall aerodynamic pressure fluctuations found in previous studies of typical configurations corrected to flight dynamic pressure (original SLA configuration)

29
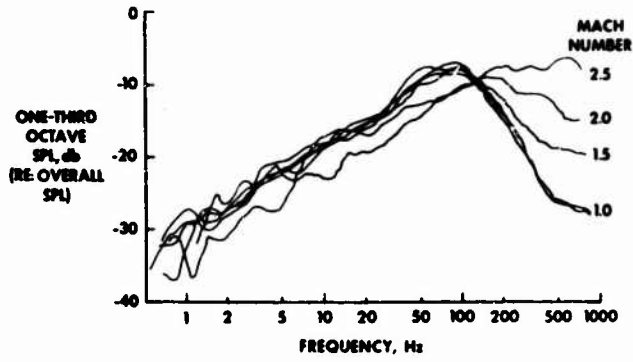
Fig. 4. Typical relative pressure spectra down-
stream of shoulder at various Mach numbers
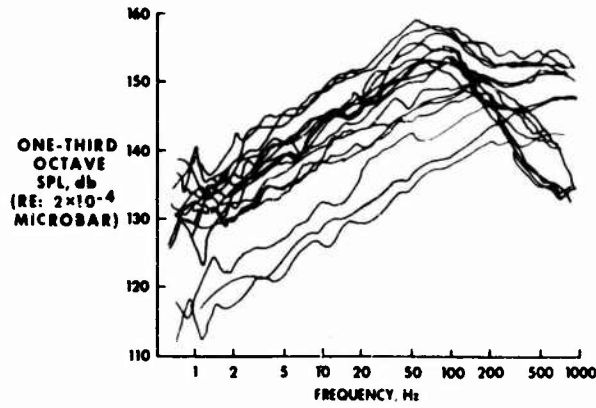
Fig. 5. Typical spectra of pressure fluctua-
tions in one-third octaves for several posi-
tions and several Mach numbers
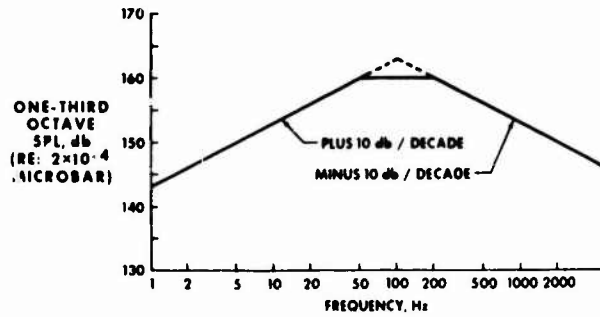
Fig. 6. Design curve for random noise spec-
trum at shoulder of Apollo vehicle with an
overall level objective of 171 db

30

The range of sound pressure spectra required to simulate the aerodynamically derived pressure spectra is shown in Fig. 7. The estimated spectrum from rocket noise at launch is also shown in Fig. 7. Note that the aerodynamically derived pressure fluctuations are more severe than the rocket noise. The judgment was that achievement of the facility design spectra with appropriate levels at the various body stations would guarantee a test envelope which would be realistically conservative.

A method was required for simulating the fluctuating pressure field around the Apollo spacecraft where the test article was a 65-ft-high stack made up of the CM, SM, and SLA on a support fixture. The test article would be 13 ft in diameter at the SM and 22 ft in diameter at the base. Since this is a large item to test, a simulation technique would have to include consideration for the practical and economical methods of exciting such a specimen.

laboratory excitation tool when used for vibration testing of large vehicles. Some of these problems are that modifications would be required to the vehicle structure for attachment of shaker armatures; that vibration response in the vicinity of the shaker attachments would be excessive, which is unrealistic; and that control difficulties for a large matrix of shakers with inputs of random excitation would be formidable. For these reasons, further considerations emphasized acoustical input methods.

During the course of the conceptual development of the SAL, three general methods of simulating the external pressure fluctuations by the use of acoustic wave impingement were proposed. These are illustrated in Fig. 8, and include (a) the reverberant field, (b) the progressive wave from either the bottom or the top of the test specimen, and (c) the multiple-source, close-coupled progressive wave.
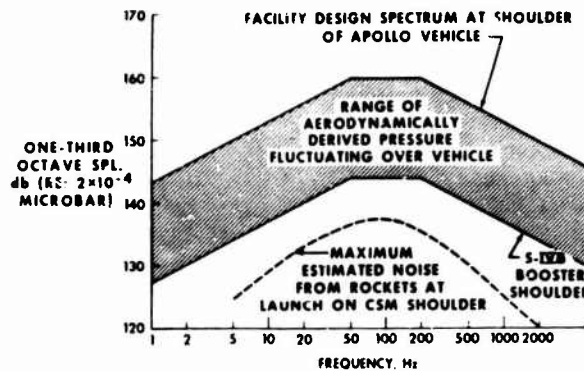
Fig. 7. Comparison of flight dynamic pressure fluctuations with facility design spectrum for Apollo vehicle

Simulation of the Pressure Fluctuations
Around the Apollo Spacecraft Vehicle

Note that the use of shakers, either singly with excitation introduced at the base of the vehicle, or in multiples, with excitation introduced at several points on the vehicle surface, was discarded as an approach for simulation of the pressure fluctuations around the Apollo spacecraft vehicle. With single-input excitation at the base of the vehicle, the desired vibration field could not be achieved because of response attenuation, especially at higher frequencies, along the structural transmission paths to points forward in the vehicle. A multiple-shaker approach would result in the more common problems encountered with this form of

A reverberation chamber approach offered considerable handling and placement flexibility for the Apollo and future spacecraft because few, if any, fixtures and ducts would be required. However, for the 270,000-cu-ft test tower required to enclose an Apollo vehicle configuration, the acoustic power requirements became rather large. For example, if the wall absorption coefficient were 0.03, the absorption would be 0.03 times 26,000 sq ft, which is 800 sabins. An input power of 2.5 million acoustic watts would be required to achieve an SPL of 170 db in the chamber if the propagation in air were linear; however, because of macrosonic attenuation, the acoustic power requirement more probably would be on the order of 5 to 7 million acoustic watts. This power requirement

31
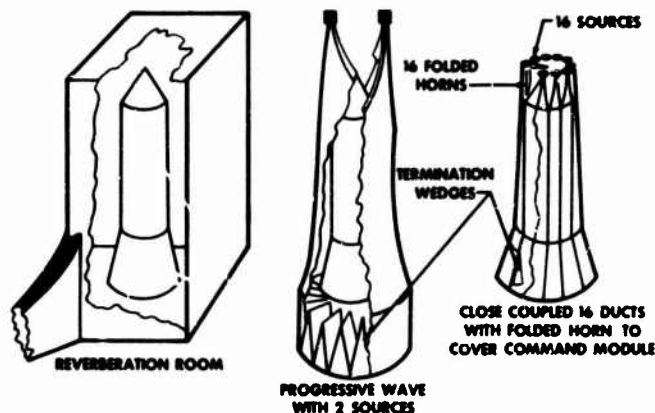
Fig. 8. Three facility concepts for SAL

would have far exceeded the most ambitious of previous facilities, and its cost would have been prohibitive.

More important, technically, the high-level sound field would surround the entire vehicle, including all sections which have much lower maximum flight levels. This would provide a quite unrealistic simulation, especially for the aerodynamic cases, and would cause much higher response of equipment and structures than occur in flight. Consequently, failures and malfunctions which might be experienced during the test would have a low probability of occurring in flight, thus potentially leading to an excessive number of structural fixes, overdesign, and overweight.

While high-level reverberant testing was impractical, it was desirable to be able to utilize the tower as a reverberation chamber at lower levels. This would allow for future reverberant tests of large equipment and comparison of the responses of vehicle structure to two different types of test environment, reverberant and progressive wave acoustic excitation. For this purpose, the internal tower dimensions selected were 90-ft height, 50-ft depth, and 61-ft width to optimize the frequency separation of the acoustic modes in the chamber. In the optimization process, a height of 90 ft was selected to accommodate the vehicle, and a width of 50 ft was selected for architectural compatibility and test-article handling space. The chamber modes were then calculated for a range of lengths between 54 and 65 ft in increments of approximately 1 ft. The 61-ft dimension provided the best results, with good frequency response obtained above approximately 3.3 times the fundamental chamber resonant frequency of 6.2 Hz (approximately 20 Hz). Hence, good

diffuse field characteristics were obtained for the entire frequency range of interest between 20 and 2500 Hz. Because of later additional architectural considerations, the basic tower dimensions were increased to 101-ft height, 56-ft depth, and 68-ft width, each dimension being adjusted by the same factor to maintain the optimum dimension ratios.

Two alternative methods of progressive wave testing using a duct-containment system were considered and are illustrated in Fig. 8. Both methods required approximately 160,000 acoustic watts of power to achieve 171 db in a 3-in.-wide annular area around the command and service module (CSM) shoulder. Both concepts allowed simulation of the SPL gradient aft of the CSM shoulder by a combination of attenuation and increase in area function. Both could be terminated in similar manner, either alongside the SLA or around a portion of a simulated S-IVB stage.

A major difference in concept was the provision of multiple-source units. In the multiple-source configuration which was adopted, 16 sources would be utilized to drive 16 longitudinal ducts in lieu of one or two sources driving a single duct. Each of the 16 sources could be driven from an independent random-noise generator which would enable limiting circumferential correlation to a duct width of 30 in., thereby improving the simulation flexibility.

A second major difference was the use of a folded horn rather than a direct horn for the CM. The principal difficulty with the direct horn was the requirement that the SPL at the nose be less than that at the shoulder. Consequently, the duct cross-sectional area would have to be greater at the nose than at the

32

shoulder with the anticipation that this area expansion followed by a contraction and then an expansion would lead to considerable acoustic-transmission difficulties. The folded horn avoided some of the difficulties since its horn area expansion nearly matched the areas required to achieve the desired SPL's. However, impedance discontinuities would occur at the throat of the folded horn. These discontinuities were minimized during the model portion of the concept study.

During the design phase, the mold lines for the horns and ducts were defined in detail. An opportunity to add, at little additional cost, the capability to drive the laboratory reverberantly with the 16 noise sources also became apparent in the design phase. This second mode of testing would be achieved by removing the ducts from the horns at the CSM shoulder and replacing them with 16 large horn flare sections. The flare sections would couple the noise sources to the room volume by using a portion of the test vehicle as the horn walls. The resulting acoustical conditions would retain progressive wave excitation over the surface of the CM and the upper surface of the SM. The lower surface of the SM and the surface of the SLA would be subjected to reverberant energy, thus affording versatility of the testing approach and an opportunity to compare the response of vehicles to both types of laboratory forcing functions.

The primary purpose of the SAL as in any ground-based experimental facility is to provide a tool which can be used to simulate one or more of the in-service environments of a spacecraft. With this tool, the experimenter may study the vibrations of either a full-scale or model vehicle to simulated environments, and then utilize the experimental results to predict the vibrations of the full-scale vehicle to actual environments. The utility of any experiment involving such simulation is proportional to the degree of confidence which can be placed in the accuracy of the vibration response predictions that can be made from the experiment. Under the proper choice of field parameters, different fluctuating pressure fields can produce essentially identical average vibration response in a structure. Thus, in general, it is not necessary that the simulated environment always be completely accurate in itself but rather that it provide an accurate vibration prediction tool. The variable parameters for optimizing simulation, which served as design requirements for the SAL, are compared with flight conditions in Table 1.

The comparisons indicate that the SAL could achieve a rather accurate simulation of

pressure field from rocket noise at launch and a less accurate simulation of the pressure field resulting from aerodynamic pressure fluctuations. The principal deficiencies of the latter simulation are (a) inability to simulate the longitudinal and lateral correlation functions except to the approximation of $(\sin ky)/ky$, where k is the acoustic wavelength constant and y is distance, for the reverberant configuration; or $\cos ky$, longitudinally, and one sixteenth of the circumference laterally in the progressive wave patterns; and (b) inability to vary the spectrum as a function of longitudinal position in either configuration.

These deficiencies result from the use of an acoustic field to simulate a nonacoustic phenomena. However, the significance of the deficiencies is still not established. Existing theory and experience indicated that their effects could be minimized through development of proper equivalent spectra for the ground simulation. Therefore, early experimental programs in the SAL, together with supporting theoretical studies [4,5], were directed toward developing the necessary equivalences and proving the results by comparing the vibration field in actual vehicles measured both in flight and in the SAL. These efforts are continuing, and results already achieved [6] toward simulation of flight response are quite promising. The following section is a detailed description of the facility, as built.

FACILITY DESCRIPTION

General

The SAL (Fig. 9) is housed in a tower which has external dimensions of 105-ft height, 60-ft depth, and 70-ft width. The tower consists of a structural steel framework with concrete panels for the exterior walls, and can accommodate a vehicle up to 30 ft in diameter and 85 ft in height. A door 40 ft high and 32 ft wide provides access for bringing individual spacecraft modules into the laboratory. The laboratory is serviced by a 75-ton fixed-point hoist which is used for stacking modular components of an integrated spacecraft, and which can be used to suspend a spacecraft during testing. A 5-ton circular bridge crane is used for general-purpose material handling and for handling test ducts. Permanent and movable platforms are located at elevations of 15, 30, 45, 60, and 75 ft. The movable platforms are 3-ft-wide catwalks which encircle the test vehicles. An elevator 6 ft wide, 7 ft deep, and 8 ft high is used for personnel and equipment access to the various levels and to the adjacent control room. Pneumatic and electrical utility

TABLE 1
Control of Fluctuating Pressure Parameters in the SAL
(Neglecting Protuberances and Yaw)

Independent Variable	Case	Function		
		Amplitude	Spectrum	Spatial Correlation
Axial location	Flight	Depends on vehicle geometry and Mach number	Depends on vehicle geometry and Mach number	Depends on vehicle geometry and Mach number
	SAL	Determined by cross-sectional area of horns and ducts and by air modulator output	Determined by finite length effects and absorption of power by vehicle and ducts and by air modulator output	Cannot be varied
Time	Flight	Variable	Variable	Variable
	SAL	Stepwise approximation or possibly continuous variation	Stepwise approximation or possibly continuous variation	Stepwise approximation or possibly continuous variation
Axial separation	Flight	—	—	Variable
	SAL	—	—	Either $\cos ky$[a] in progressive wave mode or $\sin ky/ky$[a] in reverberant mode
Circumferential separation	Flight	—	—	Variable
	SAL	—	—	Variable to within 1/16 of circumference in progressive wave mode; approximately $\sin ky/ky$[a] in reverberant mode

[a]k = acoustic wavelength constant; y = distance.
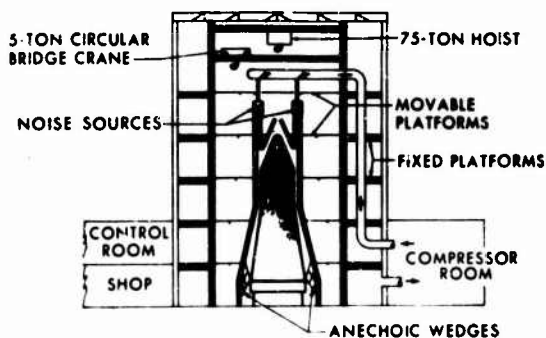
Fig. 9. Spacecraft Acoustic Laboratory

connections, communications stations, and instrumentation and cable chases are located throughout the laboratory.

Two modes of testing are presently available in the laboratory: progressive wave, the primary mode; and progressive wave/reverberant fill-in, the secondary mode. In progressive wave tests, the exposed surface of a test vehicle is enveloped by controlled high-intensity sound. Sixteen separate progressive wave sound fields are directed downward over the vehicle in separate encircling ducts, as shown in Fig. 9. The cross-sectional area of the ducts is adjustable so that specified SPL's can be achieved along the longitudinal axis of the test vehicle. Sound energy is supplied by 16 noise sources, or air modulators, which are electrically programmed and have an output of 10,000 acoustic watts each. The air modulators are suspended from the top platform in the tower and are attached to coupling horns which are connected to the ducts. The air modulators are independently controlled so that the

34

correlation of the acoustic fields between the ducts can be programmed. The 160,000 acoustic watts of power generated by the air modulators provides an overall SPL of 169 db at the horn/duct interface.

In progressive wave/reverberant fill-in testing, the ducts are removed from the horns and replaced with extension horn flare sections which couple the acoustic energy to the acoustic response modes of chamber volume. Thus, the lower portion of the vehicle is subjected to reverberant loading.

The air modulators require a large volume of compressed air (approximately 27,000 standard ft^3/min) which is supplied by a constant-flow centrifugal air compressor driven by a 4500-hp electric motor. The compressor is located in an adjacent building and draws its supply of air from within the tower, making the air system a closed loop, with the tower volume serving as a plenum. Air manifolds are connected by hoses to the air modulators.

Apollo Test Configuration

The SAL horn/duct system is presently configured specifically for the Apollo spacecraft (Fig. 10). In this configuration, the complete Apollo test article (consisting of a CM, an SM, an SLA, and an LM located inside the SLA) is positioned atop a Saturn instrument unit (IU) and a base fixture (which simulates the S-IVB forward skirt). The entire stack is in a vertical orientation. The dome of a forward tank of the S-IVB booster is also mounted, consistent with flight location, inside the S-IVB forward skirt to assure proper internal acoustical boundary conditions. (Standard longitudinal Apollo station numbers are used to identify measurement locations. These station numbers along the longitudinal axis are identified as X$_\bullet$---- (with up to four digits to fill the blanks). In SAL, measurement locations from X$_\bullet$ 552 (bottom of the SLA) to X$_\bullet$ 1260 (top of the upper terminator) are available.) The circular duct system is positioned around the entire Apollo vehicle stack (Fig. 11) to contain the high-energy acoustic progressive waves which are generated above the stack and passed aftward over the outer shells of the vehicles. Approximately 75 percent of the acoustic energy passes down over the SM. The remainder is directed via a splitter arrangement in the initial, or transition, horn section through a reverse, or folded, horn back up over the face of the CM. Anechoic termination wedges are located at the end of each duct run and each horn run to assure that a plane-wave condition is maintained.
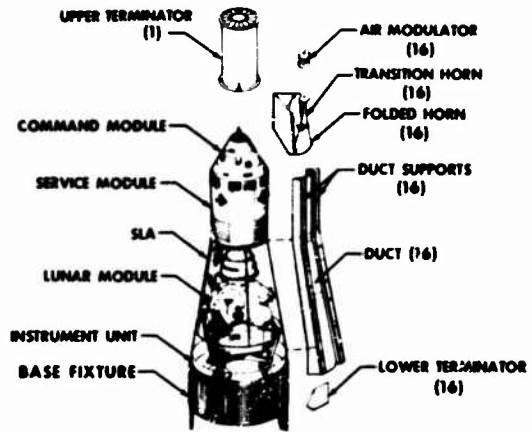
Fig. 10. Arrangement of test article and horn/duct system

This is necessary to preclude the occurrence of standing acoustic waves and to assure compliance with plane-wave propagation objectives. The latter allows the SPL to be increased or decreased along the length of the specimen by moving the outer wall of the duct in or out with respect to the vehicle outer shell (that is, the depth of the duct is variable). The spectral shape of the acoustic waves is controlled by appropriate programming of the electrical input signal to the driver coil of the air modulator which generates the acoustic waves. The acoustic levels are controlled by the programmed output of the air modulator and by the radial placement of the duct with respect to the outer face of the vehicle shell. The duct is divided into 16 acoustically separate channels so that many combinations of levels, shapes, and correlations can be programmed around the circumference of the test article.

The transition horns (Fig. 12), which couple the air-modulator acoustic output with the folded horn/duct system, are constructed of epoxy fiber glass and have access ports for mounting microphones so that the microphone diaphragms are flush with the internal wall of the horns. The transition horns are bolted to the steel folded horn sections which surround the CM. A steel upper terminator unit having 16 compartments, each lined abundantly with fiber-glass absorptive material and fitted with fiber-glass wedges, is bolted to the top of the 16 folded horn sections. The V-shaped duct supports (Fig. 13), which are bolted to the lower faces of the folded horn sections and extend downward over the SM, SLA, and IU, are constructed of plywood faced with sheet metal. The outer walls of the ducts (Fig. 14) are steel rolled to a curvature that is concentric with the

35
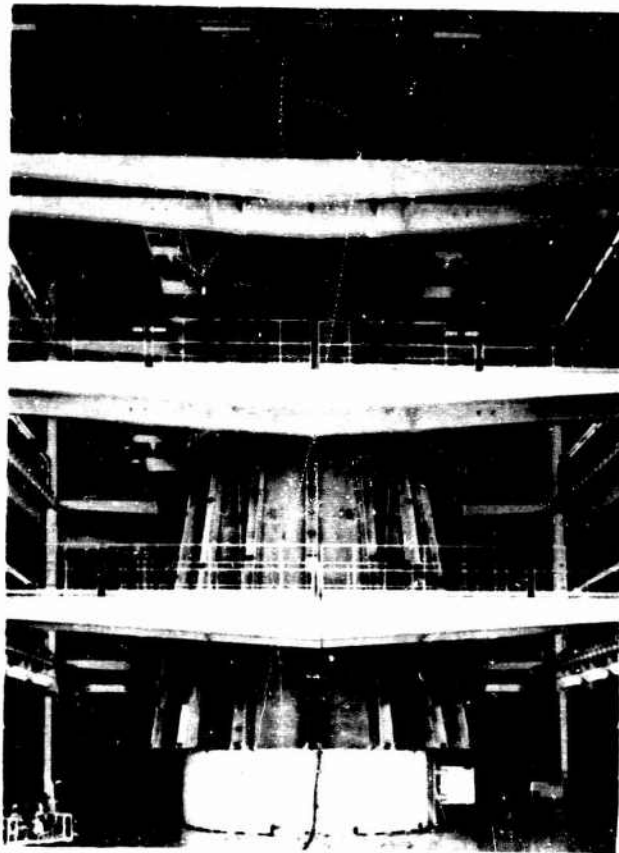
Fig. 11. Apollo vehicle in SAL after
installation of duct system
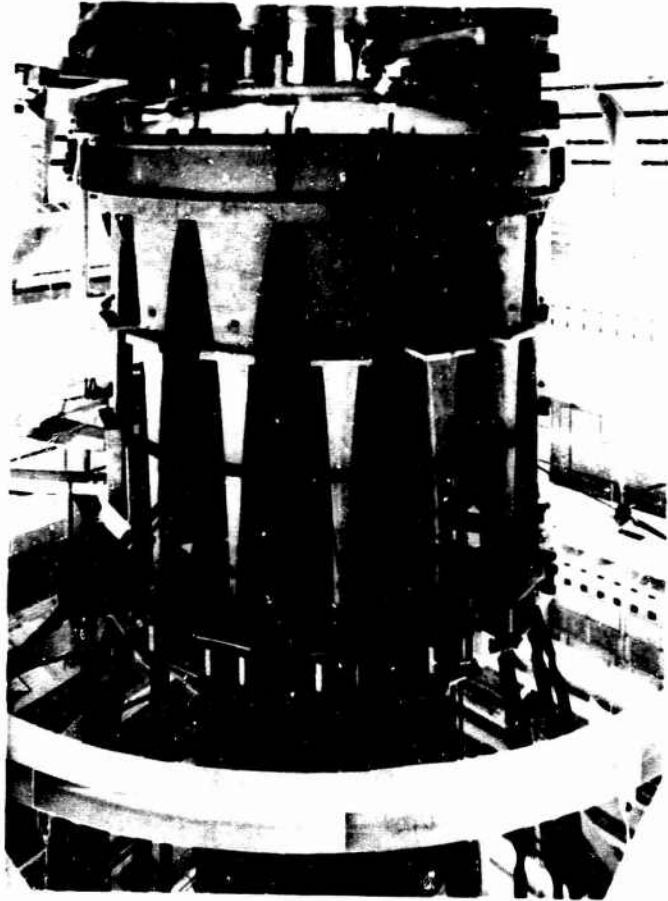
Fig. 12. SAL horn assembly with air
modulators installed

37
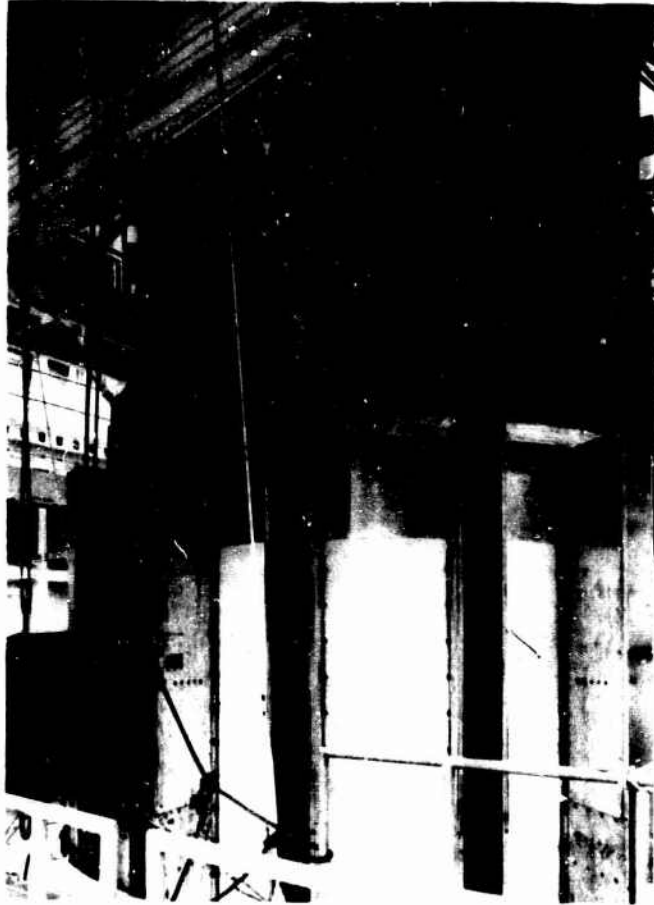
Fig. 13. Ducts removed showing contact of V-shaped
duct supports with outer shell of SM vehicle
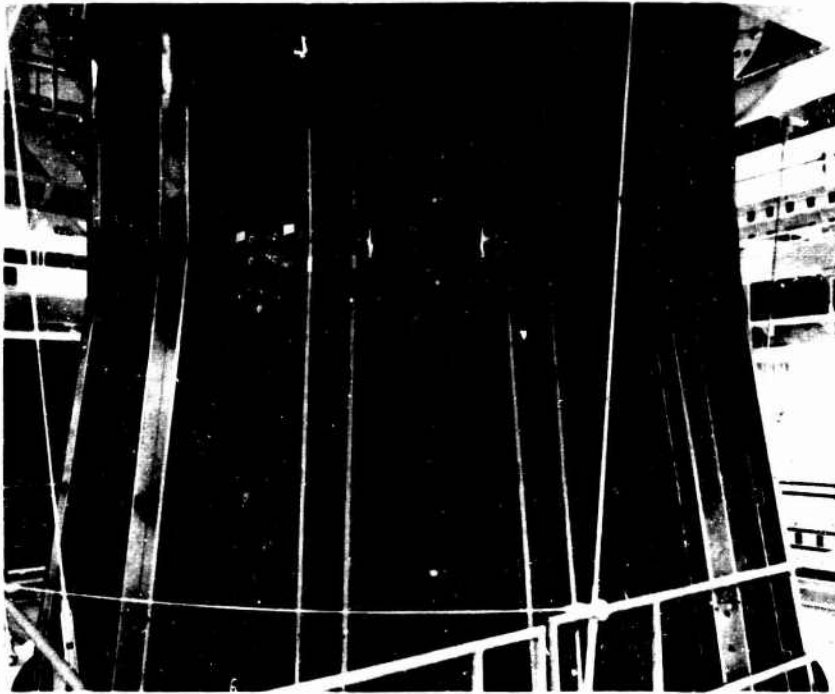
Fig. 14. Interface of SAL ducts covering SM
with ducts covering SLA

surface of the test article. Slotted tabs are provided on the outer walls of the ducts and multiple bolting locations are provided on the V-shaped duct supports to allow radial adjustment of the cross-sectional area of the ducts. The cross-sectional area of each duct is bounded by the outer wall, two walls of the V-shaped duct supports, and the surface of the test vehicle. In a similar fashion, the surface of the CM serves as a fourth horn boundary in the reverse horn sections. Fiber-glass wedges, which serve as lower terminators, are positioned at the bottom of each duct in the area of the IU and base fixture. When the reverberant flare system (Fig. 15) is used in lieu of the duct system, the acoustic progressive waves are coupled directly to the room and no anechoic terminators are used. All steel walls of the horn/duct assemblies are coated with several thick layers of viscoelastic damping compound. The weight of the horn/duct assemblies is supported by the building platforms through hangar rods and bolting arrangements so that no load is exerted on the test vehicle by the test hardware. Soft, highly compliant sealing hoses provide the only contact between the horn/duct systems and the test vehicle. The sealing hoses run longitudinally along the vehicle and separate the horn/duct walls from the vehicle surface. Acoustical

isolation between adjacent horns and adjacent ducts is provided by the sealing hoses without interference with the vibration response of the surface of the test vehicle. During assembly of the horns and ducts around the vehicle, illumination checks are made with electrical lights for duct leaks which, when found, are eliminated by the application of rubber sealing compound. A hyperbolic-exponential design with an aspect ratio of 0.6 was used for the expansions of all horns, and a design cutoff frequency of 25 Hz was used throughout with the exception of the reverberant flare sections where 50 Hz had to be used because of space limitations (Fig. 16).

The air modulators (Fig. 17) are connected to the top of the initial horns with a quick-disconnect arrangement. Ancillary equipment items, including a cooling system and a dc field supply, are located on adjacent platforms. The air modulators are linear-vane devices with electromagnetically driven cylindrical valves and were developed specifically for this facility. The units are water cooled with a vacuum-assisted return system. The modulator valves are suspended on continuous rubber diaphragms and are driven inductively by variable electrical programming signals interacting with magnetic fields [7].

39

Fig. 15. SAL reverberant flare system
installed around Apollo vehicle

Fig. 16. SAL reverberant flare system
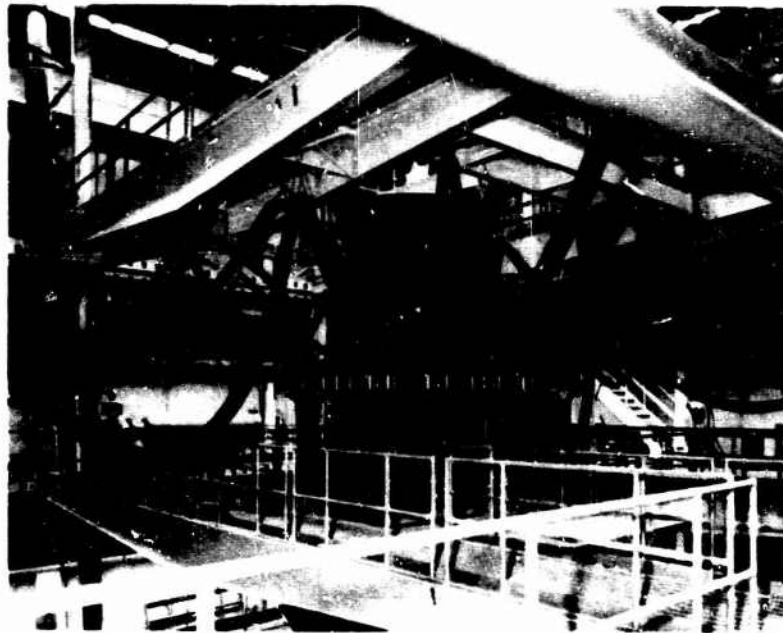
Fig. 17. Access to the horn assembly and air modulators
of the SAL via movable platforms

Control and Instrumentation

The control system equipment, located in a room adjacent to the acoustic tower, consists of 16 control and power channels, one for each of the 16 air modulators (Fig. 18). Each channel includes a separate electrical white-noise generator and one-third octave band shaper for random programming and a separate 3000-w power amplifier so that acoustic energy can be produced by the separate air modulators which is uncorrelated between ducts. The amplified programming signals are connected via cables to the air modulators in the tower. Through patching changes, one white-noise generator and shaper can be used to drive all amplifier and air modulator channels to obtain an all-correlated acoustic condition between the ducts. Intermediate correlation combinations are also possible. Oscillators are available and the air modulators can be driven sinusoidally or sinusoid programming can be mixed with random programming. While versatility of control is provided, a single master-gain control is used to increase and decrease the output levels of all air modulators simultaneously during a test run. The rapid attainment of either test levels or shutdown was designed into the system to minimize undesired excitation and structural fatigue of the test vehicle. Other operational features include equipment malfunction alarms and automatic shutdown, emergency termination switches for the amplifier system and the air compressor, an arrangement allowing for selection of any control channel for monitoring by the test conductor, an environmental condition (temperature, humidity, and pressure) recording system, a flexible control and data instrumentation patching capability, plug-in modular components for quick replacement of malfunctioning units, intercom and television systems, and an analog data acquisition system consisting of signal-conditioning amplifiers and magnetic tape recorders. Presently, the data acquisition system can accommodate 35 channels of horn/duct microphone measurements, 160 channels of test vehicle microphone and accelerometer measurements, and 50 channels
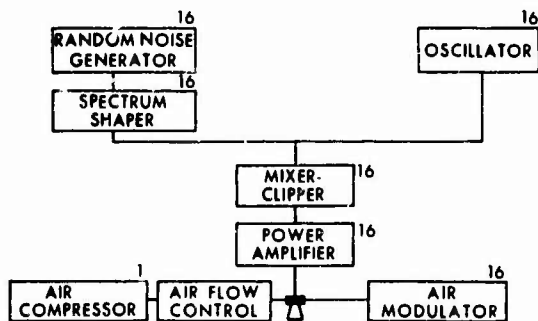
Fig. 18. SAL control system

of strain-gage measurements simultaneously. Multiple test runs with repatching can be used to obtain a larger number of response measurements on the test vehicle.

Each air modulator is calibrated using a plane-wave tube (especially constructed for the purpose) before being installed in the SAL for a testing operation. All tests of airframe vehicles are preceded by a calibration test series using a boilerplate vehicle. During these calibration tests, the amplitudes and spectral shapes are adjusted sequentially in each duct at planned test levels. This procedure assures appropriate compensation for individual air modulator/duct anomalies that may be present, and assures correct settings at high levels where acoustical nonlinearities occur. The controls for each channel are then documented and the test stack is torn down. The boilerplate dummy vehicle is replaced with the actual spacecraft test article and the horn/duct systems reinstalled. A low-level test run for checking the test environment and for ranging of data acquisition equipment precedes high-level runs. For the high-level runs, the test conductor uses a single master-gain control to apply acoustic excitation to the vehicle. Tape-recorded test data can be reduced with either analog or digital equipment at data reduction facilities located elsewhere at MSC.

FACILITY PERFORMANCE

The major features of the facility performance for both progressive wave duct and reverberant modes of operation are reviewed in this section. In addition, some of the detailed performance characteristics of the coupling horns and ducts are examined, and the problem associated with coupling the progressive wave duct to the vehicle are discussed. Vibration responses obtained with accelerometers at three locations on the SLA for both progressive wave duct and reverberant excitation are compared. Vibration responses obtained with accelerometers at eight locations on the SM for both progressive wave duct and flight excitation are presented.

Progressive Wave Performance

As described in previous sections, the progressive wave mode of operation allows variation of the overall SPL axially along the test article for all stations below the CSM shoulder. Furthermore, this mode allows freedom in selecting the spectrum and level for each duct and the correlation parameters among

various ducts. Therefore, for any individual duct, the spectrum throughout the duct has a definite relation to the spectrum at all other points along the duct. The relationship may be varied only by changing the axial variation of the duct cross-sectional area, the characteristics of the acoustical termination, or the axial impedance characteristics of the vehicle.

Air modulators were designed to meet the requirements of this facility, providing a maximum of 10,000-w acoustical power output over a frequency range of 30 to 1000 Hz. The high-frequency performance of the facility is thus limited by the capability of the noise source above 1000 Hz, whereas the low-frequency performance is controlled by the horn cutoff characteristics and the terminating impedances. Within these frequency response constraints, a large variety of spectra can be generated as indicated by the range of spectra measured in several experiments at the CSM shoulder, station X_a 1008 (Fig. 19). Figure 20 shows that the overall level can be varied over at least 30 db from 140 to 169.5 db at the CSM shoulder station. Note that these particular spectra were chosen for specific experimental objectives and do not represent all possible spectra. For example, spectra which peak at either the low-frequency, middle-frequency, or high-frequency ends of the overall envelope indicated in the figure may be produced.

Figure 21 gives the spectra resulting at the Apollo shoulder for one setting of the electronic spectrum shaper and for various voltage amplitudes across the air modulator. Note that all spectra are essentially similar below 500 Hz.
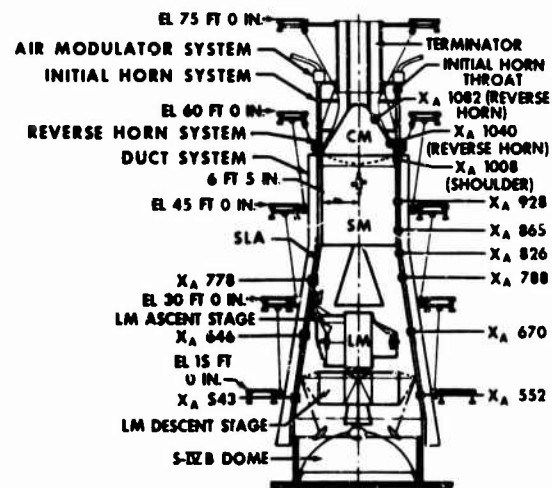
Fig. 19. Measurement locations for Apollo tests in the SAL

43
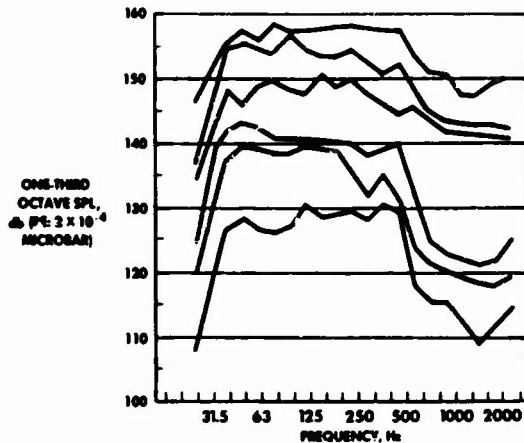
Fig. 20. Typical spectra in
SAL at Apollo shoulder

Fig. 21. Spectra obtained at Apollo
shoulder in SAL by varying overall
power input to noise makers

However, in the frequency range above 500 Hz, there is considerably less roll-off for the high-level spectra than for the lowest level spectra. This nonlinear property, termed macrosonic attenuation, results from the distortion of high-level acoustic energy in its propagation in the initial horn. The distortion produces a triangular waveform which, when fully developed, will give a roll-off of approximately 3 db/octave. For the data in Fig. 21, the highest level spectra is approaching the theoretical 3-db/octave roll-off.

For some applications, the presence of distortion at high frequency is undesirable. For the majority of applications, however, the distortion is most useful, since it provides the only currently available method of extending the spectrum beyond the controllable limits of the acoustic noise source.

The variation of SPL along the axis of the vehicle is accomplished by varying the cross-sectional area of the ducts. The variation permits a change of area along the SM from the 90-sq-in. fixed cross section at the shoulder to as much as 450 sq in. at the base of the SM. The area along the SLA can vary from a minimum of 90 sq in. at the top of the SLA to a maximum of approximately 750 sq in. at the base. Part of the variation along the SLA comes from the increase in diameter of 13 ft at the top to 22 ft at the base, and the remainder comes from the ability to vary the radial dimension (or depth) of the duct from 4.5 to 15 in.

Figures 22a and 22b illustrate the axial range of variation of SPL which has been found

for the Apollo configuration. The ideal variation of SPL for both minimum and maximum duct spacings compares quite closely with that measured in the high-frequency region. At low frequencies, however, the decrease of SPL along the vehicle is greater than that resulting from the area variation alone. The effect of frequency is best illustrated in Fig. 23, which gives the measured one-third octave band spectra in decibels relative to the shoulder spectra for four locations down the side of the test article. The high-frequency levels in Fig. 22 represent the average of the three one-third octave bands centered on 800 Hz (from Fig. 23); the low-frequency levels were derived from the six one-third octave bands centered on 112 Hz.

Thus, Fig. 23 shows that the transition between the low- and high-frequency region occurs just above 250 Hz. As will be seen later, the maximum absorption of acoustic power by the vehicle structure occurs just below 250 Hz, with a considerable decrease in acoustic absorption at higher frequencies. Therefore, the additional decrease in SPL along the axis of the vehicle for the low-frequency region is attributed to the absorption of acoustic power by the vehicle.

The mechanism for this absorption can be seen from a simplified acoustic model of the duct/vehicle system as a duct with a continuous resistive absorber forming one side. Analysis of the model indicates that the attenuation in decibels along the duct from absorption of acoustic power should vary directly with axial distance and inversely with radial duct dimension

44
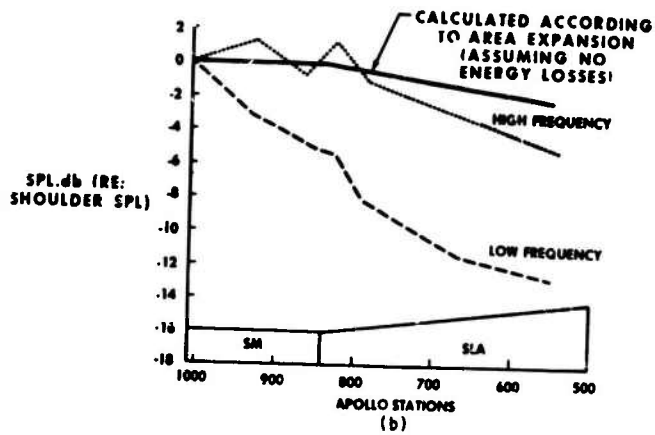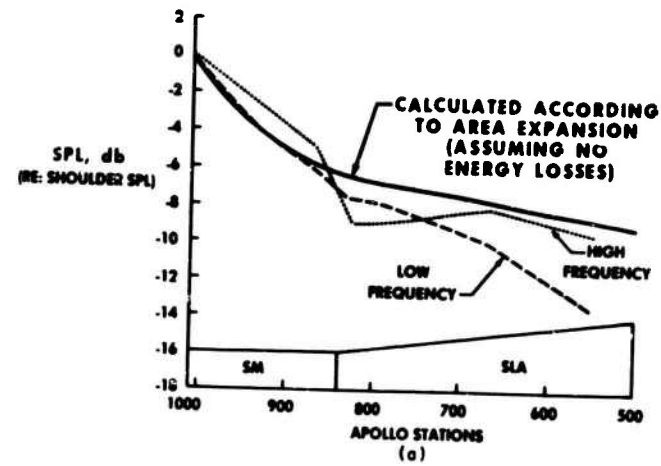
Fig. 22. Axial variation in SPL for
maximum duct spacing
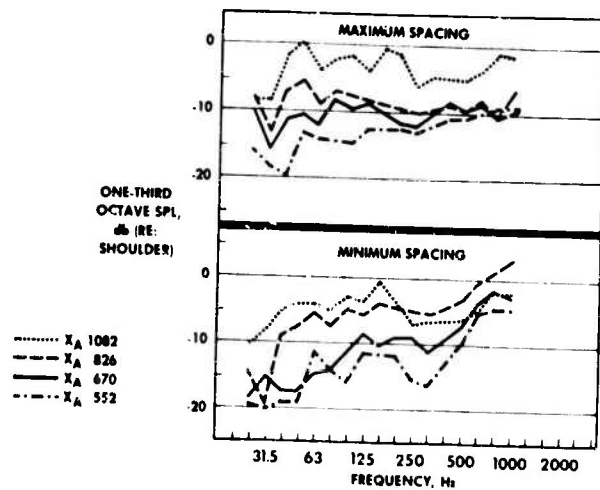
Fig. 23. Spectra in ducts for
two-duct spacing from Apollo

(or depth) for the Apollo structure. Therefore, if a lesser low-frequency SPL gradient along the vehicle were desired, it would be necessary to increase the depth of the duct at the shoulder to obtain lower attenuation. Of course, the increase of area at the shoulder will have a side effect of reducing the maximum SPL in the duct at the shoulder. The simplified analysis also suggests that if the progressive wave duct mode of testing were utilized for vehicles of lower surface weight than that of Apollo (approximately 2 lb/ft^2), careful consideration would have to be given to the duct depth vs SPL gradient requirements.

The utilization of 16 ducts and their associated air modulators enables a controlled variation of the circumferential spatial correlation of the sound field along the vehicle. As discussed in previous sections, this acoustic system, together with its electronic controls, can operate in any mode from "all ducts correlated" to "all ducts uncorrelated." The practical achievement of the "all ducts correlated" condition is yet to be demonstrated in the facility. Early experiments revealed that it was difficult to maintain unity correlation from duct to duct over a wide frequency range, primarily because of variations among the acoustic noise sources. These variations among noise sources also made it difficult to obtain identical spectra and amplitudes among the ducts. The variation in SPL or in the one-third octave band SPL's for all 16 ducts operating in the uncorrelated mode is shown in Fig. 24. As shown from the data envelopes, when the overall SPL's are controlled to within ±1.5 db, the SPL's in one-third octave bands remain within ±2 to 3 db over a substantial portion of the frequency range. However, deviations up to 4 db are noted in the high-frequency end of the spectra. The increase in deviation in high frequency for the spectra is associated with the fact that the

levels in this frequency range are generated both by controlled modulation and nonlinear distortion of noise from lower frequency modulation. In any event, the overall variation illustrated in Fig. 24 is considered quite acceptable for practical test purposes.

A great number of interesting experimental results have been derived from the facility. Many of these experiments are directed toward obtaining better understanding of detailed factors which affect the overall performance of the facility. Although space does not permit discussion of all investigations here, two of the detailed factors have general application to progressive wave duct excitation of aerospace vehicles and are discussed briefly in the following paragraphs.

Horn Performance

In the design of a high-intensity acoustic facility, horns are employed to give a smooth transition from the very small area of the air modulator throat to a large area at the entrance to a test section. Ideally, the horns should be perfectly terminated in impedances which match the characteristic impedance of air (or ρc) and act as perfect couplers for the energy over the entire frequency range. However, in any finite-length horn/duct system, the termination is always less than perfect and will cause reflected waves. The reflections result in the buildup of standing waves, which may be found experimentally by probing the sound field along the axis of the horn. A typical result of such a probe is given in Fig. 25 for the initial horn and for three discrete frequencies.

At 400 Hz, a variation of SPL along the axis departs from the ideal horn area expansion by less than 1 db. However, at 100 Hz and
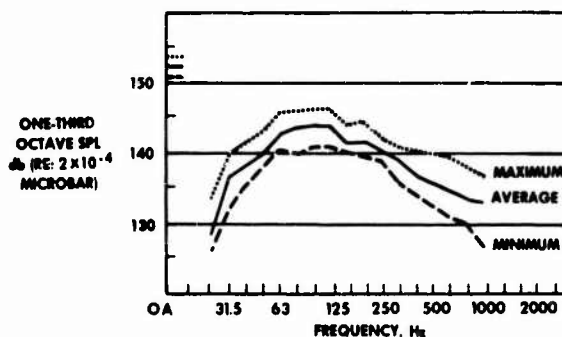
Fig. 24. Typical envelope of SPL variation in SAL for 16-duct operation

46
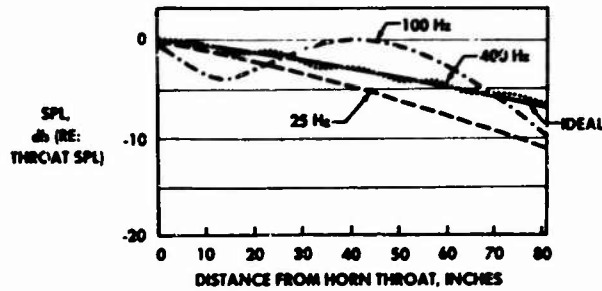
Fig. 25. Axial variation in SPL of initial horn
for single-frequency excitation

lower frequencies, a greater difference is found between the ideal and the real horn. The difference can be quantified in terms of the standing-wave ratio, which is the peak-to-peak difference in decibels of the departure of the pressure amplitude from the mean. This behavior can also be related to the effective absorption coefficient of the termination to the horn (and is a measure of the quality of the termination).

Both the standing-wave ratio and the effective absorption coefficient for the initial horn, reverse horn, and reverberant flare horn are given in Figs. 26a, 26b, and 26c, respectively. The effective absorption for the initial horn approaches 100 percent for frequencies above 150 Hz. However, below 100 Hz, the absorption varies between 70 and 90 percent, depending on frequency and type of termination. Although the
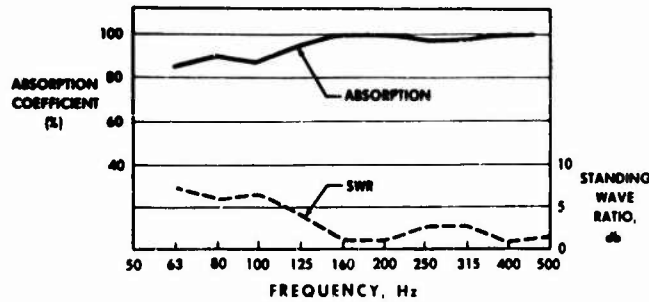
Fig. 26a. Typical initial horn characteristics
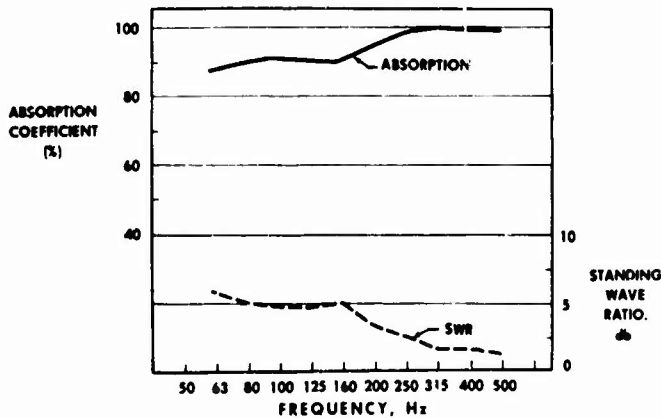
Fig. 26b. Typical reverse horn characteristics

47
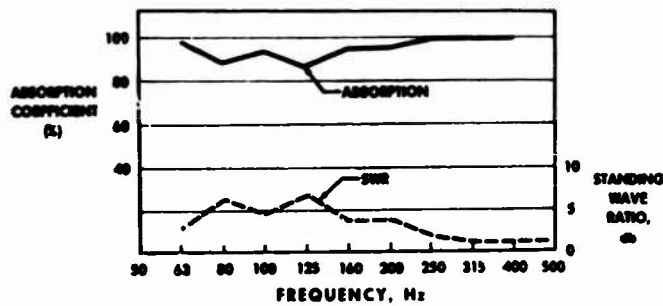
Fig. 26c. Typical reverberant flare characteristics

absorption for most acoustical purposes is generally of primary interest, the standing-wave ratio is perhaps more meaningful from the point of view of assessing facility performance, since it gives twice the maximum deviation from the mean SPL in terms of decibels. Also, as seen in Fig. 26, the standing-wave ratio is a more sensitive indicator than the absorption coefficient in detecting minor departures from the ideal.

Duct Seals

The sealing of the individual ducts to the vehicle to prevent leakage of sound into adjacent ducts is necessary to maintain independent noise fields and for the adequate acoustic termination of each noise source. A leak along the duct acts as a distributed inductive shunt and causes a significant degradation of the low-frequency performance of the entire system, in addition to providing added attenuation along the duct. The potential seriousness of the situation is illustrated in Fig. 27 which gives results from a one-third scale model of a typical duct section studied during the design of the facility. Spectra are given for three stations located in the parallel section of the duct, varying between 2 and 80 in. from the interface between the horn and duct. The data for the

O 2 IN. BELOW HORN / DUCT INTERFACE
△ 40 IN. BELOW HORN / DUCT INTERFACE
□ 80 IN. BELOW HORN / DUCT INTERFACE
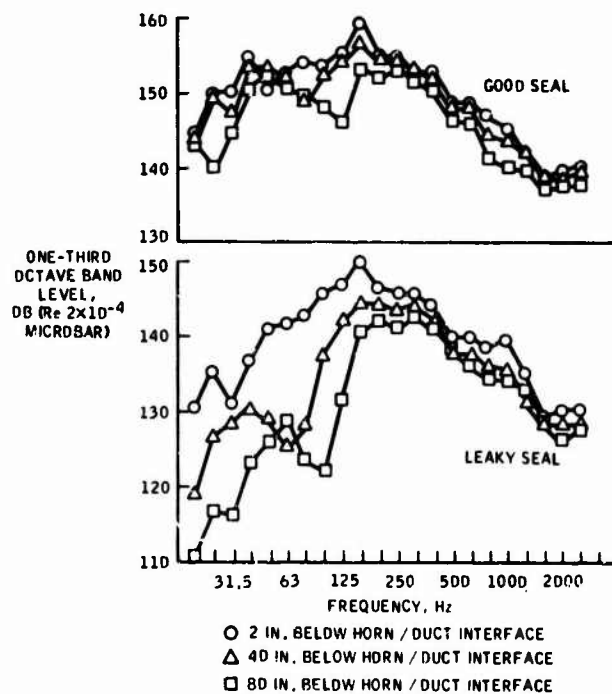
Fig. 27. Effect of seal on acoustic performance of a duct (taken from a one-third scale model)

48

2-in. location in Fig. 27 demonstrate that the overall frequency response of the horn/duct configuration rolled off below 100 Hz. However, with a tightly sealed configuration, the low-frequency performance is significantly improved with the low-frequency cutoff occurring at approximately 30 Hz. Furthermore, the results for locations farther down the duct show that considerable attenuation is occasioned by the leak.

These two effects of improper sealing make it essential to seal the vehicle to the duct acoustically. However, the sealing requirement conflicts somewhat with the requirement that the presence of the duct shall not inhibit the vibration response of the vehicle. This potential problem area was recognized early in the design concept study and resulted in experimental studies of various types of sealing devices to meet both criteria. The final result for the ducts along the Apollo vehicle is a 1-in.-diam rubber hose of low durometer, supplemented

The seal design, which gives a reasonable noise reduction, simultaneously enables achievement of designed low-frequency response performance characteristics.

To test the possible interference of the sealed ducts with the vibration response of the vehicle, experiments were conducted in which the vehicle was mechanically excited, both with and without the acoustic duct system. A typical vibration response, measured in one-third octave bands, for a boilerplate CM is given in Fig. 29 for both cases. For convenience, the vibration response is expressed in decibels relative to 10^{-6} g. Little variation was experienced throughout the spectrum. Figure 30 gives a summary of the differences in response measured in the SLA at six accelerometer locations for mechanical excitation, both with and without the duct system coupled to the vehicle. Again, the variation appears to be within the statistical accuracy of the data. These and other experiments demonstrated that the seals
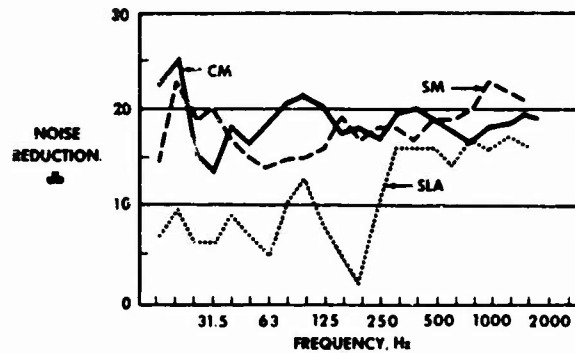
Fig. 28. Typical noise reduction between adjacent ducts

with plastic sealants over local contour variations about the vehicle mold lines.

The noise reduction between adjacent ducts (Fig. 28) is approximately 15 to 20 db over both the CM and the SM. However, the noise reduction between these same ducts, when measured at the base of the SLA, is only 5 to 10 db for frequencies below approximately 300 Hz and increases to approximately 20 db above that frequency. This lower noise reduction at the base of the SLA is suspected to result from the reradiation of energy by the vehicle into adjacent ducts. This would also explain the increase of the noise reduction to the 20-db level at frequencies above the principal response frequencies of the vehicle, as discussed previously and exhibited in the axial attenuation of Fig. 22.
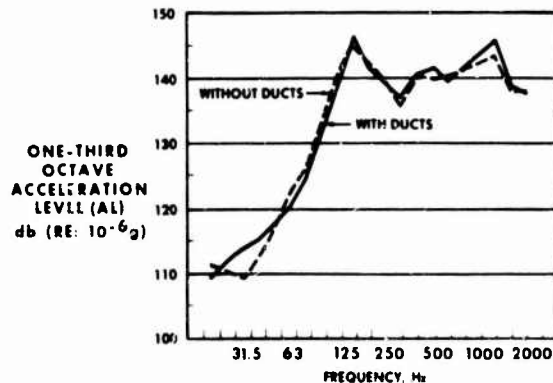
Fig. 29. Typical response of boilerplate 1:50 CM with and without ducts installed

49
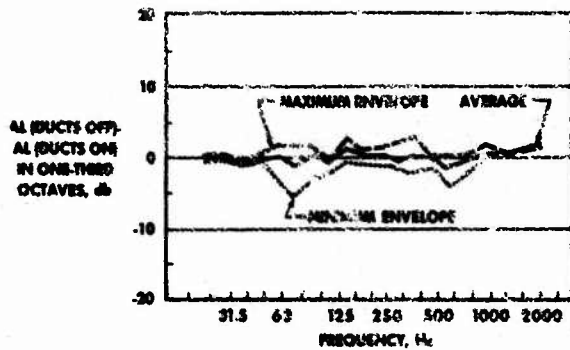
Fig. 30. Difference in airframe SLA
response with and without ducts in-
stalled for six measurement locations

currently in use are more than adequate for the Apollo vehicle. However, if vehicles of signifi- cantly lower surface weight were to be tested in a similar configuration, it would be necessary to demonstrate again the adequacy of the seals.

Reverberant Performance

The second basic mode of operation pro- vided in the SAL is the semireverberant mode discussed in a previous section. Although the principal experimentation to date has been with the progressive wave mode, the measurements with the reverberant mode indicate that it will also furnish a practical tool for certain Apollo test applications.

The acoustical absorption provided inside the SAL is given in Fig. 31. The absorption below approximately 1200 to 1600 Hz averages a little over 4000 sq ft, resulting in an absorp- tion coefficient of approximately 0.12, based on a wall surface area. The absorption coefficient is approximately eight times higher than would be expected in a standard hard-walled reverbera- tion chamber. However, it is not the result of the classical acoustic absorption expected from soft resistive absorptive materials, rather it is the result of steel gratings provided at every platform level, of the vehicle, and of the various steel piping and other systems provided in the tower for general facility operation. The in- crease in absorption illustrated in frequencies above 1600 Hz is the result of natural air
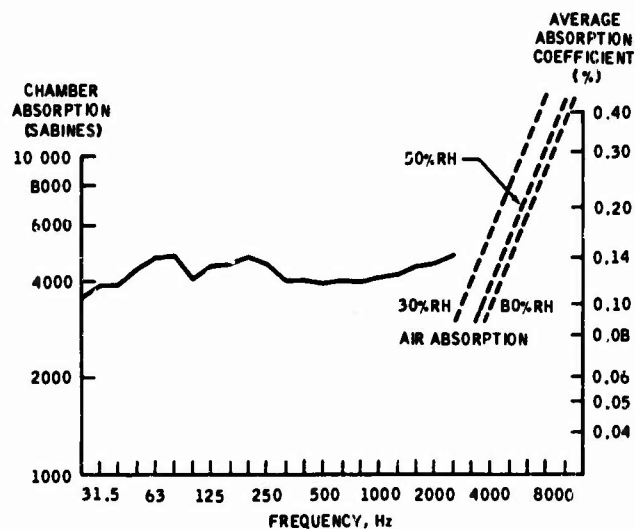
Fig. 31. SAL chamber absorption

50

absorption in the room and is expected to become asymptotically proportional to the square of frequency.

Figure 32 gives the range of SPL's measured along the SLA immediately adjacent to the skin and in the general chamber volume. The levels are the result of a reasonably flat input spectrum at almost full acoustic power. Note that the levels adjacent to the SLA are within 1 or 2 db of those predicted for the launch case. Therefore, this configuration has utility for some test purposes utilizing the SLA.

Fig. 33. Sound pressure spectra for SAL reverberant flare operation
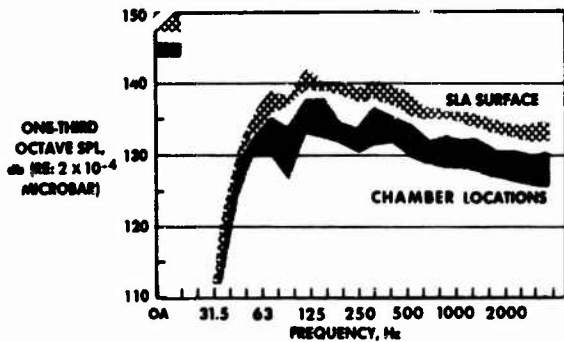
Fig. 32. Range of sound pressure spectra for SAL reverberant flare operation

The difference between the SPL's in the general chamber volume and those adjacent to the actual structure, as illustrated in Fig. 32, is important. Although the usual practice for equipment testing is to specify and measure the average level in the general volume of a reverberant chamber, the levels which are most important for full vehicle testing are those adjacent to the skin. Thus, in designing a vehicle test, differences between the chamber reverberant level and the pressure on the skin of the order of those shown in Fig. 32 must be considered in specifying and measuring the test spectrum.

The relative spectra between the Apollo shoulder station and the four longitudinal stations along the test article are given in Fig. 33. These data, which are measured at the same stations utilized in Fig. 23, show the type of variation of axial sound pressures which might be expected from a combination of a close-coupled horn/vehicle configuration in a reverberant chamber. Naturally, the absolute magnitude of the difference between the close-coupled region and the throat of the horn in the reverberant chamber is dependent on both the coupling area and the absorption of the chamber.
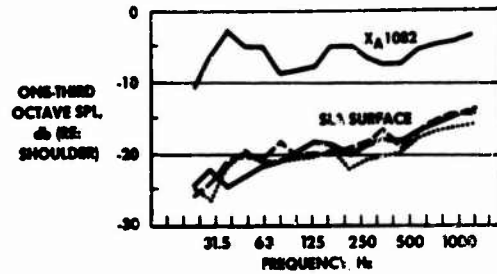
Vibration Response

The ultimate intent of the acoustic facility is to produce a vibration field within the vehicle which is similar to that actually encountered in its mission performance. The transfer function, which relates the average vibration within the vehicle to the surface acoustic pressures, is known to be a function of the type of external pressure of the fluctuating field. Figure 34 gives the transfer function for three accelerometers located on the SLA for both the progressive wave duct and reverberant field excitations. The data show that the shapes of the transfer functions are almost identical and the absolute magnitudes are similar, although the reverberant sound field appears to produce a response averaging approximately 3 db higher than that produced by progressive wave-duct excitation.

Note that the frequency response characteristics and the magnitude of the responses which govern the transfer functions are a function of the SLA structure, size, stiffness, mass, and damping, as well as the characteristics of the room and the method of excitation, and therefore cannot be applied to other vehicles without suitable correction.

Figure 35 gives the space-average fluctuating pressure spectra measured on the surface of the SM during Apollo flights. In an attempt to match the SM vibration response in SAL, an acoustic spectrum (Fig. 35) was applied to a prototype airframe (honeycomb structural shell) SM with the progressive wave-duct configuration. Figure 36 presents the resulting two vibration response spectra for flight and laboratory cases. Each curve represents an average of eight accelerometers located on the SM outer shell with the locations in the laboratory test closely duplicating those in flight. Further indications of good response simulations attainable in SAL are presented in Ref. [6],

51
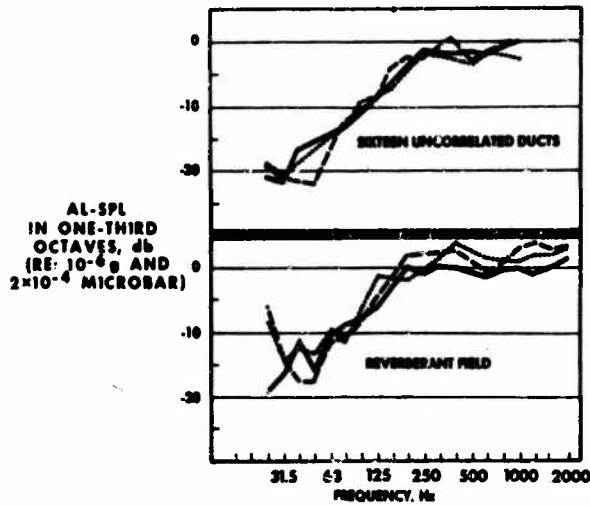
Fig. 34. SLA response characteristics at
three locations for two acoustic fields
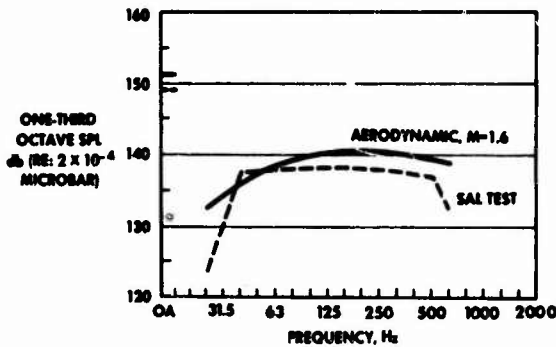
Fig. 35. Space average pressure
spectra on Apollo SM
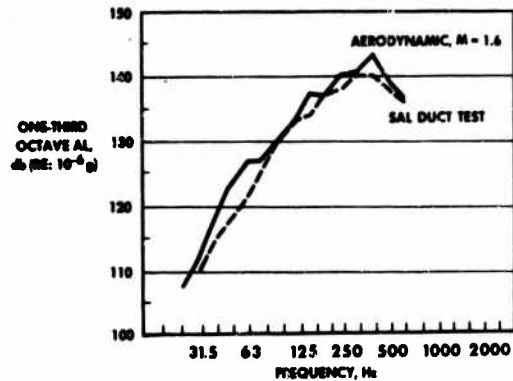
Fig. 36. Average vibration response of
Apollo SM for flight and SAL pressure
fields

which discusses a specific test program in the
facility.

CONCLUDING REMARKS

Simulation of vehicle vibration response to
the acoustic waves propagating forward from
the first-stage booster engine at liftoff is rea-
sonably straightforward through application of
progressive acoustic waves in the laboratory.
However, simulation of vehicle vibration re-
sponse to aerodynamically induced fluctuating
pressures through the transonic and max Q
flight regimes by using acoustic progressive
waves in the laboratory requires adjustments
to the correlation, amplitude, and spectral
shapes of the laboratory composite wave en-
ergy. In other words, the laboratory acoustic

environment applied to the vehicle is not nec-
essarily a duplication, acoustically, of the flight
fluctuating pressure environment when attempt-
ing to achieve duplicate vehicle vibration re-
sponse in the laboratory. Until adjustment cri-
teria can be developed for the wide range of
fluctuating pressure environments and the
vehicle structural characteristics which are
possible, testing will probably follow a two-step
procedure. The first step will be to program
the laboratory environment to match the meas-
ured or predicted service environment in ac-
cordance with the amplitude and spectral shape.
Comparison of vehicle vibration responses
obtained from the first step with service vibra-
tion responses will then lead to the second step
of adjusting the laboratory environment conditions

52

including phase correlation coefficients, if possible, to achieve a duplication in the laboratory of the service vibration responses.

Checkout and development tests have proved the practicality and workability of the fluctuating pressure simulation approach embodied in the SAL for full-scale ground testing of large vehicles. Examination of acoustic performance data has shown that the design requirements for the SAL have been met or exceeded. Vehicle vibration responses have been obtained in the SAL for the Apollo which closely duplicate responses measured in flight.

The SAL has been and currently is supporting the Apollo program with evaluations of structurally complete prototype spacecraft. Further use of this unique facility in support of the Apollo applications program is scheduled, and application of this simulation technique to future programs, such as the Manned Orbital Laboratory and the Mars mission, having vehicles with new shapes and sizes, is possible with merely a modification of a portion of the acoustic test hardware.

REFERENCES

1. K. McK. Eldred, "Concept Study for Simulation of Fluctuating Pressure Loads on the Apollo Vehicle in the Acoustic Laboratory," Wyle Lab. Rept. WR 63-11, Sept. 1963

2. F. M. Murray, "Acoustical Consulting Relative to the Acoustical Laboratory, Building 49, NASA Manned Spacecraft Center at Clear Lake," Wyle Lab. Rept. WR 64-6, Oct. 1984

3. G. W. Jones, Jr., and J. T. Foughner, Jr., "Investigation of Buffet Pressures on Models of Large Manned Launch Vehicle Configurations," NASA TN-D-1633, May 1963

4. K. McK. Eldred, "Basic Considerations in the Development of Vibro-Acoustic Test Methodology for the MSC Spacecraft Acoustic Laboratory," Wyle Lab. Tech. Rept. WR 66-33, June 1966

5. R. W. White, "Predicted Vibration Responses of Apollo Structure and Effects of Pressure Correlation Lengths on Response," Wyle Lab. Rept. WR 67-4, Mar. 1967

6. W. D. Dorland, R. J. Wren, and K. McK. Eldred, "Development of Acoustic Test Conditions for Apollo Lunar Module Flight Qualification," Shock and Vibration Bull., 37 (Part 5) Jan. 1968

7. Anon., "Model EPT-200 Electro-Pneumatic Transducer, Instruction Manual," Ling Electronics Rept. EPT-200-85-1, 1965

DISCUSSION

Mr. Sommers (The Boeing Co.): Did you take radiation damping into account when testing with and without the shrouds?

Mr. Wren: Yes; we ran that test in three ways. I mentioned two. We did it with no shrouds, ducts, or duct supports — completely naked if you like. We ran it with only the V supports and the sealing hoses in place. Finally, we ran it with the duct systems and the V supports in place. The two curves shown were the two limits. I did not show the middle curve. They overlay quite well. Actually, we tried hoses with pressure when we first started, trying to achieve acoustic isolation from duct to duct. We quickly found out that this was not necessary. We changed the rubber composition and the diameter of the hose during these studies.

Mr. Morrow (LTV Research Center): What was the difference in propagation levels at the high and low frequencies with the ducts sealed?

Mr. Wren: It was 20 or 30 db. We attributed that difference to absorption of the energy of the propagating wave by the vehicle. It turns out that the major response of the adapter section, which is where the problem was, is 250 Hz or thereabouts. The low-frequency curve that we plotted was 6 octave bands in that vicinity, so that is why it absorbed so much energy.

Mr. Morrow: Why did you get the additional loss at low frequencies if you did not seal the ducts?

Mr. Wren: Because it presented a low-frequency shunt.

Mr. Dorland (NASA Manned Spacecraft Center): You have to present the right kind of

acoustic load to the transducer to get it to generate properly in that low end. If there is a leak in the duct, you will have a problem getting the energy out of the air modulator itself. The second point is that all these data were taken with the ducts completely uncorrelated, so that there was no energy transfer.

*   *   *

THEORETICAL STUDY OF ACOUSTIC SIMULATION
OF IN-FLIGHT ENVIRONMENTS*

R. W. White
Wyle Laboratories
Huntsville, Alabama

Progressive wave and reverberant acoustic tests are often used for qualification of aerospace structures subjected to unsteady aerodynamic environments. Acoustic simulation of these in-flight environments is achieved if the structural vibration response to the acoustic excitation is equivalent, over the frequency range of interest, to that which occurs during flight. To determine the degree of response simulation that could be expected for such testing of the Apollo vehicle, responses of the spacecraft lunar module adapter were estimated for a modified progressive wave field, a reverberant acoustic field, and for boundary-layer turbulence. Using an equivalent, uniform, pinned-end cylindrical shell, space-average power spectral densities of acceleration were computed from 10 to 1000 Hz. The classic modal analysis method employing 570 independent degrees of freedom was used in the computations. The pressure fields were assumed to be homogeneous with rectangular space correlation patterns, and to have uniform power spectra over the shell. Theoretical and experimental results are compared; these indicate that approximate simulation is possible over a broad frequency range.

INTRODUCTION

During launch and flight through the atmosphere, the external skin of the Apollo spacecraft is exposed to high-level fluctuating pressure environments from rocket exhaust noise and aerodynamic turbulence. As a result, significant vibration levels could be encountered throughout the vehicle since much of the structure consists of relatively lightweight materials. To ensure against fatigue failures and malfunctions, structural vibration qualification and evaluation tests of Apollo were performed at the Spacecraft Acoustic Laboratory (SAL) at the Manned Space Center (MSC) in Houston, Texas.

The SAL facility is designed to test the Apollo in a stacked flight configuration using an acoustic field to simulate the launch and in-flight environments. Figure 1 shows this configuration to consist of the command module, the service module, the spacecraft lunar module adapter (SLA), the lunar module housed in the SLA, and the instrument unit located just below the SLA. The MSC acoustic facility is capable of generating over the structure a modified progressive wave field or a reverberant acoustic field. The progressive wave field is generated within a shroud that is constructed around the vehicle. This shroud, shown diagrammatically in Fig. 2, consists of 16 axially oriented ducts which are contoured to the external skin of the vehicle. These ducts extend along the full length of the vehicle and are uniformly spaced around the entire circumference. Adjacent ducts are separated by a radial wedge-shaped baffle whose inner edge is fitted with a hollow pressurizable rubber hose that runs the full length of the baffle and which rests lightly against the vehicle skin. The purpose of the rubber insert is to provide an acoustic seal between ducts with minimum structural constraint. The vehicle skin forms the inner wall of each duct; and a vertical flat plate between baffles forms the outer wall. The radial position of the outer wall can be adjusted so that the cross-section area of the duct can be varied along the vehicle axis.

Each duct is equipped with an independently driven noise source which delivers sound through a horn and into the duct at the interface between the command module and the service module. From this juncture, sound waves propagate up over the command module to an

---
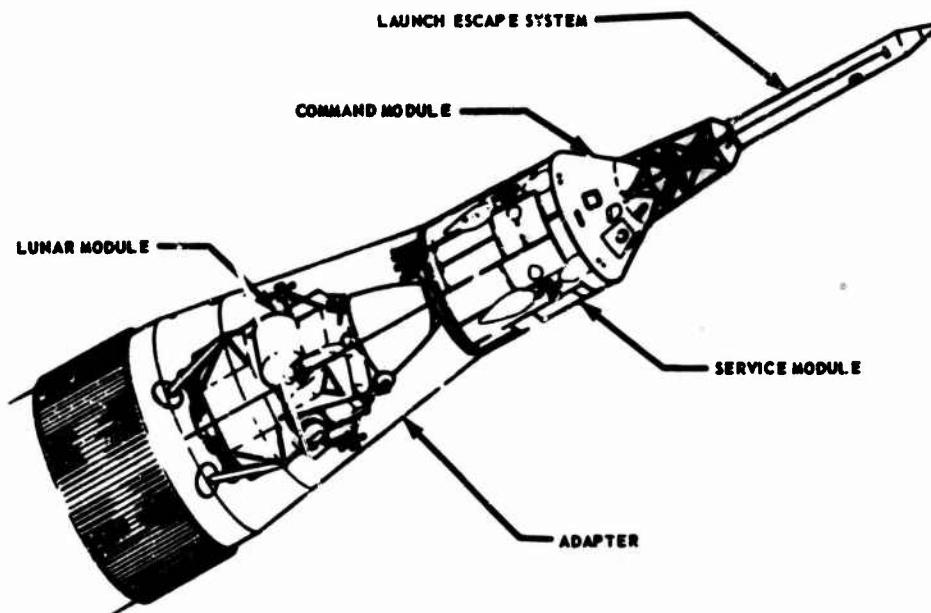
Fig. 1. Apollo spacecraft and
instrument unit

LAUNCH ESCAPE SYSTEM

COMMAND MODULE

LUNAR MODULE

SERVICE MODULE

ADAPTER

RUBBER SEAL

SHROUD

22°-30'

22°-30'

TYPICAL CHAMBER
16 PLACES

SECTION A-A
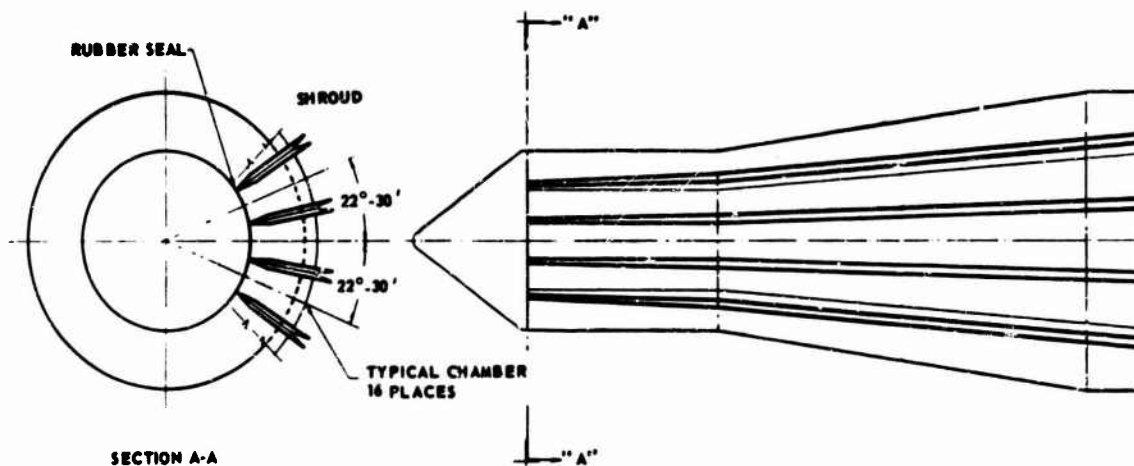
Fig. 2. Progressive wave shroud system
for Apollo acoustic tests

acoustic termination at the apex, and downward
over the service module and SLA. When the
16 noise sources are driven by independent
random electrical signals, the modified pro-
gressive wave field that is generated consists
of a pattern of 16 uncorrelated duct fields.
However, the sound fields in any two or more
ducts can be correlated by sending a common
electrical signal to the noise sources which

drive those ducts. Thus many pressure corre-
lation patterns can be generated over the struc-
ture. As a limiting case, all 16 ducts can have
correlated sound fields corresponding to a true
progressive wave propagating along the vehicle
axis.

The shroud system has three primary
functions. First, the ducts provide a means

56

for controlling the circumferential pressure correlation lengths so that both launch noise and aerodynamic turbulence can be simulated approximately. The acoustic pressures associated with launch noise are fairly well correlated around the vehicle, whereas the hydrodynamic pressures associated with aerodynamic turbulence have relatively small correlation areas over the skin. Second, the pressure profiles along the vehicle axis can be controlled through adjustment of the duct cross-section area. Third, confinement of a high percentage of a high percentage of the acoustic energy within the ducts provides for an efficient use of acoustic energy generated in the laboratory.

The shroud and noise sources are housed within a closed acoustic chamber. Therefore, a reverberant acoustic field can be developed around the vehicle by removing the system of ducts but retaining the noise sources and coupling horns. In the Apollo tests, both the modified progressive wave field and a reverberant acoustic field were employed.

The modified progressive wave field represents a unique method for simulating various types of distributed pressure environments. However, because of the lack of control on the acoustic wavelengths along the ducts axes, the pressure correlation patterns of real environments cannot be perfectly simulated. On the other hand, there will exist for each environment a particular duct correlation pattern which will give optimum simulation of the vibration response of the structure. If the laboratory-induced vibration response characteristics are essentially the same as those of the environmentally induced response, the desired simulation will have been achieved.

To take full advantage of the capabilities of the SAL facility, it is necessary to understand the effects of pressure correlations on structural response in terms of the sensitivity of response levels to changes in correlation patterns. Thus comparisons of the vibration responses to boundary-layer turbulence, a diffuse acoustic field, and modified progressive wave fields having various duct correlation patterns would show the degree of response simulation that could be achieved by the SAL facility. As a theoretical approach to this problem, vibration response spectra resulting from these environments were determined analytically for a uniform pinned-end cylinder which has overall dimensions, mass, and stiffnesses similar to those of the SLA; these computed responses were then compared for a flat pressure spectrum level of $1 \text{ (psi)}^2/\text{Hz}$. From this comparison and from a knowledge of the real environmental pressure

spectrum, it is possible to estimate the acoustic test spectrum required to achieve response simulation over the frequency range of interest. For this purpose, the analysis is a comparative type of analysis as opposed to an absolute response predictor.

The frequency range in which significant vibration response levels of the SLA can be expected is 10 to 1000 Hz. In the low-frequency range of 10 to 100 Hz, the structural resonances are well separated and the response is modal in character. For the intermediate frequency range of 100 Hz to the shell ring breathing frequency of 180 Hz, the modal bandwidths begin to overlap so that there is a transition from modal to nonmodal response as frequency increases. Above 180 Hz, the resonance frequencies are closely spaced with considerable bandwidth overlap, and the resulting vibration exhibits a relatively smooth response spectrum. In the laboratory tests, it is desirable that response simulation be achieved in each of these frequency ranges; thus the analytical study should have the capability of estimating responses over the entire frequency band of 10 to 1000 Hz.

For this purpose the classic modal analysis method was chosen, and all of the 570 idealized shell modes having resonance frequencies between 10 and 1000 Hz were included as independent single-degree-of-freedom systems. For each mode, structural and radiation damping were lumped into an equivalent viscous damping. With this method the above frequency-dependent vibration characteristics of the shell can be reproduced; and the two key parameters which influence vibration response, namely, modal density and elastic wave velocity, can be properly included. Such an approach has reasonable engineering accuracy in the low- and intermediate-frequency ranges where the individual modes are well separated. At high frequencies where the modal bandwidths overlap, the accuracy of the method is limited by damping coupling between modes; however, for a comparative analysis, these inaccuracies are offset to a degree by the fact that the influence of damping coupling on response should be similar for all three types of environments. Furthermore, all of the high-frequency modes are excited to roughly the same response level, so that the power flow between modes should be minimal. The chief advantages of the modal analysis technique is that the response equations can be readily programmed for a digital computer; and although the equations are lengthy, efficient programs can be developed which compute two-decade response spectra having high resolution in running times of 5 to 10 min.

57

In this paper, the pertinent structural properties of the SLA are discussed, followed by a development of the free vibration mode shapes and resonance frequencies of the equivalent idealized cylindrical shell. Then a brief derivation of the response equations is presented along with a discussion of the narrow-band spatial correlation functions used for the various fluctuating pressure environments. Finally, the analytically computed response spectra are compared to show the degree of simulation of in-flight environments that can be achieved in the SAL facility.

FREE VIBRATION CHARAC-TERISTICS OF SLA

Structural Properties

The SLA is a truncated conical shell composed of a set of honeycomb panels which are flush mounted in a light framework of axial and circumferential stiffeners, as seen in Fig. 3. This shell has a vertical height of 336 in., a slant angle of approximately 8.6 deg, a slant height of 349 in., and a mean radius R of 104 in. The honeycomb panels have, approximately, an overall thickness of 1.70 in., aluminum face-sheet thicknesses of 0.015 in. and 0.032 in., and an overall weight per unit area, μg, of 2.0 lb/ft^2 or 0.0139 lb/in.^{2}

Because of the small slant angle, it is expected that the vibration response of the SLA will be approximately equal to that of a cylindrical shell of length $L_x = 349$ in. and radius $R = 104$ in. The honeycomb panels are expected to dominate the shell stiffness; hence the idealized cylindrical is assumed to consist only of the above honeycomb skin. For simplicity, the ends of the uniform cylinder are assumed to be tangentially pinned. Assuming that only the facesheets provide the shell stiffness, the moment of inertia, I, per unit of length of the cross-section area is 0.0287 in.^{3} With a Young's modulus $\Sigma = 10^7$ lb/in.^{2} and a Poisson's ratio $\nu = 0.36$, the plate bending stiffness $D = EI/12(1 - \nu^2) = 3.24 \times 10^5$ lb-in. The in-plane extensional stiffness $K_e = 10^7 (0.032 + 0.015) = 4.7 \times 10^5$ lb/in.
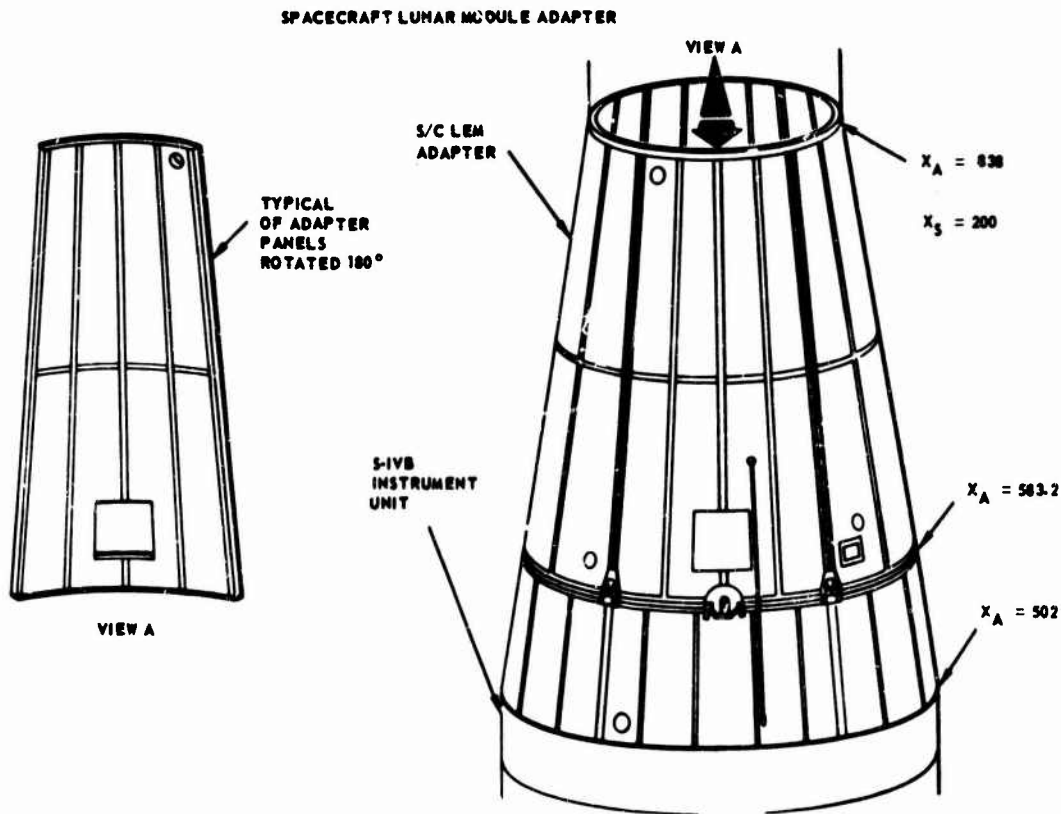
SPACECRAFT LUNAR MODULE ADAPTER

Fig. 3. General configuration of SLA skin structure

Mode Shapes and Resonance Frequencies

Each mode of vibration of the cylinder wall is characterized by m $(= 1, 2, 3, \ldots)$ elastic half-waves parallel to the shell axis, and by $n (= 0, 1, 2, \ldots)$ complete elastic waves around the circumference. For tangentially pinned ends, the mode shapes vary as $\sin m\pi \bar{x}$ along the axis where $\bar{x} = x/L_x$. Because of symmetry, the modes shapes vary either as $\sin 2n\pi\bar{y}$ or $\cos 2n\pi\bar{y}$ around the circumference of the cylinder where $\bar{y} = y/L_x$; and these two orthogonal components are distinguished by the integers $i = 1, 2$. Further, each mode (mni) has a radial deflection component $\phi_{mni}(x,y)$ and a tangential deflection component $\psi_{mni}(x,y)$; and thus a single mode shape is defined by the pair of functions $[\phi_{mni}(x,y), \psi_{mni}(x,y)]$, where

$$\phi_{mn1}(x,y) = \psi_{mn2}(x,y) = \sin m\pi\bar{x} \sin 2n\pi\bar{y}$$
$$\psi_{mn1}(x,y) = \phi_{mn2}(x,y) = \sin m\pi\bar{x} \cos 2n\pi\bar{y} \tag{1}$$

Because of the uniformity of the mass distribution, the orthogonality condition for these modes is expressed as

$$\int_0^1 \int_0^1 \left[\phi_{mni}(x,y) \, \phi_{rsj}(x,y) \right.$$
$$\left. + \psi_{mni}(x,y) \, \psi_{rsj}(x,y) \right] d\bar{x} \, d\bar{y} = 0, \quad (mni) \neq (rsj)$$
$$= \xi_{mni}, \quad (mni) = (rsj)$$

where $\xi_{mni} = 1/2$ for all modes. The generalized mass $M_{mni} = \xi_{mni}M_0$, where $M_0 (= \mu L_x L_y)$ is the total mass of the shell, so that $M_{mni} = M_0/2$ for all modes. Since the $(mn1)$ and $(mn2)$ modes shapes are geometrically similar, these modes have the same resonance frequency, ω_{mn}, defined by [1]

$$\omega_{mn} = 2\pi f_{mn}$$

$$= \frac{1}{R\sqrt{\mu}} \left[K_e \, \frac{\lambda_m^4}{(\lambda_m^2 + n^2)^2} + \frac{D}{R^2} (\lambda_m^2 + n^2 - 1)^2 \right]^{1/2}$$
$$\text{rad/sec} \quad (2)$$

with $\lambda_m = m\pi R/L_x$. The resonance frequencies determined by Eq. (1) are reasonably accurate for the lower order modes of the SLA; and they have approximately the correct frequency separation for both the lower and the higher order modes. The distribution of resonance frequencies in the range of 0 to 1000 Hz is shown in Fig. 4 where it is seen that the lowest frequency is $f_{13} = 20$ Hz. A large number of resonance

frequencies are seen to occur in the neighborhood of $f_{10} = 175$ Hz, which is the frequency for the highest modal density of the shell. Below and above 175 Hz, the modal densities dN/df are approximately [2]

$$\frac{dN}{df} = \frac{9}{16\pi} \frac{L_x}{f_{10}} \left(\frac{f}{f_{10}} \right)^{1/2} \sqrt{\frac{K_e}{D}} = 0.43 \left(\frac{f}{f_{10}} \right)^{1/2} \quad f < f_{10}$$

$$= \frac{L_x}{4} \sqrt{\frac{K_e}{D}} = 0.60 \, \frac{\text{modes}}{\text{hertz}} \quad f_{10} < f \tag{3}$$

It is to be noted that the modal density above 175 Hz is constant, and is equal to one half of the modal density of a simply supported, flat rectangular plate with edge dimensions L_x, L_y. The frequency separation between modes in this region is 1.67 Hz.

EQUATIONS OF MOTION

If $\ddot{q}_{mni}(t)$ denotes the generalized acceleration of the (mni) mode, then the net instantaneous acceleration $\ddot{U}(x,y,t)$ at point (x,y) is expressed as

$$\ddot{U}(x,y,t) = \sum_{mni} \phi_{mni}(x,y) \, \ddot{q}_{mni}(t), \tag{4}$$

where each term in this summation represents the acceleration response of a single mode. The power spectral density $S[\ddot{U}(x,y,t); \omega]$ of the acceleration $\ddot{U}(x,y,t)$ is defined as

$$S[\ddot{U}(x,y,t); \omega] = \frac{1}{\sqrt{2\pi}} \int_{-\infty}^{\infty} \overline{\ddot{U}(x,y,t) \, \ddot{U}(x,y,t+\tau)}$$
$$\times \, e^{i\omega\tau} \cdot d\tau, \tag{5}$$

where the bar $\overline{(\quad)}$ denotes time average. Substituting Eq. (4) into (5) gives

$$S[\ddot{U}(x,y,t); \omega] = \sum_{mni} \sum_{rsj} \phi_{mni}(x,y) \, \phi_{rsj}(x,y)$$
$$\times \, S[\ddot{q}_{mni}(t), \ddot{q}_{rsj}(t); \omega] \tag{6}$$

where $S[\ddot{q}_{mni}(t), \ddot{q}_{rsj}(t); \omega]$ denotes the cross power spectral density of the modal accelerations $\ddot{q}_{mni}(t), \ddot{q}_{rsj}(t)$. When $(rsj) = (mni)$, this cross power spectral density reduces to the power spectral density, $S[\ddot{q}_{mni}(t); \omega]$, for a single mode. It is convenient to deal with an acceleration spectral density, $S[\ddot{U}; \omega]$, which is space averaged over the surface of the shell, and which is defined as

59
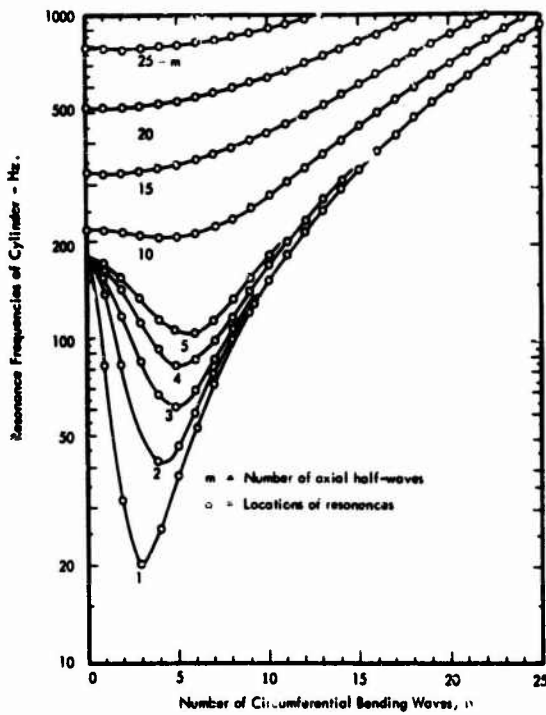
Fig. 4. Distribution of resonance frequencies of cylinder with circumferential and axial mode numbers

$$S[\ddot{U};\omega] = \int_0^1 \int_0^1 S[\ddot{U}(x,y,t);\omega]\, dx\, d\bar{y}. \quad (7)$$

Such a spectrum is independent of position (x,y); and by orthogonality of the mode shapes $\phi_{mni}(x,y)$, $\phi_{rsj}(x,y)$, this spectrum is also independent of the modal acceleration cross spectra appearing in Eq. (6). Substituting Eq. (6) into (7) gives

$$S[\ddot{U};\omega] = \sum_{mni} a_{ni}\, S[\ddot{q}_{mni}(t);\omega]$$

$$a_{ni} = \int_0^1 \int_0^1 \phi_{mni}^2(x,y)\, d\bar{x}\, d\bar{y}$$

$$= \begin{cases} 0, & n = 0,\ i = 1 \\ 1/2, & n = 0,\ i = 2 \\ 1/4, & n = 1, 2, 3, \ldots;\ i = 1, 2. \end{cases} \quad (8)$$

Each mode of vibration is assumed to respond independently so that $q_{mni}(t)$ satisfies the equation of motion for a single-degree-of-freedom system, namely

$$\ddot{q}_{mni}(t) + \frac{\omega_{mn}}{Q_{mn}} \dot{q}_{mni}(t) + \omega_{mn}^2\, q_{mni}(t) = \frac{F_{mni}(t)}{M_{mni}}, \quad (9)$$

where Q_{mn} is, approximately, the dynamic magnification factor at resonance, and $F_{mni}(t)$ is the generalized force defined by the equation

$$F_{mni}(t) = L_x L_y \int_0^1 \int_0^1 P(x,y,t)\phi_{mni}(x,y)\, d\bar{x}\, d\bar{y}. \quad (10)$$

The external fluctuating pressure loading at point (x,y) is denoted as $P(x,y,t)$. For a stationary and ergodic random pressure excitation, the solution of Eq. (7) for $S[\ddot{q}_{mni}(t);\omega]$ is [3]

$$S[\ddot{q}_{mni}(t);\omega] = \frac{1}{M_{mni}^2} \left[\frac{\omega}{\omega_{mn}}\right]^4 H^2\left(\frac{\omega}{\omega_{mn}}\right) S[F_{mni}(t);\omega] \quad (11)$$

where $S[F_{mni}(t);\omega]$ is the power spectral density of the generalized force, and $H^2(\omega/\omega_{mn})$ is the dynamic magnification factor for the single-degree-of-freedom system,

$$H(\omega/\omega_{mn}) = \left\{\left[1 - \left(\frac{\omega}{\omega_{mn}}\right)^2\right]^2 + \frac{1}{Q_{mn}^2}\left(\frac{\omega}{\omega_{mn}}\right)^2\right\}^{-1/2}$$

From Eq. (10), the generalized force spectrum can be written as

$$S[F_{mni}(t);\omega] = L_x^2 L_y^2 \int_0^1 \int_0^1 \int_0^1 \int_0^1$$

$$\times\ S[P(x,y,t),\ P(x',y',t);\omega]$$

$$\times\ \phi_{mni}(x,y)\phi_{mni}(x',y')\, d\bar{x}\, d\bar{y}\, d\bar{x}'\, d\bar{y}' \quad (12)$$

where $S[P(x,y,t),\ P(x',y',t);\omega]$ is the cross power spectral density of the pressures acting at points (x,y) and (x',y'). This pressure cross spectrum is a complex quantity which in general has a nonzero real and imaginary part termed the cospectrum and the quad spectrum, respectively. Based on the assumption of stationarity of the pressures, it is easy to show that the double space integral in Eq. (12) of the pressure quad spectrum is zero. Assuming that the pressure spectral density, $S[P;\omega]$, has a uniform distribution over the shell, the pressure cospectrum can be written as

$$\text{Real }\left\{S[P(x,y,t),\ P(x',y',t);\omega]\right\} = S[P;\omega]\,C(x,y,x',y';\omega) \quad (13)$$

60

where $C(x,y,x',y';\omega)$ is a narrow-band pressure correlation coefficient, at frequency ω, between the pressures at (x,y) and (x',y'). Assuming further that the pressure correlation patterns on the shell are rectangular and that the pressure field is homogeneous along both the x and y axes, this correlation coefficient can be simplified to the following product form:

$$C(x,y,x',y';\omega) = C(\zeta;\omega)\, C(\eta;\omega)\,. \qquad (14)$$

where $\zeta = x - x'$ and $\eta = y - y'$. Here, $C(\zeta;\omega)$ denotes the narrow-band pressure correlation coefficient along the cylinder axis; $C(\eta;\omega)$ is a similar coefficient along the circumference. Thus, substituting Eqs. (1), (13), and (14) into (12) gives

$$S[F_{mni}(t);\omega] = L_x^2 L_y^2\, S[P;\omega]\, j_m^2(\omega)\, j_{ni}^2(\omega) \qquad (15)$$

where the joint acceptances $j_m^2(\omega)$, $j_{ni}^2(\omega)$ are

$$j_m^2(\omega) = \int_0^1 \int_0^1 C(\zeta;\omega)\, \sin m\pi\bar{x}\, \sin m\pi\bar{x}'\, d\bar{x}\, d\bar{x}' \quad (16)$$

$$j_{n1}^2(\omega) = \int_0^1 \int_0^1 C(\eta;\omega)\, \sin 2n\pi\bar{y}\, \sin 2n\pi\bar{y}'\, d\bar{y}\, d\bar{y}' \qquad (17)$$

$$j_{n2}^2(\omega) = \int_0^1 \int_0^1 C(\eta;\omega)\, \cos 2n\pi\bar{y}\, \cos 2n\pi\bar{y}'\, d\bar{y}\, d\bar{y}'\,. \qquad (18)$$

Substituting Eqs. (11) and (15) into (8), and noting that the generalized mass $M_{mni} = \mu L_x L_y/2$, gives the following response equation:

$$S[\ddot{U};\omega] = \frac{1}{\mu^2}\, S[P;\omega] \sum_{mni} \beta_{ni}\left[\frac{\omega}{\omega_{mn}}\right]^4$$
$$\times H^2\left(\frac{\omega}{\omega_{mn}}\right) j_m^2(\omega)\, j_{ni}^2(\omega)\,. \qquad (19)$$

$$\beta_{ni} = 0,\ n = 0,\ i = 1$$
$$= 2,\ n = 0,\ i = 2$$
$$= 1,\ n = 1,2,3,\ldots;\ i = 1,2\,.$$

From the above definition of $H(\omega/\omega_{mn})$, it can be shown that $[\omega/\omega_{mn}]^4\, H^2(\omega/\omega_{mn}) = H^2(\omega_{mn}/\omega)$, which simplifies the form of Eq. (19). Also, the summation over $i = 1,2$ in Eq. (19) can be eliminated by defining a new coefficient β_n and a new joint acceptance $j_n^2(\omega) = j_{n1}^2(\omega) + j_{n2}^2(\omega)$, so that from Eqs. (17) and (18)

$$S[\ddot{U};\omega] = \frac{1}{\mu^2}\, S[P;\omega] \sum_{mn} \beta_n\, H^2\left(\frac{\omega_{mn}}{\omega}\right) j_m^2(\omega)\, j_n^2(\omega) \qquad (20)$$

$$\beta_n = 2,\ n = 0$$
$$= 1,\ n = 1,2,3,\ldots$$

$$j_n^2(\omega) = \int_0^1 \int_0^1 C(\eta;\omega)\, \cos 2n\pi\bar{\eta}\, d\bar{y}\, d\bar{y}'\,. \qquad (21)$$

In this analysis, the response-to-pressure ratio $S[\ddot{U};\omega]/S[P;\omega]$ is computed in units of $g^2/(psi)^2$; and therefore if μg is the surface density of the shell in pounds per square inch, then

$$\frac{S[\ddot{U};\omega]}{S[P;\omega]} = \frac{1}{(\mu g)^2} \sum_{mn} \beta_n\, H^2\left(\frac{\omega_{mn}}{\omega}\right) j_m^2(\omega)\, j_n^2(\omega)\,. \qquad (22)$$

Equation (22) is the desired form of the response equation.

Joint Acceptance Transformation

The joint acceptance expressions (16) and (21) involve double integrations over one of the coordinate axes of the cylinder. For each of these expressions, a coordinate transformation can be made which will permit one of the integrals to be evaluated directly so that the joint acceptance can be written as a single integral. Consider first expression (16). The product $\sin m\pi\bar{x}\, \sin m\pi\bar{x}'$ can be written as

$$\sin m\pi\bar{x}\, \sin m\pi\bar{x}' = \frac{1}{2}\,[\cos m\pi\bar{\zeta} - \cos m\pi\bar{\xi}]$$

where $\bar{\zeta} = \bar{x} - \bar{x}'$, $\bar{\xi} = \bar{x} + \bar{x}'$. Transforming the variables of integration $(\bar{x}, \bar{x}')$ to the new variables $(\bar{\xi}, \bar{\zeta})$, the region of integration $0 \le x \le 1$, $0 \le \bar{x}' \le 1$ is transformed as shown in Fig. 5. Integrating first over $\bar{\xi}$, the joint acceptance $j_m^2(\omega)$ can be rewritten as

$$j_m^2(\omega) = \frac{1}{4} \int_{\bar{\zeta}=-1}^1 C(\bar{\zeta};\omega) \int_{\bar{\xi}=|\bar{\zeta}|}^{2-|\bar{\zeta}|} \times [\cos m\pi\bar{\zeta} - \cos m\pi\bar{\xi}]\, d\bar{\xi}\, d\bar{\zeta}\,.$$

Performing the integration over $\bar{\xi}$ gives

$$j_m^2(\omega) = \frac{1}{2} \int_{\bar{\zeta}=-1} C(\bar{\zeta};\omega)\left[(1 - |\bar{\zeta}|)\cos m\pi\bar{\zeta} + \frac{1}{m\pi}\sin m\pi\,|\bar{\zeta}|\right] d\bar{\zeta}\,. \qquad (23)$$
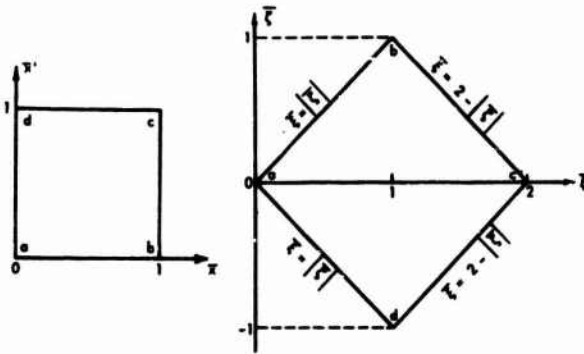
61

Fig. 5. Transformation of the region of
integration for joint acceptances

The correlation coefficient $C(\bar{\zeta};\omega)$ is the normalized time average of the product of the filtered narrow-band pressure components acting at two points on the shell which are separated by an axial distance ζ; and hence $C(\bar{\zeta};\omega) = C(-\bar{\zeta};\omega)$. Thus Eq. (23) can be reduced to the form

$$j_m^2(\omega) = \int_{\bar{\zeta}=0}^1 C(\bar{\zeta};\omega)\left[(1-\bar{\zeta})\cos m\pi\bar{\zeta} + \frac{1}{m\pi}\sin m\pi\bar{\zeta}\right]d\bar{\zeta}.$$

(24)

Similarly, the joint acceptance $j_n^2(\omega)$ given by Eq. (21) can be expressed as

$$j_n^2(\omega) = 2\int_{\bar{\eta}=0}^1 (1-\bar{\eta})\, C(\bar{\eta};\omega)\cos 2n\pi\bar{\eta}\; d\bar{\eta}.$$ (25)

Pressure Correlation Coefficients

Three types of pressure excitation are considered in this analysis, namely, boundary-layer turbulence, reverberant acoustic field, and the modified progressive wave field. To evaluate the joint acceptance functions, it is necessary to know the space correlation coefficients $C(\bar{\zeta};\omega)$ and $C(\bar{\eta};\omega)$ for these three pressure fields.

Turbulence in an attached boundary layer is often characterized as a convected pressure field whose internal pressure distributions change slowly with time in the moving frame of reference. For a frozen pressure field convected at velocity U_c, the cross power spectral density of the pressures at two points along the flow axis is $S[P;\omega]e^{-i\omega\zeta/U_c}$, the real part of which is $S[P;\omega]\cos\omega\zeta/U_c$. Thus, the axial space correlation coefficient $C(\bar{\zeta};\omega) = \cos\gamma_x\bar{\zeta}$, where $\gamma_x = \omega L_x/U_c$. Time variations of the pressures within the moving frame of reference lead to

decay of the axial correlations with separation distance. The decay is often approximated by the exponential factor $e^{-\delta_x|\bar{\zeta}|}$, where δ_x is an empirically determined parameter. Normal to the flow axis, the space correlations exhibit primarily an exponential decay with separation distance. Thus the narrow-band space correlation coefficients for boundary-layer turbulence are often approximated by the equations

$$C(\bar{\zeta};\omega) = e^{-\delta_x|\bar{\zeta}|}\cos\gamma_x\bar{\zeta}$$

(26)

$$C(\bar{\eta};\omega) = e^{-\delta_y|\bar{\eta}|}$$

Space correlations obtained from subsonic wind tunnel data are summarized in Figs. 6 through 9. Using Maestrello's [4] data in Figs. 6 and 7 [4-7], the exponential decay parameters may be approximated as $\delta_x = 0.10\gamma_x$, $\delta_y = 2\gamma_y$, where $\gamma_y = \omega L_y/U_c$. Based on these expressions for δ_x and δ_y, the low-frequency components of the pressure are correlated over large distances. However, correlation lengths must be limited to distances which are of the order of the boundary-layer thickness, δ_b. This effect is shown by the data of Bull et al. [7] in Figs. 8 and 9, where it is seen that the low-frequency correlations are a function of the boundary-layer displacement thickness δ^*. An approximate correction for this effect was made by choosing δ_x and δ_y equal to the following:

$$\delta_x = 0.10\,\omega L_x/U_c + 0.265\, L_x/\delta_b$$
(27)
$$\delta_y = 2\,\omega L_y/U_c + 2L_y/\delta_b.$$

For the present analysis of the SLA, the boundary-layer thickness was estimated to be $\delta_b = 12$ in. Also, on the basis of Willmarth and Wooldrige's [6] data, the convection velocity U_c was assumed to equal the broad-band convection
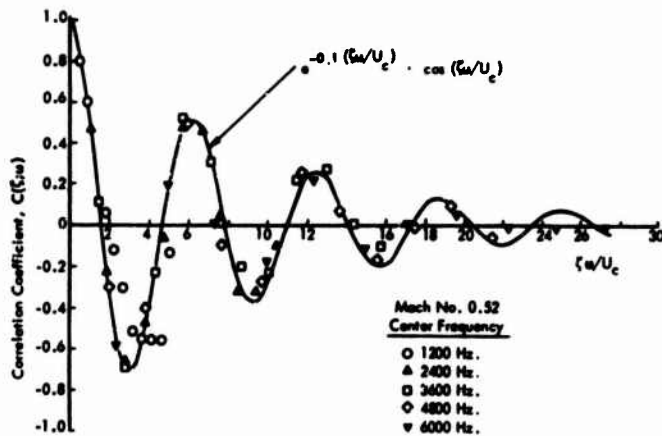
62

Fig. 6. Narrow-band longitudinal space correlation
coefficient for boundary-layer turbulence [4]

---- Gardner, (Theoretical), Reference 5)
○ Maestrello, Center Frequency 1200 Hz.,(Reference 4)
▲ Maestrello, Center Frequency 2400 Hz.,(Reference 4)
▣ Maestrello, Center Frequency 3600 Hz.,(Reference 4)
● Willmarth and Wooldridge, Center Frequency, 500 Hz.,(Reference 6)
♦ Bull, Center Frequencies at 1260, 2000, 3200, and 5000 Hz.,(Reference 7)
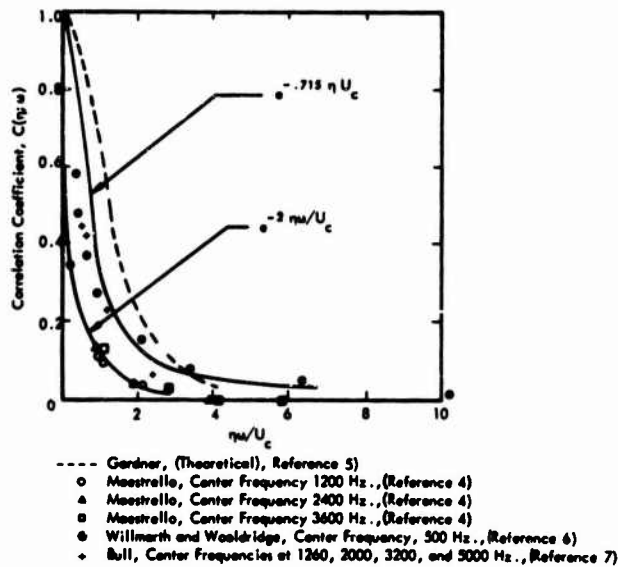
Fig. 7. Narrow-band lateral space correlation
coefficient for boundary-layer turbulence

velocity of $0.8\ U_\infty$, where U_∞ is the free stream velocity. Convection velocities used in the analysis are $U_c = 9810$ in./sec at Mach 1 and $U_c = 15,900$ in./sec at Mach 2.

For a reverberant acoustic field impinging on a flat wall, Eckhart [8] shows that the space correlation coefficient is $(\sin kr)/kr$ where k is the wave number and r is the separation distance. In keeping with the rectangular correlation pattern, this functional form was used for the correlation coefficients along the x and y axes. Thus

$$C(\zeta;\omega) = \frac{\sin \gamma_x \bar{\zeta}}{\gamma_x \bar{\zeta}}$$

(28)

$$C(\zeta;\omega) = \frac{\sin \gamma_y \bar{\eta}}{\gamma_y \bar{\eta}}$$

where, if c_0 denotes the speed of sound, and λ denotes the acoustic wavelength,

$$\gamma_x = kL_x = \omega L_x/c_0 = 2\pi L_x/\lambda$$
$$\gamma_y = kL_y = \omega L_x/c_0 = 2\pi L_y/\lambda .$$

(29)

63
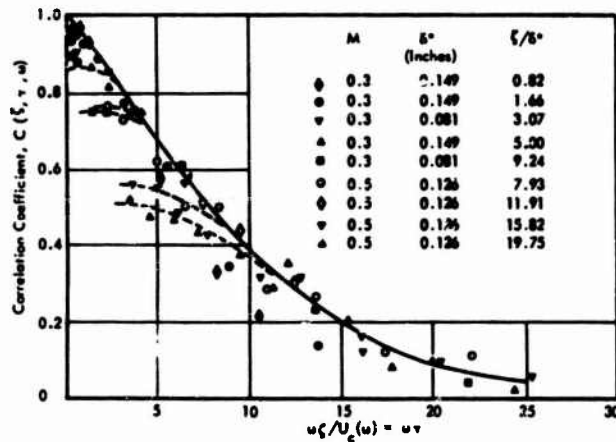
Fig. 8. Narrow-band longitudinal space-time correlation coefficients for wall pressure field from boundary-layer turbulence [7]
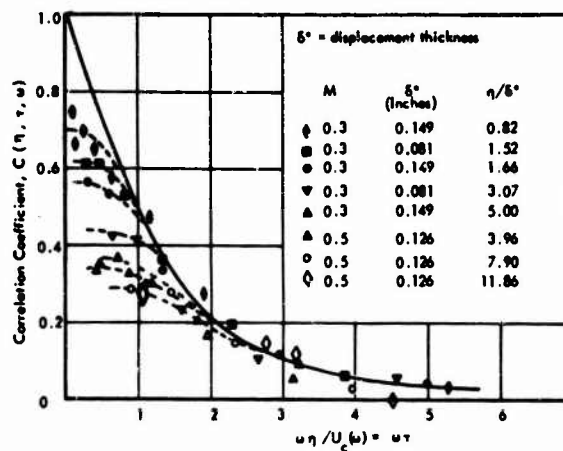
Fig. 9. Narrow-band lateral space-time correlation coefficients for wall pressure field from boundary-layer turbulence [7]

Although these correlation functions correspond to a diffuse field on a flat surface, they are reasonably good approximations for a cylindrical surface immersed in such a field. For the latter case, Wenzel [9] has determined more exact correlations and shows that $C(\zeta; \omega)$ and $C(\eta; \omega)$ are also functions of L_y/λ. These results are compared with the approximations of Eq. (29) in Figs. 10 and 11. The correlation $C(\zeta; \omega)$ is relatively insensitive to L_y/λ, while $C(\eta; \omega)$ is more sensitive. In view of the lengthy computations leading to the improved correlations, it is necessary for the present analysis to use the approximations (29).

For the modified progressive wave field, the axial correlation coefficient is $C(\zeta; \omega) = \cos \gamma_x \zeta$, where $\gamma_x = \omega L_x/c_0$. The lateral correlation coefficient is assumed to be unity across the width of a single duct or a group of adjacent correlated ducts. Responses for various duct correlation patterns were obtained. If N denotes the number of uncorrelated spans around the circumference, with all adjacent ducts within a span being perfectly correlated, then correlation patterns used correspond to N = 1, 2, 4, 8, and 16. Here N = 1 signifies that there is essentially one duct since all ducts are correlated; N = 2 implies that eight ducts on each side are

64
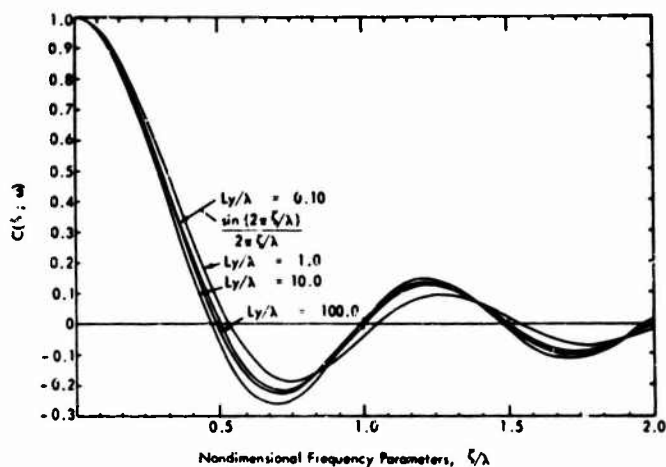
Fig. 10. Narrow-band longitudinal space correlation coefficient on surface of a cylinder immersed in a reverberant acoustic field [9]
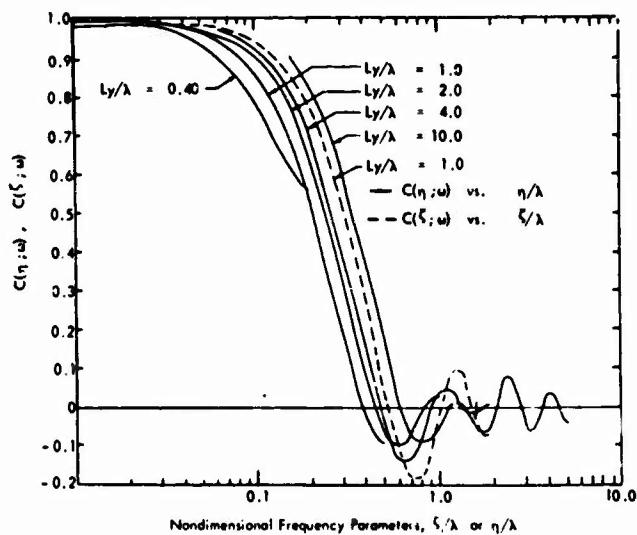
Fig. 11. Narrow-band longitudinal and lateral space correlation coefficient on surface of a cylinder immersed in a reverberant acoustic field [9]

correlated, but that the two sets of eight ducts are uncorrelated; and N = 16 means 16 uncorrelated ducts.

Joint Acceptance for Boundary-Layer Turbulence

The expression for the joint acceptances of the axial modes of the cylinder for boundary-layer turbulence can be obtained by substituting Eq. (26 into (24) and performing the necessary integration, giving

$$j_m^2(\omega) = \frac{2}{(m\pi)^2 \Delta^2} \left\{ P \left[1 - (-1)^m e^{-\delta_x} \cos \gamma_x \right] \right.$$

$$\left. + 4(-1)^m q e^{-\delta_x} \sin \gamma_x + \frac{m\pi}{2} r\Delta \right\}. \quad (30)$$

where

$$\Delta = \left[1 + \left(\frac{\gamma_x}{m\pi} \right)^2 + \left(\frac{\delta_x}{m\pi} \right)^2 \right]^2 - 4 \left(\frac{\gamma_x}{m\pi} \right)^2$$

65

$$P = \left[1 - \left(\frac{\gamma_x}{m\pi}\right)^2 + \left(\frac{\delta_x}{m\pi}\right)^2\right]^2 - 4\left(\frac{\gamma_x}{m\pi}\right)^2\left(\frac{\delta_x}{m\pi}\right)^2 \cdot$$

$$q = \left(\frac{\gamma_x}{m\pi}\right)\left(\frac{\delta_x}{m\pi}\right)\left[1 - \left(\frac{\gamma_x}{m\pi}\right)^2 + \left(\frac{\delta_x}{m\pi}\right)^2\right]$$

$$r = \left(\frac{\delta_x}{m\pi}\right)\left[1 + \left(\frac{\gamma_x}{m\pi}\right)^2 + \left(\frac{\delta_x}{m\pi}\right)^2\right] .$$

For $L_x = 349$ in. and $\delta_b = 12$ in., the ratio $L_x/\delta_b = 29.1$; and hence according to Eq. (27), $\delta_x > 7.7$. Because of this, the terms in Eq. (30) which contain the factor $e^{-\delta_x}$ are negligibly small so that Eq. (30) can be reduced to the following approximation:

$$j_m^2(\omega) \doteq \frac{2}{(m\pi)^2}\left[\frac{P}{\Delta^2} + \frac{m\pi}{2}\frac{r}{\Delta}\right] . \qquad (31)$$

Numerical values of $j_m^2(\omega)$ were determined for $m = 1, 2, \ldots, 20$ using (31), and the results are shown in Fig. 12 as a function of the non-dimensional frequency parameter $2L_x f/U_c$, where f denotes the frequency in hertz. Also shown in Fig. 12 are the actual frequency scales for free stream Mach numbers of 1 and 2. The joint acceptances are maxima at the coincidence condition $\gamma_x = m\pi$, or $2L_x f_c/U_c = m$ where f_c denotes the coincidence frequency for the mth mode. Note that in terms of f_c, $\gamma_x = m\pi(f/f_c)$.

At frequencies well below coincidence, the joint acceptances can be estimated by setting $\gamma_x = 0$ and $\delta_x = 0.265 L_x/\delta_b = 7.7$, which leads to the approximation

$$j_m^2(\omega) \doteq j_m^2(0) \doteq \frac{m^2 + 4.75}{(m^2 + 6.05)^2} , \quad f \ll f_c .$$

Thus for large values of m, $j_m^2(\omega) \doteq 1/m^2$ when $f \ll f_c$. The maximum, or coincidence, values of $j_m^2(\omega)$ can be estimated readily for say $m > 5$ by noting that $\gamma_x = m\pi$ and $\delta_x/\gamma_x = 0.10 + 7.7/m\pi < 1$, so that $\Delta = -P \doteq r^2 \doteq (2\delta_x/\gamma_x)^2 \ll 1$. From (30) then, $j_m^2(\omega) \doteq (\delta_x - 1)/2\delta_x^2$. However, since $\delta_x = 0.10 m\pi + 7.7 > 7.7$, the approximate expression for $j_m^2(\omega)$ at coincidence reduces to

$$j_m^2(\omega) \doteq \frac{1}{2\delta_x} = \frac{1}{0.628 m + 15.4} , \quad f = f_c = \frac{mU_c}{2L_x} .$$

This equation defines the envelope of the peak values of $j_m^2(\omega)$ in Fig. 12.

At frequencies which are well above coincidence, $\gamma_x \gg m\pi$ so that $\Delta \doteq P \doteq (\gamma_x/m\pi)^4$ and $r = (\delta_x/m\pi)(\gamma_x/m\pi)^2$. Thus $P/\Delta^2 = (m\pi/\gamma_x)^4$, $m\pi r/2\Delta = \delta_x(m\pi/\gamma_x)^2/2 \gg (m\pi/\gamma_x)^4 = P/\Delta^2$. Hence, Eq. (31) reduces to the following expression which describes the high-frequency roll-off of $j_m^2(\omega)$ in Fig. 12:
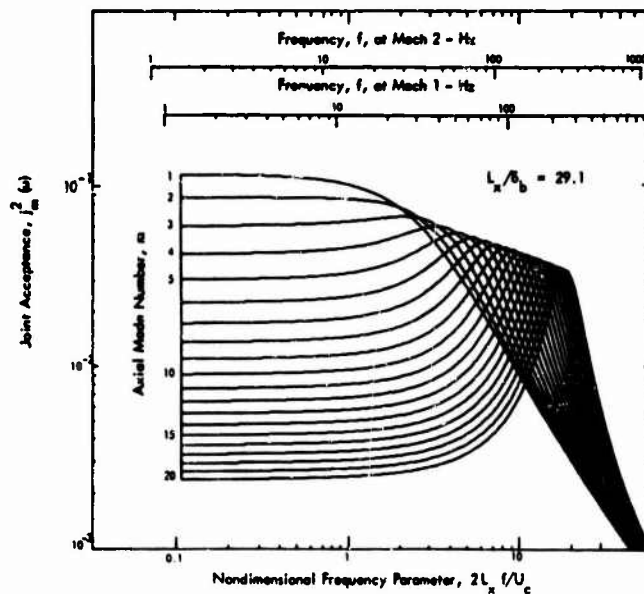
Fig. 12. Joint acceptances of axial shell modes of cylinder for boundary-layer turbulence

$$j_m^2(\omega) \doteq \frac{1}{m\pi}\frac{r}{\Delta} \doteq \frac{\delta_x}{\gamma_x^2}$$

$$= \frac{0.10}{m\pi}\left(\frac{f_c}{f}\right) + \frac{7.7}{(m\pi)^2}\left(\frac{f_c}{f}\right)^2$$

$$= \frac{0.446}{f} + \frac{153.5}{f^2} \quad \text{at Mach 1}$$

$$= \frac{0.725}{f} + \frac{405}{f^2} \quad \text{at Mach 2}$$

$$\left.\right\} \, f_c \ll f \,.$$

The joint acceptance $j_n^2(\omega)$ is obtained by substituting Eq. (26) into (25) and integrating, giving

$$j_n^2(\omega) \doteq \frac{2\delta_y}{(2\pi n)^2 + \delta_y^2} + 2\frac{(2\pi n) - \delta_y}{[(2\pi n)^2 + \delta_y^2]^2}(1-e^{-\delta_y}). \tag{32}$$

From (27), it is seen that $\delta_y > 108$; and for this reason only the first term in Eq. (32) is significant.

Numerical evaluations of Eq. (32) are shown in Fig. 13 for various ring modes and as a function of the nondimensional frequency parameter $L_y f/U_c$. In this case the joint acceptances are fairly insensitive to frequency and are approximately proportional to $1/n^2$ for large values of n.

Joint Acceptances for Reverberant Acoustic Field

The joint acceptance expressions for a reverberant acoustic field are obtained by substituting Eq. (28) into (24) and (25) and performing the necessary integrations. The resulting expressions are summarized below:

$$j_m^2(\omega) = \frac{1}{(2\pi)^2 m L_x/\lambda}\left\{\text{Cin}\,[\pi\,(m + 2L_x/\lambda)]\right.$$
$$\left. - \text{Cin}\,(\pi\,|m - 2L_x/\lambda\,|)\right\}$$
$$+ \frac{1}{4\pi L_x/\lambda}\left\{\text{Si}\,[\pi(m + 2L_x/\lambda)] - \text{Si}\,[\pi(m - 2L_x/\lambda)]\right\}$$
$$+ \frac{1}{(m\pi)^2}\frac{1 - (-1)^m \cos\,(2\pi L_x/\lambda)}{1 - (2L_x/m\lambda)^2}\,, \tag{33}$$

where

$$\text{Cin}\,(z) = \int_0^z \frac{1 - \cos x}{x}\,dx \quad \text{(cosine integral)}$$

$$\tag{34}$$

$$\text{Si}\,(z) = \int_0^z \frac{\sin x}{x}\,dx \quad \text{(sine integral)}$$
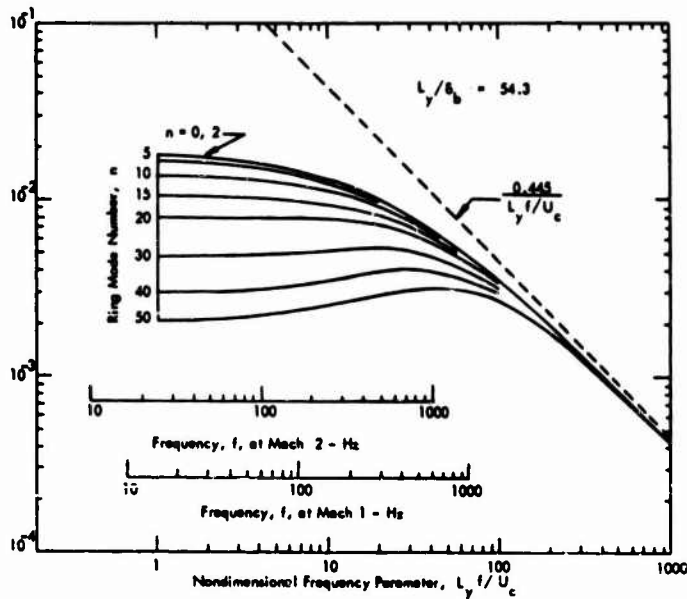
Fig. 13. Joint acceptances of cylinder ring modes for boundary-layer turbulence

67

$$j_n^2(\omega) = \frac{1}{2\pi(L_y/\lambda)} \left\{ \text{Si}\left[2\pi(n+L_y/\lambda)\right] - \text{Si}\left[2\pi(n-L_y/\lambda)\right] \right\}$$

$$+ \frac{1}{2(n\pi)^2} \frac{1 - \cos(2\pi L_y/\lambda)}{1 - (L_y/n\lambda)^2} \quad \text{at } n \neq 0$$

$$= \frac{\text{Si}(2\pi L_y/\lambda)}{\pi L_y/\lambda} - \frac{1 - \cos(2\pi L_y/\lambda)}{2\pi^2(L_y/\lambda)^2} \quad \text{at } n = 0.$$

$$(35)$$

Convenient expressions for the numerical evaluation of the $\text{Si}(z)$ and $\text{Cin}(z)$ integrals are given by Abramowitz [10]. These consist of power series expansions for small values of the argument ($0 < z < 1$), rational fraction approximations for intermediate values of the argument ($1 < z < 50$), and asymptotic expansions for large values of the argument ($50 < z$). These approximations are also summarized in Ref. [11].

Numerical values of $j_m^2(\omega)$ and $j_n^2(\omega)$ were obtained using Eqs. (33) and (34), and the results are presented in Figs. 14, 15, and 16 as functions of mode number and the nondimensional frequency parameters $2L_x/\lambda$ ($= 2L_x f/c_0$) and $2L_y/\lambda$ ($= 2L_y f/c_0$). Maximum values of these joint acceptances occur at the coincidence conditions $2L_x f_c/c_0 = m$ for the axial modes and $L_y f_c/c_0 = n$ for the ring modes. Above coincidence for each mode the joint acceptances approach values which are inversely proportional to frequency but which are independent of the order of the mode.

Joint Acceptances for Modified Progressive Wave Field

The joint acceptances of the axial modes for the modified progressive wave field are obtained by substituting $C(\bar{\zeta};\omega) = \cos\gamma_x\bar{\zeta}$ into Eq. (24) and integrating. The well-known result obtained by Powell [3] for this case is

$$j_m^2(\omega) = \frac{2}{(m\pi)^2} \frac{1 - (-1)^m \cos\gamma_x}{[1 - (\gamma_x/m\pi)^2]^2} \quad \gamma_x \neq m\pi$$

$$(36)$$

$$= \frac{1}{4} \quad \gamma_x = m\pi.$$

The condition $\gamma_x = m\pi$ is associated with acoustic coincidence of the axial modes; and since $\gamma_x = \omega L_x/c_0$, the coincidence frequency $f_c = mc_0/2L_x = 19.2 \, m$. In terms of f_c, $\gamma_x = m\pi(f/f_c)$. At frequencies which are well below coincidence, $j_m^2(\omega) \doteq (f/f_c)^2$ for $m = 2$,
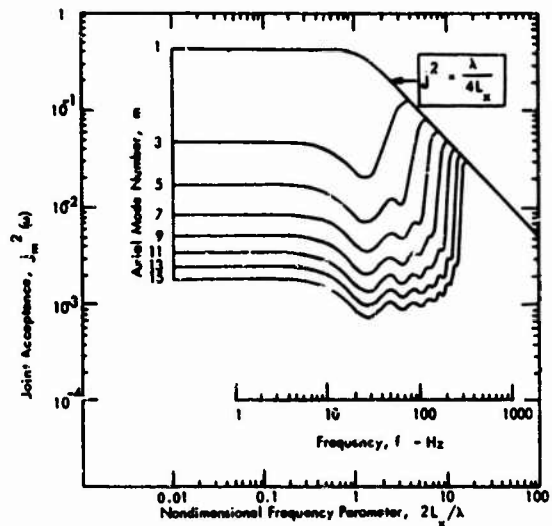
Fig. 14. Joint acceptances of odd-numbered axial modes of cylinder for reverberant acoustic field

$4, 6, \ldots,$ and $j_m^2(\omega) \doteq (2/m\pi)^2$ for $m = 1, 3, 5, \ldots$. At frequencies which are above coincidence, the peak values of $j_m^2(\omega) \doteq (2/m\pi)^2 (f_c/f)^4$. As shown by Fig. 4, the modes $(1,3)$, $(2,4)$, $(3,5)$, $(4,5)$, $(5,5)$, $(5,6)$, $\ldots$ have resonance frequencies which are near the axial coincidence frequency $f_c = 19.2 \, m$. The remaining modes, as well as all of the modes above about 250 Hz have resonance frequencies above the coincidence frequency, which implies that for most modes of the cylinder, the acoustic wavelengths are shorter than the elastic wavelengths at the resonance frequencies of the modes. This condition would not be true for the lower order modes ($m < 20$) of a pinned-pinned beam of length 349 in. which had the same stiffness and mass properties as the SLA, since the resonance frequencies ($f_m = 1.22 \, m^2$) of such a beam would be much lower than those of the SLA for the same axial mode number. The relatively high resonance frequencies of the lower order modes of the SLA are due to the extensional stiffness K_e introduced by the cylindrical nature of the structure.

For N uncorrelated sound fields around the circumference of the vehicle, the joint acceptance $j_n^2(\omega)$ for the nth ring mode is N times the joint acceptance of that mode when driven by one of the N sound fields. Thus for unit space correlation across the width of a single span, and for an antimode of the nth mode located at the center of the span, the joint acceptance for N sound fields is
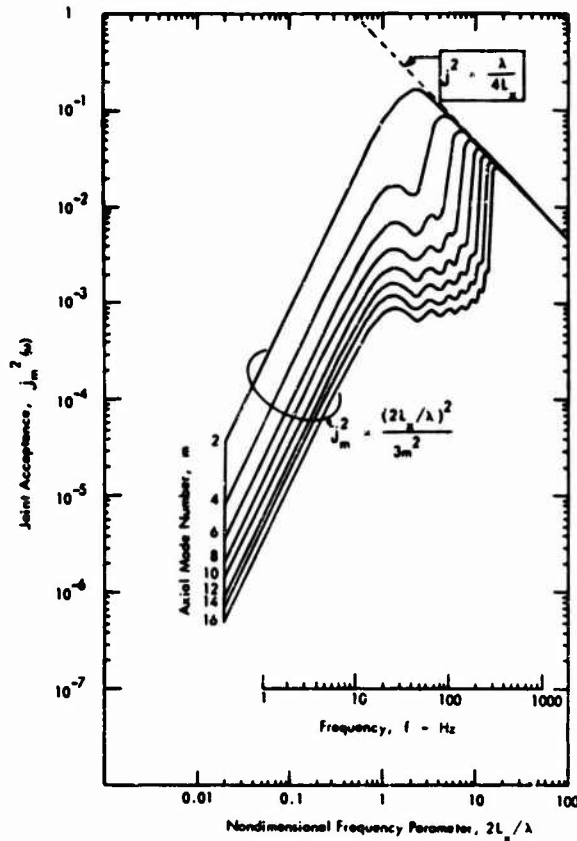
Fig. 15. Joint acceptances of even-
numbered axial modes of cylinder
for reverberant acoustic field

$$j_n^2(\omega) = N \left[\int_{-1/2N}^{1/2N} \cos 2\pi n\bar{y} \; d\bar{y} \right]^2$$

$$= \frac{1}{N} \left[\frac{\sin \, n\pi/N}{n\pi/N} \right]^2 . \qquad (37)$$

From Eq. (37), the greatest values of $j_n^2(\omega)$ for a fixed N occur for the ring modes $n < N$; and, $0.10 \leq N j_n^2(\omega) \leq 1.00$ for $0 \leq n \leq 0.75\,N$. Thus, for example, the only ring modes having a significant amount of excitation for $N = 16$ are $0 \leq n \leq 12$, and of these, the greatest excitation occurs for the lower order ring modes.

VIBRATION RESPONSE EVALUATION

A digital computer program was developed for numerical evaluation of the frequency Eq. (2), the response Eq. (22), and the joint acceptance Eqs. (30)-(37). For each of the various environments considered, a normalized acceleration response spectrum was computed at 100 discrete frequencies per decade for the frequency range of 10 to 1000 Hz. From these discrete responses, a continuous graph of the response spectrum was constructed through the use of a plotting routine included in the program. The choice of 100 logarithmically spaced frequencies per decade provided sufficient resolution of the spectrum curves for a minimum of computing time, which was 5 to 10 min per case.

Response spectra were obtained for boundary-layer turbulence at Mach 1 and Mach 2, for a reverberant acoustic field, and for five acoustic duct correlation patterns. In these cases, the damping of each mode was chosen as 3-1/3 percent of critical damping so that $Q_{mn} = Q = 15$. For purposes of comparison, response spectra for boundary-layer turbulence at Mach 1 were also determined for $Q = 5, 25$. The computed response spectra are shown in Figs. 17 through 21.

69
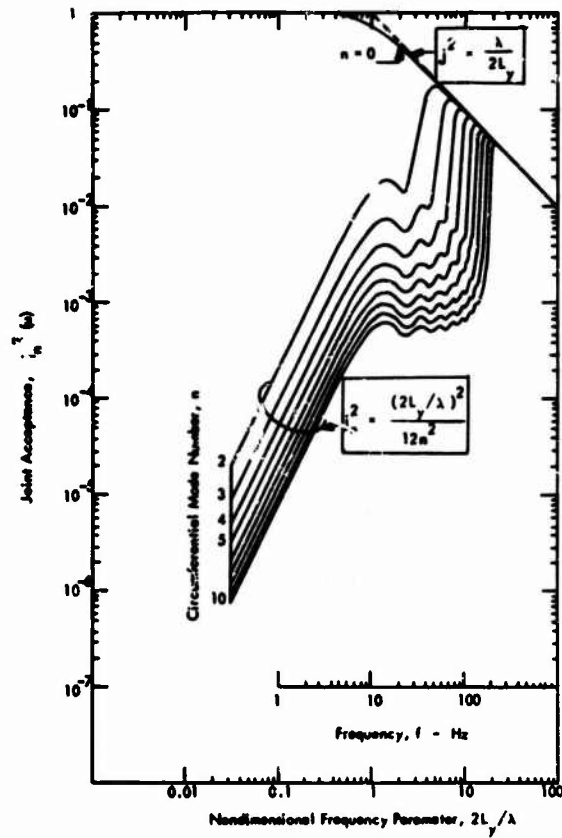
Fig. 16. Joint acceptances of circumferential ring modes of cylinder for reverberant acoustic field
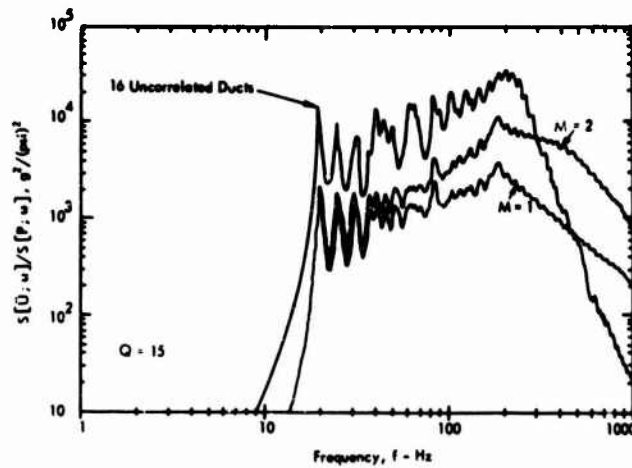
Fig. 17. Cylinder response to boundary-layer turbulence, at Mach 1 and 2 and 16 uncorrelated ducts
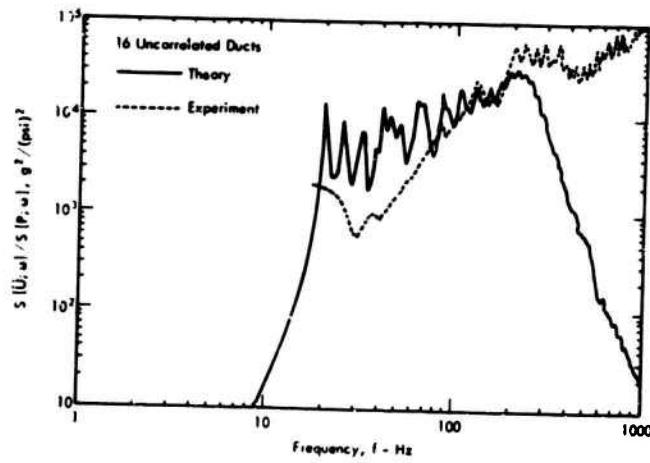
Fig. 18. Comparison of theoretical and experimental
response for 16 uncorrelated ducts
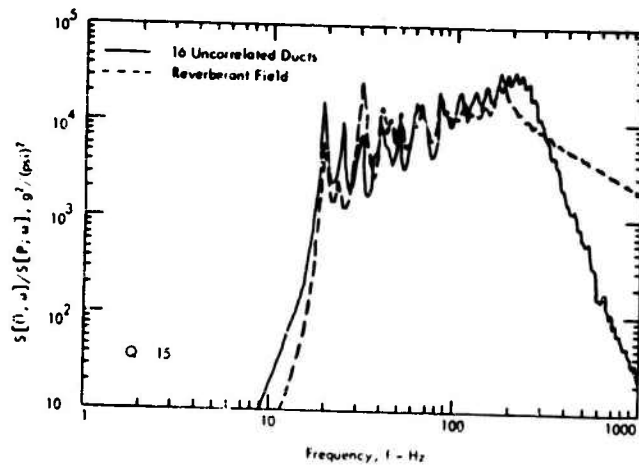
Fig. 19. Cylinder response to reverberation
acoustic field and 16 uncorrelated ducts
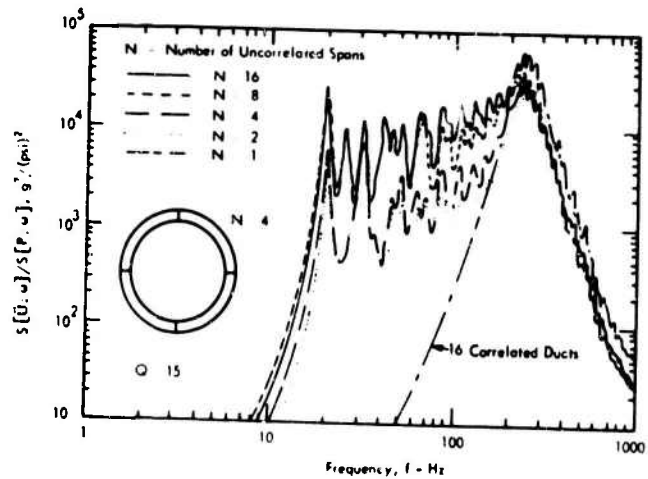
Fig. 20. Cylinder response for various duct
correlation patterns, with 16 ducts oper-
ating (all ducts within a span are corre-
lated; only adjacent ducts can be correlated)

71
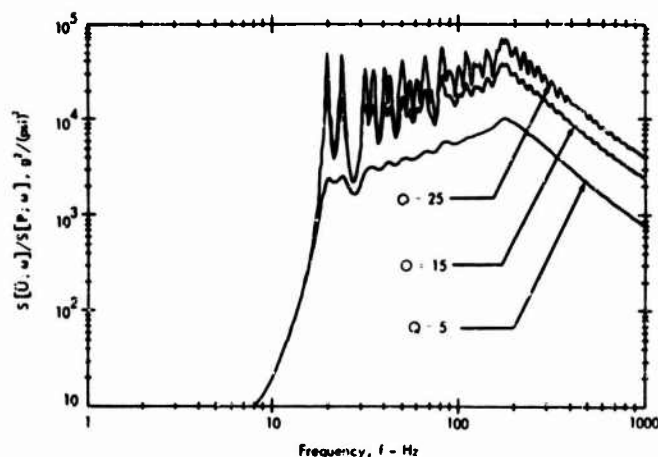
Fig. 21. Cylinder response for boundary-layer
turbulence at Mach 1 for three values of damping

The analytical response spectra are seen to be distinctly modal in character in the low-frequency range. This results from the fact that the resonance frequencies of the lower order modes are well separated as shown in Fig. 4. At the higher frequencies, the overlapping of the modal bandwidths produces a nonmodal type of response having a relatively smooth spectrum. The modes which contribute significantly to the response at any frequency f have resonance frequencies lying in a narrow frequency band of width f/Q centered on frequency f. In general, the greater the number of modes in this band, the greater is the response level at f. Thus below 175 Hz, the response spectrum levels increase with frequency because of the increasing modal density as defined by Eq. (3); and the response levels are maximum near 175 Hz where the modal density is largest. Beyond this frequency, the modal density is constant and the theoretical decrease in response is controlled by the joint acceptance functions.

The response spectrum for 16 uncorrelated acoustic duct fields ($N = 16$) is shown in Fig. 17. The significant feature of this spectrum is that above about 250 Hz, the spectrum levels are roughly proportional to f^{-5}. The joint acceptances of the ring modes $0 \leq n \leq 12$ lie in the range $1/160 \leq j_n^2(\omega) \leq 1/16$, with $j_n^2(\omega) \leq 1/160$ for $n \geq 13$; and hence only the modes $n \leq 12$ can have a significant response. With n so restricted, the near resonance modes at any frequency $f > 250$ Hz correspond approximately to a single value of m as can be seen in Fig. 4. For example, at 500 Hz the dominant modes are $m = 19$ and $0 \leq n \leq 12$. Thus, the theoretical

high-frequency responses must follow the variation of $j_m^2(\omega)$ with frequency where m is also frequency dependent. For frequencies $f > 250$ Hz, $f \doteq f_{m0}$, and from Eq. (2) $f_{m0} \doteq 175 [1 + 0.50 (m/10)^4]^{1/2}$. From Eq. (36), the maximum value of $j_m^2(\omega) = \{(2/m\pi)/[1 - (2L_x f/mc_0)^2]\}^2$. These two expressions define the variations of $j_m^2(\omega)$ and m with frequency; and their numerical evaluations would show the high-frequency roll-off seen in Fig. 17.

A comparison of the theoretical response spectrum and the spectrum obtained experimentally in the SAL facility is shown in Fig. 18 for the case of 16 uncorrelated ducts. The normalized experimental spectrum was obtained by averaging the measured responses at several locations on the SLA. The agreement is reasonably good except in the high frequency range above 300 Hz where the actual responses tend to follow mass law. To resolve this difference, it would be necessary to study both the type of structural response that occurs in this frequency range and the experimental acoustic correlation functions. Similar experimental data were obtained for two uncorrelated spans ($N = 2$), and in this case the agreement between theory and experiment is very good below 300 Hz with a similar mass law response at the high frequencies.

The response spectra for boundary-layer turbulence at Mach 1 and Mach 2 are compared in Fig. 17 with the response spectrum for 16 uncorrelated ducts. For $N = 16$, the ducts are more efficient in generating structural vibration than boundary-layer turbulence in the lower frequency range. Response levels are

72

greatest when the pressure correlation lengths match the elastic half wavelengths, which is approximately the condition for the lower order modes for duct excitation. The aerodynamic correlation lengths are much shorter than the elastic wavelengths of the low-order modes, thus causing a lower response than acoustic excitation. Theoretically, the reverse situation is true at the higher frequencies. The axial coincidence frequency for Mach 1 is $f_c = 14.1$ m, and for Mach 2, $f_c = 22.8$ m. Comparing these frequencies with the resonance frequencies shown in Fig. 4, it is seen that for frequencies above 250 Hz, all of the modes are above coincidence and the axial joint acceptances and responses roll-off between f^{-1} and f^{-2}. The above-coincidence condition for turbulence excitation differs from that of acoustic excitation in that the aerodynamic field is not well correlated over the surface of the shell as are ideal acoustic waves.

The theoretical responses to 16 uncorrelated ducts and a reverberant acoustic field are compared in Fig. 19. Except for differences in individual resonance peaks, the two response spectra are nearly equal below 200 Hz. Measured responses for these two forms of acoustic excitation indicate a similar result with the one-third octave band responses to a reverberant acoustic field being slightly higher (Eq. (3b)) than for the duct excitation. Above 300 Hz, the theoretical response to a reverberant acoustic field rolls off as f^{-1} in contrast to that for duct excitation. In practice, this large difference in the two responses does not appear, however. The high-frequency variation of the response to a reverberant field can be predicted easily as follows. Above 300 Hz, the resonance frequencies of all the near resonance modes lie above the acoustic coincidence frequency. Thus as shown in Figs. 14, 15, and 16, $j_m^2(\omega) j_n^2(\omega) = \lambda^2/8L_x = c_0^2/8L_x^2 f^2$. Thus Eq. (22) reduces to the form

$$\frac{S[\ddot{U};\omega]}{S[P;\omega]} = \frac{c_0^2}{8L_x^2 f^2 (\mu g)^2} \sum_{mn} \beta_n H^2 \left(\frac{f_{mn}}{f}\right) .$$

Let $\delta f (= df/dN)$ denote the frequency separation between resonances and let $\beta_n = 1$. This equation can then be rewritten as

$$\frac{S[\ddot{U};\omega]}{S[P;\omega]} = \frac{c_0^2}{8L_x^2 f^2 (\mu g)^2} f \frac{dN}{df} \sum_{mn} H^2 \left(\frac{f_{mn}}{f}\right) \frac{\delta f}{f} .$$

Since the modal density dN/df is constant above 180 Hz, the summation can be replaced by an integral over the resonance frequencies, giving as an approximation

$$\frac{S[\ddot{U};\omega]}{S[P;\omega]} = \frac{c_0^2}{8L_x^2 (\mu g)^2} \frac{1}{f} \frac{dN}{df} \int_0^\infty H^2(\Omega) d\Omega$$

$$= \frac{c_0^2}{8L_x^2 (\mu g)^2} \frac{1}{f} \frac{dN}{df} \frac{\pi Q}{2} .$$

Thus, the high-frequency response spectrum for reverberant acoustic excitation is proportional to f^{-1} as shown in Fig. 19.

The effect on response of using different duct correlation patterns is shown in Fig. 20. For $N = 1$, the sound fields in all ducts are correlated giving a uniform distribution of acoustic pressures around the circumference; and as a result, the ring bending modes cannot respond theoretically, and the low-frequency response is negligible. As the number of uncorrelated spans N increases towards $N = 16$, the low-frequency response increases. The high-frequency mass law effect shown in Fig. 18 is expected to be similar in practice for all N.

The theoretical effect of various values of damping on response is shown in Fig. 21 for boundary-layer turbulence at Mach 1. The low-frequency modal response spectrum is proportional to Q^2, while the high-frequency nonmodal type of response is proportional to Q.

CONCLUSIONS

The theoretical results indicate that acoustic testing with 16 uncorrelated duct fields provides the capability for simulating vibration response to in-flight environments over a broad frequency range. For the lower frequency range, the predicted laboratory and flight responses shown in Fig. 17 can be aligned by proper choice of the acoustic spectrum level and by shaping of this spectrum. At the higher frequencies, the analysis gives a better prediction of response to a reverberant field excitation than for duct excitation. Measured responses for these two acoustic environments are similar in the high-frequency range; and furthermore, Figs. 17 and 19 show that analytically the responses to a reverberant field are similar to those for boundary-layer turbulence. Thus computed responses for a reverberant field and turbulence might be used to determine the high-frequency spectrum level required for response simulation when employing the ducts. This should give a high-frequency acoustic test spectrum level which is nearly equal to the in-flight pressure spectrum level. The implication of these conclusions is that the

73

response levels of the lower order structural modes are more sensitive to pressure correlation lengths and patterns than are the higher order modes.

Although the analysis procedure developed for this study was designed only to compare responses for different fluctuating pressure environments, there is a natural interest in using this tool as an absolute response predictor when it appears to be valid. The comparisons between theoretical and measured responses in the lower frequency range indicate that the analysis method has reasonable engineering accuracy for acoustic environments for the lower order modes. Measured vibration responses of the SLA for Spacecraft 9 flight also agree very well with computed responses for boundary-layer turbulence below 200 Hz when the flight pressure spectrum level is assumed to be 125-130 db. In the latter case, the average slope of the measured vibration spectrum is nearly the same as predicted analytically. The Spacecraft 9 flight data cannot be used for comparison above about 200 Hz because of instrumentation cutoff.

To study the differences between measured and predicted responses at the higher frequencies, additional data will be required to define better the high-frequency dynamic characteristics of the structure and the acoustic pressure correlations of the test environments. For duct excitation, the theoretical responses of the higher modes decrease rapidly with increasing frequency because of the increasing number of plane acoustic wavelengths per elastic wavelength along the vehicle axis and because of the uniformity of the structural mode shapes. Under these circumstances, the pressures within many of the oppositely phased acoustic half wavelengths cancel, and the effective force driving the structure is small. This degree of input pressure cancellation does not occur,

however, if the vibration correlation areas are small compared with the pressure correlation areas or if the pressure correlation areas are small compared with the vibration correlation areas. At high frequencies the latter case is true for both the reverberant and the turbulence pressure excitations; and this explains why the predicted responses to these environments do not roll off as rapidly as for duct excitation. For the duct analysis, both the structure and the acoustic field within each duct were assumed to be well correlated. Since the SLA is composed of a set of panels mounted in a framework, it is likely that some panel decoupling will occur at high frequencies so that the vibration correlation areas may be limited to one or only a few adjacent panels. Thus, even if the acoustic field within each duct is well correlated, the high-frequency panel response levels will be much greater than those predicted for the coupled shell. Thus for more accurate high-frequency predictions, it would be desirable to have measured data for both the structural and pressure correlation areas.

Many refinements could be made in the digital computer program which were considered to lie beyond the scope of the present study; and it is felt that such refinements would greatly enhance the value of the existing program. The manner in which damping is included in the analysis could be improved by separating structural and radiation damping, and by allowing damping to be a function of frequency. As additional measured data become available for the turbulent pressure cross power spectra, more accurate treatment of the space correlation functions can be made. The subject program along with an existing similar program for a flat plate are capable of analyzing uniform structures. It is believed that still other efficient programs can be developed for stiffened shell and plate structures.

REFERENCES

1. "Structures and Mechanical Systems Course Number A-512S," North American Aviation, Inc., Apr. 1965

2. M. Heckl, "Vibrations of Point-Driven Cylindrical Shells," J. Acoust. Soc. Amer., 34(10): (1962)

3. A. Powell, "On the Response of Structures to Random Pressures and to Jet Noise in Particular," Ch. 8 of Random Vibration (S. H. Crandall, Ed.) (MIT Press, Cambridge, Mass.), 1958

4. L. Maestrello, "Measurement and Analysis of the Response Field of Turbulent Boundary Layer Excited Panels," J. Sound and Vibr., 2(3): (1965)

5. S. Gardner, "On Surface Pressure Fluctuations Produced by Boundary Layer Turbulence," Acoustica, 16, No. 2 (1965-66)

6. W. W. Willmarth and C. E. Wooldrige, "Measurements of the Fluctuating Pressure at the Wall Beneath a Thick Turbulent Boundary Layer," J. Fluid Mech., 14(Part 2) (1962)

7. M. K. Bull, J. F. Wilby, and D. R. Black-
    man, "Wall Pressure Fluctuations in
    Boundary Layer Flow and Response of
    Structures to Random Pressure Fields,"
    ○ University of Southampton AASU Rept.
    243, July 1963

8. C. Eckart, "The Theory of Noise in Con-
    tinuous Media," J. Acoust. Soc. Amer.,
    25(2):195 (1953)

9. A. Wenzel, "Surface Pressure Correlation
    Function for a Cylinder in a Diffuse

    Reverberant Sound Field," Wyle Lab. Res.
    Staff Rept. WR 66-14, 1966

10. M. Abramowitz and I. A. Stegun, Handbook
    of Mathematical Functions, American
    Mathematical Series 55 (U.S. Dept. of
    Commerce, National Bureau of Standards,
    Washington, D.C.), 1964

11. R. W. White, "Predicted Vibration Re-
    sponses of Apollo Structure and Effects of
    Pressure Correlation Lengths on Response,"
    Wyle Lab. Res. Staff Rept. WR 67-4, 1967

DISCUSSION

Mr. Dorland (NASA Manned Spacecraft Center): The detailed analysis that supports this presentation will be released in due time as a NASA contract report.

Mr. Ross (Aerospace Corp.): On the curve with the 16 uncorrelated ducts and the Mach 1 and Mach 2 modulator turbulence curves, I assume that the latter two curves refer to your convected turbulence model. If so, do you have any experimental verification or check on the relative position of these curves?

Mr. Eldred: At this time we do not have anything that we completely believe in. On the SLA we have measured vibration results from three pickups up to about 250 cycles where telemetering cuts everything off. It is just when the aerodynamic response becomes most interesting. We do know that we can duplicate the response in the 16-duct configuration, plus or minus a couple of decibels, throughout the whole one-third octave band spectrum at those three pickup locations. We know what sound pressure it takes to do that. What we do not have is any sound pressure measurements or point pressure measurements on the SLA; so the only things that we can compare with are the simple analytical models which are not always the most trustworthy things for the modern aerospace vehicle. We definitely need some data.

* * *

DATA HANDLING METHODS FOR LARGE VEHICLE TESTING

Daniel J. Bozich
Wyle Laboratories
Huntsville, Alabama

Environmental testing of large aerospace vehicle structural systems requires a
great number of measurements to describe adequately the response of the vehicle
system to simulated environments. These environmental control and response
measurements comprise the full range of acoustic, aerodynamic, vibration, and
thermal parametric relationships. Analog-digital data acquisition computer sys-
tems and digital data reduction techniques have made practical the large-scale
data processing tasks associated with several hundred response measurements ac-
quired on line from a single test.

Several techniques for acquiring periodic (sinusoidal), random, and aperiodic
(transient) response signals in real time utilizing on-line analog-digital computer
systems are reviewed, along with the associated digital data reduction methods.
Existing systems and their capabilities are discussed. Spectral densities and
three-dimensional resonant mode shape plots are a few of the examples shown of
digitally produced information from test data.

Recent developments in hardware and software techniques, which promise to revo-
lutionize the application of computers to large vehicle testing, are discussed. In-
cluded is a preview of the use of special integrated-circuit hardware and the use of
the fast Fourier transform (FFT) method for analyzing data.

INTRODUCTION

Measurement requirements for adequately
describing the responses of modern aerospace
vehicles to simulated mission environments
have increased dramatically over the past five
years because of the need for higher reliability
on space-oriented missions. Increased num-
bers of measurement transducers, signal con-
ditioning instrumentation channels, data ac-
quisition systems, and data processing systems
were required to handle this unprecedented flood
of data. More sophisticated analysis methods
were demanded, resulting in the extraction of
additional volumes of information from the
swelling mass of acquired data.

Five years ago, 60 channels of broad-band
data acquired in real time was considered a
large test requirement. Three years later,
data acquisition requirements had grown to ap-
proximately 540 broad-band response measure-
ments from a single test. Coupled with this
requirement was the need to perform close to
100 full-scale tests within a six-month period,
realizing about 20,000 separate response meas-
urements which were to be analyzed and reduced
within the same six-month period. To meet
these demands, new data processing conceptions
and data systems were developed.

Development of second-generation (transis-
torized) computer systems occurred concur-
rently with the rising need for increased quan-
tities of data. The widespread use of analog-
digital data systems began with the advent of
high-speed computer systems whose internal
processing cycle times were in the range of 2
μsec or less. As a result, high-resolution
analog-to-digital data conversion systems could
now be interfaced directly as "standard" peri-
pheral equipment to (on-line) digital computer
systems, thus creating analog-digital data sys-
tems. Prior to this development, analog-to-
digital data conversion was accomplished with
special systems which digitized and recorded
data directly (off line) onto digital magnetic
tape for later processing on digital computer
systems. These off-line systems were rela-
tively inflexible and expensive. Analog-digital
data systems have been subsequently designed
and constructed to be directly coupled (on line)
with several hundred wideband signal condition-
ing instrumentation channels, which are in turn
coupled with response measurement transducers
attached to test specimens.

This paper contains a brief summary of the
development of analog-digital data systems for
on-line automatic instrumentation calibration
and validation, on-line data acquisition, and

high-speed digital data analysis, interpretation, and summarization. Several examples illustrate the utility of analog-digital data systems for handling a broad range of test data-processing requirements.

DATA ACQUISITION REQUIRE-MENTS AND TECHNIQUES

The countdown preceding a large-scale environmental test requires the performance of several key checks to assure successful test response data acquisition. Check procedures include instrumentation system continuity and noise floor determinations, pretest instrumentation calibrations, quick-look verification of acquired test data, and, of course, final processing of all data as the final test validation. Comparing pretest and posttest calibration values locates instrumentation channels which become damaged or otherwise uncalibrated during the test. This simple automatic check helps identify and eliminate questionable data. Quick-look verification that test data were acquired properly aids in obtaining an early release of the test setup for subsequent tests.

Rapid computation of the first four statistical moments from short samples of data taken from each channel is a task which is easily accomplished by an on-line analog-digital data system. The evaluation of these quantities successfully performs the system continuity and noise checks, pre- and postcalibrations, and the quick-look data verifications for all data channels for all types of data. The first moment, the mean, evaluates the constant or dc bias component of the data sample. The mean-square fluctuation of the data sample about the mean value is represented by the second moment, the variance (the square root of the variance is the standard deviation — rms value — of the signal about the mean value). The symmetry of the amplitude probability density distribution about the mean value is evaluated by the third moment, the skewness. For symmetrical distributions, the skewness equals zero. Bottoming, or one-sided signal clipping, is an example of unsymmetrical amplitude distributions. The fourth moment, the kurtosis, evaluates the distribution of amplitudes about the mean value of the data sample. A normal distribution has a kurtosis coefficient of 3.0, whereas a sinusoidal signal yields a value of 1.5. Kurtosis coefficients between 1.5 and 3.0 indicate a mixed random and sinusoidal signal. Values greater than 3.0 indicate a preference of the amplitudes for values near the mean, such as would occur in signal overdriving (clipping) or nonlinear responses. A quick scan

of the computer printouts of these values for each data channel will check system noise, loose transducers, bad instrumentation, loose cabling, ground loops, signal overdriving, low signal levels and the like.

Parameters which must be known prior to data acquisition include actual maximum frequency range of each data channel, calibration sensitivity values of each channel, sinusoidal sweep rate (if applicable), channels whose joint statistical relationships are to be determined, minimum required analysis resolution bandwidth, and maximum estimated test specimen dynamic magnification factor. Details on the relationship of these parameters with respect to data acquisition utilizing on-line analog-digital data systems are contained in Ref. [1].

Random or transient response data which are to be crosscorrelated or otherwise jointly related must be acquired within the same time interval, that is, grouped so that they are sampled and submultiplexed together. Since all channels, in general, cannot be acquired at the same time, these channel groups need to be defined prior to the test to assure proper acquisition. References [1-3] contain detailed descriptions of the use of analog-digital data systems for random data acquisition.

Acquisition of sinusoidal sweep response data requires sampling the reference sweep oscillator signal simultaneously with each data signal. The use of a reference signal allows the accurate determination of the phase and amplitude relationships between all data channels. This method is similar to optical holography inasmuch as a monochromatic (sinusoidal) reference signal is used to establish the phase and amplitude relationships between all transducer signals at all frequencies. Three-dimensional displays can then be made of the motion of the test specimen at any frequency within the sweep range. At system resonances, these three-dimensional displays are the driven-resonant mode shapes of the specimen. References [1] and [4] contain detailed descriptions of the application of an analog-digital data system to sinusoidal sweep (or step) response data acquisition.

ANALOG-DIGITAL DATA SYSTEMS

Analog-digital data systems can be described as either on line or off line. An on-line system is capable of acquiring data directly from the test in real time and is also able to analyze and process these data. An off-line system comprises two systems: an on-line

real-time data acquisition system and a separate off-line data analyzing and processing system. The two sections of the off-line system can be remote from each other.

Another form of an off-line system uses an on-line analog data acquisition system which records the data in real time on analog magnetic tape. These data tapes are then played back to either an on-line or off-line analog-digital data system in either real time or scaled time; i.e., the tapes are recorded at a lower or higher tape speed to facilitate scaling the data frequency range to be compatible with the analog-to-digital (A/D) conversion rate of the on-line system. This type of data acquisition is very useful for short-duration transient (shock) tests, for remote hazardous test locations, and for either very low or very high frequency dynamic test data.

To date, several versions of each of the aforementioned types of systems are in operation. To cover even a few of these systems in detail would be a formidable task; therefore, only a general on-line system is discussed in this paper. Reference [1] contains detailed descriptions of a broad range of analog-digital data systems which can acquire random, sinusoidal sweep (or step), and transient (aperiodic) data coupled on line with either tests or analog magnetic tape recorders.

Figure 1 illustrates a signal conditioning instrumentation system which can condition multiple sets of matched transducers through the use of a multiple-position coaxial switching network between the transducers and the signal conditioning instrumentation. This scheme multiplies the number of data measurement points which can be handled by a specific

analog-digital data system. The analog outputs from the signal conditioning instrumentation are connected to the inputs of two multiplexers, as seen in Fig. 2. The multiplexers are connected to two A/D converters, which are in turn connected to two computer input control communication channels. The converted data are then transferred to computer core memory in blocks which are subsequently transferred as records onto digital magnetic tape for storage. Basically these two schematics cover the essentials of most on-line analog-digital data systems. The system illustrated in Figs. 1 and 2 is described in detail in Refs. [1] and [3].

The techniques for acquiring data properly are generally concerned with programming the multiplexer. Random and transient data require that groups of channels be sampled at the requisite rate sequentially within the group, repeating the sequence until the required number of samples (record length) has been obtained for each channel. Two or more multiplexers are usually sampled simultaneously and with similar group designations. Sinusoidal sweep (or step) data, on the other hand, are sampled using both multiplexers simultaneously such that the reference channel on one multiplexer is sampled with each channel of the requisite group, which is sequenced repeatedly until the required number of samples have been obtained from the group. The process is then switched to the next group and repeated until all channel groups have been sampled, after which the entire procedure is repeated until the test ends. Details of these procedures are contained in Refs. [1], [3], and [4].

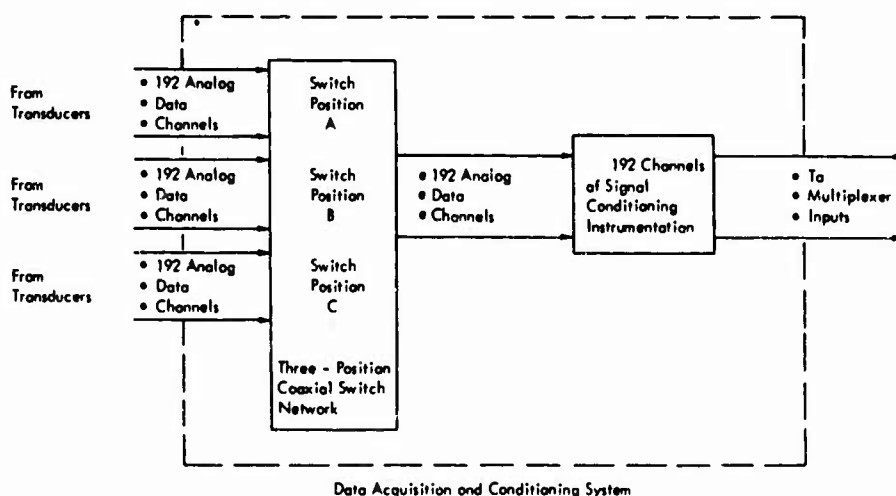Future on-line analog-digital data systems will comprise real-time data acquisition,

Data Acquisition and Conditioning System

Fig. 1. Multiple switching between matched sets of transducers to one set of signal conditioning instrumentation
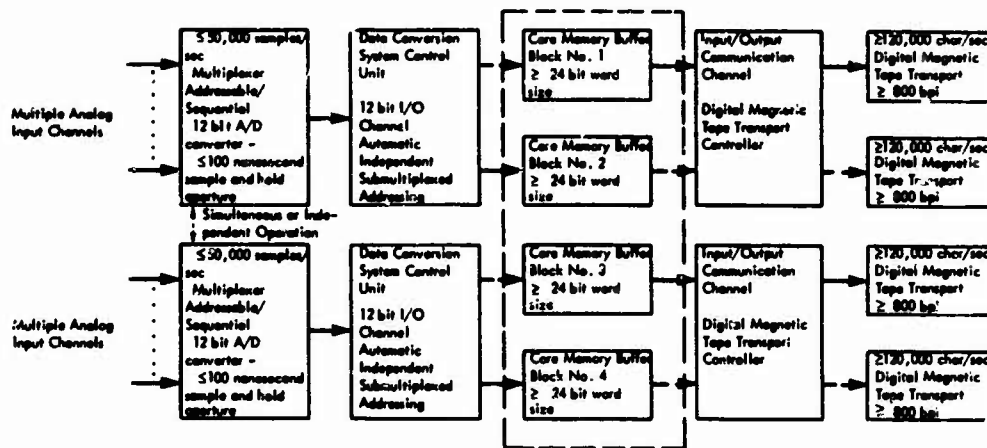
79

Fig. 2. Data flow diagram of up to 50,000-sample/sec analog-digital synchronous or independent dual-channel data acquisition using on-line digital computer control

real-time test monitoring and control, and both real- me and off-line data processing. Time sharing and multiprogramming, recent developments for second-generation computer systems and the faster integrated-circuit third-generation computer systems, can be used to advantage in performing real-time data acquisition and test control at the same time. However, only a limited amount of real-time data processing can be performed for a large test involving hundreds of response measurements.

Projected fourth-generation computer systems, wh'ch are discussed in Refs. [5] and [6], reveal new conceptions which will increase the data system's ability to perform real-time data processing. The fourth-generation system will be specialized to perform the various tasks involved with the entire on-line test process by the addition of replaceable "microprograms" to a computer system largely comprised of large-scale integration (LSI) logic hardware. The LSI systems will be from 10 to 100 times faster than present systems.

Micrograms, which are used to a limited extent in third-generation computer systems, are special hardware units which perform the operations of normally programmed subroutines at extremely high speed. These units can be stored like tape reels or disk packs and simply plugged into the system as required. In other words, production program subroutines are implemented in LSI circuitry. The micro-programs which include high-speed micro-memory buffer units have been termed "firmware" in Ref. [5] in contrast to the terms "hardware" and "software" in common usage today.

DIGITAL DATA REDUCTION

Analysis methods developed for use on digital computer systems have led to significant improvements in time-series data analysis techniques. A continuous random response signal becomes a discrete time series when the signal is sampled periodically such that there are equal time increments between the discrete samples. These time increments can be shortened (compressed) to scaled time increments within the computer system during processing, thereby allowing the data processing to proceed at the computer's higher internal operational speed. Since all computer operations are related to the system internal basic cycle time, it can be assumed that the faster the system, the faster the data processing. Of course, with the new developments of time sharing and multiprogramming ushered in with integrated-circuit third-generation computers, and the addition of peripheral hardware units (firmware) which add special high-speed algorithmic sub-routines to third- and fourth-generation computer systems, as needed, the future for digital data processing is virtually unlimited.

Time-series digital data analysis techniques have existed in the literature for quite a long time; however, these methods saw only limited use until high-speed computer systems were developed. Historically, the direct digital computation of PSD functions from response time-series data was slow compared with the lagged products method for computing time-correlation functions which are transformed to obtain the desired PSD functions. The latter PSD function was computed with constant frequency spacing

80

over the frequency range of the data, i.e., with a constant resolution bandwidth. Figure 3 is a PSD function obtained from a time-series data record using a straight lagged products correlation method. This particular PSD function was computed from a 32,000-sample time series obtaining a constant 6.65-Hz resolution bandwidth from 5 through 1000 Hz. The total computer time required for computation and plotting was about 7 min.

Constant-bandwidth analyses of acoustic and vibration responses do not match the response characteristics of the physical systems. Constant-bandwidth analyses become costly when analyzing wideband data which require narrow resolution bandwidths at low frequencies. A constant percentage resolution bandwidth is best suited for assuring equal resolution throughout the response frequency range. Therefore, a new analysis technique was developed which yields a constant resolution bandwidth in each octave; it starts with a specific narrow bandwidth at the lowest end of the frequency range, and then as the frequency doubles, the bandwidth within the next higher octave of the range doubles, and so forth until the upper frequency limit of the range is reached. This technique not only gives higher resolution at low frequencies but also gives essentially "equal" resolution at all frequencies. Reference [3] contains a detailed description of this "selective bandwidth" analysis technique. Figure 4 contains a PSD obtained by the selective bandwidth method from the same data used for Fig. 3. The computer time required was about 5 min. A comparison of Figs 3 and 4 quickly illustrates the increased resolution obtained at low frequencies

Fig. 4. PSD obtained by selective-bandwidth method, channel 2

without any apparent loss of information at higher frequencies.

References [7] and [8] describe a recently developed technique for obtaining Fourier transforms of discrete time-series data. This method, known as the fast Fourier transform (FFT), can be used to compute PSD's and cross-PSD's directly from time-series data extremely fast, in fact, much faster than the lagged products technique for most cases of interest. This method has been incorporated into the selective-bandwidth analysis program, resulting in a marked decrease in computer analysis time. Figure 5 is a PSD function of the same data

Fig. 3. PSD obtained by constant-bandwidth method, channel 2

Fig. 5. PSD obtained by fast Fourier transform selective-bandwidth method, channel 2

81

used in Figs. 3 and 4. The only difference between this PSD and that shown in Fig. 4 was the use of the combined FFT selective-bandwidth analysis program. The required computer time was about 2.5 min, which is one-half of Fig. 4's time. Future program refinements should reduce this time to about 1 min.

Figure 6 illustrates a selective-bandwidth PSD function of another response time series. The cross-PSD function of the data used for Fig. 4 and for Fig. 6 is shown in Fig. 7. Note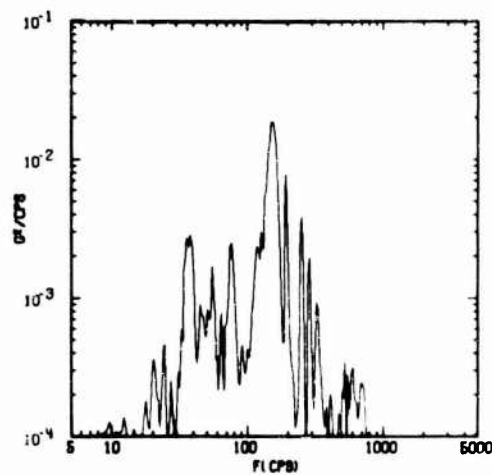 that the magnitude of the cross-PSD function, the phase angle magnitude, and the phase angle sign are plotted separately. The gain factor and phase angle, transfer functions and phase angle, spatial correlation function, and coherence function of these two sets of data can also be plotted, since they are all functions made up of different combinations of the PSD's and the cross-PSD.

Fig. 7. Cross-PSD obtained by selective-bandwidth method, channel 2 vs channel 3
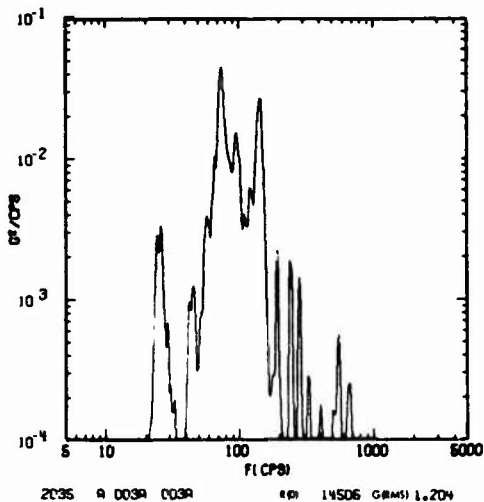

Fig. 6. PSD obtained by selective-bandwidth method, channel 3

The FFT selective bandwidth analysis program has the highly desirable added feature of obtaining a cross-PSD from the Fourier coefficients obtained in computing the PSD's for a pair of channels. In other words, a cross-PSD is obtained almost "free." The lagged products technique requires about four times the computer time to compute a PSD to obtain two PSD's and one cross-PSD; whereas the FFT technique requires only about twice the single PSD computation time for the same three functions. For example, the PSD's of Figs. 4 and 6 and the cross-PSD of Fig. 7 required a total of about 20 min of computer time using the lagged-products selective-bandwidth analysis program,
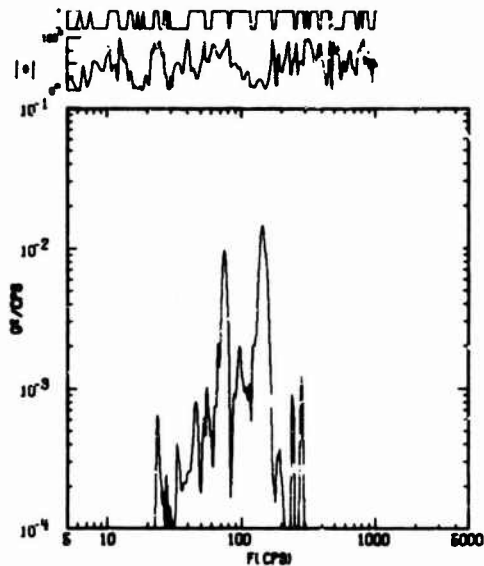
while the FFT selective bandwidth analysis program would require slightly more than 5 min.

A group of PSD's can be summarized by a single set of curves which depict the maximum value, minimum value, and average value in each bandwidth for all of the channels in the group. The PSD amplitude probability distribution of the separate PSD values of the group within each band could also be obtained, and the mean and some percentile PSD amplitude value other than the maximum, such as the 97.5 percent value, of the distribution would be determined. These summary response envelopes are used to set design and test criteria on similar structures, validate tests, review test results quickly, etc. Figure 8 illustrates a maximum, average, and minimum envelope plot for a set of three PSD's.

Another form of data summary is obtained from data of sinusoidal sweep (or step) tests. The data acquisition technique, described above and in Refs. [1] and [4], using the sinusoidal sweep (or step) oscillator as a reference signal which is sampled along with each data signal, allows the accurate determination of the relative response amplitudes and phases of all the transducers attached to a vibrating structure or located in a force field. Therefore, three-dimensional pictorial displays of the response at any or all frequencies within the sweep frequency range can be constructed. These three-dimensional response plots are
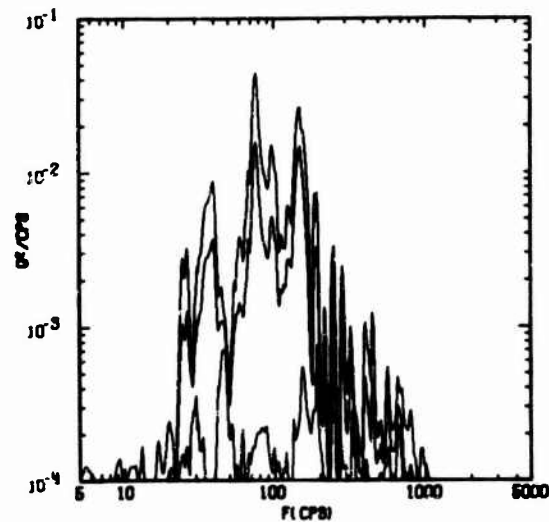
Fig. 8. Maximum, average, and minimum
envelopes of three PSD density plots

the driven mode shapes of the structure when
they are obtained at a resonant frequency of the
structure. Figures 9 and 10 show the first and
second normalized mode shapes of a uniform
flat rectangular honeycomb panel which was
pinned at the four corners and at the center
point of each side. Twenty-five evenly spaced
accelerometers were used to measure the ver-
tical responses of the panel, which were then
analyzed and subsequently used to construct
these figures. The vertical lines show the ac-
tual normalized amplitudes.

Figure 11 is an illustration of the second
vertical normalized resonant mode shape of a
complex telescope obtained from measured
data. These data, however, were obtained by
recording the responses of 15 accelerometers
and the sinusoidal sweep oscillator on analog
magnetic tape. This process was repeated four
times with the accelerometers in four different
positions. The analog tapes were played back
to the on-line analog-digital data system and
analyzed separately; then the four sets of data
were combined into the three-dimensional
driven mode shape shown in Fig. 11. This ex-
ample illustrates the accuracy and utility of the
data system for large vehicle tests.

The first lateral vibration mode of a large
space vehicle interstage cylindrical skirt struc-
ture is shown in rolled-out format from 0 to
360 deg in Fig. 12. One hundred and sixty

accelerometers were used to measure this re-
sponse mode. Note that the upper edge (right
side, z direction) is constrained to move only
laterally; thus there are only two zero cross-
ings, whereas the center motion shows the
classic figure 8 first bending mode of a cylin-
der as seen by the four zero crossings. The
bumps in the response surface are due to heavy
component equipment and supporting structure.

Another use of three-dimensional data
summarizing is shown in Fig. 13, which shows
the pressure distribution measured on the
rotor blade of a helicopter averaged over three
revolutions.

CONCLUSIONS

The accuracy and speed of digital computers
coupled with their ability to perform many tasks
and make numerous comparisons and decisions
automatically make analog-digital data systems
indispensable aids in large environmental tests.
The application of on-line analog-digital sys-
tems to environmental test response measure-
ments and the development of digital data anal-
ysis techniques are briefly reviewed in this
paper. Although far from exhaustive, it is
hoped that this brief introduction to digital data
handling techniques will encourage their in-
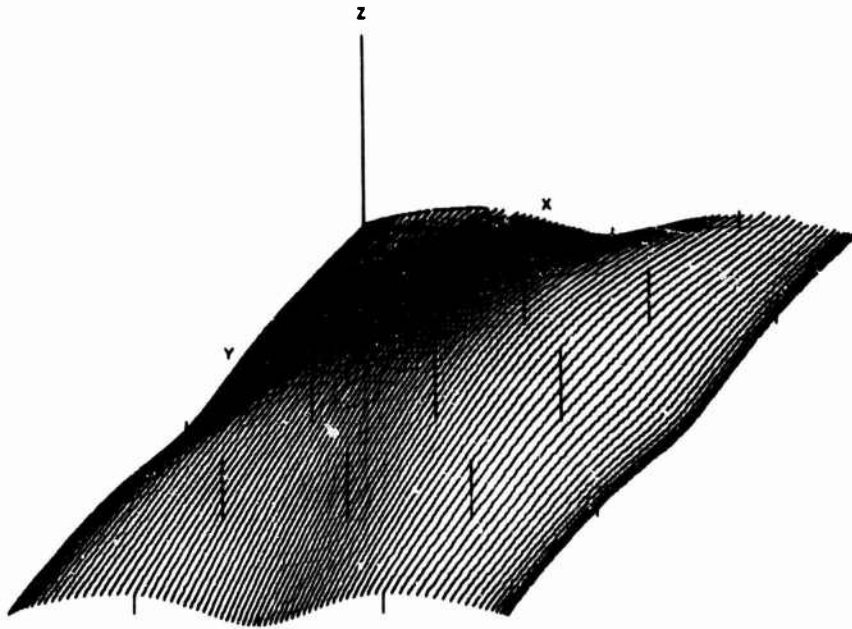creased use in future tests.

Fig. 9. Flat rectangular uniform honeycomb panel (pinned at corner and at midpoints of each side — 266.2-Hz, vertical resonant mode)
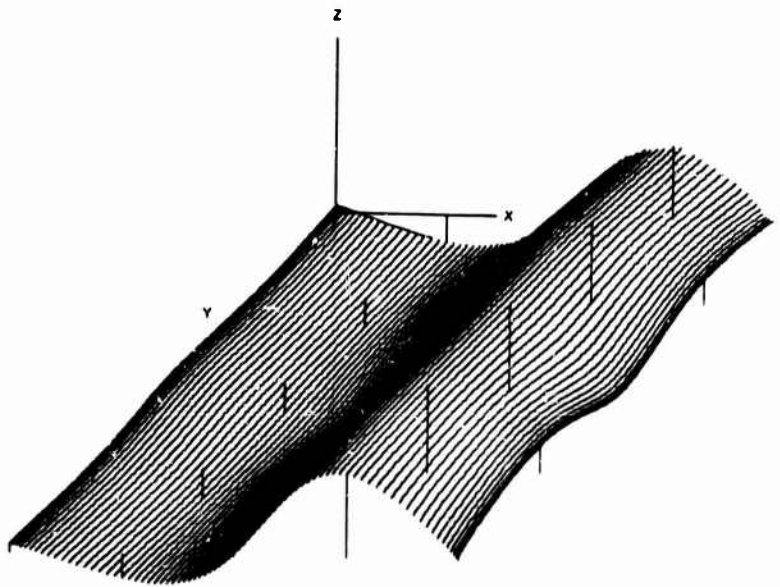
Fig. 10. Flat rectangular uniform honeycomb panel (pinned at each corner and at midpoints of each side — 420-Hz, vertical resonant mode)
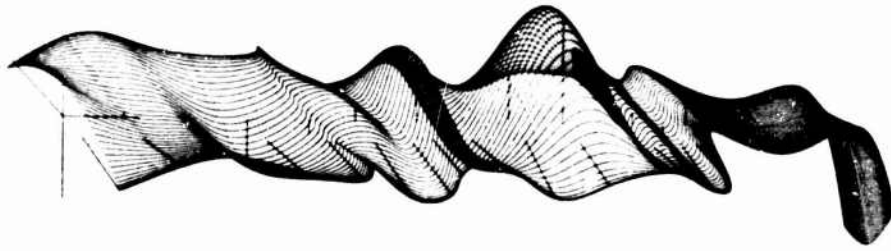
Fig. 11. Complex space telescope resonant mode at 160-Hz vertical acceleration (z axis)
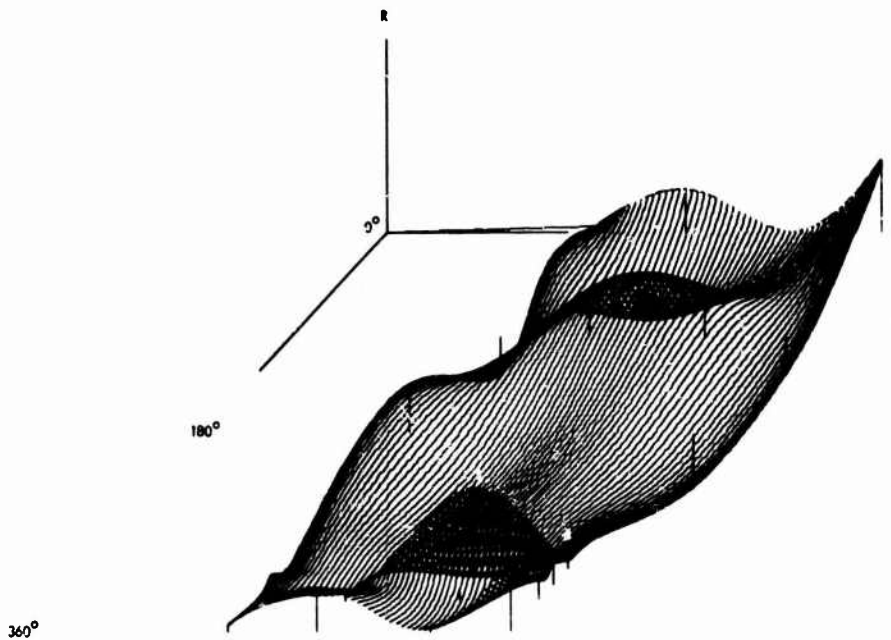
Fig. 12. Forward skirt -- 57-Hz, lateral resonant mode
(upper half of skirt unrolled 0-360 deg)

The future holds virtually unlimited applications for these systems. Time sharing, multiprogramming, firmware (or microprograms), megacycle sampling rates, etc., are the developments which will bring about the universal trend toward the increased use of analog-digital data systems on everyday problems. There are many applications of such systems, including on-line medical analyses of hospital patients; automobile engine trouble diagnosis; all types of environm l testing and monitoring; oil exploration; earthquake monitoring, analysis, and prediction; and on-line research and analysis of complex operations.

One of the most important advantages of analog-digital data systems is their ability to be programmed to summarize and categorize thousands of information records into a few summary plots or tables so that management decisions can be made in timely fashion. Increased use of data interpretation is needed since these systems can produce information faster than an army of engineers can digest it. Prevention of such an "information explosion" can be accomplished by using the system to make many important observations and decisions about the test results and present only summaries of the most interesting data.

85
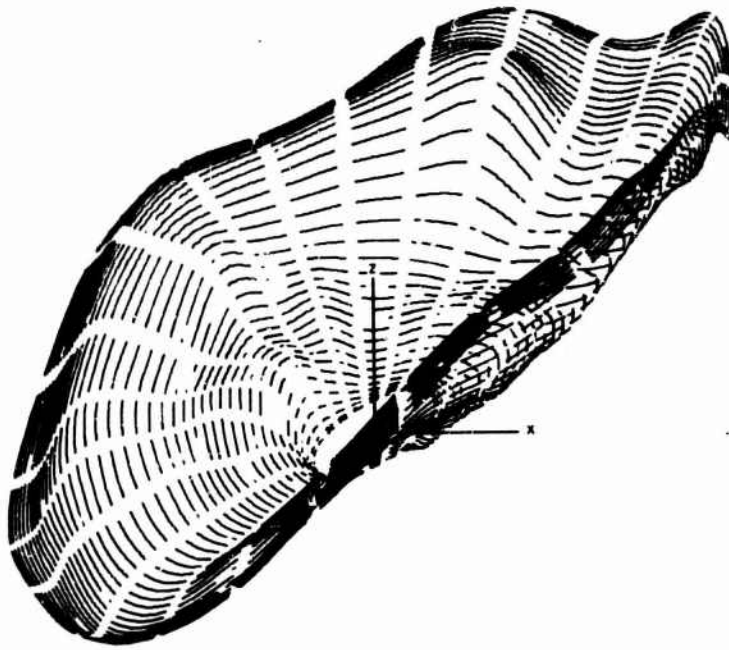
Fig. 13. Pressure distribution measured on the blade
of a helicopter, averaged over three revolutions

REFERENCES

1. D. J. Bozich, "Real-Time Acquisition of Acoustic and Vibration Data With an On-Line Digital Computer," paper 6.2-4-66, presented at the 21st Ann. ISA Conf. and Exhibit, New York, Oct. 24-27, 1966

2. J. S. Bendat and A. G. Piersol, Measurement and Analysis of Random Data (Wiley, New York), 1966

3. D. J. Bozich, "Digital Analysis of Saturn Environmental Test Response Data," Shock and Vibration Bull. 36 (Part 6):55 (1967)

4. D. J. Bozich, "Utilization of a Digital Computer for On-Line Acquisition and Analysis of Acoustic and Vibration Data," Shock and Vibration Bull. 35 (Part 4):151 (1966)

5. A. Opler, "Fourth-Generation Software," Datamation, 13(1):22 (1967)

6. G. M. Amdahl and L. D. Amdahl, "Fourth-Generation Hardware," Datamation, 13(1): 25 (1967)

7. J. W. Cooley and J. W. Tukey, "An Algorithm for the Machine Calculation of Complex Fourier Series," Mathematics of Computation, 19 (90):297 (1965)

8. W. M. Gentleman and G. Sande, "Fast Fourier Transforms-For Fun and Profit," Proc. Fall Joint Computer Conf., pp. 563-577, 1966

DISCUSSION

Mr. Smith (Martin-Marietta Corp.): I can certainly see the usefulness of the computer, particularly with respect to mode shapes, where it applies to such things as panels. But, on the entire vehicle where the control system interacts and we need accurate definition of the mode shapes, what kind of accuracy can you have with a system calibrated in the fashion that you have

described? Can you give me some idea of the accuracy on the orthogonality of the modes?

Mr. Bozich: I hope that people won't misunderstand what I meant by "mode shape." I put that in quotes because this system is not the true free vehicle. It is being driven, and the shape that we turn out is a resonant response

86

shape which includes the non-phase-related drivers. For instance, if you had eight shakers that were slightly out of phase, this would show up in the shape. If you can drive the vehicle so that these shapes do represent the true mode shapes, then I would expect that the measured mode shape on the low frequencies should show the orthogonality conditions. Again, this is just a conjecture; I do not think it can be proved in a real case.

Mr. Smith: Do you know if orthogonality checks have been performed on any of the modes?

Mr. Bozich: There are none that I know of to date. We have had only this rectangular panel to work with but we would like to work on the problem further.

*   *   *

DEVELOPMENT AND VERIFICATION OF THE VIBRATION
TEST REQUIREMENTS FOR THE APOLLO
COMMAND AND SERVICE MODULES

Dan E. Newbrough
General Electric Company
Houston, Texas

Richard A. Colonna
NASA Manned Spacecraft Center
Houston, Texas

and

James R. West, Jr.
North American Rockwell Corporation
Downey, California

Demonstration of the structural capability of the Apollo command and service modules for withstanding flight environments necessitated extensive vibration test programs, of which a significant part was full-scale command module and service module acoustic tests. Verification of vibration test requirements brought about several interesting problems in flight test simulation. Analyses and manipulations of the acoustic test data resulted in some unique Apollo vibration criteria and procedures. The documentation of these techniques is considered important in the development of manned spacecraft vibration criteria.

At Apollo liftoff and during atmospheric flight, the command and service modules are exposed to intense noise which produces high-amplitude structural vibration. The design and test vibration criteria for this environment were derived originally by analytical prediction methods. Acoustic tests of the command and service modules structural test vehicles conducted in the North American Aviation, Inc., Los Angeles Division acoustic test facility demonstrated that the responses were generally greater than predicted and that increases in vibration test requirements were required in many cases.

A brief narrative of the developments leading to the present vibration environment definition for the command and service modules is presented. The basis for the vibration environment initially defined is discussed; the acoustic test programs carried out on the command and service modules are described briefly; the vibration criteria redefinition resulting from the acoustic tests is examined; and data obtained from unmanned Apollo flights are presented.

INTRODUCTION

The Apollo spacecraft is designed to fly on the free world's largest rocket propulsion system. Pressure fluctuations generated by these launch vehicles at liftoff and by aerodynamic flow during atmospheric flight produce severe structural vibration. The random aerodynamic excitation patterns and the complex structure of the spacecraft make accurate prediction of the vibratory response very uncertain. Initial vibration criteria were derived from analytical predictions and extrapolation of flight data from other programs. Subsequent refinements to these criteria have been obtained by conducting Apollo spacecraft acoustic tests and by acquiring flight acoustic and vibration data on three unmanned Apollo spacecraft. The spacecraft

acoustic tests were conducted in the North American Aviation, Inc., Los Angeles Division (NAA LAD) acoustic test facility on command module (CM) and service module (SM) structural vehicles with mass-simulated equipment. The response data obtained from these tests demonstrated the need for substantial increases in the vibration levels for much of the Apollo spacecraft and brought about a major requalification test program.

This paper describes the Apollo spacecraft launch and boost vibration environment and the developments leading to the present Apollo vibration criteria. It discusses the use of ground acoustic tests to develop and substantiate qualification test requirements, and compares the ground test results with flight data.

89

SPACECRAFT

The CM, the SM, and the spacecraft lunar module adapter (SLA) are shown in Fig. 1. The CM is the spacecraft control center, housing the flight crew, the equipment to control and monitor the spacecraft systems, and the equipment required for the comfort and safety of the crew. As seen in Fig. 2, the CM consists of two structures, an inner pressure cabin of aluminum and an outer structure of stainless steel which supports the ablative heat shield. Between these two structures are unpressurized compartments which contain the earth landing equipment and most of the CM reaction control system (RCS). Insulation is provided on the inner surface of the heat shields.
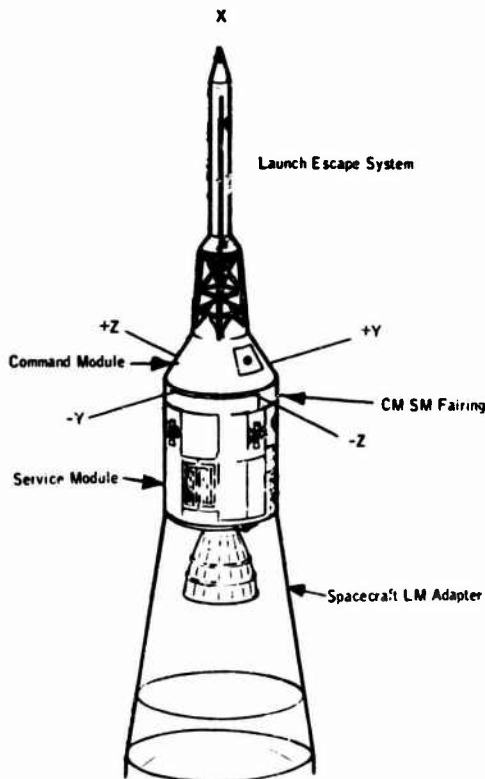

Fig. 1. Apollo CM, SM, and
SLA flight configuration

The SM (Fig. 2) contains the service propulsion system (SPS) engine and propellants and the SM RCS cryogenic storage provisions, fuel cells, etc.; it provides the support surface for space radiators for the electric power and environmental control systems. The SM consists of forward and aft bulkheads connected by six shear beams radially disposed about a central cylinder. These beams support the 1-in.-thick honeycomb sandwich outer-shell panels. The sectors between the radial beams are used for propellant tanks and equipment installation. The central cylinder and aft bulkhead support the SPS engine and two large SPS helium tanks.

The SLA (Fig. 3) provided the structural connection between the SM and the launch vehicle. Its primary purpose is to house the lunar module (LM). The construction of the SLA consists primarily of attachment rings and honeycomb sandwich panels 1.7 in. thick.
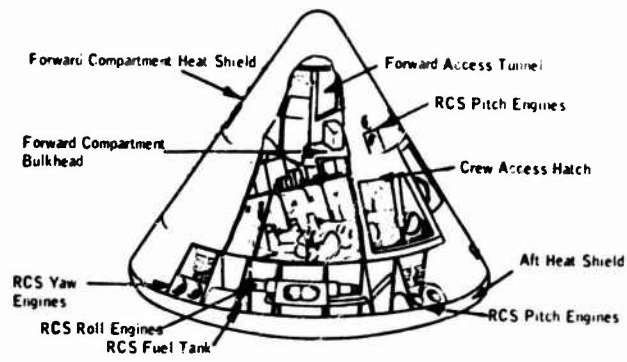
FLIGHT VIBRATION ENVIRONMENT

Acoustic and Aerodynamic Fluctuating Pressures

During the atmospheric portion of an Apollo flight, the CM and SM structure is exposed to intense aerodynamic and acoustic excitation, which produces high-amplitude structural vibration. At liftoff, intense noise is generated in the turbulent boundary between the rocket engine exhaust and the surrounding atmosphere and is radiated to the surface of the spacecraft. After liftoff, the radiated engine noise diminishes rapidly with time as the vehicle moves away from the reflective surface of the launch pad. The engine noise on the spacecraft at liftoff is not as severe as the aerodynamic noise encountered later in flight, except on the aft portion of the SLA. As the spacecraft velocity increases, the aerodynamic excitation resulting from turbulent airflow over the spacecraft surfaces increases. Near sonic velocity, airflow separations occur on the SM, causing a transient peak in the sound pressure levels (SPL's). Beyond sonic speed, steady flow conditions are reestablished, with a resulting reduction in the fluctuating pressure level. However, as the dynamic pressure increases, the fluctuating pressure levels again increase until another peak value is obtained near Mach 1.6. The noise levels then diminish as the spacecraft rapidly climbs out of the atmosphere.

Command Module

Data acquired from three fluctuating pressure transducers on an early Apollo boilerplate vehicle (BP-13) flown on a Saturn were used to formulate the CM aerodynamic noise criteria. The average one-third octave band SPL's of these data are shown in Fig. 4. These maximum levels occurred at approximately Mach 1.55, near the max Q region, and compared favorably with data measured during wind-tunnel model tests.

90

Forward Compartment Heat Shield
Forward Access Tunnel
RCS Pitch Engines
Forward Compartment Bulkhead
Crew Access Hatch
RCS Yaw Engines
Aft Heat Shield
RCS Roll Engines
RCS Fuel Tank
RCS Pitch Engines

COMMAND MODULE

Forward Bulkhead
Sector Equipment
SM to CM Fairing
Fuel Storage
Oxidizer Storage
Oxidizer Storage
SM RCS Motor (4 sets)
Radial Web Beam
He Tanks
H₂ TANK
O₂ Tanks
Fuel Cells
H₂ TANK
Fuel Storage
Aft Bulkhead

SERVICE MODULE

Fig. 2. Apollo general configuration

Adapter

S-IVB Instrument Unit
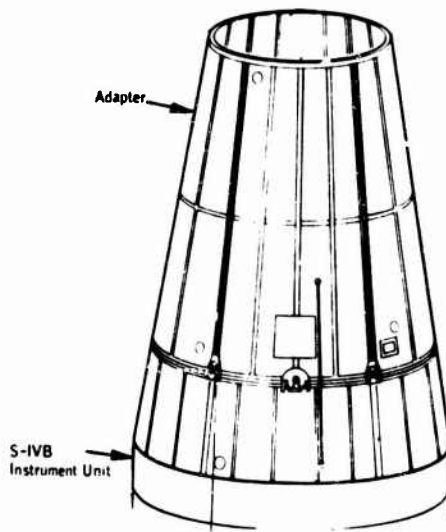
Fig. 3. Spacecraft LM adapter

91
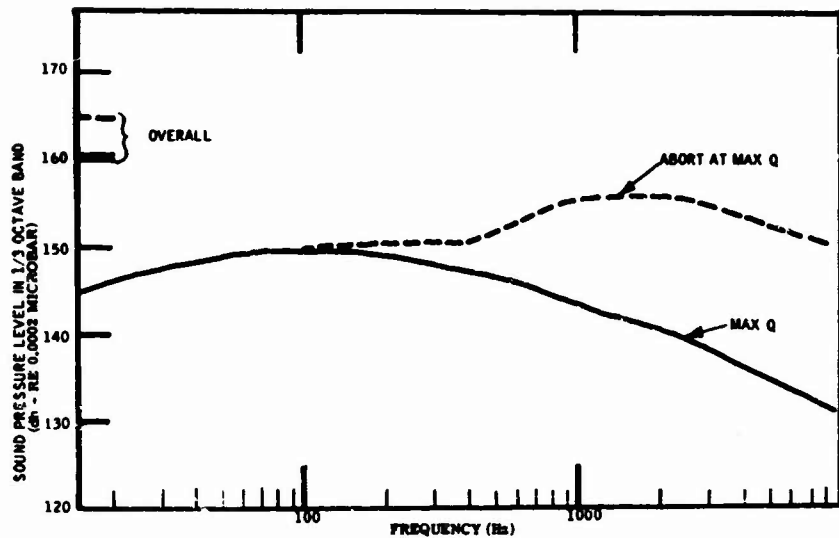
Fig. 4. CM external flight noise levels

It was also necessary to determine the CM noise level during an abort at or near the max Q region as a special case of the atmospheric flight criteria. Data taken during abort tests were analyzed and used as the basis for the max Q abort levels shown in Fig. 4. The lower frequency portion of the abort spectrum shows little change, but in the higher frequency SPL's are increased because of the presence of the added turbulence generated by the launch escape system (LES) rocket motor exhaust impinging directly on the CM surface.

Service Module

A large quantity of aerodynamic noise data on the SM was obtained from wind-tunnel tests and boilerplate flights. A typical plot of overall SPL vs body station is shown in Fig. 5. The general trend of the fluctuating pressure levels measured for Mach 1.6 is presented; local variations from turbulent flow around protuberances, such as the RCS engines, are not included. The spectral characteristics of the noise data at various body stations were found to be similar.

Fig. 5. Variation of aerodynamic noise along Apollo spacecraft, Mach 1.6

92

It was assumed that the integrated vibration response of the SM was the result of a spatial average exterior sound pressure field instead of local pressures at any SM point. Reference [1] presents the analyses used in arriving at th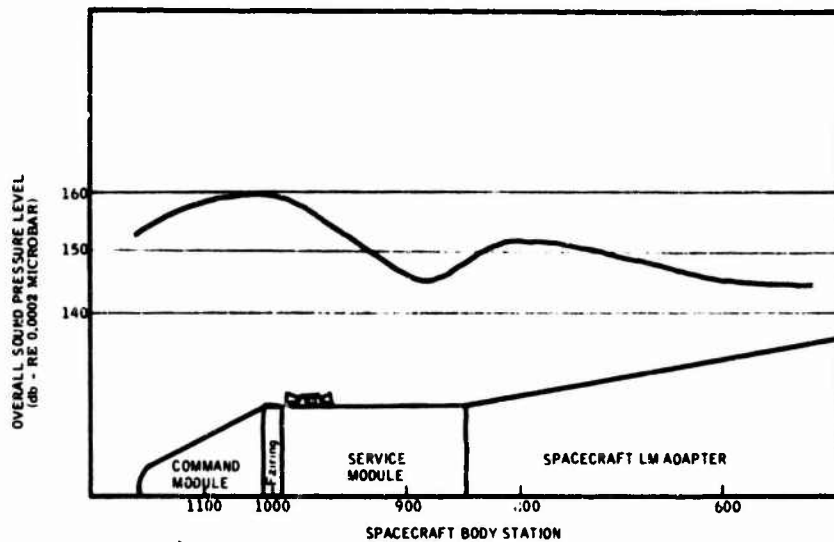is assumption. The overall spatial average SPL of 152 db was used as the SM external aerodynamic noise criteria for the critical max Q condition. The spectrum derived for the SM aerodynamic noise criteria is shown in Fig. 6.

The boilerplate flight data were also analyzed to determine the spectral characteristic of the transient peak noise level associated with flow separation near Mach 1. The spectral characteristic of this transient was found to be similar to that of the max Q condition over most of the SM surface area, exhibiting an average overall SPL 4 db higher than the max Q level. Therefore, the average noise levels associated with the Mach 1 transient condition were determined to have the same spectral shape as the max Q condition and to have an overall SPL of 156 db.

Spacecraft LM Adapter

Data from Apollo scale-model wind-tunnel tests were analyzed to determine SPL variations for the region of the SLA. Comparisons were made for all recorded Mach numbers of the data from four transducers mounted on the model along the length of the SLA section.

A time scale was constructed from nominal Saturn trajectory Mach numbers vs time. The resulting plot of the SLA overall SPL's vs time for the four test transducers, shown in Fig. 7,

indicates that the peak aerodynamic SPL's for all SLA transducers occur at about 63 sec after liftoff or at Mach 1.0. Figure 8 presents the spatial average noise levels of the one-third octave band SPL data for Mach 1, adjusted to the full-scale vehicle configuration.

Vibratory Response Predictions

Initial vibration criteria for the spacecraft were developed by analytical methods using data from other aerospace programs, scale-model wind-tunnel results, and accepted statistical techniques for predicting the vibration environment of a vehicle exposed to an acoustic field. The primary prediction technique used was that developed by Mahaffey and Smith [2] from measured vibrations of aircraft structure in jet-engine noise fields. This technique allows grouping of data according to the types of structure from which they were obtained, and allows the vibration environment for each type to be defined in terms of percentile or confidence intervals. The resulting spacecraft vibration criteria are presented in Fig. 9.

VEHICLE ACOUSTIC TEST PROGRAM

SM 007 Acoustic Tests

The SM 007 acoustic tests were conducted on a production SM in the NAA LAD acoustic test facility. Figure 10 is a diagram of the test setup. For the SM test, equipment weighing 5 lb or more was mass simulated except on the radial beams, where no mass simulations were included. No attempt was made to represent
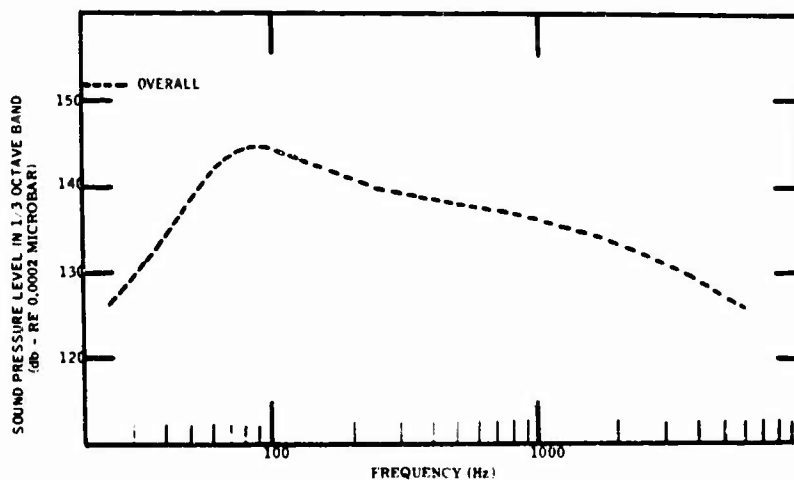

Fig. 6. SM external acoustic spectra, max Q flight

93
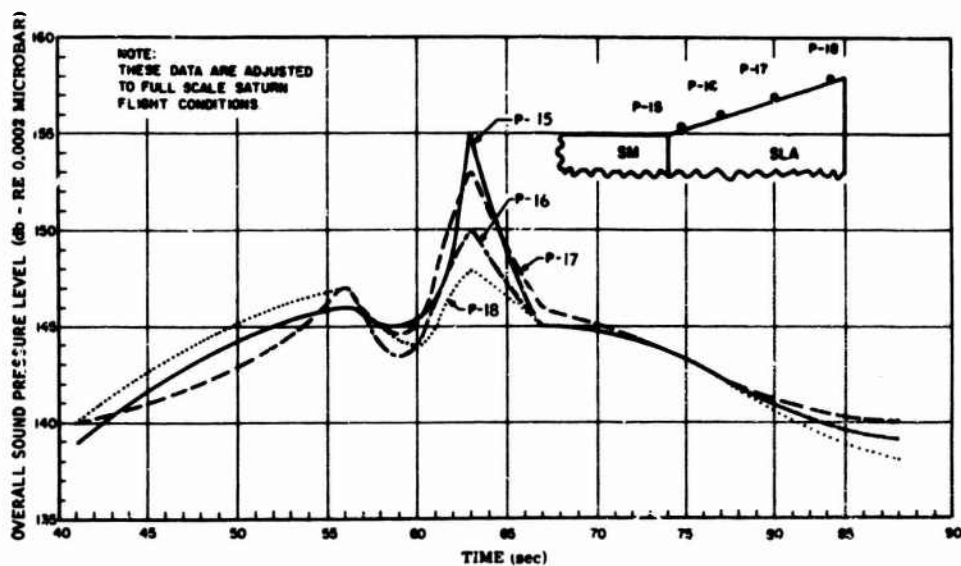
Fig. 7. SLA exterior SPL variation during launch and boost
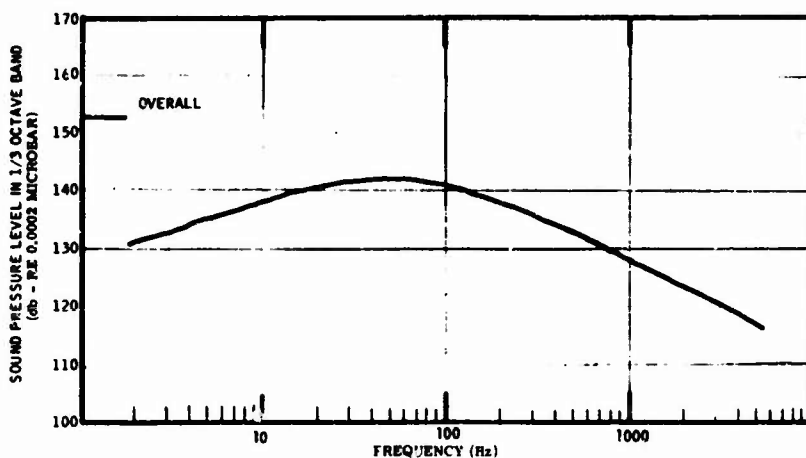
Fig. 8. SLA average external acoustic spectra, Mach 1

wiring or plumbing except on the aft bulkhead. Mass simulations of the fuel cells and cryogenic tanks were attached to the basic equipment mounts. The SPS propellant tanks were of aluminum construction and contained water, simulating a 20 percent fuel load. Acoustic insulation of the SM forward and aft bulkheads was used to reproduce end conditions of the CM to SM area and SM to SLA area. A 2-g static load was imposed on the SM to simulate the acceleration loading condition at max Q. A total of 252 vibration response measurements were made on primary and secondary structures, and 15 microphones were positioned around and inside the SM.

The SM 007 structure was exposed to 31 sinusoidal and random acoustic tests that varied in overall SPL from 130 to 160 db. Figure 11 presents acoustic spectra for the highest noise levels obtained during the tests. For comparison, the predicted transonic and max Q fluctuating pressure spectra are also shown. The SM circumferential acoustic field was not uniform, varying as much as 7 db.

After the final test run, inspection revealed cracks in some of the radial beam shear webs and in some of the equipment support brackets of the RCS panels. In addition, several broken tension straps between radial beam inner caps

Fig. 9. Original CM and SM
vibration criteria

95

Fig. 10. SM 007 acoustic test setup
(external microphones are shown)

Fig. 11. Comparison of SM maximum
acoustic spectra, flight vs test

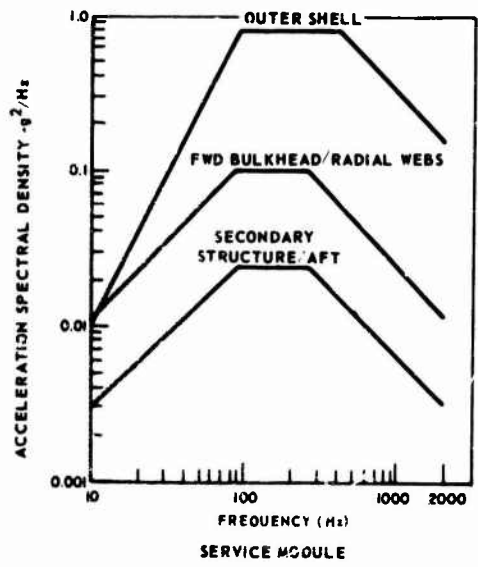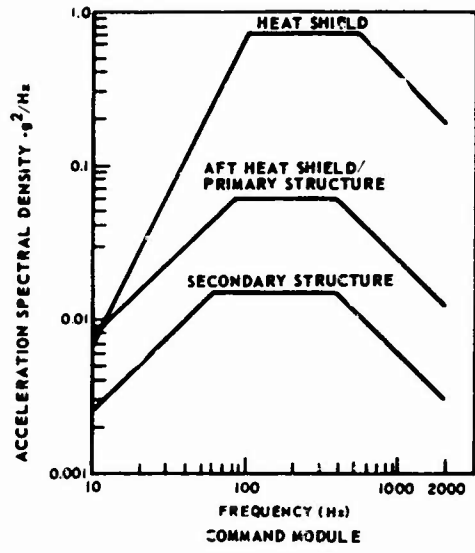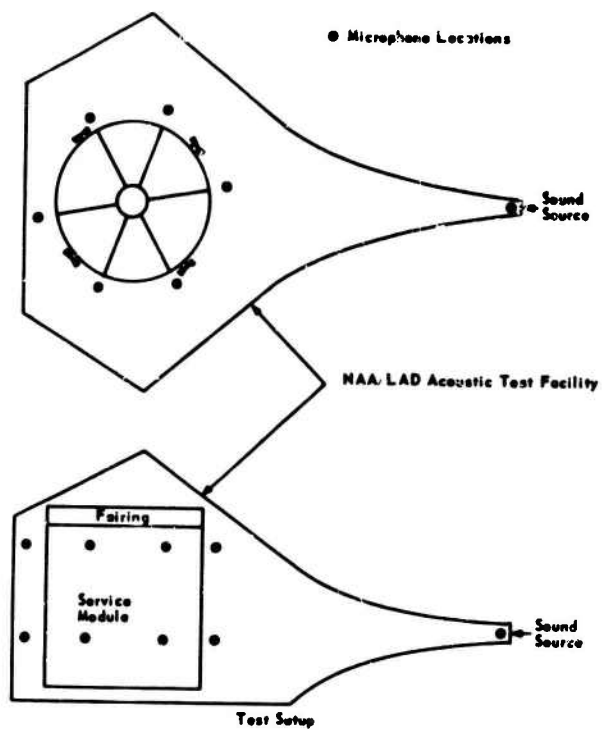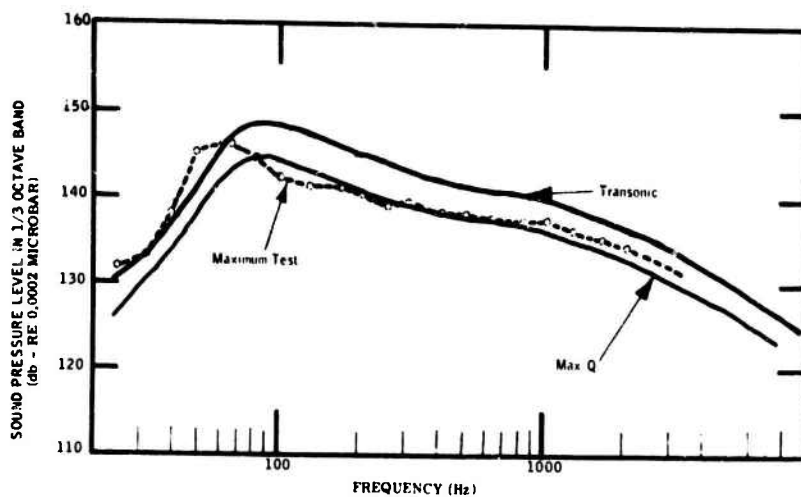were found. No damage was found in the external panels or the forward and aft bulkheads. The vibration response of much of the SM structure was greater than predicted. The outer shell levels were 12 db over predicted levels, and the aft bulkhead and radial beam levels were 8 to 10 db over those predicted.

CM 007 Acoustic Tests

The CM, which was subjected to acoustic tests, consisted of a spacecraft structure including forward compartment, crew compartment, and aft heat shield, but utilizing cork in place of the forward and crew compartment heat shields and the ablative material. All major components were either mass simulated or represented with prototype or mockup hardware. The quantity of the mass simulation was insufficient to allow definition of all equipment vibration requirements without any further extrapolation of the recorded response data.

The CM was oriented in an upright attitude in the NAA LAD facility and positioned on an acoustic closeout between itself and the facility floor. Figure 12 is a diagram of the test setup. Vibration responses were recorded at 129

locations, and acoustic measurements were recorded at 12 positions around and inside the CM.

The acoustic environment was imposed laterally from one direction and, as in the case of the SM, did not provide a uniform acoustic field around the test specimen. The maximum variation in one-third octave bands around the CM was 5 db. The applied broad-band acoustic spectrum was developed from the instrumented flights of Apollo boilerplate vehicles and from scale-model wind-tunnel test data. Four tests were performed, varying in overall SPL from 135 to 156 db. The highest test levels are shown in Fig. 13, along with the expected max Q flight environment.

No structural failures occurred in the CM as a result of these tests, and the resulting data generally substantiated the predicted primary structural response. However, the internal secondary structure responded approximately 6 db higher, and the forward and crew compartment heat shields responded approximately 10 db higher than predicted. Noise reduction properties of the CM were measured and used to determine the maximum expected acoustic level of 125 db in the crew compartment during flight.
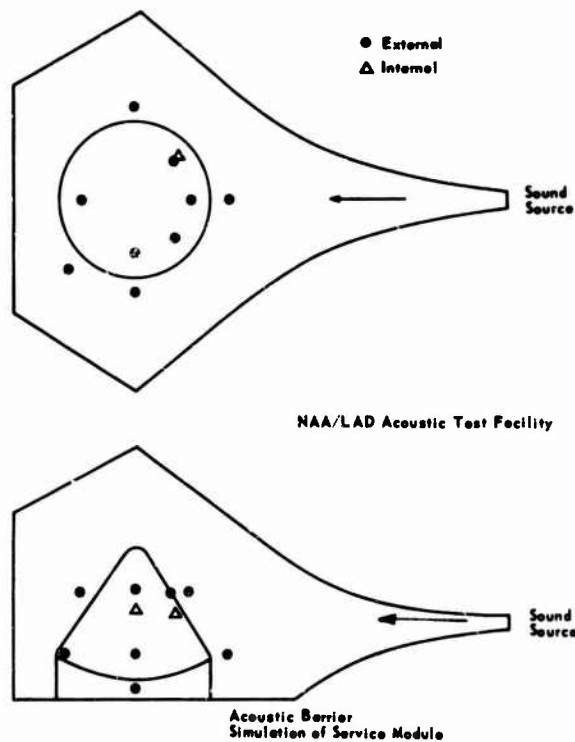

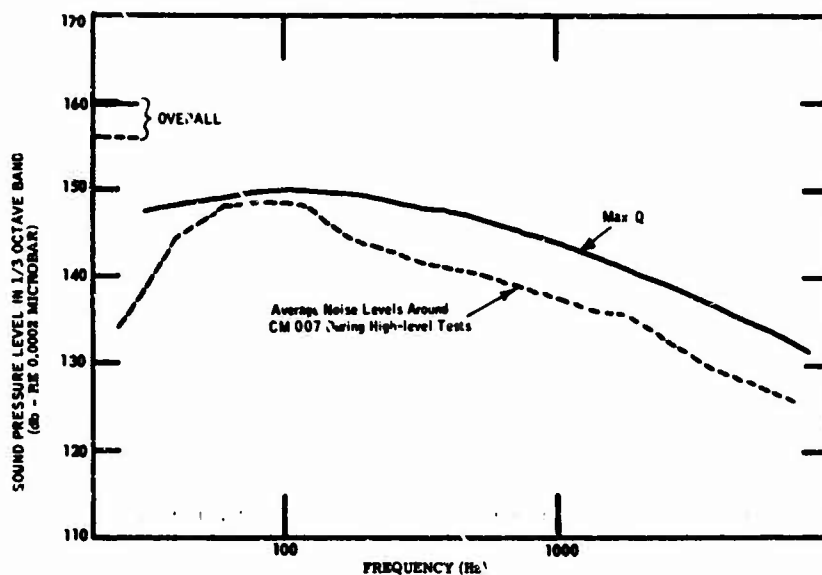Fig. 12. CM 007 acoustic test setup

97

Fig. 13. Comparison of aerodynamic noise and
CM acoustic test spectra

Follow-on Tests

As a result of the high SM vibration responses and fatigue failures of the SM elements, several acoustic tests were performed on another SM. These tests were performed to assess the effectiveness of varying mass loading on specific areas of the SM and to evaluate the radial beam shear web response characteristics when loaded with different configurations of damping tape. This SM (006) was complete as to basic structure, except boilerplate SPS fuel and oxidizer tanks were substituted and all equipment and supporting structure were omitted. Fuel and oxidizer tank loads were simulated with water, and the max Q inertial loading (2 g) was simulated with a static loading fixture. Nine tests were performed, each in excess of 2 min. The first test run was conducted with an overall acoustic level of 128 db, the second run at 138 db, and the remaining seven runs were carried out at 143 db.

The responses from the SM 006 tests were slightly lower than the responses of the SM 007 tests, but generally substantiated the previous results. The addition of damping tape to the thin webs of the radial beams was effective to the extent of mass added, and the addition of masses to these webs produced response reductions from 6 to 15 db, depending upon the mass amounts. However, the additional mass added to the webs had very little effect on the response of the beam caps or surrounding structure. Addition of mass to the SM shelves and bulkheads

resulted in considerable attenuation at frequencies in excess of the members' fundamental frequency. During these tests, no failures of the radial beam shear webs or other components occurred. Subsequent fatigue testing of the radial beams indicated that the radial beam fatigue strength was satisfactory to perform the designed missions and that the failures experienced during the SM 007 testing were unrealistic with respect to flight conditions because of excessive test time at nonrepresentative mass loaded conditions.

TEST DATA EVALUATION AND DERIVATION OF THE REVISED VIBRATION ENVIRONMENT

The acquisition of data from the CM 007 and SM 007 acoustic tests and the resulting revisions to the spacecraft vibration environment were accomplished after the equipment qualification test program was well underway. The revised vibration environment was devised as follows:

The CM, SM, and SLA were divided into the following zones:

Command Module

Forward and crew compartment heat shield
Crew compartment inner structure sidewalls
Aft heat shield

98

Aft equipment compartment
Main display console
Left-hand equipment bay
Right-hand equipment bay
Crew support system
Main display console
Lower equipment bay
Forward bulkhead
Crew compartment inner structure
Aft bulkhead

Service Module

Outer shell
RCS quadrant panels
CSM fairing
Forward bulkhead
H_2 tank shelf
Upper O_2 tank shelf
Lower O_2 tank shelf
Radial beam caps
Radial beams
Helim pressure panel
Helium tank

Spacecraft Lunar Module Adapter

Outer shell forward of LM attachment
 frame
Outer shell aft of LM attachment frame

The large number of zones was chosen to provide greater flexibility and to minimize impact to the equipment vibration qualification test programs.

Data recorded during the acoustic tests were reduced to narrow-band acceleration spectral density curves. These data had to be scaled to the maximum expected flight conditions because the test facility was unable to match the flight conditions, as shown in Fig. 13, and because the data from some of the lower level test runs had to be used in the criteria definition of some zones. In some cases, it was necessary to scale the data at particular frequencies as much as 25 db. Normally, scaling vibration response in this manner produces conservative results, since structural nonlinearities tend to limit the structural response. The scaled data were grouped into composites according to the zonal descriptions above. The vibration criteria, in general, represent the envelope of the composite for the given zone. However, narrow spectral peaks that protruded up to 3 db above the spectral envelope were allowed to be "clipped" by this envelope, provided that the rms g value of the envelope was equal to 1.5 times the rms g value of the composite plot. Figure 14 presents a typical SM zone with corresponding envelope of the range of adjusted
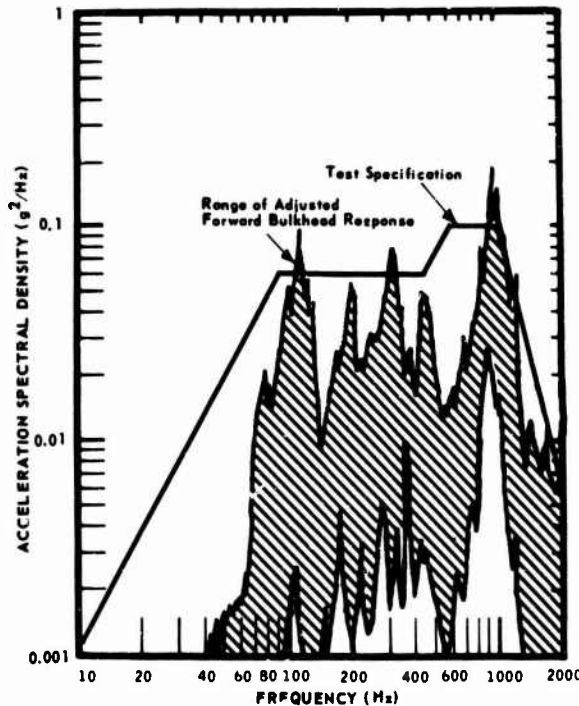

Fig. 14. Typical vibration specification
derivation, SM forward bulkhead

data plotted for the max Q flight condition. A comparison of this method of enveloping data and the statistical analysis of a large quantity of Titan data indicated that this method produced levels which were approximately equal to the 90th percentile probability of the Apollo test data.

Two vibration levels, A and B, were derived for the SM and SLA. Level A criteria represented the max Q portion of the flight, while the level B criteria represented the higher excitation associated with the transient flow separation near Mach 1. The durations were defined for the purpose of testing as 140 sec for level A and 10 sec for level B. The total test duration of 150 sec was derived from the flight time, which was established as the time that a spacecraft would be exposed to SPL's in the range 10 db down from those expected at max Q. This exposure duration was then increased by a factor of 1.5 to obtain the 150 sec.

The CM vibration criteria were also specified at two levels, one representing max Q flight and the other representing excitation expected during an abort at max Q using the LES. The test time for the max Q condition was set at 140 sec, and the abort condition was defined at 10 sec.

The vibration environment for the SLA was determined from SM 007 outer shell response data scaled to the predicted SLA acoustic levels. These adjusted SM 007 data were enveloped and reduced 6 db to compensate for the increased mass per unit area of the SLA panels as compared with the SM 007 outer shell panels.

FLIGHT VIBRATION DATA EVALUATION

A large number of vibration measurements were acquired during the A-004 LES development flight of CSM 002 at NASA's White Sands Missile Range using the Little Joe II launch vehicle. Since A-004 was flown at a lower maximum dynamic pressure than the expected design limit, some scaling of the data was required. From Fig. 15, it can be seen that the A-004 dynamic pressure was 635 psf at Mach 1.6; the Saturn max Q, which is considered to be the design limit condition, is 800 psf. In addition, A-004 was flown at an angle of attack of 4 deg, whereas the design limit condition is 0 deg. Therefore, the acoustic excitation levels for A-004 that occurred at Mach 1.6 can be shown to be approximately 2 db lower than the design limit condition.

The internal vibration data measured on CM 002 were linearly adjusted to compensate for differences in fluctuating pressure level and were found to compare favorably with the CM vibration criteria. However, the vibration levels on the crew compartment heat shield were found to exceed the CM 007 test-derived vibration levels. All of the crew compartment heat shield data were reassessed, and revised vibration cirteria were developed by enveloping composites of the flight data.

One usable fluctuating pressure measurement was made on the A-004 SM. The spatial average of all the measured Apollo wind-tunnel and boilerplate flight data for the forward end of the SM was determined, and the comparison of this spatial average and the A-004 measurement is shown in Fig. 16. The A-004 measured SM vibration levels were then increased by the difference between the two spectra shown in Fig. 16 to determine the design limit vibration condition.

The vibration data from eight measurements on the A-004 SM outer shell were enveloped, as shown in Fig. 17. The conservative shape of the envelope above 400 Hz was to compensate for the telemetry channel limitations. This envelope was then raised by the SPL differences of Fig. 16. Next, data measured during the SM 007 tests at eight locations similar to the A-004 SM measurements were also enveloped. The difference in the outer shell response envelope using data from all 180 SM 007 measurements and the data from SM 007 locations that were similar to the A-004 SM locations, as shown in Fig. 18, was determined to be the difference in response criteria based on a large and small data sample. This difference was added to the scaled A-004 SM outer shell data to produce vibration criteria that were representative of a larger sample of data. Since it was generally believed that the excitation of both primary and secondary structure was induced by mechanical excitation from the SM outer shell, the difference between the SM 007-derived outer shell criteria and the A-004 SM modified outer shell criteria was applied to each SM zone to develop the final SM zonal vibration criteria.

Flight vibration levels recorded on AS-201 (CSM 009) consisted of only one SM and four CM broad-band vibration measurements. Six other SM vibration measurements were obtained over standard IRIG telemetry channels, but were restricted to frequencies below 300 Hz and were of limited value. The AS-201 CSM vibration levels, when adjusted for differences in max Q, were generally lower than those measured on
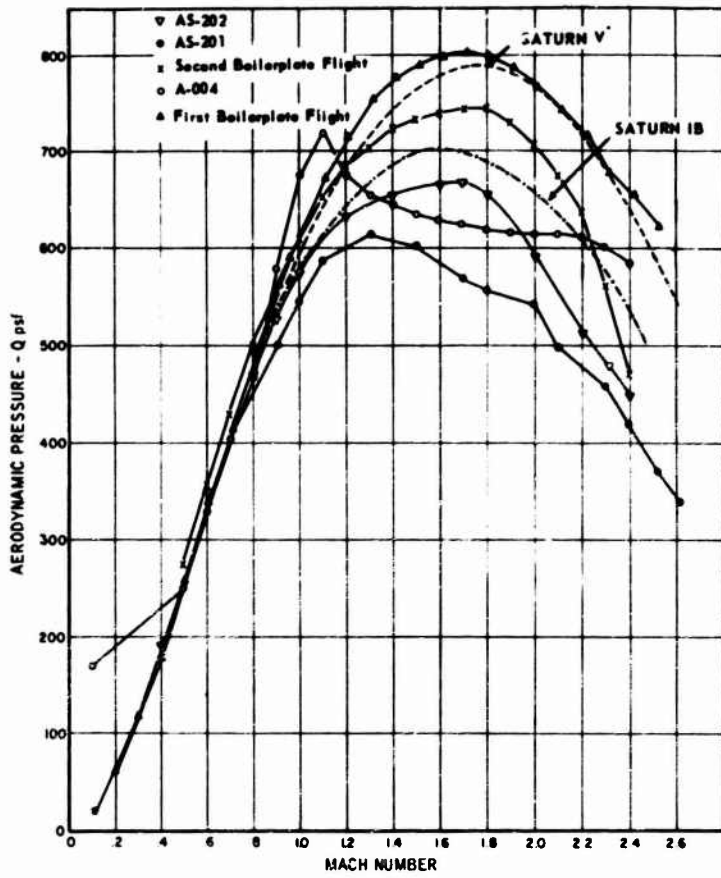
100

Fig. 15. Comparison of various Apollo flight trajectories,
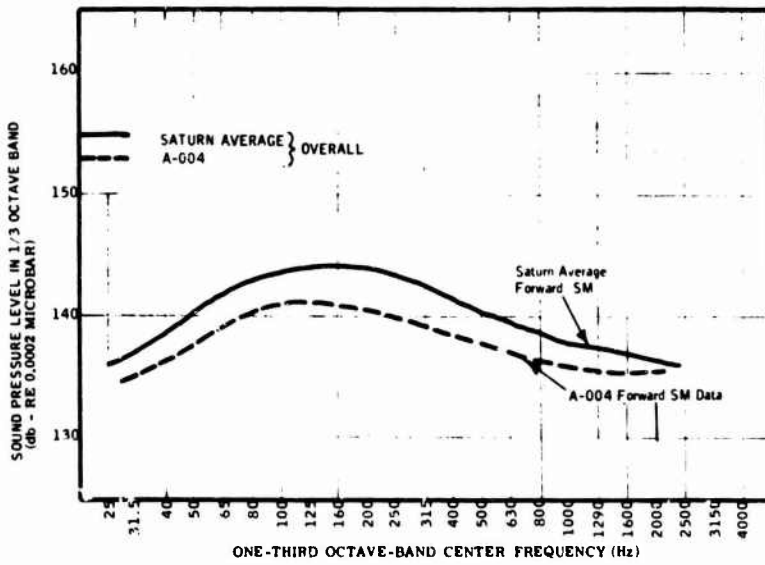Mach number vs aerodynamic pressure

Fig. 16. Comparison of average forward SM exterior
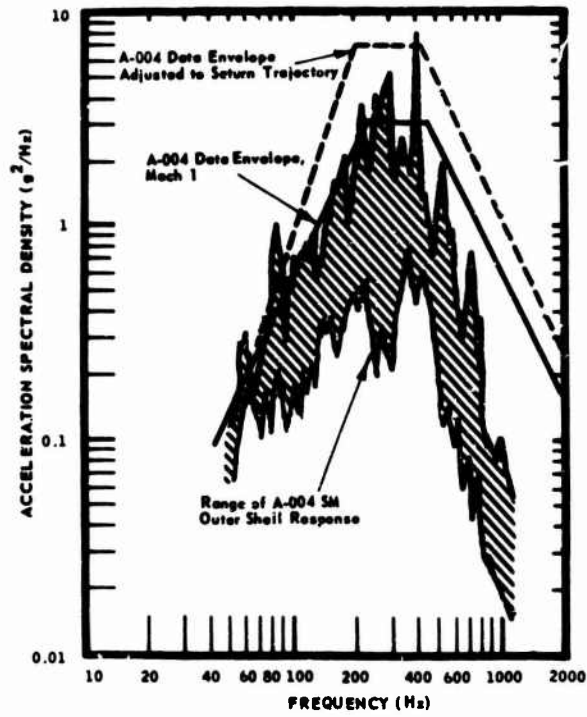SPL's with A-004 measured SPL's

101

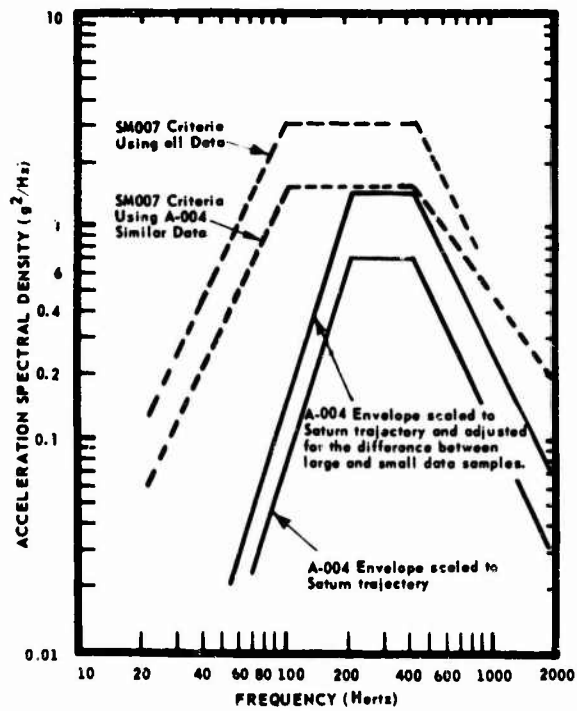Fig. 17. Composite vibration data and
envelope, A-004 SM outer shell

Fig. 18. Distribution differences between
A-004 SM and SM 007 vibration data envelopes

102

A-004 CSM. Because of the limitations of these data, no change was made to the CM or SM criteria.

Three measurements on the AS-201 SLA indicated that the vibration responses at liftoff were generally higher than predicted and higher than during subsequent transonic or max Q flight. Descriptions of these recorded flight spectra are included in Ref. [3]. Revised SLA vibration criteria were constructed from an envelope of the highest aerodynamic vibration responses (level A), and from an envelope of the vibration responses at liftoff (level B). The maximum vibration levels did not occur on the SLA during transonic flight, but instead occurred at liftoff. Therefore, for the SLA, level B was redefined as a liftoff vibration criterion.

The vibration instrumentation used on AS-202 (CSM 011) was essentially the same as on CSM 009, except for the relocation of five broad-band vibration measurements from the CM interior primary structure to the guidance and navigation base and main display panels. The AS-202 flight vibration data, after being adjusted for differences in dynamic pressure, confirmed the AS-201 data. Accordingly, no changes to the CSM or SLA vibration criteria resulted from the AS-202 flight.

CONCLUSION

This paper describes the contribution made by vehicle acoustic tests in the development of the present Apollo spacecraft launch and boost vibration environment. The importance of the CM and SM 007 acoustic tests must be stressed, since these vehicle tests provided necessary insight for evaluating the complex impedance environment and the intricate CM and SM structural response. The zoning, scaling, and enveloping techniques employed in analyzing the test results provided sufficient margin to account for unknown factors, such as the relative effectiveness of aerodynamic and acoustic noise in inducing vibration in the Apollo structure and the effects of variation in launch trajectories.

The revised vibration criteria derived from these acoustic tests generally represented increases in vibration levels. Flight data obtained after the vehicle acoustic tests indicate that the revised vibration criteria were sufficient to represent the Apollo design limit flight environment.

The inadequacy of existing analytical prediction techniques for providing accurate definition of the vibration environment for the Apollo CM, SM, and SLA structure must be underscored. Early predictions were as much as 10 db less than measured flight vibration environments, and only the vehicle-level acoustic tests provided the means for defining adequate vibration criteria.

REFERENCES

1. C. L. Stevens, "Vibration Response of Apollo Shell Structures to Acoustic and Aerodynamic Noise," Proceedings of the 13th Meeting of the Institute of Environmental Sciences, Vol. II, pp. 619-627, April 1967

2. P. Mahaffey and K. Smith, "A Method for Predicting Environmental Vibration Levels in Jet Powered Vehicles," Noise Control, July and Aug. 1960

3. W. D. Dorland, et al., "Development of Acoustic Test Conditions for Apollo Lunar Module Flight Qualification," Shock and Vibration Bull. 37, Part 5, 1968

DISCUSSION

Mr. Morse (TRW Systems): I notice that you had about 13 zones in each of the areas. How many locations did you instrument to differentiate these zones? Also, were the spectral shapes as well as the levels different for each of these zones? In other words, did you have to develop 13 or 26 different spectra and levels for the equipment that goes in the different areas?

Mr. West: There was much instrumentation on these acoustic tests. In the case of the service module about 195 measurements were made, and about 125 on in the command module. We did have to develop criteria for each one of these zones, because they did differ in spectral distribution as well as in level.

*   *   *

103

DEVELOPMENT AND VERIFICATION OF THE APOLLO
LUNAR MODULE VIBRATION TEST REQUIREMENTS

Dan E. Newbrough
General Electric Company
Houston, Texas

and

Murray Bernstein and Eugene F. Baird
Grumman Aircraft Engineering Corporation
Bethpage, New York

The Apollo lunar module (LM) size, weight, and configuration have given rise to problems in determining equipment vibration requirements and in verifying structural adequacy for anticipated mission environments. The application of large-scale vibration testing has played a prominent part in qualifying the LM for its intended mission.

The LM is subjected to mechanical excitation from on-board engine firings and from acoustic excitation during launch and boost. The LM engine firing conditions were simulated by replacing the ascent stage and descent stage engines with vibration test fixtures and applying shaped random excitation. Simulation of the LM launch and boost vibration environments required use of the unique vibration and acoustic test facility at the Manned Spacecraft Center (MSC), Houston, Texas. Testing in this facility resulted in expeditious certification of the LM structure and allowed completion of the necessary equipment qualification testing.

The initially predicted LM vibration and acoustic environment is described, and the LM structural vehicle vibration test program is outlined. A brief account of the LM dynamic tests conducted at MSC and the data evaluation are presented. Test results are compared with original predictions, and the effectiveness of the vehicle dynamic test program in certifying the LM for its intended mission is examined.

INTRODUCTION

The Apollo lunar module (LM) spacecraft must withstand severe vibration environments during earth launch and boost and during lunar descent and ascent flight. The complex configuration of the LM has made the prediction of vibration requirements and the demonstration of structural adequacy a difficult endeavor. Derivation of the LM vibration criteria began with analysis of Apollo scale-model wind-tunnel unsteady-pressure data and predictions of primary structure response. Refinement and verification of the vibration predictions were accomplished with vehicle-level dynamic tests.

Simulation of the vibration environment required test programs that provided both mechanical and acoustic excitation of the spacecraft. Vehicle-level vibration tests to simulate LM rocket engine excitation were conducted at Grumman Aircraft Engineering Corporation (GAEC), Bethpage, New York; acoustic tests to simulate launch and boost were conducted in the unique facilities at the Manned Spacecraft Center (MSC), Houston, Texas.

This paper examines the development of the LM vibration criteria from initial predictions to existing specifications. Data evaluation and significant observations from the vehicle dynamic test programs are briefly discussed, and the effectiveness of the LM vehicle vibration test program in satisfying qualification test objectives is presented.

SPACECRAFT

The LM vehicle shown in Fig. 1 consists of a descent stage and a separate ascent stage interconnected at four points. The basic descent stage structure is a 65-in.-deep cruciform consisting of a central engine compartment and four propellant tank compartments. The four landing gear legs are mounted on four member
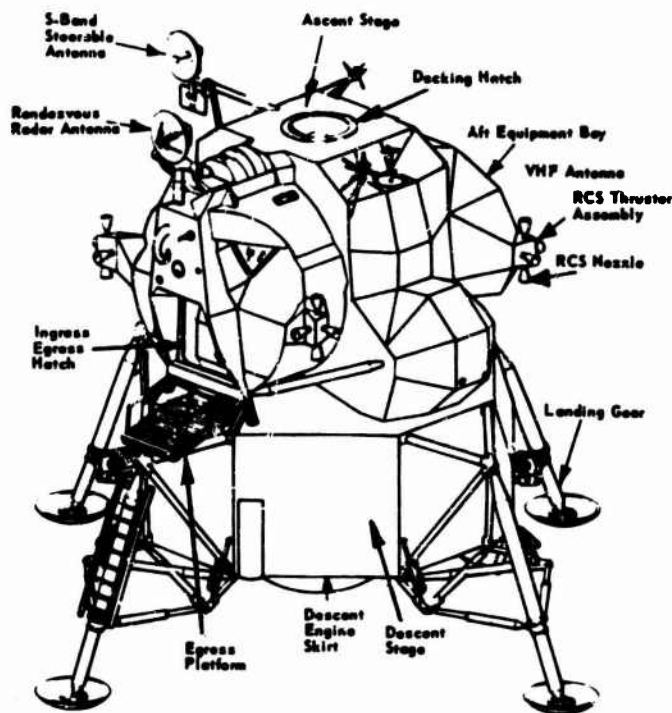
Fig. 1. Apollo lunar module

trusses which also act as supports when the vehicle is inside the spacecraft LM adapter (SLA) during launch. Auxiliary equipment, such as helium and oxygen tanks and the Apollo lunar surface exploration package, are mounted in the four quadrants of the descent stage cruciform. The ascent stage is constructed of two cylindrical sections capped by forward and aft machined bulkheads, with a major intermediate bulkhead separating the crew area from the aft cabin. The ascent engine is mounted from the midsection floor. Two spherical propellant tanks are supported from bulkheads, principally by struts. Much of the electronic equipment is located in the aft equipment bay and is mounted on a vertical rack supported by struts that extend off the rear bulkhead.

LAUNCH AND BOOST EXCITATION

The LM is exposed to both low-frequency mechanical vibration and high-frequency acoustic excitation during liftoff and atmospheric flight. Mechanically induced vibration transmitted from the SLA panels through the support trusses is limited to low-frequency vibration amplitudes. Above 12 Hz, the LM vehicle is effectively decoupled from the SLA and experiences only high-frequency acoustic excitation. The induced LM high-frequency vibration is closely related to the SLA internal acoustic environment. These noise levels follow the typical rocket booster flight profile of decreasing rapidly after liftoff and then increasing to a peak near Mach 1, as presented in Fig. 2. These external noise levels induce SLA panel vibration, which generates a quasi-reverberant acoustic field inside the SLA. The internal SLA noise is considered to be the most significant source of LM excitation. A detailed discussion of the mechanics of internal SLA noise generation is presented in Ref. [1].

Initial estimates for the LM launch and boost acoustic environment were based on unsteady pressure measurements obtained from scale-model wind-tunnel tests and from early Apollo boilerplate flights. The SLA external noise levels presented in Fig. 3 were the results of these early analyses. It is assumed that the LM spatial average peak external acoustical levels would produce vibration responses similar to those experienced by upper stages of launch vehicles. Following this assumption, the LM vibration levels for the ascent and descent stage structures, presented in Fig. 4, were predicted using procedures derived by Barrett [2]. These procedures allow extrapolation of a large number of vibration measurements compiled on launch vehicles to any dynamically similar structural configuration,
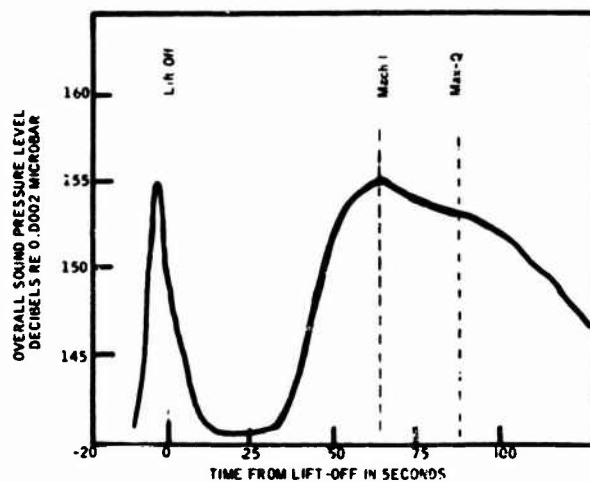
106

Fig. 2. Typical sound pressure level on an
Apollo SLA during launch and boost
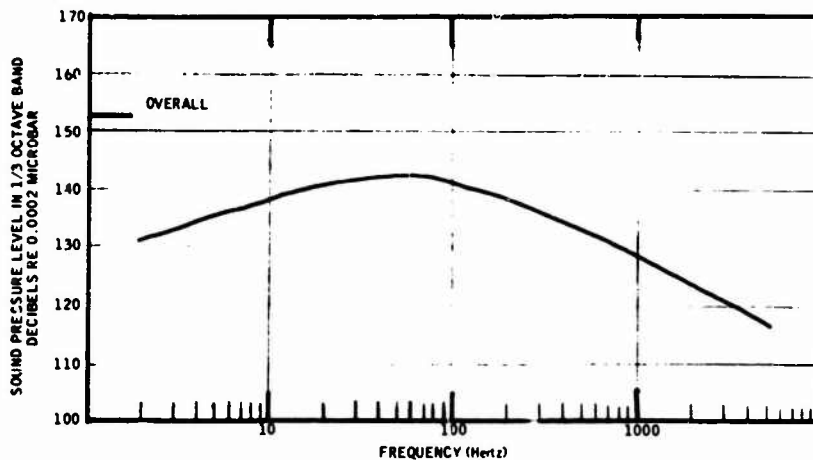
Fig. 3. SLA average external acoustic spectra,
Mach 1 flight condition

and account for variations in acoustic levels, mass density of structural members, and component weight on supporting structure. In addition, these levels were supplemented by the vibration requirements of Military Standard 810 [3], and those defined by North American Aviation, Inc., for the Apollo command module. The resulting LM criteria were a composite of these requirements. It should be noted that many LM equipment items, such as valves, regulators, and switches, were assigned a vibration test requirement before a definite LM location was known. These vibration levels were derived from Military Standard 810 and were specified approximately 10 db higher than primary structure requirements to compensate for unknown

amplification resulting from mounting configuration.

ENGINE-INDUCED EXCITATION

The LM spacecraft also experiences vibration induced by the LM ascent and descent stage rocket engines and the reaction control system (RCS) engines. Figure 5 presents the initially predicted vibration requirement for these engine firing simulations. Originally, a mathematical model of the LM, consisting of about 140 degrees of freedom for half of the vehicle, was derived. Unsteady thrust values determined from the LM engine test-stand firings were applied as a

Fig. 4. Original LM primary structure
random-vibration criteria, launch and boost

Fig. 5. Original LM primary structure
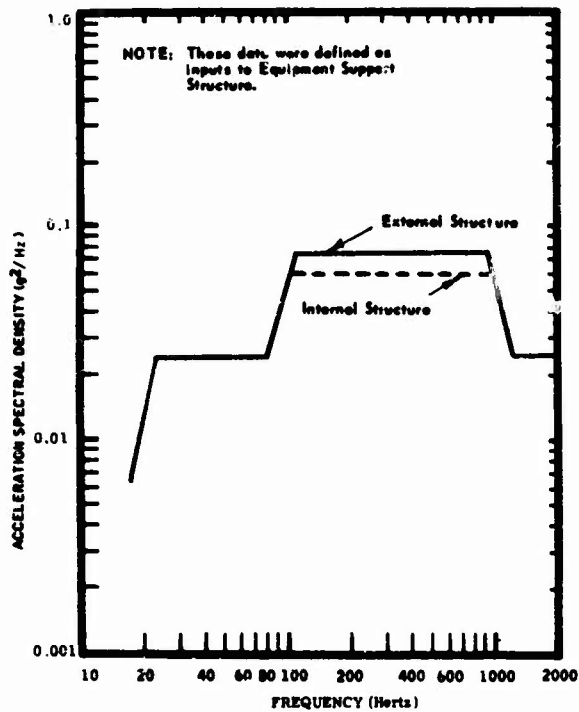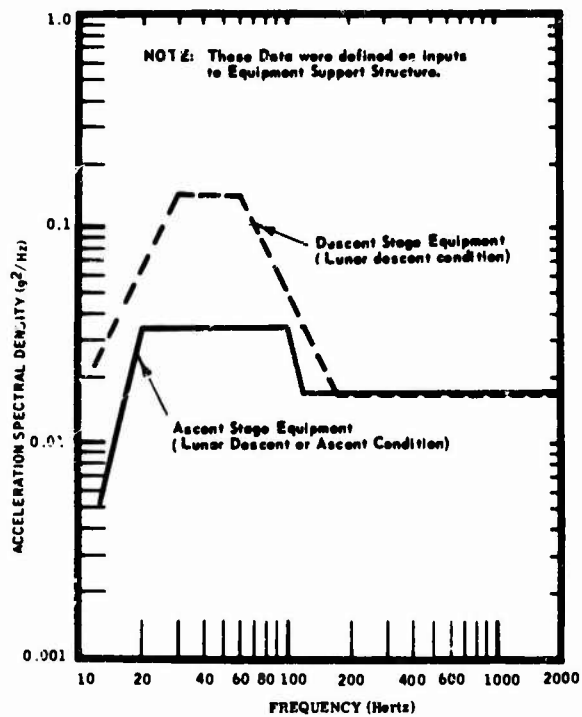random-vibration criteria, lunar descent
and lunar ascent

108

forcing function to this model. The resulting vibratory motion on various portions of the vehicle was calculated, and an envelope drawn to cover all but the responses at the engine support points. This analysis was adequate up to about 100 Hz for the descent stage configurations and up to about 250 Hz for the ascent stage configuration. Levels above that frequency were obtained by extrapolating to 2000 Hz.

VEHICLE VIBRATION AND ACOUSTIC TEST PROGRAM

To verify the predicted vibration requirements, a structural prototype vehicle (LTA 3) was subjected to tests which simulated the induced vibration during the various mission phases. This vehicle included mass simulations of all flight hardware weighing more than 20 lb and all those known to be susceptible to vibration. In addition, models of the navigation sensors, mounted on the top of the forward portion of the ascent stage, and elements of the life support system, mounted in various cabin locations, were also included. All tanks were filled with referee fluids and were at weights representative of the proper flight conditions. Main engine propellant lines and representative sets of RCS lines, water glycol lines, and representative wiring harnesses were included. Because of safety limitations, propellant lines were pressurized to only 50 psi, about 20 percent of normal operating pressure.

A total of 540 accelerometers were used so that vibration environments could be determined directly for a majority of the equipment. In this test program, emphasis was placed on defining individual equipment requirements rather than defining a zonal representation. Most measurements were made at the interfaces between support structure and equipment, and some were made on control panels and tanks. The large number of measurements required a series of repeated test runs in many of the configurations since the capacity for recording vibration data was limited. Prior to each run, the correct accelerometer range setting was determined by a full-level test run for 10 to 15 sec and immediate data reduction and review. About one third of the accelerometers were located on primary structure, and the rest were on secondary structure. Strain gages were mounted on the struts supporting the LM in the SLA and on the supports that attach the LM engines to the primary structure.

LM Engine Firing Simulation

Figure 6 shows the LTA 3 vehicle mounted for the engine-induced vibration tests. The
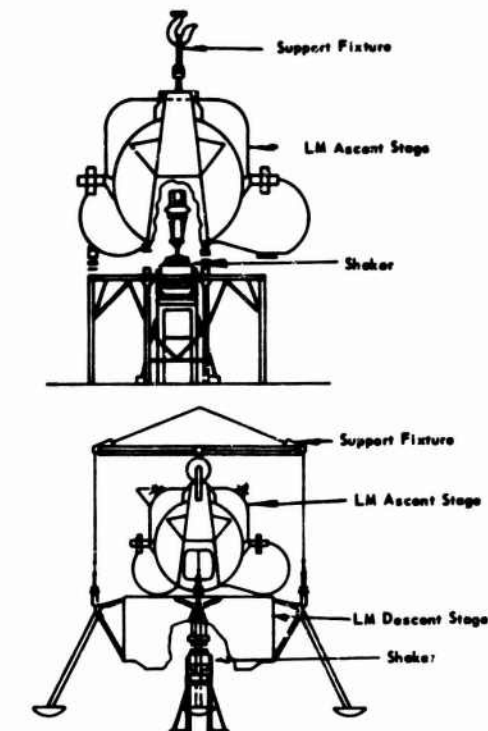
Fig. 6. Configuration of LTA 3 during vibration tests, engine firing simulation

oscillating forces applied for the descent engine were determined from measured loads on the engine gimbal ring during test firings. Differences in dynamic characteristics of the engine test stand and the vehicle were resolved by conducting exploratory sinusoidal tests of LTA 3 before the measured forces were applied. The force spectra for the ascent engine were most difficult to determine because the data recorded during test-stand engine firings had a very low signal-to-noise ratio. Therefore, conservative values were adopted for the magnitudes of the forces, and were adjusted by the spectra measured on the injection head of the test-stand engines. The RCS engines are located in clusters of four thrusters supported by struts off the primary structure. There are two forward clusters and two aft clusters. Vibratory forces were also applied to the RCS cluster mounting struts to determine the induced accelerations. These forces were determined from load time histories measured when the RCS thrusters were firing on a very rigid stand. Random vibration, used to represent the unsteady portion of the force, was combined with low-frequency sinusoidal vibration in the range expected to be excited by the pulsing nature of these thruster firings.

The maximum ascent stage vibration, resulting from ascent engine firing excitation, produced equipment responses in a few areas that were higher than predicted. Over portions of the frequency range, vibration requirements for the ascent engine firing condition had to be increased for about 15 items, mostly those mounted close to the engine. Ascent stage response to descent engine excitation was less than predicted, and there appeared to be less actual transmission between stages than originally estimated. The maximum response in the descent stage, resulting from descent engine inputs, was representative of predicted values. Vibration induced by the RCS thrusters was significant only for certain display panels in the forward area of the cabin, and for some components in the aft equipment bay. The data obtained from these tests permitted reductions in vibration requirements for much of the LM equipment.

Launch and Boost Simulation

The launch and boost low-frequency mechanical vibration and high-frequency acoustic excitation are generally more severe than the engine firing vibration conditions. Some equipment located near the LM engines experiences high vibration during engine firing conditions, but most of the LM structure and equipment have higher responses during launch and boost. Therefore, accurate simulation of the launch vibration environment was a necessary part of the LM certification program.

For the low-frequency tests, the LTA 3 was mounted on the lower portion of the SLA,

which was supported on a Saturn instrument unit (IU) as shown in Fig. 7. Shaker forces were applied to a large structural base ring which supported the IU. The launch and boost vibration tests consisted of sine sweeps of 4 to 20 to 4 Hz, with the motion of the LM primary structure and the LM-SLA outrigger attachment points limited to 0.2-in. double amplitude. The location of the controlling transducers was based on low-level mode surveys conducted previously. Figure 8 indicates typical maximum velocities measured during excitation of one axis. As was expected, the maximum control point at low frequencies was on the vehicle; above 12 Hz, it was on the outrigger attachment points. A typical example of the shaker force required to generate these responses is shown in Fig. 9. Also plotted on these curves are the measured forces applied to LTA 3 from the calibrated outrigger struts. The main differences between the force curves occur above 12 Hz. These differences can be explained by noting that the test control procedures required a constant displacement on the LTA 3-SLA configuration, and higher accelerations and forces were induced by the shakers into the SLA base as the frequency increased. The higher input forces did not produce increased loads on LTA 3, since the test vehicle is essentially isolated from the SLA above 12 Hz.

The high-frequency launch and boost acoustic tests of the structural prototype were conducted in the NASA MSC Spacecraft Acoustic Laboratory. Figure 10 is a diagram of the test configurations. Detailed descriptions of the facility design and operation are contained in Ref. [4].

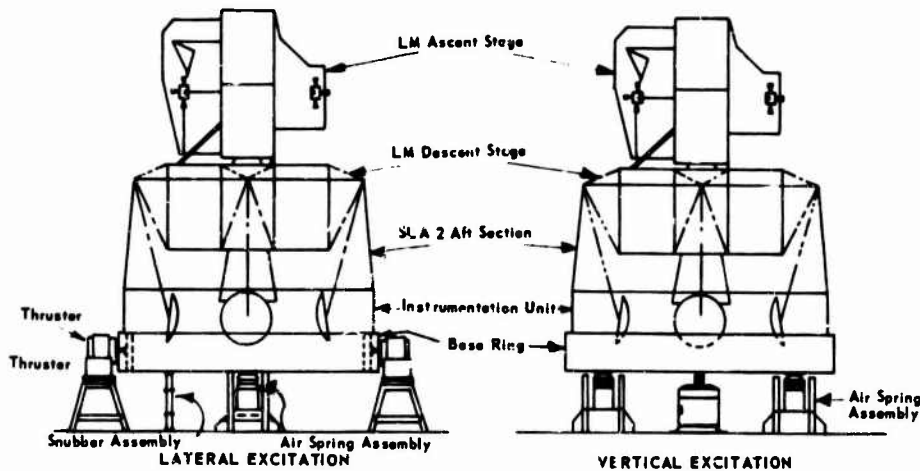Selection of the test acoustic spectrum and control pattern was difficult because of the lack

Fig. 7. Configuration of LTA 3 during low-frequency
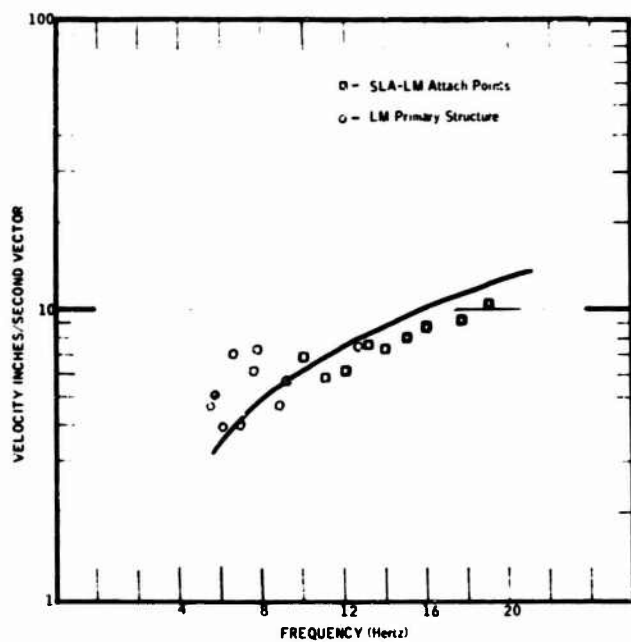vibration tests, launch and boost simulation

110

Fig. 8. LTA 3 maximum velocity during low-frequency vibration tests, launch and boost simulation, y-axis excitation
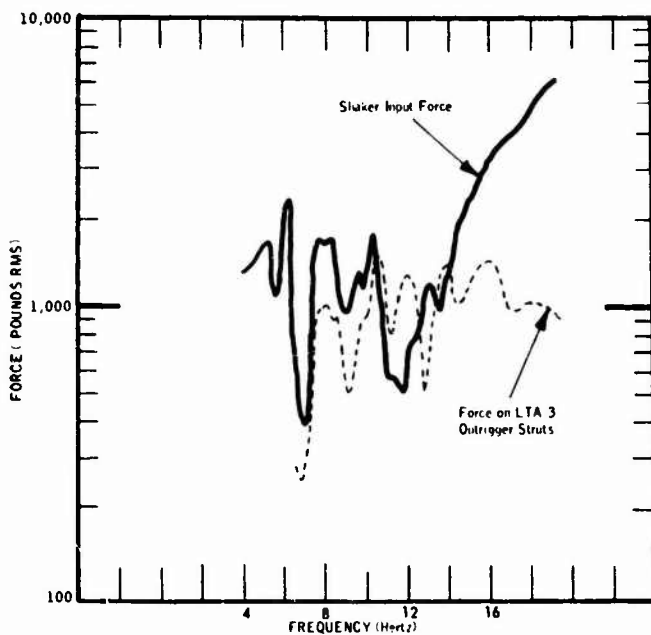

Fig. 9. LTA 3 forces measured during low-frequency vibration tests, launch and boost simulation, x-axis excitation
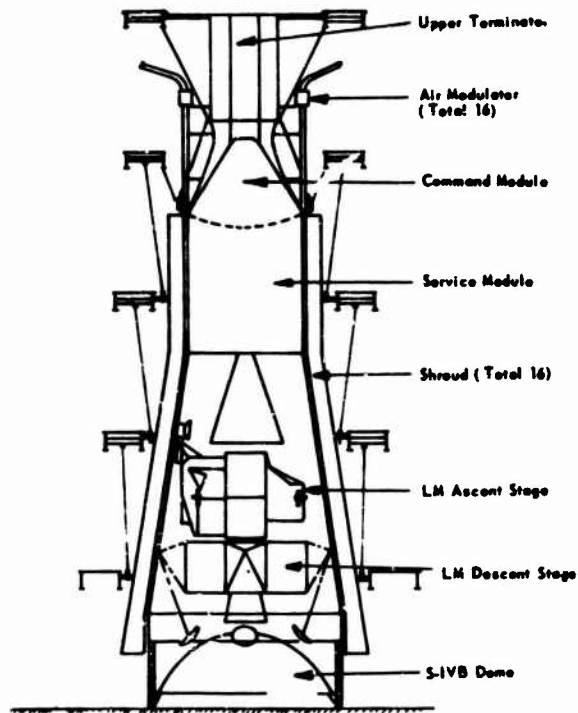
111

Fig. 10. Configuration of LTA 3 during
acoustic tests, launch and boost simulation

of appropriate flight acoustic data and because of uncertainties in the response of the test structure to the pattern of applied acoustic pressures generated in the facility. In particular, there was concern that the difference in spatial correlation characteristics between the test facility and the actual launch vehicle might prevent adequate simulation of the environmental vibration. This problem is described in detail in Refs. [1] and [4]. It was necessary to base the test control on flight vibration data, since no actual SLA flight acoustic data were available. The control procedure that finally evolved was to adjust the applied external SLA fluctuating pressures so that the responses measured on three SLA accelerometers during the test would match a maximum envelope determined from flight data measured at the same locations during Apollo spacecraft flights AS-201 and AS-202. The SLA flight vibration levels were adjusted to account for the anticipated differences in the liftoff acoustic and aerodynamic noise generated by Saturn IB and Saturn V launch vehicles, and it was these adjusted vibration levels that were generated on the test SLA.

The acoustic tests were conducted in three parts to allow all the required data to be

recorded. Between high-level test runs, before repatching instrumentation for the next run, all recorded data were played back on oscillographs and reviewed for adequacy.

DATA EVALUATION AND OBSERVATIONS

The recorded data from all accelerometers were reduced to acceleration spectral density plots, which were then grouped into composites to represent the environment for each item of equipment on the vehicle. Envelopes were drawn through the composites so that no narrow-band spectrum peaks were clipped more than 3 db. Figure 11 presents a typical LM equipment envelope requirement. Note that minimum vibration requirements were specified no lower than 0.005 g²/Hz.

Response data from the low-frequency tests were reviewed to establish equipment vibration test requirements. The maximum equipment displacement criteria, resulting from this test, were about 2.5 times the response control level. The data review also revealed that some primary structure points responded with motions greater than the control limit. The placement
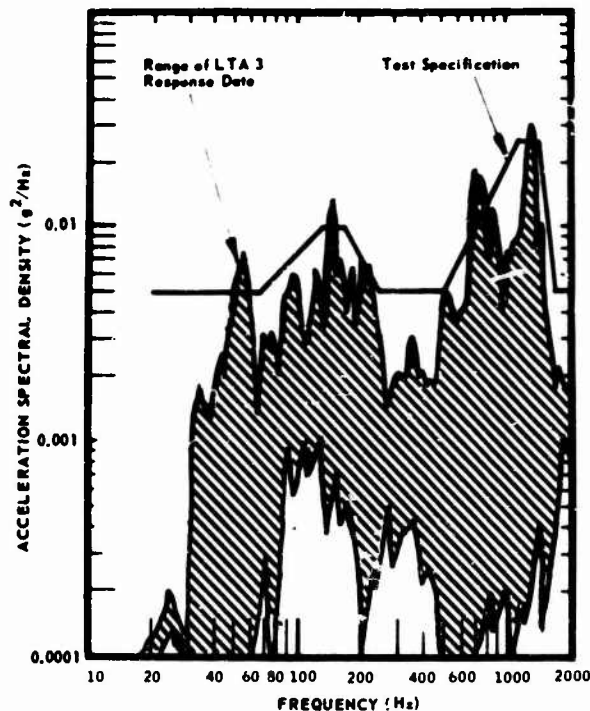
112

Fig. 11. Typical specification derivation,
LM fuse assembly 1, launch and boost
random vibration

of the control transducers was based on the
results of the low-level modal surveys, in which
the vehicle support conditions were somewhat
different. This may account for the discrepancy
between estimated and measured maximum mo-
tion locations.

Sinusoidal test requirements up to 100 Hz
were determined from the maximum random
level in the range between 20 and 100 Hz by
calculating a sine input which would give the
same peak response as the three-sigma ran-
dom response when calculated for a single-
degree-of-freedom system. This sinusoidal
requirement was maintained as a part of the
qualification test because it avoids random
testing difficulties at low frequencies and it
provides additional assurance of adequacy under
the anticipated environment.

A comparison of the original LM primary
structure estimates with envelopes of primary
and secondary structure, obtained from the
acoustic tests, is shown in Fig. 12. The pri-
mary structure composite shown is from an
envelope of 75 vibration measurements made
on the ascent stage. Fifteen measurements (20
percent) exhibited narrow-band peaks that

exceeded the original requirements by more
than 1 db. Twenty percent seems like a large
number, and had not been anticipated. How-
ever, when the acceleration spectral density
plots were subdivided into 50-Hz intervals and
compared with the predicted criteria, only 1
percent of all the 50-Hz bandwidths were higher
than the original primary structure estimates.

The envelope drawn for secondary struc-
ture, in Fig. 12, was from a composite of 282
ascent stage measurements. Note that the dif-
ference between primary and secondary struc-
ture envelopes is small and indicates little dif-
ference between maximum motion points.

The only common characteristic notable in
all of the vibration data from the ascent stage
and descent stage data was a peak in almost all
plots at about 40 Hz. This corresponds to one
of the higher frequency modes measured in the
launch and boost configuration. At higher fre-
quencies, there are larger differences in the
vibration environment in various locations.

An interesting and somewhat disconcerting
phenomenon encountered during the low-
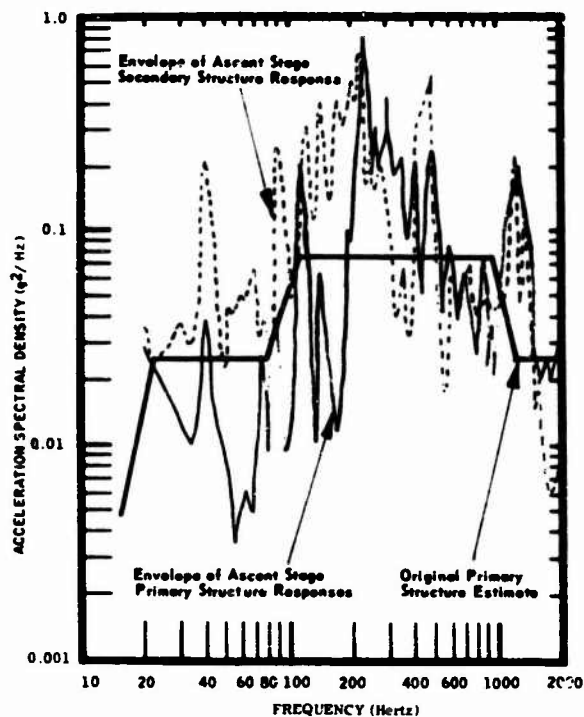frequency launch and boost tests was a definite

113

Fig. 12. Comparison of LM predicted vibration criteria with LTA 3 acoustic test data

high-frequency content noted in many of the acceleration signals. To determine whether the high-frequency response was being generated within the measuring instrumentation, accelerometers were physically removed from the structure and left in place on isolators with no change in the connecting cables. A review of the output of these disconnected accelerometers indicated large reductions in high-frequency content compared with runs made when they were mounted on the structure. Apparently, the high-frequency acceleration resulted from phenomena associated with panel buckling or impacting of various adjacent structural elements. It is believed that this high-frequency response to low-frequency excitation was sufficiently accounted for during the high-frequency acoustic tests.

Several design changes were implemented as a result of the vibration tests on LTA 3. On the ascent stage, the bonding technique used to mount thermal shield supports was altered as a result of poor adhesion and failure during the test. The end covers on the aft equipment rack rails were redesigned because cracks were found after the LTA 3 vibration and acoustic tests, although metallurgical analysis indicated that stress corrosion probably caused the fault.

The major change on the descent stage was an increase in skin gage in the beam panels. The type of attachment used for the thermal shielding support straps was also changed.

The resulting random-vibration equipment test requirements were higher than those initially estimated on 40 items of equipment out of a total of about 250. Since much of the equipment had not yet been qualified, the results were used to change requirements without specifying additional tests. In some instances where equipment had not yet completed scheduled overstress testing, an additional overstress test became a necessary requirement to qualify equipment.

CONCLUSION

The Apollo lunar module spacecraft is an extremely complex dynamic structure. Prediction of the LM vibration environment by use of analytical or empirical methods employed on other spacecraft programs was very uncertain. Therefore, conservatism was included in the definition of equipment test requirements to compensate for this uncertainty and to allow necessary margins of safety for a man-rated spacecraft.

114

Refinement of the original LM vibration estimates could only be accomplished with vehicle-level dynamic tests. The primary factors in achieving these vehicle tests were accurate definition of the LM excitation environment and available facilities in which to conduct the tests. At the time of the LTA 3 test program, SLA response data had been measured on two successful unmanned flight vehicles, and LM engine excitation levels had been acquired from test-stand firings to provide authentic engine-firing vibration input levels. The GAEC test facilities were adequate to support LTA 3 for the LM engine simulation tests, and the MSC acoustic facility provided the necessary control flexibility to generate the SLA flight response. Therefore, the LM test program relied largely upon vehicle-level vibration tests, with emphasis directed toward acoustic testing in the MSC facility. This procedure was a highly desirable approach, since accurate simulation of the SLA panel flight response was necessary to generate the acoustic forcing function of the LM. It is of interest to note that the LM structural response to descent engine firing as determined on the LTA 3 has been confirmed by recent propulsion-structural tests in the high altitude chamber at the MSC White Sands test facility.

The large number of vibration measurement locations used for these vehicle tests was selected so that individual equipment vibration test requirements could be derived. Since the LM is not easily subdivided or broken down into zoned vibration criteria, this procedure allowed detailed definition of all LM equipment vibration levels.

Comparison of the vehicle test results with initial LM vibration predictions shows the uncertainty in the original prediction techniques. The apparent difference points up the justification for vehicle-level dynamic tests. The techniques used in developing the LM vibration criteria should provide insight for future vibration test programs of large, structurally complex spacecraft.

REFERENCES

1. W. D. Dorland et al., "Development of Acoustic Test Conditions for Apollo Lunar Module Flight Qualification," Shock and Vibration Bull. No. 37, Part 5, 1968

2. R. E. Barrett, "Techniques for Predicting Localized Vibration Environments of the Rocket Vehicles," NASA Tech. Note D-1836, Oct. 1963

3. "Military Standard — Environmental Test Methods for Aerospace and Ground Equipment," USAF MIL-STD-810, June 1962

4. R. J. Wren et al., "Concept, Design, and Performance of the Spacecraft Acoustic Laboratory," Shock and Vibration Bull. No. 37, Part 5, 1968

*   *   *

115

SATURN S-II, S-IVB, AND INSTRUMENT UNIT SUBASSEMBLY
AND ASSEMBLY VIBRATION AND ACOUSTIC
EVALUATION PROGRAMS

Richard W. Schock and Johnnie M. Everitt
Marshall Space Flight Center
Huntsville, Alabama

and

John R. Seat
Brown Engineering Company
Huntsville, Alabama

The major factor governing design of rocket-vehicle secondary structure and com-
ponent parts is the low- and mid-range frequency response of the primary struc-
ture shell to acoustic excitation associated with engine and aerodynamic noise.

Until recently, laboratory simulation of these imposed acoustic environments has
been impossible because of facility size and power limitations. However, recent
advances in facility capability have provided means by which full-sized assemblies
can be exposed, in ground test, to simulation of vehicle boost vibration and acoustic
environments. Marshall Space Flight Center has made extensive use of these capa-
bilities in ground-test developmental programs on S-II, S-IVB, and instrument unit
assemblies and subassemblies. Presented are: (a) a summary of these tests; (b)
the philosophy of the utilization of assembly tests; (c) methods of establishing test
environments; (d) advantages and limitations of this type of testing; (e) a compari-
son of test results to other types of ground tests and flight environments; and (f)
conclusions, derived from these comparisons, on the usefulness and validity of this
type of ground test.

INTRODUCTION

During liftoff and flight, rocket vehicle
structures are subjected to considerable noise-
generated vibration. The Saturn V vehicle,
being developed for manned space exploration,
is the largest and most powerful of the present
generation of booster vehicles. The 7,500,000
lb of thrust produced by the five F-1 engines
burning on the first stage (S-IC) of the Saturn V
generate over 200,000,000 acoustic watts of
energy. This sound field and the aerodynamic
noise of transonic flight develop approximately
90 percent of the vibratory forces present in
the upper stages of the vehicle. The other 10
percent is produced by mechanical energy
transmitted through the structure (see Fig. 1).

While both the engine-generated noise and
aerodynamic noise are described as acoustic,
their characteristics differ markedly. The
pressure fluctuations produced by the F-1 en-
gine jetstream turbulence are predominately
low frequency (peaking below 100 cps as shown
in Fig. 1), directional, and highly correlated,
and they affect large sections of the vehicle.
The aerodynamic noise caused by shock oscil-
lations at transonic speeds, separation at
supersonic speeds due to shock/boundary-layer
interaction, and turbulence in the boundary
layers at maximum dynamic pressure is higher
in frequency, much less correlated, and a less
effective vibration exciter. There is insufficient
energy to drive primary structure. Because of
these characteristics, the structural effects are
more localized. The engine noise predominates
during ignition, liftoff, and the early boost
phases of flight, and the aerodynamic noise
reaches a maximum during Mach 1, max Q
flight.

The forcing environment affecting vehicle
vibration then can be spectrally separated by
the dynamics engineer into two areas of
importance:

1. Low-frequency vibration (~ 300 cps) —
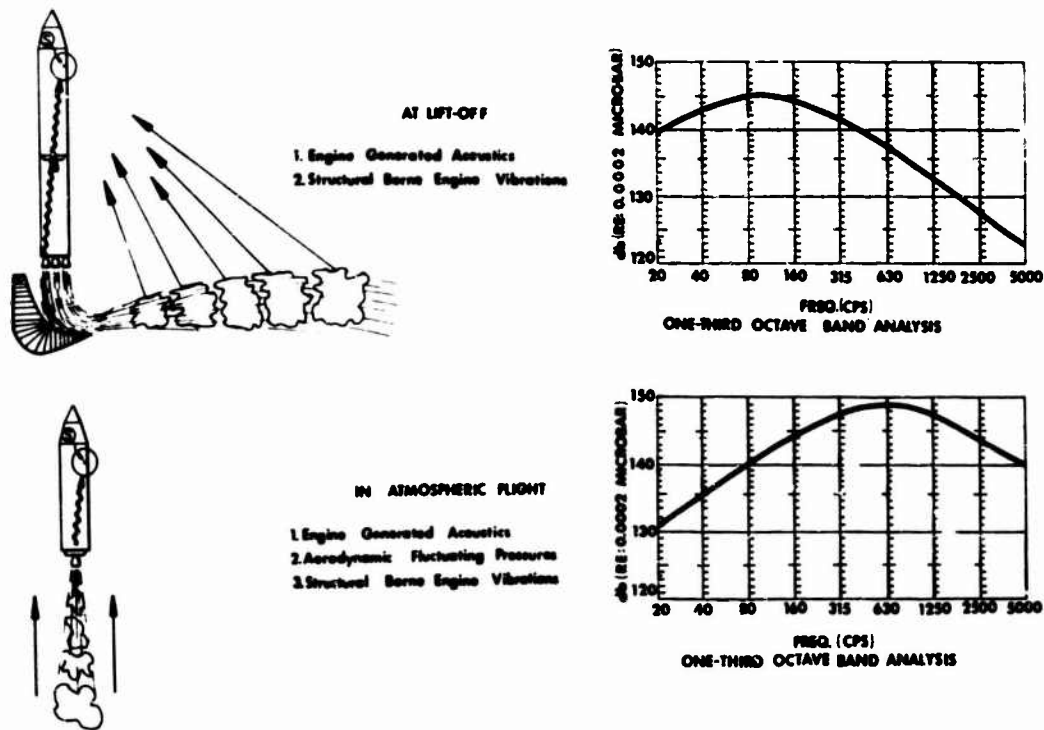affecting large areas of the vehicle primary and
secondary structure;

Fig. 1. Sources of vibration

2. High-frequency vibration (>300 cps) — affecting localized areas of the vehicle structure.

It should be recognized that this separation is a broad generalization and that there is considerable spectral overlap in both areas. The structures tested to date characteristically locate the dividing line around 300 cps. This is graphically demonstrated in Fig. 2, which compares primary structural responses measured during acoustic and random mechanical vibration. The left-hand graph shows the response to acoustic excitation, while the right-hand graph compares the response to broad- and narrow-band mechanical excitation of a typical shell structure. The solid lines show the input and response to the broadband excitation, and the dashed lines show the narrow-band input and response. Note that both curves roll off rapidly above 300 cps, indicating location of the dividing line for the generalized (large area) and localized condition.

Discussions and publications under the general heading of component and subassembly level testing emphasize testing for the localized condition, but relatively few efforts have been directed toward simulation of the low-frequency condition which requires testing of large

structural assemblies. The reasons are many, but they can be categorized as follows:

1. Facility size and power limitations;

2. Vehicle test requirements — low-frequency environments are not as significant or detrimental on small vehicles.

Only recently, and in close association with development of the Saturn vehicles, have facilities developed to the extent that makes assembly testing practical.

This paper presents a two-part discussion on assembly testing. Part 1 presents a general discussion on the philosophy of assembly testing, discusses some of the advantages and limitations, presents a brief summary of the major programs directed by Marshall Space Flight Center (MSFC), and submits a general discussion on development of a typical program, covering such items as program objectives, specimen choice, test specification development, test setup, test techniques, instrumentation requirements, and typical results. Part 2 presents a more detailed technical discussion of test results, drawing comparisons between assembly test, other types of ground tests, and
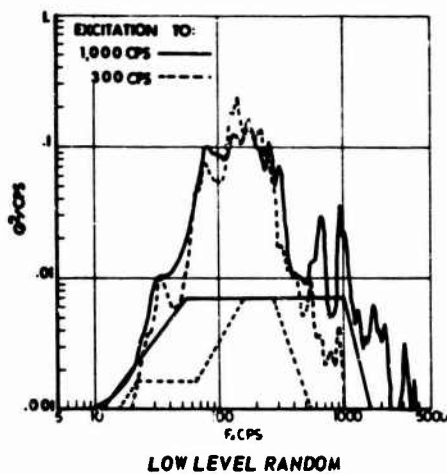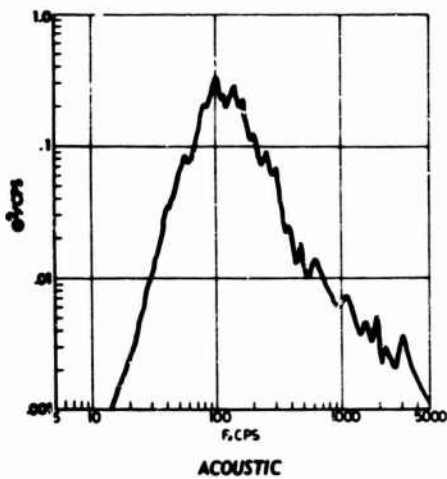
118

ACOUSTIC

LOW LEVEL RANDOM

Fig. 2. Unloaded struc-
tural response

measured flight results. Also included are con-
clusions about the use and validity of large as-
sembly tests and recommendations for future
work in the field.

PART 1

Philosophy

The philosophy behind all large assembly
testing is that the test specimen shapes and
controls its own vibration response by its mass
distribution and mechanical impedance charac-
teristics. This simulates the way the natural
vibration environment is controlled during
flight. Flight responses in a vehicle are a
function of the shell's acceptance of the forcing
environment, mass distribution, and the struc-
ture's mechanical impedance. The stiffened

shell of the flight vehicle absorbs acoustic
energy that in turn drives the nonacoustically
susceptible primary structure. The process
can be reversed for test, with the primary
structure excited to produce representative
flight responses in the stiffened shell. Figure
3 compares flight and mechanically induced
test responses from the uprated Saturn I in-
strument unit (IU). From this type of compari-
son it can be concluded that realistic low-
frequency tests can be made when the proper
excitation is applied to a sufficiently large as-
sembly. The result is a force-controlled test
of the primary and secondary structural areas
of interest. Three modes of excitation are em-
ployed in the full test program:

1. Sinusoidal sweep (5-300 cps) — at rep-
resentative levels to evaluate structural
transmissibilities and interaction character-
istics in support of analysis;

2. Random vibration (10-300 cps) — shaped
to predicted flight levels to evaluate the struc-
tural response under simulated flight conditions;

3. Broadband random acoustic excitation
(40-5000 cps) — at maximum facility levels to
validate and support mechanical vibration test.
Several sound pressure levels (SPL's) are
usually employed to enable extrapolation to
other levels.

Technical Discussion

The Saturn vehicles are large-diameter,
cylindrical-shell structures made of light skin
panels stiffened by stringers and ring frames
or of the newer honeycomb materials. These
types of structure are extremely susceptible to
the high-energy pressure fluctuations produced
during rocket flight. As stated earlier, the
large panel surfaces absorb these pressure
fluctuations and convert the acoustic energy to
mechanical energy in the structure. At the
lower frequencies, this mechanical energy af-
fects large sections of the structure. This re-
sults in coupling and interaction between adjacent
structural segments and components; i.e., each
area affects all other areas to some degree,
either reducing or amplifying the vibration.

Large assembly tests have been developed
to simulate this environment under controlled
laboratory conditions where engineering evalua-
tion of their influence can be made. The forcing
environment on the Saturn V booster is of pre-
dominately low frequency, as shown on Fig. 1,
and is well correlated. The structural vibra-
tion can be laboratory simulated by using either
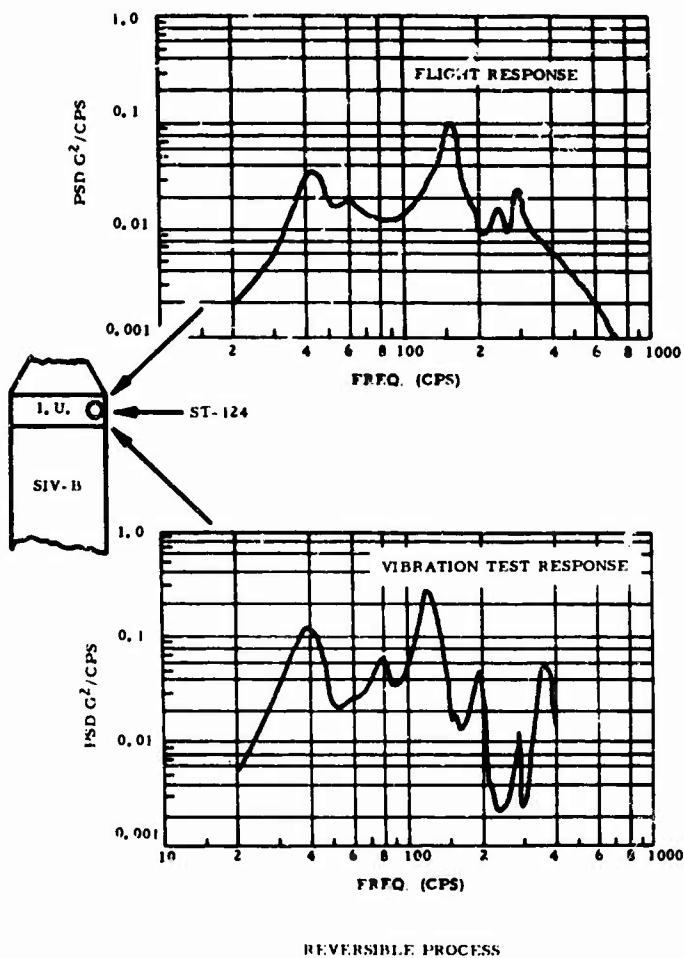mechanical or acoustic excitation. Below 300

119

Fig. 3. Flight and mechanically induced test
responses of the uprated Saturn I IU

cps the structures cannot distinguish between
mechanical and acoustical excitation (Fig. 3).
This is discussed in detail during the data
presentation.

The objectives of assembly testing are:

1. To determine the integrity of the pri-
mary and secondary structure under simulated
worst-case conditions;

2. To define mode shapes and response
characteristics of the primary and secondary
structure;

3. To determine interaction characteris-
tics at all levels of assembly;

4. To supplement theoretical dynamic anal-
ysis with test results;

5. To evaluate the adequacy of component
and subassembly level qualification pecifica-
tions and tests prior to flight.

Summary of Large Assembly Tests

Table 1 presents a summary of the large
assembly tests conducted on the Saturn program
under MSFC responsibility since 1963. All of
the tests except the instrument unit tests were
conducted at independent test laboratories under
supervision of the respective stage contractors.
The instrument unit tests were conducted under
direct contract between the test laboratories

120

TABLE 1
Saturn V Test Summary

Specimen	Approx. Weight (lb)	Number of Vibration Axes	Maximum Excitation			Test Facility
			Mechanical		Acoustic (db)	
			Sine (g)	Random (g^2/cps)		
Saturn V IU	4,000	3	—	—	153	Wyle, Huntsville, Alabama
S-IVB stage (Saturn V) forward skirt	6,000	3	6	0.04	—	Thiokol, Brigham City, Utah
S-IVB thrust complex	20,000	6	4	0.08	—	Thiokol, Brigham City, Utah
S-II stage (Saturn II) forward skirt	12,000	4	2.3	0.033	155 (overall)	Wyle, Huntsville, Alabama
S-II thrust complex	42,000	5	1.8	0.011	155 (overall)	Wyle, Huntsville, Alabama
S-II aft interstage	18,000	3	4.2	0.033	155 (overall)	Wyle, Huntsville, Alabama

and MSFC. See Figs. 4 through 10 for a pictorial presentation of this summary. Figure 10 shows the placement of the specimens in the assembled vehicle.

As Table 1 shows, assembly tests have progressed to very large, massive, complex structures. It should be noted that there are no assembly tests included on the first stage of the Saturn vehicles. Dynamic testing for these structures is effectively accomplished during their static firing tests — the booster stage creates its own worst-case environment, which the upper stages do not encounter until boost flight. Their static firing environments average 10-20 db below the boost environments at low frequencies (5-400 cps). To limit the scope of this paper, and because the S-II stage was the most thoroughly tested, the remainder of Part 1 concentrates on the test accomplished on the second stage (S-II) of the Saturn V vehicle. All tests were conducted at Wyle Laboratories in Huntsville, Alabama, during 1966 and early 1967.

Choosing the Specimen

The most desirable specimen configuration for an assembly test would be a complete stage or vehicle with all flight components installed and operating. This is impractical in most cases, however, because of specimen size and weight, test complexity, facility costs, schedules, etc. The S-II assembly tests were made on three convenient sections, forward skirt,

thrust complex, and aft interstage. These sections were logical choices because they contain almost all of the stage's operational components and because the stage is designed and manufactured in these subassemblies for ease of handling prior to final stage assembly. Their upper and lower interfaces consist of beefy primary structure ring-frames which mate to adjacent S-II or adjoining stage structures.

The test specimens were assembled from flight-type primary and secondary structure with mass, stiffness, and center of gravity simulated for most of the components. These components included such items as electrical components, fuel tank bulkheads, and the engines. Other items such as valves and feedlines were flight hardware. Dummy electrical components were used because they are infinitely less expensive and are technically acceptable at the test frequencies (below 300 cps), and because flight components are usually unavailable for specimen assembly. Valves and lines, however, are almost impossible to simulate and are normally included in flight configuration.

Test Environments

Vibration — The technique used to establish the mechanical vibration test environments for the three assemblies was the "similar structures" or Barrett technique which has been successfully used by MSFC to establish component specifications [1,2]. Vibration data

121

Fig. 4. Test specimens for Saturn V large assembly tests
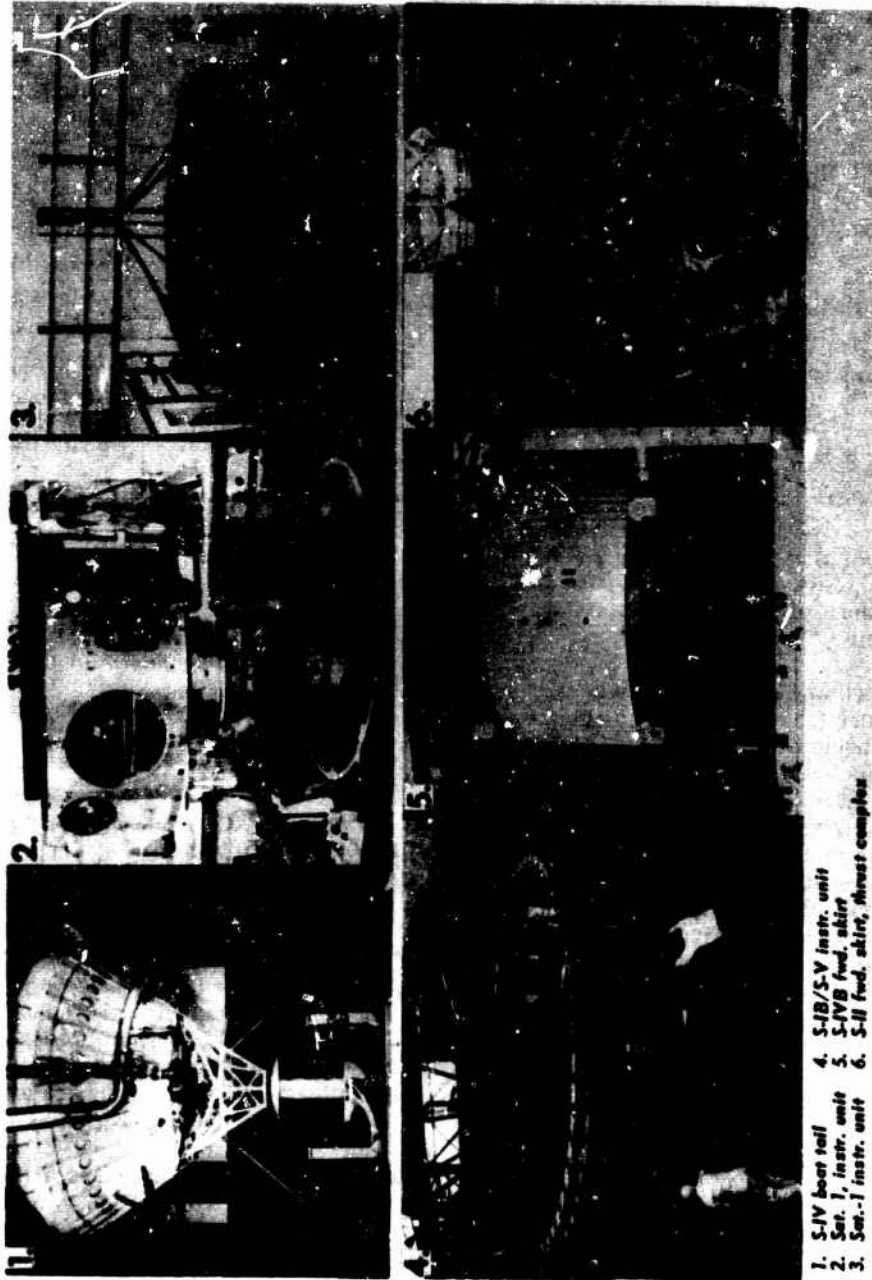
1. S-IV boat tail
2. Sat. 1 instr. unit
3. Sat.-1 instr. unit
4. S-IB/S-V instr. unit
5. S-IVB fwd. skirt
6. S-II fwd. skirt, thrust complex

122

1. S-IB/S-V instr. unit lat. axis test check out
2. S-IB/S-V instr. unit lat. axis test set-up
3. S-IB/S-V instr. unit - localized test set-up
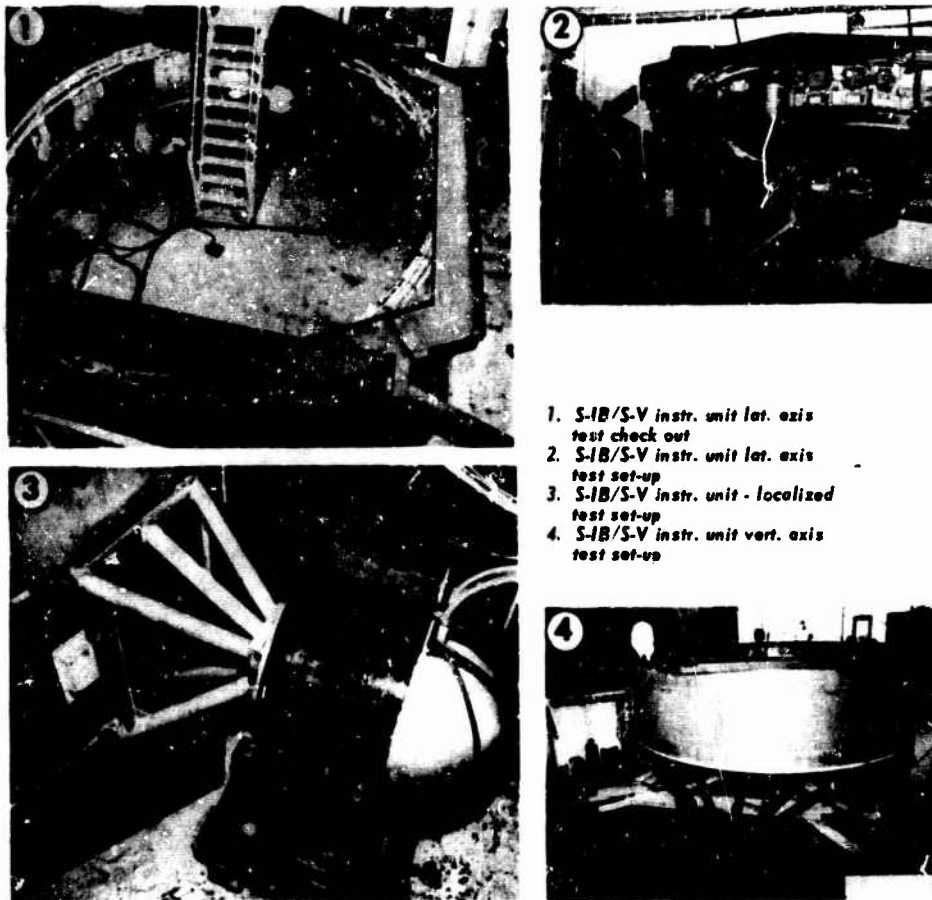4. S-IB/S-V instr. unit vert. axis test set-up

Fig. 5. Test specimens for Saturn V large assembly tests

from response measurements made on dynamically similar types of basic structure (i.e., similar inertial, damping, and elastic properties) during static firings or flights were statistically evaluated. Probability estimates of the environments were derived on a spectral basis. The statistically derived environments thus established were used as the reference levels, from which the environment for a new similar type of basic structure was extrapolated. Consideration is given in the extrapolation technique to the inertial properties of the new structure, new noise sources, distance from the noise sources, and aerodynamic configuration changes. The reference data came primarily from S-IC static firings and S-I and S-IB flights.

Experience has shown that assembly test environments based on extrapolation from the statistical mean of the reference data yields flight level responses in the primary and secondary structures of the test specimens. As a precaution against overtesting, response

measurements located at critical points on the test specimen are "red lined" at maximum predicted flight levels and monitored during each test run.

Acoustic — Acoustic specifications were based on theoretical-empirical methods derived by Dyer [3] and Bolt Beranek and Newman Inc. [4].

Test Setup

Vibration — Combination of the input specifications with the mass of the S-II thrust complex and the mass of the fixture, and consideration of normal fixture dynamic characteristics produce exciter force requirements approaching 400,000 lb. The magnitude of this force almost dictates the use of hydraulic shakers, especially when economics and the limited range (400 cps) test requirements are considered. Remaining factors to be considered then

123
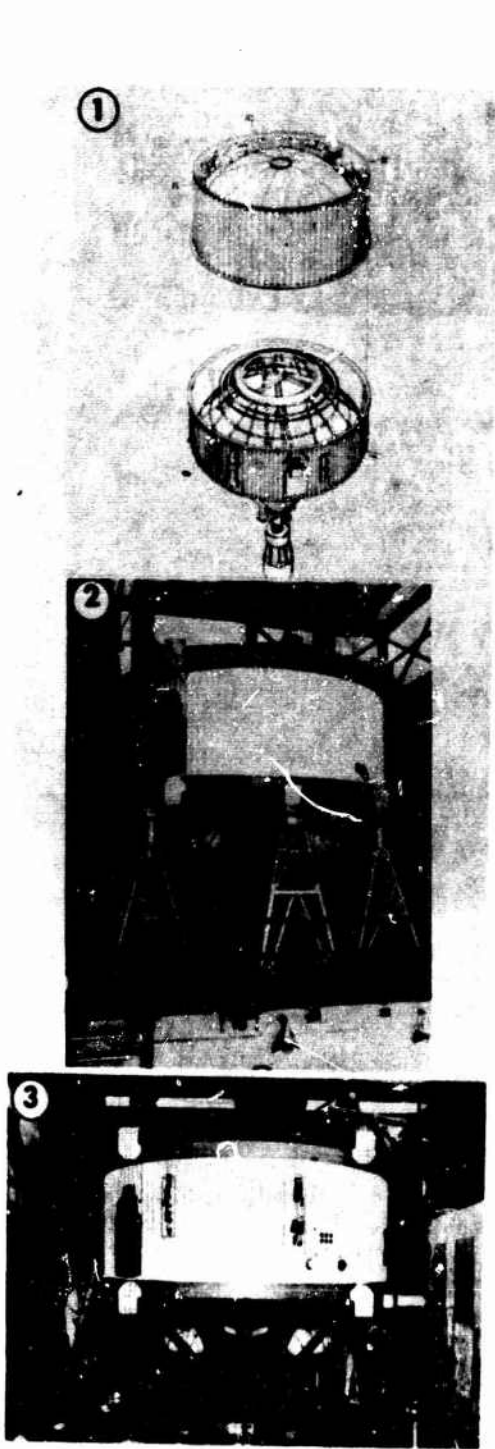
1. S-IVB vibration test specimens
2. S-IVB boat tail lateral axis test set-up
3. S-IVB boat tail vertical axis test set-up

Fig. 6. Test specimens for Saturn V large assembly tests
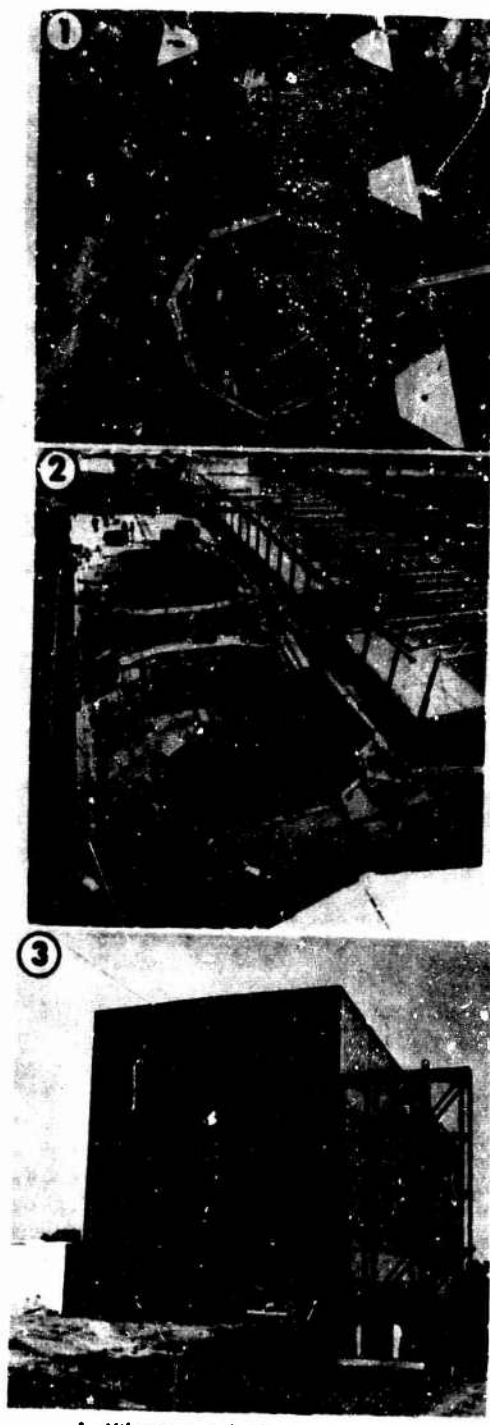
1. Vibration test facility construction - four lateral seismic masses are complete
2. Vibration test facility pits near completion
3. Vibration test facility - high bay building near completion

Fig. 7. Vibration test facilities for Saturn V large assembly tests

124

1. S-II thrust complex on transporter
2. S-II thrust complex and vertical fixture
3. S-II thrust complex being placed on vertical fixture

Fig. 8. S-II thrust complex test arrangement

Fig. 9. Lateral vibration setup

125

Fig. 10 - Specimen configuration
for Saturn V assembly test

For the S-II program the low-frequency conditions were simulated with an eight-exciter, 400,000-force-lb Hydrashaker system used in conjunction with massive steel drive fixtures and sophisticated control electronics. Pit-type reaction masses were designed and built to react the forces, and a complex flexuring system was developed to restrain the cross-axis motion of the specimen. Figure 11 shows the mechanical vibration test setup for longitudinal and lateral testing of the thrust complex. Vibration forces were transmitted from the eight exciters to the specimen by 15,000-lb steel fixtures. The fixtures were designed to distribute the exciter loads uniformly to the 33-ft-diam specimen interfaces. It was recognized that the stiffness-controlled fixtures rigidly attached to the "soft" test specimen created locally unrealistic vibration conditions. However, the structural areas of interest were generally located away from this unrealistic zone in areas where the input environment had been shaped by the structure, as discussed earlier. The areas of interest were not influenced by the rigid attachment joints. When structural areas of interest were located within the fixture influence zones, a transition segment was used. The transition segments were designed to simulate the radial response characteristics of the stage structure adjacent to the test specimen.

Input control to the averaged primary structure levels, established as described earlier, was maintained at the rigid fixture interfaces. Sinusoidal and random excitations were applied to the specimen in five axes: one longitudinal or flight axis and four lateral axes acting through the centerline of the structure and separated by 45 deg. The number of axes required for a test depends on dynamic analysis and engineering judgment of the ability of the fixture to excite the structure. Five axes proved to be more than required for the S-II program; one longitudinal and two lateral axes would have been sufficient. The control circuitry for both the sine and random tests is shown in Figs. 12 and 13.

Acoustic — Figure 14 shows the thrust complex mounted on the S-II aft interstage in the 100,000-cu-ft acoustic reverberation chamber at Wyle. The specimen was isolated from the concrete floor by the rubber tires on the transporter and shielded from unwanted acoustic leakage to the inside of the specimen by 15-db attenuation shields located on top and around the bottom of the specimen. This forced the acoustic energy to pass through the exterior shell as it does under operational conditions where continuous structures are present. The overall SPL required in the acoustic test specification was beyond the facility capability, so

were (a) how the load should be applied, (b) how many exciters are required, (c) how the exciters should be arranged, and (d) how they should be controlled to meet the test requirements.

These decisions are generally the responsibility of the testing laboratory, with the test requirements, test specimen configuration, and test specifications used as guidelines. Since these are always considered as evaluation tests, the decisions are seldom easy, usually requiring much arbitration and compromise based on numerous technical and program considerations.
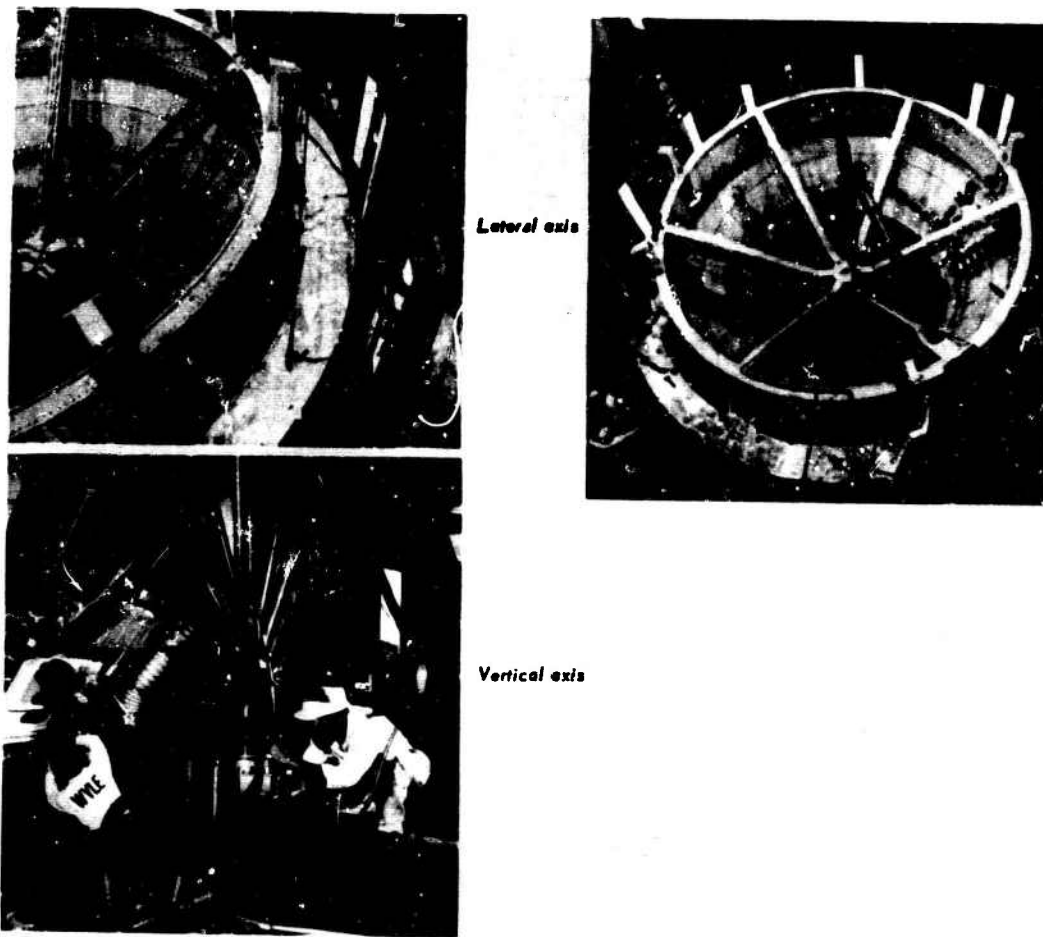
126

Lateral axis

Vertical axis

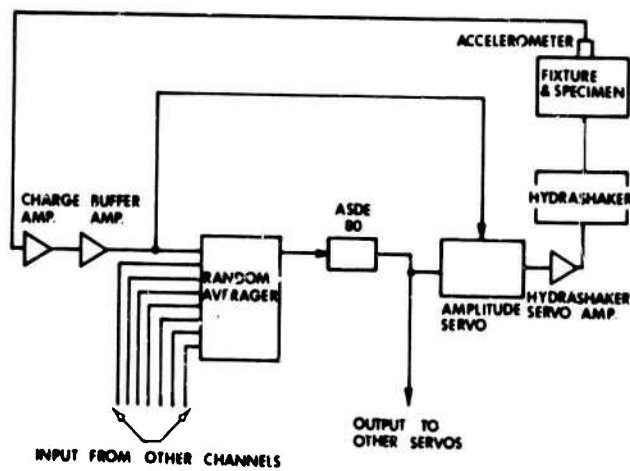Fig. 11. Setup for thrust complex vibration test

Fig. 12. Control circuitry for random vibration test
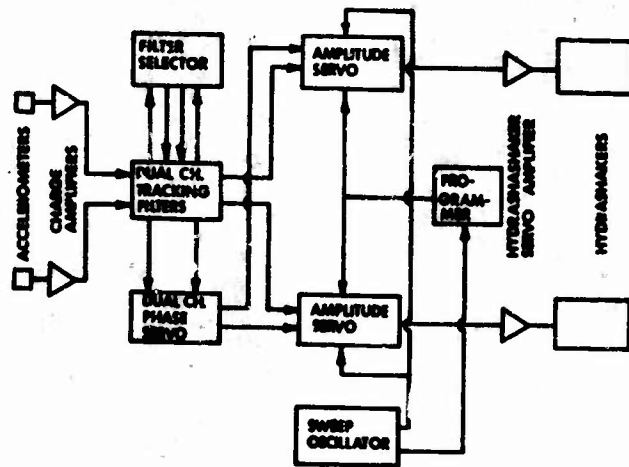
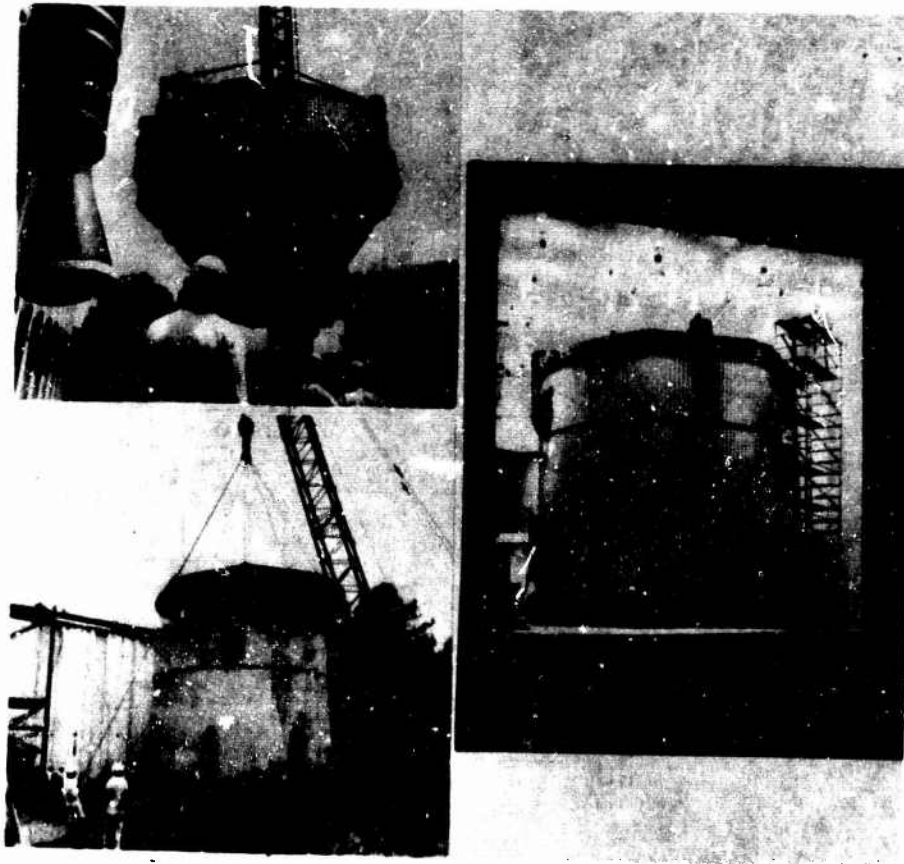Fig. 13. Control circuitry for
sine vibration test

Fig. 14. Thrust complex mounted on S-II
aft interstage for acoustic test

128

reduced step levels were used, increasing in 3-db steps. Tests were run at 149, 152, and 155 db, with the energy concentrated to meet specified levels below 400 cps during the 155-db test run. Typical structural responses are shown in Fig. 15. As noted above this gives spectral coverage of the critical structural frequencies and the ability to extrapolate data to higher SPL's. The acoustic levels roll off significantly below 40 cps and above 400 cps. Figure 16 shows the test specifications required for both the vibration and acoustic tests. Typical levels achieved during the S-II tests are shown on the same figure. Test results gave excellent control tolerances: ±1 db on the sine and ±3 db on the random average of eight control points for vibration, and ±2 db for the control microphone during the acoustic tests.

Instrumentation

Of great importance for any vibration or acoustic test is establishing the number and location of all response transducers. For the S-II program, an attempt was made to monitor flight measurement locations and the inputs to all components. Unloaded primary structure (ring frame and stringer) data were also of primary importance for comparison with theoretically determined specifications. Saturn V flight data will be compared with the test data when it becomes available for proof of test validity.

A total of 564 response measurements was recorded during the acoustic test of the thrust complex and aft interstage. A maximum of 200 could be recorded during any run, so a total of three runs was required at each SPL. In spite of the large number of measurements taken, additional locations would have been very useful. This was particularly true when interest was concentrated in a certain location because of a failure.

Data Reduction

Over 20,000 bits of data were obtained from the S-II assembly test program. These were recorded and reduced by an on-line, 200-channel digital computer system (Control Data 3200). The sine data were presented in the form of peak g vs frequency and transmissibility vs frequency. The random data from the mechanical vibration tests were reduced to power spectral density utilizing constant-bandwidth, 10-cps filters and presented as g^2/cps vs frequency. Random data from the acoustic tests were treated in the same way except for reduction with 20-cps filters. More detailed analyses, such as reduction with narrow and variable bandwidth filters, crosscorrelations, and mode shapes, were accomplished and are currently being evaluated. Even with this large quantity of data, more could be utilized.
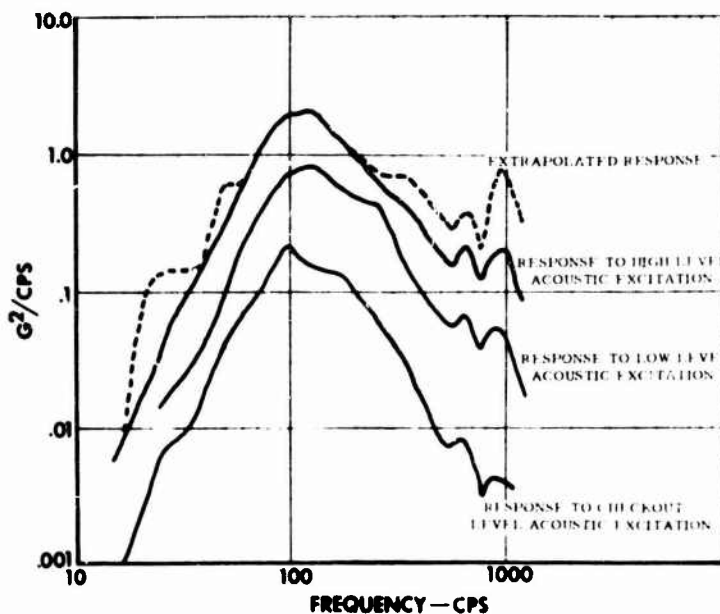

Fig. 15. Extrapolated radial responses to Saturn V predicted flight-level acoustic environment, based on response to three levels of acoustic excitation (average of six unloaded ring-frame and stringer measurements)
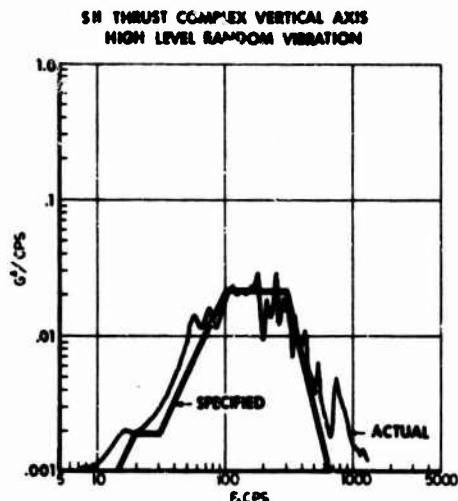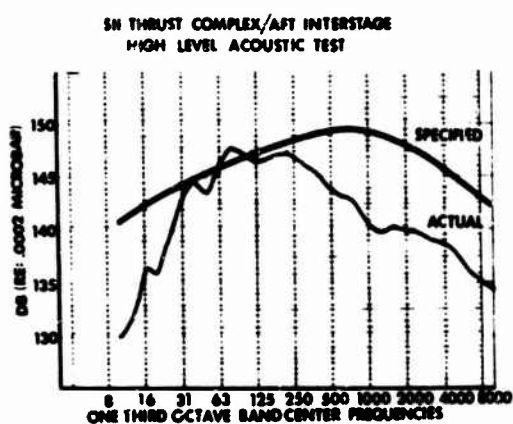
129

Fig. 16. Specified vs achieved test level
for vibration and acoustic tests

PART 2

Data Evaluation and Comparisons

In general, the following questions arise
concerning the use and application of assembly
testing:

1. What are the test facility capabilities?

2. Can these facilities provide a simulation
of the flight environment?

3. What can be learned from assembly test-
ing that cannot be determined by analysis or
component test?

These questions and other interesting and sig-
nificant aspects of assembly testing are dis-
cussed and evaluated in the subsequent para-
graphs.

To illustrate the capability of large rever-
berant acoustic chambers for exciting full-scale
structures, two representative examples from
the S-II thrust-complex acoustic test are

presented. The first example is the response
of unloaded primary structure at station 118.5
of the S-II stage interstage. This location is 80
in. from the fixture-specimen interface restraint
and 40 in. from the forward ullage motor fitting.
This location is well removed from either fix-
ture restraint or component loading and is there-
fore considered unloaded primary structure.
Figure 17 illustrates the measurement location
at ring-frame station 118. Since the acoustic
chamber was incapable of meeting the predicted
acoustic SPL for the entire frequency spectrum,
a compromise was selected that would attempt
to meet predicted levels in the frequency ranges
most critical to secondary support bracketry
and primary structure: 30-250 cps. In the re-
maining frequency ranges, the SPL was allowed
to roll off. The resulting acoustic environment
is shown in Fig. 18. The unloaded primary
structure response is shown in Fig. 19. The
response in the frequency range above 300 cps
shows the effect of the corresponding acoustic
environment roll-off. Of note is the 50-300-cps
modal response corresponding to the 153-db
SPL. This is especially indicative of this large
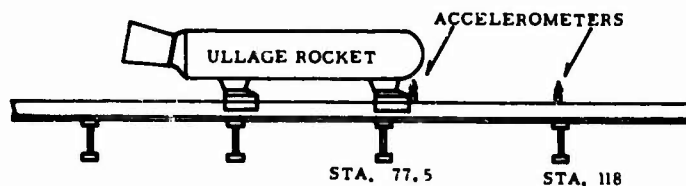chamber's low-frequency reverberant capability,

Fig. 17. Instrumentation locations, S-II
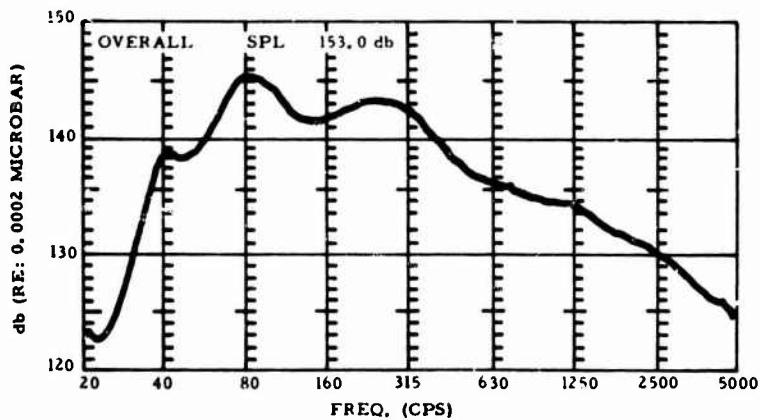interstage unloaded and loaded structure
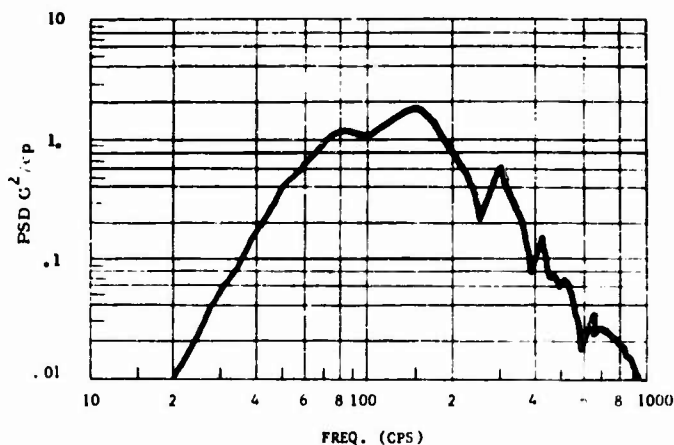
130

Fig. 18. S-II interstage acoustic environment

Fig. 19. Unloaded S-II interstage radial vibration
response to acoustic excitation

which was a unique requirement to simulate the singular low-frequency acoustic environment generated by the S-IC stage at liftoff. As an illustration of the acoustic forcing capability for relatively heavily loaded structure, an ensemble of the input vibration measurements of the 500-lb S-II stage ullage motor is included in Fig. 20. The acoustic environment of Fig. 18 is still appropriate. The response at 30 cps is a rigid body mode of the ullage motor on the supporting shell structure. The notch area indicates the lack of rigid body modes in that frequency range, i.e., low structural mobility. The vibration level increasing to 100 cps is the support structure response to the resonance of the ullage motor and support brackets. Beyond approximately 100 cps, the primary support structure is essentially decoupled from the ullage motor and the interstage response is in effect unloaded.

The greater high-frequency response of the loaded structure is associated with a localized resonance of the monitoring accelerometer mounting location.

Unfortunately no direct comparison can be made between flight data and assembly response to acoustic excitation, since all acoustic tests were on Saturn V hardware and attempted to simulate the anticipated Saturn V liftoff environment. The best comparisons available are those between the uprated Saturn I IU flight data from AS 204 and 202 flights and the Saturn V IU acoustic tests. The two structures are essentially identical although exposed to different acoustic environments. Figure 21 illustrates these acoustic environments. The flight measurement was obtained on the instrument unit during uprated Saturn I liftoff. The test
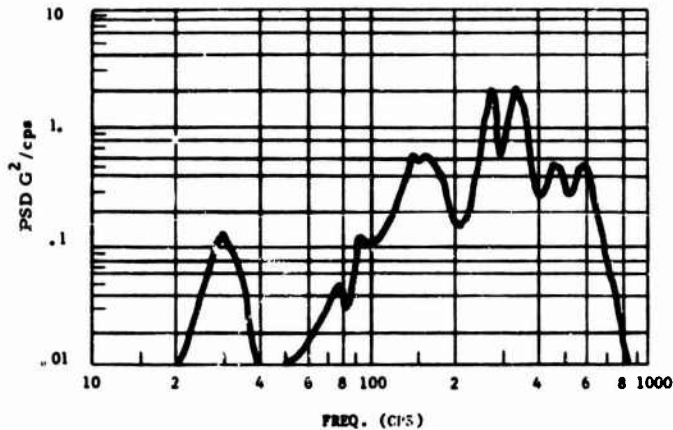
131

Fig. 20. Loaded S-II interstage radial vibration
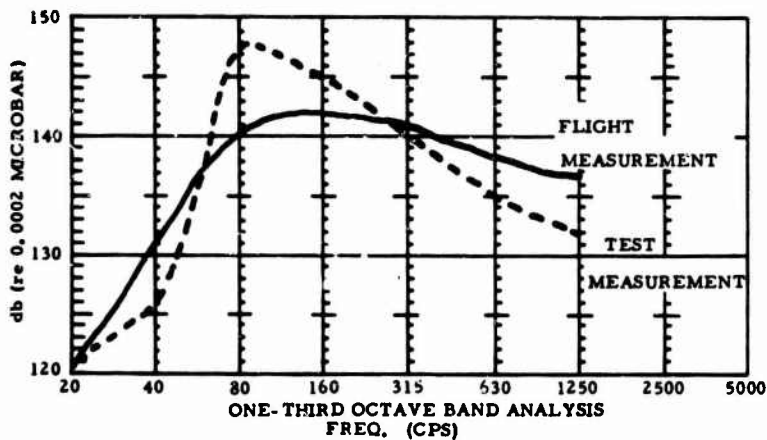response to acoustic excitation

Fig. 21. Comparative acoustic environments for
uprated Saturn I IU and Saturn V IU

measurement was obtained during the Saturn V IU acoustic test. It is emphasized that the test measurement is not intended as a simulation of the flight measurement but is an attempt to simulate Saturn V liftoff environment which has a higher low-frequency SPL than the uprated Saturn I. The two curves are shown to facilitate comparison of the resulting vibration response.

Comparative vibration response levels on the stabilized platform (ST-124) are shown in Figs. 22 and 23. Instrumentation locations associated with these curves are shown in F g. 24. As illustrated in Figs. 22 and 23, th   e modes are apparent in both the flight and test response; however, the magnitude of the response varies greatly at 280 cps. The acoustic test vibration response is much higher than the flight data, even though the acoustic test SPL is lower than flight SPL. The greater 280-cps acoustic test response is considered to be a reverberant-chamber reinforcing effect which does not exist in flight. Also apparent is the inability of the acoustic chamber to force a response at 40 cps because of the sharp chamber ro" 'f. In Fig. 23, superimposed on the acoustic st response, is the mechanical random-excitation response 21X07R, which well supplements the acoustic test response in the low-frequency range. Figures 25 and 26 compare the flight, acoustic test, and vibration test responses at the flight control computer support. In general the vibration response data support the trend expected from a comparison of the acoustic excitation in Fig. 21. Higher response levels were obtained during test in the 200-1000-cps range than during flight. As noted in the analysis of ST-124 data, mechanical

132
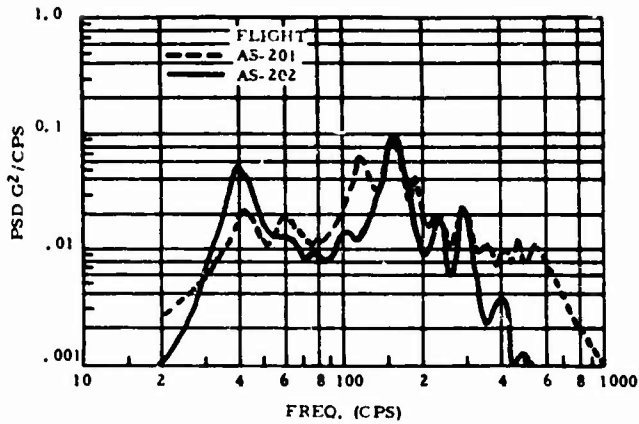
Fig. 22. Saturn IB IU stabilized platform, flights
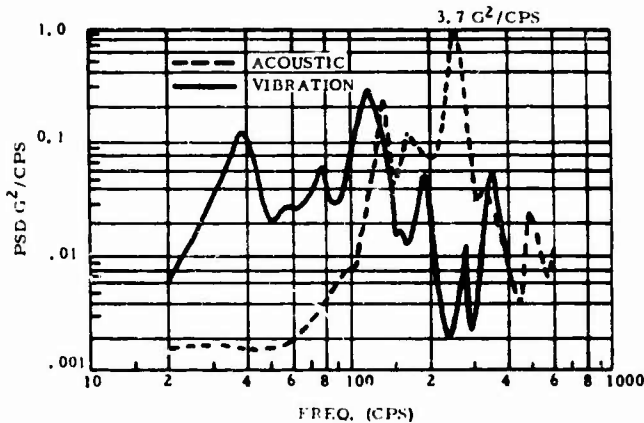AS201 and AS202, measurement E9-603

Fig. 23. Saturn V IU stabilized platform acoustic
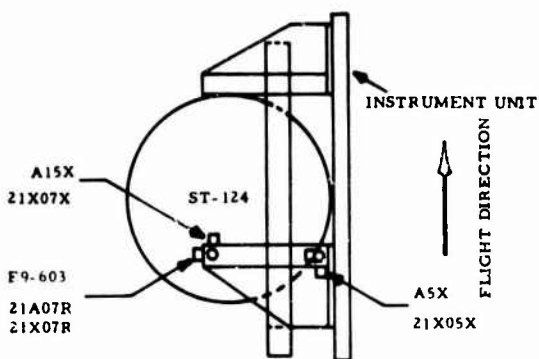and vibration test, measurement E9-603

Fig. 24. Instrumentation locations, sta-
bilized platform (ST-124) (E9-603: radial
flight measurement; 21A07R: corre-
sponding radial vibration response meas-
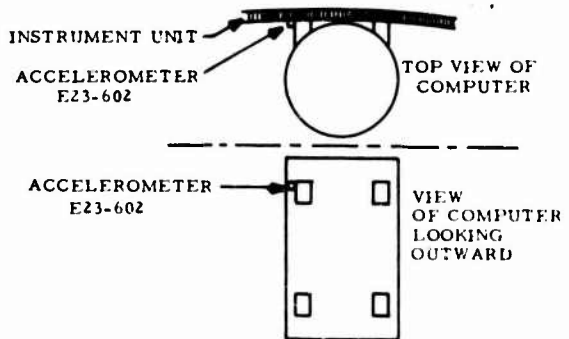urement during acoustic test)

Fig. 25. Instrumentation location
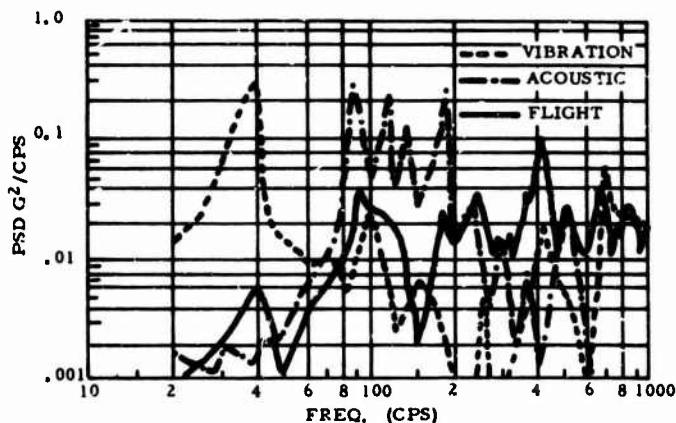for flight control computer

133

Fig. 26. Flight control computer, comparative
environments, flight AS201, acoustic test and
vibration test

vibratio..s are a very efficient excitation for
low-frequency modes.

Transmissibility and Rigid
Body Modes

One of the primary assets of assembly
testing is the capability of defining transmis-
sibility factors of secondary support structure
with actual primary structure impedance. Usu-
ally, secondary support transmissibility is cal-
culated by analyzing or testing the response of
the item when supported by an infinitely rigid
mass. For example, the transmissibility of
component support structure or the response of
a component is obtained from a component test
with the specimen support bracketry attached
to a rigid slip plate. Generally this method
yields acceptable results when the secondary
support structure is relatively "soft" compared
with the primary supporting structure. The
method becomes less applicable when the sup-
port structure impedance approaches the im-
pedance of the primary structure in the
component-secondary bracket resonance-
response range. In other words, the secondary-
support bracket stiffness is approximately equal
to the stage primary structural stiffness. At
the other end of the spectrum, a condition can
exist where the secondary-support bracket
stiffness is much greater than the primary
structure. This latter condition is discussed
and illustrated here. When this condition exists,
the rigid body modes of the component/support
bracketry on the "soft" supporting primary
structure will obviously not be obtained in a
component-support bracketry test but are par-
ticularly evident in an assembly test. From a
secondary-structure design standpoint, the

rigid body modes are generally not a considera-
tion if the secondary bracketry design is based
on an infinite primary structure-support im-
pedance, since the maximum resulting loads
will be defined by the latter analysis. However,
if in specific instances a component has an
actual functional frequency in the rigid body
mode range, then a potential problem may go
undetected unless an analysis or test is per-
formed utilizing the primary structure dynamic
characteristics. An example of this possibility
is illustrated in Figs. 27 and 28. The instru-
ment unit stabilized platform is supported by a
very stiff magnesium casting, and the assembly
is attached to a relatively soft honeycomb shell,
1 in. thick, 30 in. high, and 260 in. in diameter.
Figure 27 shows the result of a component
evaluation test with the magnesium support
casting attached to a slip plate. The response
A15X and input A5X measurement locations are
shown on Fig. 24. Although the overall response
of the bracket is highly damped, resonance fre-
quencies at 100, 190, and 250 cps are noted.
Figure 28 shows the result of the instrument
unit assembly sine-sweep test with measure-
ments in the identical position as in the compo-
nent test. These measurements indicate a sig-
nificant rigid body mode at 93 cps, another at
100 cps which masks the 100-cps component-
support bracket resonance but is of greater
magnitude, and the 250-cps resonance indicated
by the component test but of significantly less
magnitude. Lacking the rigid body data, one
could conclude that any actual low-frequency
functional sensitivity in the 40-60-cps range
would not be a problem; however, the assembly
test data point out that indeed a major problem
may exist. The example is presented to il-
lustrate the point that rigid body and low-
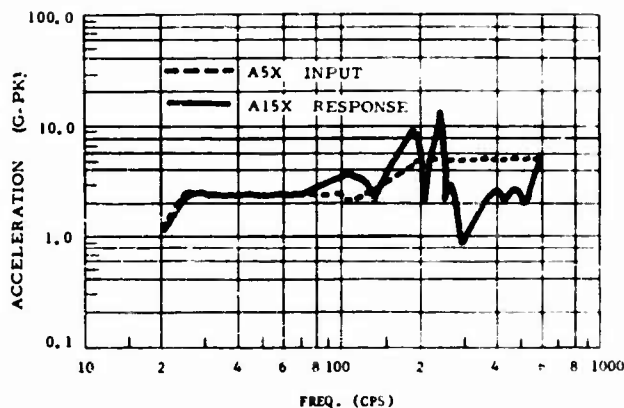frequency structural modes may be overlooked

134

Fig. 27. Stabilized platform (ST-124) component
test: longitudinal sinusoidal input (A5X) and re-
sponse (A15X)
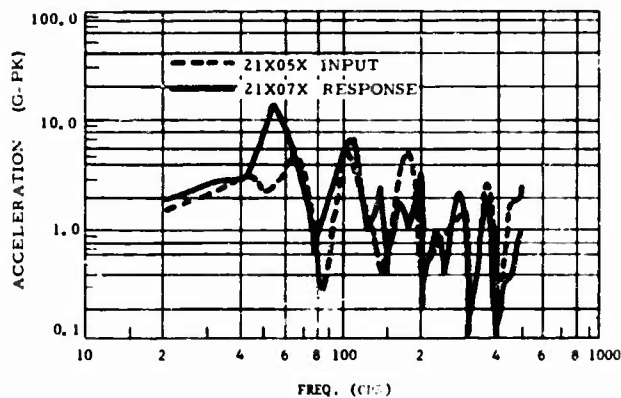
Fig. 28. Stabilized platform (ST-124) assembly
test: longitudinal sinusoidal input (21X05X) and
response (21X07X)

and undetected in component tests but can be
diagnosed in assembly tests. The case illus-
trated was selected because it particularly em-
phasized the point; but it could not be considered
as a typical case since the magnesium bracket
was deflection-designed and, as such, would be
much stiffer than a load-designed bracket.

Comparison of Acoustic and
Mechanical Excitation

Figures 29 and 30 illustrate a comparison
between measured S-II thrust structure response
to acoustic and random mechanical excitation.
The data are presented to illustrate that, with
sufficient reverberation chamber capacity,
low-frequency structural modes of significant

magnitude can be excited on relatively dense,
loaded structures. In doing this, one sacrifices
other high-frequency areas of the spectrum.
The response curves are not meant to imply
that the acoustic excitation is more efficient
than mechanical excitation in low-frequency
ranges, since the full capacity of the mechani-
cal excitation was purposely being limited by
the expected vibration response. In fact, me-
chanical excitation is not only a more efficient
exciter in the low-frequency range but generally
more practicable, unless existing acoustic fa-
cilities can efficiently obtain the required low-
frequency spectrum. In either case, a supple-
mental high-frequency acoustic test is needed
to cover the complete spectrum. A supplemen-
tal high-frequency acoustic test is, without
doubt, the most efficient method of obtaining

135
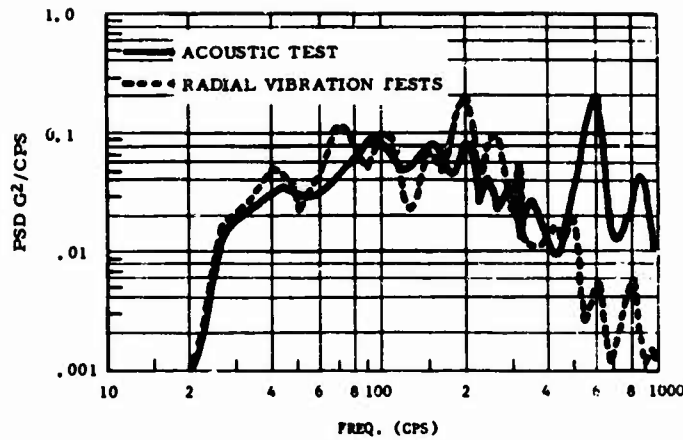
Fig. 29. S-II stage thrust complex acoustic and
radial vibration inputs to equipment container 207
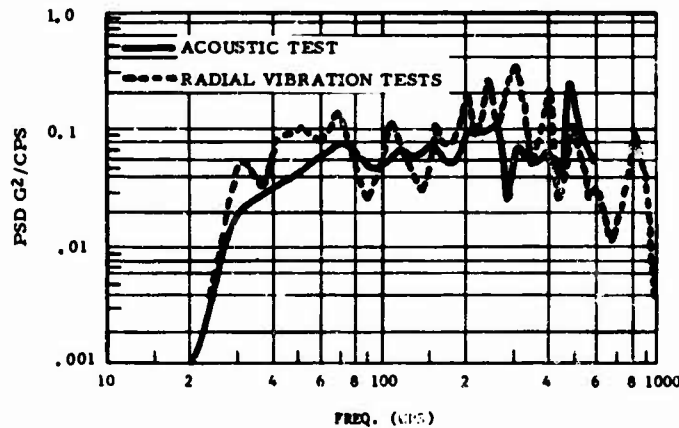
Fig. 30. S-II stage thrust complex acoustic and
radial vibration inputs to equipment container 209

high-frequency excitation, since Hydrashaker
frequency response and fixture design severely
limit the mechanical forcing capability.

CONCLUSIONS

Conclusive evidence exists to support the
use of assembly testing. Although large assem-
bly testing should not be used as a substitute
for component qualification tests, it provides
an invaluable supplemental program to accom-
plish the objectives outlined here. These objec-
tives cannot be accomplished by any other test
means. Program costs associated with test
facility construction and activation are high.
Now that facilities are available, however,
actual test costs are not excessive when

compared with large complex component quali-
fication tests. For shell-type structures, ac-
ceptable full-spectrum test results can be ob-
tained from either acoustic tests or vibration-
acoustic tests, depending on the low-frequency
capability of the acoustic chamber. Acoustic
tests are generally simpler and cheaper, pro-
vided that a facility is available to obtain the
required acoustic environment; however,
acoustic-chamber-to-flight-environment trans-
fer functions must be established. Tests to date
show significantly higher acoustic test response
levels than are anticipated during flight.

The following are recommended:

1. Expand assembly test programs to in-
clude operational components. Operational

136

components on the assembly test would provide a means for final-system verification prior to flight.

2. Expand assembly test programs to include acceptance testing of the flight systems in place of individual component acceptance tests.

3. Expand assembly test programs to study the effects of vehicle static, thermal, and propellant-mass pressure loading on the stage structural response characteristics.

4. Expand assembly test programs to include localized impedance tests. The impedance values could be combined with measured response accelerations to establish force spectra for use in component qualification test programs.

Each of the above recommendations, including acoustic-chamber-to-flight transfer functions, has been implemented at MSFC and the results will be used in all future programs.

REFERENCES

1. R. E. Barrett, "Techniques for Predicting Localized Vibratory Environments of Rocket Vehicles," NASA TN-1836, Oct. 1963

2. R. E. Barrett, "Statistical Techniques for Describing Localized Vibratory Environments of Rocket Vehicles," NASA TN-2158, July 1964

3. Ira Dyer, "Estimation of Sound Induced Missile Vibration," Ch. 9 in Random Vibration (S. H. Crandall, Ed.), Technology Press of the Massachusetts Institute of Technology, Cambridge, 1958

4. Bolt Beranek and Newman, "Structural Response to Inflight Acoustics and Aerodynamic Environments," Repts. 1417 and 1418, Job No. 11212, July 1966

DISCUSSION

Mr. Sickmeier, General Motors Corp.: You mentioned during your opening remarks that these structures receive high static and vibratory loads. I have yet to hear any comments concerning how these combined loads are actually treated either in test or analysis.

Mr. Everitt: Currently the combined loads are not treated in test; they are treated in analysis. Generally speaking, the vibration loads that we are talking about are affecting, for a stress man, localized areas of the structure. He would classify it as secondary structure. Therefore the vibration does not contribute significantly to the static load environment for the basic vehicle.

Mr. Kachadourian, General Electric Co.: Our findings are quite different from yours as far as complete system vibration testing is concerned. We get considerable difference in

responses from a mechanical vibration test than we do from actual flight, or from an acoustic test. Possibly the difference is that you are using multiple shaker systems and that you are only going up to 400 Hz. We found that most of our significant vibration due to acoustic excitation is in the high frequency range, say from 200 to 1000 Hz. I noticed in a lot of your data that you did get differences in the 200-600 Hz range.

Mr. Everitt: You will get differences in the 200-600 Hz range after you get away from the primary structure such as the ring frames, stringers, etc. In the primary structure the mechanical vibration and the acoustic vibration does agree very well.

Mr. Kachadourian: Well, being concerned about component environments I think mechanical vibration loses a lot of its validity in the high frequency range.

*   *   *

137

DEVELOPMENT OF ACOUSTIC TEST CONDITIONS FOR
APOLLO LUNAR MODULE FLIGHT CERTIFICATION

Wade D. Dorland, Robert J. Wren
NASA Manned Spacecraft Center
Houston, Texas

and

Kenneth McK. Eldred
Wyle Laboratories
El Segundo, California

An acoustic test of an Apollo lunar module test article was performed prior to flight to verify structural and component integrity. Since the lunar module is enclosed within a spacecraft/lunar-module adapter during the first-stage boost when the dynamic pressure environments are encountered, the test was performed in accordance with criteria based on measurements of spacecraft/ lunar-module adapter vibration response. The test operations were conducted in the Manned Spacecraft Center Spacecraft Acoustic Laboratory, which employs a progressive-wave mode of acoustic excitation and has a duct system tailored to the outer moldline of the Apollo spacecraft. In the lunar module qualification test, the acoustic spectrum imposed on the spacecraft/lunar-module adapter was nearly as predicted for frequencies above 315 Hz, whereas the low-frequency spectrum contained more energy than predicted. The measured spacecraft/lunar-module adapter responses provided an excellent fit to the flight envelope.

INTRODUCTION

Verification of the capability of the Apollo lunar module (LM) to sustain the dynamic loads experienced during launch necessitated the performance, prior to the launching of the first LM vehicle, of a comprehensive ground test program to qualify the structure and system components for flight. As a part of this ground test program, an acoustic test was performed to simulate realistically the dynamic pressure environment which exists during the launch-and-boost phase of an Apollo mission. (The expression "dynamic pressure" refers to the acoustic and high-frequency, unsteady fluctuating-pressure components of the total pressure environment. "High frequency" in this context refers to that part of the audio spectrum between 20 and 2500 Hz.) Since the LM acoustic testing imposed certain uncommon environmental simulation requirements, the resulting test operation incorporated several newly devised experimental techniques which are considered to be an important contribution to acoustic testing technology.

Throughout the launch-and-boost phase, the LM is located within the spacecraft-LM adapter (SLA). The LM is attached at four points to the SLA, which is a truncated cone 28 ft long that fairs the spacecraft into the Saturn IVB (S-IVB) stage (Fig. 1). During the initial phase of flight, the dynamic environment exterior to the vehicle has three distinct characteristics of interest:

1. Booster noise at liftoff, a zero-velocity condition;

2. Aerodynamic excitation in the transonic-velocity condition;

3. Aerodynamic excitation in the supersonic-velocity condition.

The environment inside the SLA, however, is a function of the dynamic energy transmitted through the structure; hence, the interior environment is largely determined by the SLA response to exterior excitation. This aspect of the LM environment introduces an unusual consideration into the determination of adequate ground test conditions, since current analytical techniques do not yield precise environmental definitions for a test article that is mounted inside an adapter. Accordingly, an experimental procedure which obviated the requirement
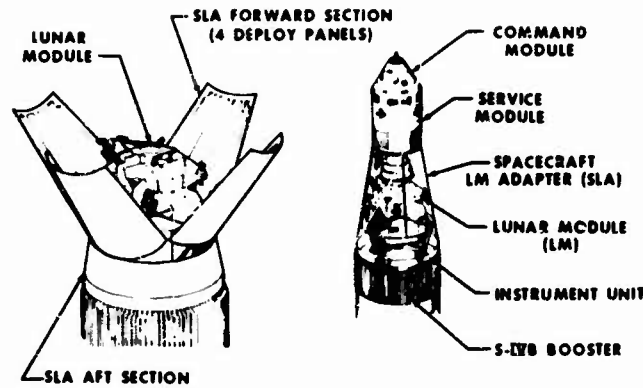
Fig. 1. Lunar module and spacecraft/
lunar-module adapter

for analytically derived test environments was needed. Such a procedure was devised for this project. The procedure was based on the rationale that the environment for the LM is a combined result of the acoustic field in the SLA and the vibration transmitted through the SLA attachment fittings. The LM environment is uniquely related to the SLA dynamic response; therefore, the proper LM environment could be obtained in the laboratory only by exciting the SLA to its flight response. To support such an experimental procedure, data available from three flight pickups (which were recorded during each of the first two Apollo flights) were used to define the required SLA vibration response. Application of this procedure enabled the adjustment of the laboratory acoustic spectrum to compensate for the difference in the spatial distribution of phase-correlation coefficients which exist in flight and laboratory environments. Hence, the acoustic field was controlled for the specified SLA vibration response rather than for faithful simulation of a predicted flight fluctuating-pressure environment. It is significant that the acoustic spectrum actually imposed on the SLA in the laboratory contained more low-frequency energy than was predicted for the liftoff environment, whereas the high-frequency spectrum (above 315 Hz) was nearly as predicted. The increased low-frequency energy was not undesirable but illustrates how the empirically determined test conditions differed from predicted conditions.

The acoustic testing of the LM test article was performed in the Manned Spacecraft Center Spacecraft Acoustic Laboratory (MSC SAL). This facility employs a progressive-wave mode of acoustic excitation and has a duct system tailored to the outer moldline of the Apollo spacecraft. These ducts, in combination with

controllable acoustic noise generators, provide the ability to control acoustic energy levels, the spectral distribution (in one-third octave bands), the longitudinal dynamic pressure profile, the circumferential dynamic pressure profile, and the approximate circumferential space correlation of the acoustic field. Prior to the LM acoustic test, a sequence of runs was performed on an Apollo spacecraft, during which the acoustic field was tailored to produce SLA response that simulated flight response.

The simulation problem is described below. This description includes the vehicle and its launch environment, the available environmental and response data, the test rationale, and the derivation of the test criteria. After a brief description of the test facility, the experimental program used to prepare the facility for the LM acoustic test is presented. In addition, the test results are presented.

APOLLO VEHICLE AND
ENVIRONMENT

The Apollo spacecraft launch configuration embodies a complex of various spacecraft and launch-vehicle modules. The spacecraft launch configuration, based on specific mission objectives, may consist of a launch escape system (LES), the command and service modules (CSM), the LM, an SLA, an SLA nose cone, and the launch vehicle which is a Saturn booster configuration. Of particular interest for ground test simulation is a spacecraft configuration of LES, CSM, and SLA launched by an uprated Saturn I booster (S-IB and S-IVB stages) or this spacecraft configuration with an LM added launched by the Saturn V booster (S-IC, S-II, and S-IVB stages). Also of interest is a mission

140

involving an LM mounted inside an SLA with a nose cone attached to the forward end of the SLA. This spacecraft configuration would be launched by an uprated Saturn I booster. In all flights, the instrument unit (IU) provides the mechanical interface between the spacecraft and launch vehicle. The external dimensions (or moldline) of the CSM, SLA, and IU remain constant. Figures 1 and 2 show the arrangement of the modules at launch.

such that each panel behaves as a continuous, curved honeycomb shell segment. The panels are joined by bolted doubler plates on internal and external surfaces. At the LM attachment station (81 in. forward of the SLA-IU interface), a light ring stiffener is employed at the joint between the forward and aft sections. The entire SLA can be considered a continuous, uniform shell composed only of the honeycomb structure used in the construction of the subpanels. This
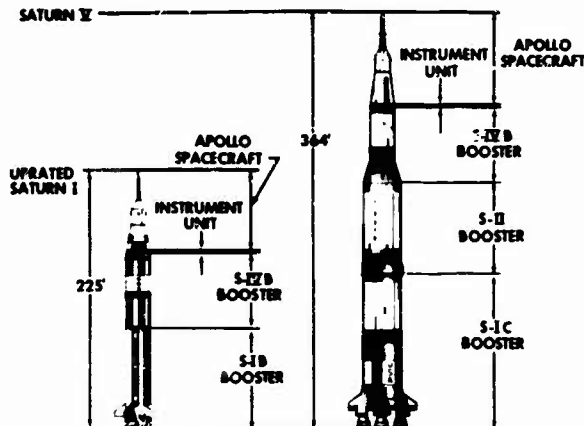

Fig. 2. Apollo spacecraft and launch vehicles

Since, as previously mentioned, the structural response of the SLA is a key factor in the LM acoustic test, the SLA structure must be described in some detail. The SLA is a truncated cone comprising eight panels. Four of the panels, such as the forward section, have linear explosive charges installed at panel junctions. During CSM-SLA separation, the charges are fired to open the four panels, which frees the CSM from the launch vehicle and exposes the LM (Fig. 1). The other four panels make up an integrated aft section which remains attached to the IU throughout the flight. The SLA diameter is 155 in. at the SM interface and 260 in. at the IU interface. The adapter is 336 in. high and has a slant height of 349 in. and a slant angle of 8.6 degrees. Each of the eight panels is constructed of several aluminum honeycomb subpanels, and the eight panels are joined by stiffeners having same radial thickness as the honeycomb face sheets. Thus, in appearance, the composite of subpanels and stiffeners forms a smooth curved surface for one panel. The structural dynamic properties of the panels are controlled essentially by the honeycomb subpanels and not by the stiffeners,

honeycomb is constructed of type 2024T-81 aluminum alloy that is 1.7 in. thick and has a surface weight density of approximately 2 lb/ft^2. The entire SLA assembly weighs approximately 3600 lb. During unmanned CSM flights, the LM is replaced in the SLA by the flight stabilizer, which is a simple crossed truss weighing approximately 60 lb. During missions which require the LM, the SLA supports the full weight of the CSM, weighing approximately 70,000 lb, and of the LM, weighing approximately 30,000 lb.

During launch and boost, the Apollo spacecraft is exposed to an acoustic environment at liftoff that is generated by the exhaust turbulence of the first-stage booster engines. Additional dynamic pressure environments envelop the spacecraft during the transonic and supersonic portions of flight, but no significant pressure environments excite the spacecraft at velocities in excess of Mach 3. In all these conditions of first-stage boost, the spacecraft/launch-vehicle configuration is the same. Accordingly, a single test-article setup is sufficient for a ground test simulation of the launch dynamic environment.

141

AVAILABLE DATA AND
TEST RATIONALE

In the development of the Apollo spacecraft, nearly all of the early effort for environmental definition was concentrated on the CSM, and only the forward section of the SLA was included in this work. After most of the early definition had been accomplished, the shape of the SLA was drastically altered, thus nullifying the validity of this work — both analytical and experimental — as applied to the SLA or the LM. The LM vehicle designers had employed a comparability technique based on Barrett's method [1,2] to establish early LM environmental descriptions. It was recognized that the LM environment was a combined result of the acoustic field in the SLA and the vibration transmitted through the SLA attachment fittings on the descent-stage outriggers. Barrett's method is an accepted procedure for deriving launch-vehicle structural test requirements. However, application of this technique to LM environment definition presented difficulties since Barrett's method is based on the assumption that similar structural configurations exhibit similar dynamic characteristics. The difference between the environmental excitation of the Saturn and LM structures contributes a significant uncertainty to the application of Barrett's method. Hence, the anticipated noise reduction of the SAL was calculated, and the resulting lower LM vibration levels were used as structural and equipment specifications for design and qualification purposes. By using this modification of Barrett's method, overly conservative vibration levels were avoided. One important test objective, therefore, was the verification of the predicted SLA noise reduction and the resulting LM vibration.

To achieve this objective, a test procedure was devised that used the limited flight data available on the response of the SLA panels to obtain the required test conditions. In this procedure, the proper LM environment could be obtained in the laboratory by exciting the SLA so that its response matched the flight data as nearly as possible. The motion of the SLA panels in response to external environmental excitation serves as a source of excitation of the internal SLA air mass; therefore, the acoustic field inside the SLA during a test closely simulates the internal SLA acoustic field during flight, if the response is the same in both the test and the flight. Hence, this excitation of the LM is realistic. Also, the LM receives a small amount of dynamic excitation through its attachment points to the SLA. Since the test configuration of the SLA and its mating components in the laboratory closely duplicate the SLA flight

configuration (with only minor exceptions), the LM excitation through the attachment points is essentially the same in both situations. Accordingly, the total dynamic excitation of the LM acoustic test closely simulates flight conditions.

TEST CONDITIONS

As mentioned above, limited SLA vibration measurements were obtained during early Apollo spacecraft launches. The measurements, which were made at three asymmetric points, indicated motion in the radial direction. (The locations of the points are shown in Fig. 3, a developed sketch of the SLA. The measurements are designated SLA-0, SLA-1, and SLA-2.) Identical measurements were made on two flights which followed very similar boost profiles. The records of overall rms vibration level (rms g) as a function of range time for all six measurements (that is, records for each of three locations during each of two flights) are shown in Fig. 4, and a tabulation of measurement parameters is given in Table 1. Inspection of these data shows that the characteristics with time of the two flights are very similar. In addition, the conditions of maximum response (that is, liftoff, transonic velocity, and supersonic velocity) are clearly evident. Plots of acceleration power spectral density (PSD) for the response at liftoff are presented in Figs. 5, 6, and 7, and one-third octave-band spectrograms for all three response conditions are plotted in Figs. 8, 9, and 10. Again, from the spectral plots, a rather remarkable repeatability of the vibration is evidenced in the two flights.

Since the electronic control system of the MSC SAL [3] provides spectral control in one-third octave bandwidths, test conditions were developed using corresponding bands. Only one spectral condition can be programmed in the test; therefore, it was necessary to reduce the number of applicable spectra to a single spectrum at each location. Examination of the spectra for the different flight times at each measurement location (Figs. 8, 9, 10) revealed that the range of spectral levels in each band was nominally 15 db or a half order of magnitude. Furthermore, the liftoff spectrum was observed to dominate, except for the very low and high frequencies where the transonic response is higher. (As a peripheral observation, supersonic response does not dominate any portion of the spectrum at any of the three locations.) Enveloping the spectral data points would produce slightly more strenuous test conditions than averaging the data, but in a flight simulation such an envelope spectrum for each location is advantageous in obtaining a reasonable,
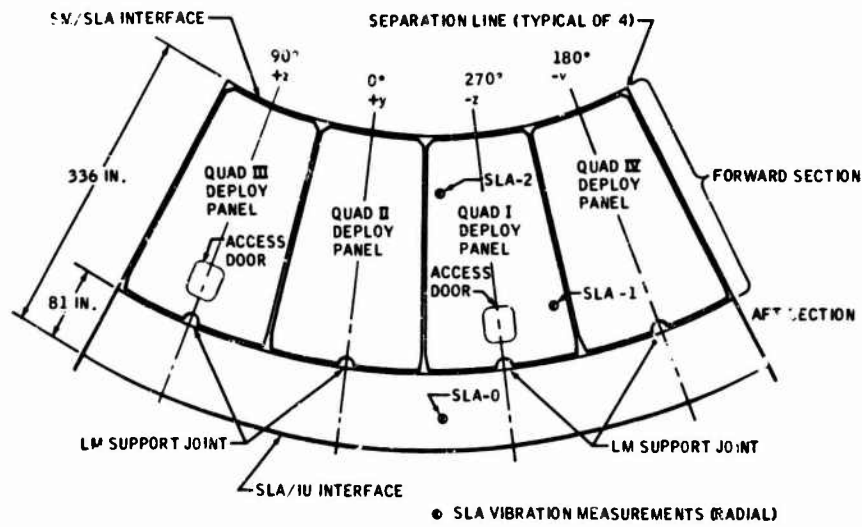
142

Fig. 3. Developed view of SLA showing location of
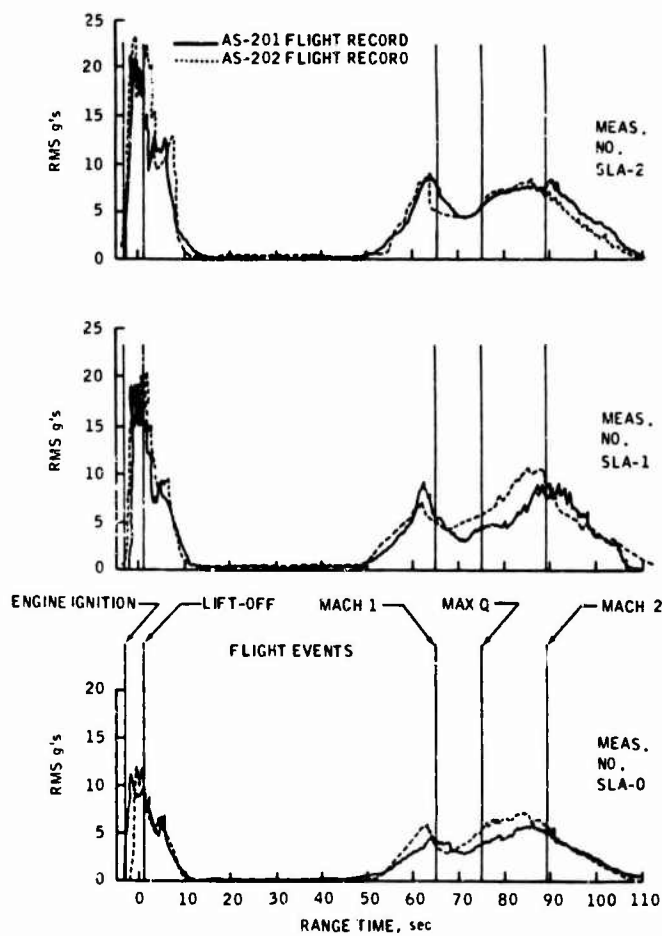skin-panel vibration measurements

Fig. 4. Launch history of SLA vibration during
Apollo missions AS-201 and AS-202

143

TABLE 1

Spacecraft/Lunar-Module Adapter Flight Measurement Parameters

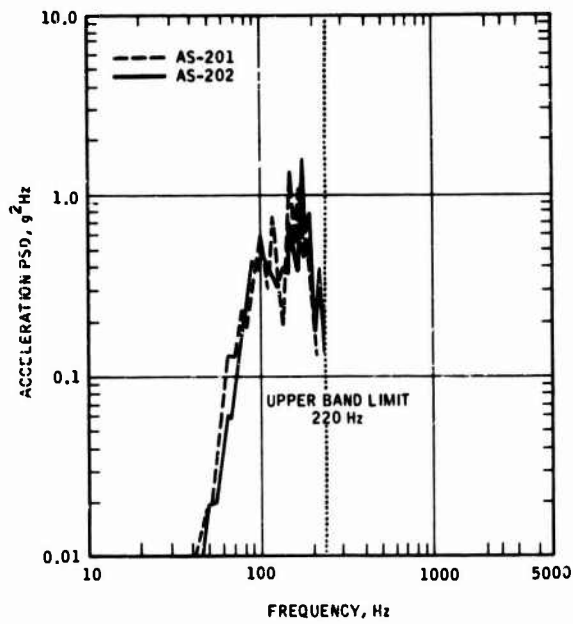| Parameter	Mission	
	AS-201	AS-202
Flight parameter time (sec)		
Engine ignition	-1.7	-1.2
Liftoff	0.37	0.93
Mach 1	65	64
Max Q	75	79.0
Mach 2	89	87
Data reduction slice time (sec)		
Liftoff	-1.0 to 1.0	-1.0 to 2.0
Transonic	61.5 to 63.5	59.5 to 62.5
Supersonic	88.0 to 90.0	84.0 to 87.0
Max Q peak value (lb/ft^2)	625	665
Nominal data bandwidth (Hz)		
SLA-0	5 to 220	5 to 220
SLA-1	5 to 330	5 to 330
SLA-2	5 to 450	5 to 450

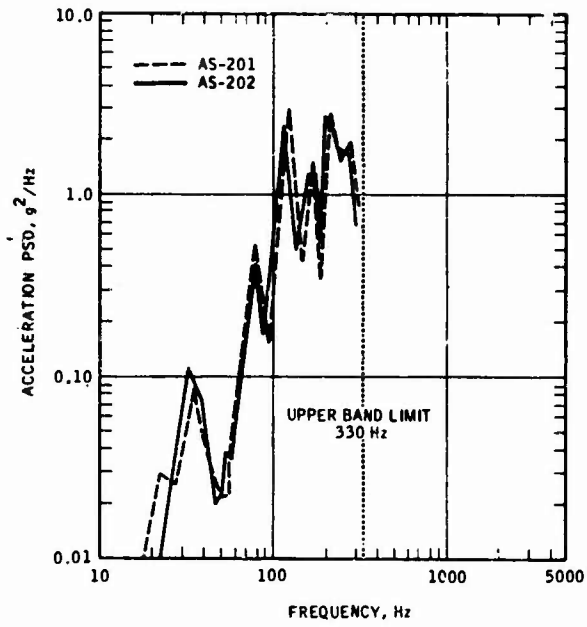Fig. 5. SLA-0 PSD at liftoff

144
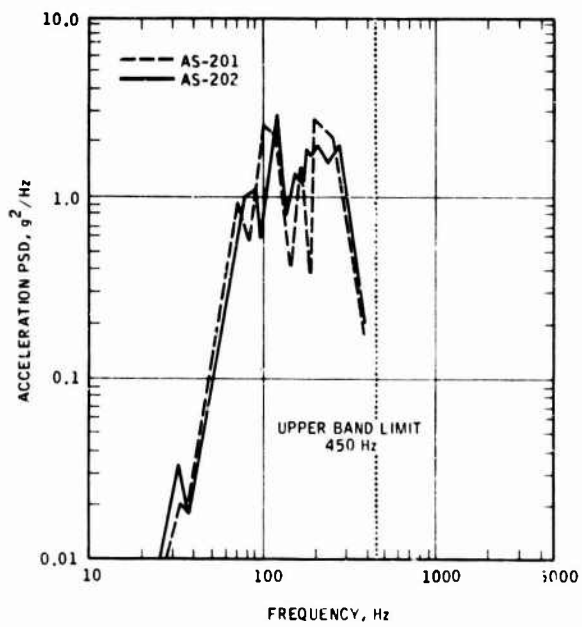
Fig. 6. SLA-1 PSD at liftoff
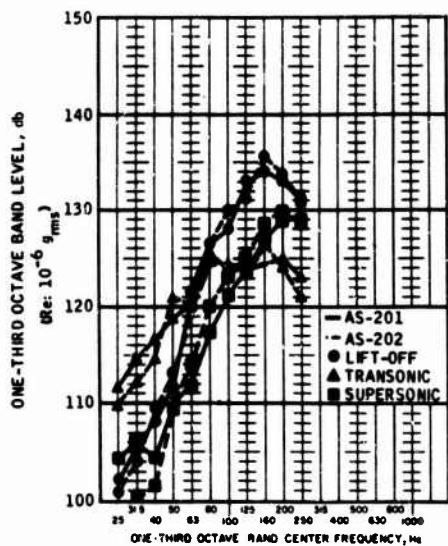

Fig. 7. SLA-2 PSD at liftoff

145

Fig. 8. SLA-0 one-third octave-
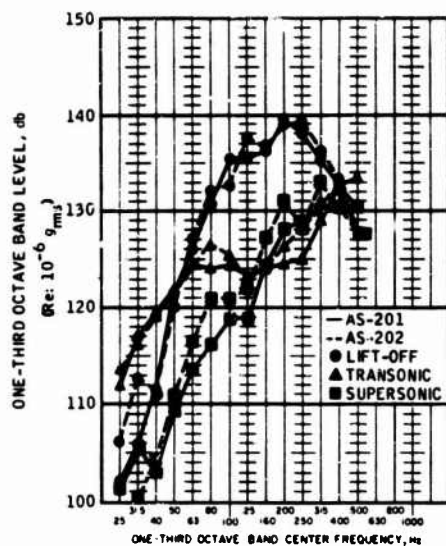band spectrogram

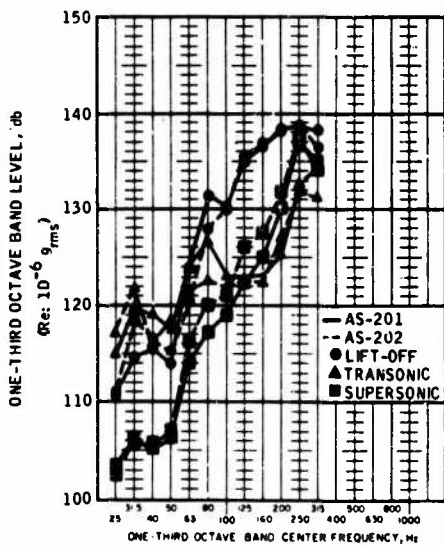
Fig. 10. SLA-2 one-third octave-
band spectrogram

Fig. 9. SLA-1 one-third octave-
band spectrogram

consideration to be included in the test condi-
tions. That is, although the LM would be
launched by both the Saturn IB and Saturn V
vehicles, the foregoing test conditions included
only environmental characteristics of the Saturn
IB launches. However, during liftoff, the Saturn
V booster noise would impose higher SPL's be-
low 100 Hz on the SLA surface, as indicated in
Fig. 11. Consequently, test conditions derived
from Saturn IB flight measurements would be
insufficient to assure that the LM would ade-
quately survive the Saturn V liftoff environment.
To overcome this problem, the envelope spec-
tra were adjusted for the difference in liftoff
environments.

Consideration was also given to increased
transonic and supersonic excitation caused by

but not prohibitive, degree of conservatism in
the test. Also, an envelope spectrum is not
likely to result in an undertest and thus pre-
clude satisfying the test requirements. Ac-
cordingly, a spectrum envelope was drawn for
each location to the highest values of Figs. 8, 9,
and 10 as the initial determination of tne test
conditions.

The domination of the resulting spectral
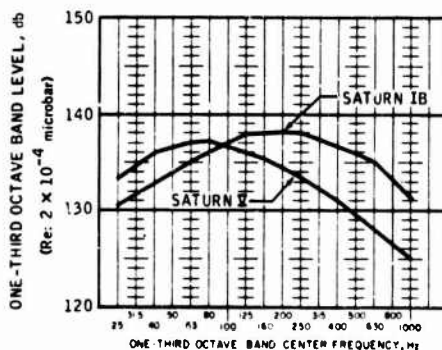envelope by liftoff conditions required another

Fig. 11. Comparison of predicted
Saturn IB and Saturn V liftoff sound
pressure spectra averaged over
SLA surface

146

higher aerodynamic pressures in Saturn V boost as compared with Saturn I boost. Nominally, the measured response of the SLA would be increased by 2 db to account for this change. But since transonic excitation of the SLA is higher than liftoff excitation only in the extreme limits of the measured spectrum, this adjustment would have negligible effect on the overall excitation levels or response characteristics. Accordingly, no adjustment was needed in the test conditions for differences in the Saturn I and Saturn V transonic dynamic pressures.

A smoothed envelope of the environment spectra from Fig. 11 and the Saturn IB environment spectrum are plotted in Fig. 12. The difference in these spectra was applied (added arithmetically) to the SLA response spectra. For example, the SLA-2 response envelope, shown by the solid curve in Fig. 13, was adjusted between 40 Hz (the lowest frequency of liftoff dominance) and 125 Hz (the highest frequency of liftoff spectral difference). The revised portion of the spectrum is indicated by the dashed curve. The resulting test spectrum for SLA-2 is shown in Fig. 13 by the dashed curve between 40 and 100 Hz and by the solid curve at all other frequencies. Similar adjustments were also made on the SLA-0 and SLA-1 measurements, thus yielding the three response-control spectra for the LM acoustic test.
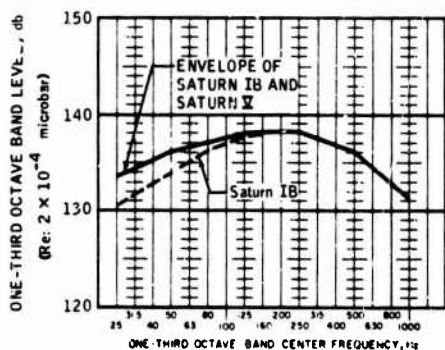
Fig. 13. SLA-2 vibration envelope adjusted for Saturn V liftoff

Fig. 12. Comparison of Saturn IB and smoothed envelope spectra at liftoff over SLA surface

FACILITY CALIBRATION PROGRAM

The MSC SAL, which was designed and equipped to perform environmental tests of full-scale manned spacecraft, is described in detail in Ref. [3]. In the LM project, the CSM and SLA were surrounded by an assembly of 16 ducts through which plane-wave acoustic energy was propagat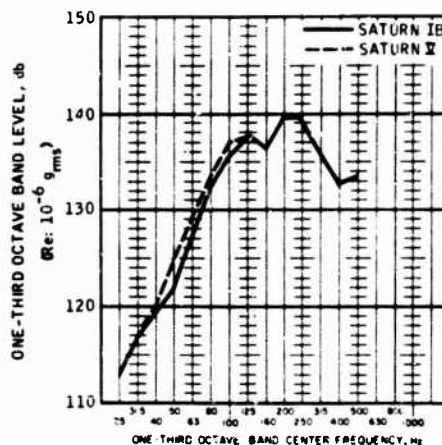ed. Each duct in this arrangement (designated the horn-and-duct system) was driven by an independent air-modulator noise source, as shown in Fig. 14. An annular sound field divided into 22.5-degree segments was thus formed. The outer wall of the ducts can be moved in and out radially to control sound levels in the longitudinal direction by varying the duct-to-test-vehicle clearance. Each air modulator is controlled by an independent channel of the SAL electronic control system where such a channel provides control of overall level, control of spectrum shape in one-third octave bands, and control of limited phase correlation between channels. Hence, the sound field can be optimized in each duct for level and spectrum, and circumferential correlation around the vehicle (that is, between ducts) can be controlled to a limited extent. The spectrum in each duct is shaped by a one-third octave-band shaper, but control is exercised by measuring the sound field in the duct at a selected point with a microphone. The shaper controls were manipulated until the required spectrum was measured. However, control below 50 Hz is limited by the rolloff characteristics of the coupling horn between the air modulator and the duct. Also, above 315 Hz, control is limited by the fact that much of the sound energy in a duct is generated by harmonic distortion of the lower frequency energy. It should be mentioned that the total weight of the horn and shroud system is supported by the SAL tower structure such that this assembly adds no load to the test vehicle. A soft uninflated hose is used to seal each radial duct wall to the test vehicle surface. Minimal restraint is exerted by these seals on the displacement of the vehicle skin.

Although the MSC SAL has the capability for adjusting and controlling the spatial
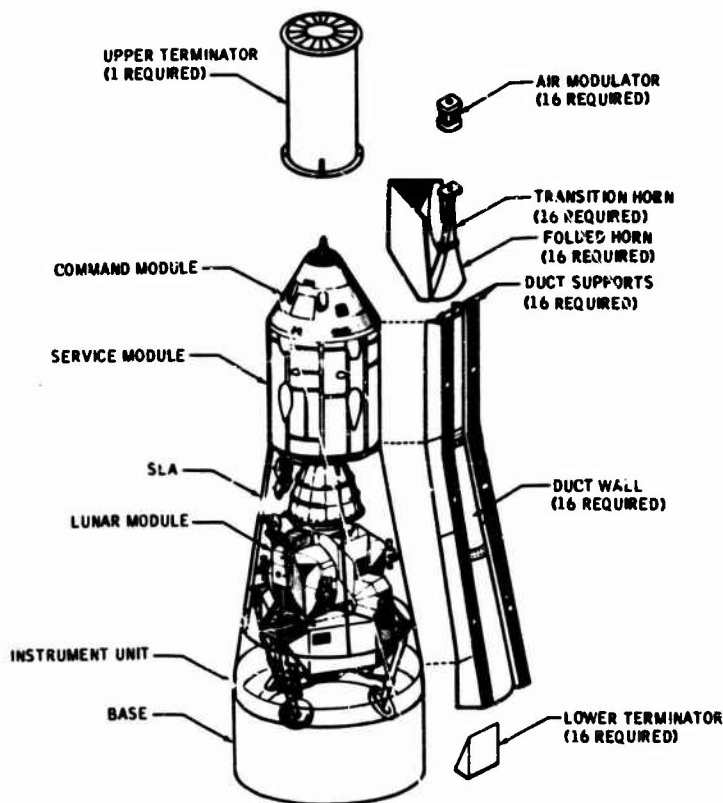
147

Fig. 14. Arrangement of test vehicle
and horn-and-duct system

correlation characteristics of the acoustic field, the best fit to the desired SLA response is obtained with a control mode in which each air modulator is controlled by a separate electronic noise generator. Previous experiments [4] have shown that the facility has greater than sufficient capability to drive the SLA to the required response levels. In other tests in the MSC SAL, the SLA has produced a very uniform response at all points on its surface; thus, it was concluded that laboratory fixtures were not introducing any undesirable anomalies into the SLA response. Further, the specific SLA being used in the laboratory has been shown to behave in accordance with the salient features of a monocoque, continuous truncated cone when excited by a dynamic forcing function.

Starting with arbitrary test conditions, the LM calibration runs were arranged to vary acoustic-field parameters until a best-fit SLA response was obtained and the sound fields within the various ducts had reasonably small variations. (At the conclusion of these runs, the ducts were disassembled, and the SLA forward and aft sections were separated in preparation for installing the LM test article.)

VEHICLE TEST PROGRAM

Test Sequence

After the LM test article was mated to the SLA, and the horn-and-duct system was assembled around the vehicle, a sequence of eight acoustic tests was performed. This sequence is tabulated in Table 2. The specific test article used for this program was LM test article 3 (LTA-3). This was a complete structural demonstrator with an unabridged complement of prototype or mass-representative equipment and subsystems. Consequently, this sequence of tests was designated the LTA-3 acoustic test.

Test Results: Acoustic Environment

The acoustic field imposed on the SLA exterior is shown in Fig. 15. The average spectrum for each of the three long tests (35 or more sec) is shown, and the envelopes show the maximum and minimum values measured in each one-third octave band in any duct during the three tests. Repeatability of the levels from test to test was quite good. This spectrum

148

TABLE 2
Lunar Module Test Article 3 LTA-3 Acoustic Test Sequence

| Test Number	Level		Duration		Remarks
	High or Low	SPL (db)	Long or Short	Time (sec)	
1	Low	139	Long	65	Facility checkout run
2	High	152	Short	18	Establish data acquisition system gain settings
3	High	152	Long	42	Data acquisition with channels 1 to 275
4	High	152	Short	19	Establish data acquisition systems gain settings
5	High	152	Long	38	Data acquisition with channels 276 to 550
6	High	152	—	5	Prematurely terminated by equipment malfunction
7	High	152	Short	18	Establish data acquisition system gain settings
8	High	152	Long	41	Data acquisition with all channels missed on previous runs
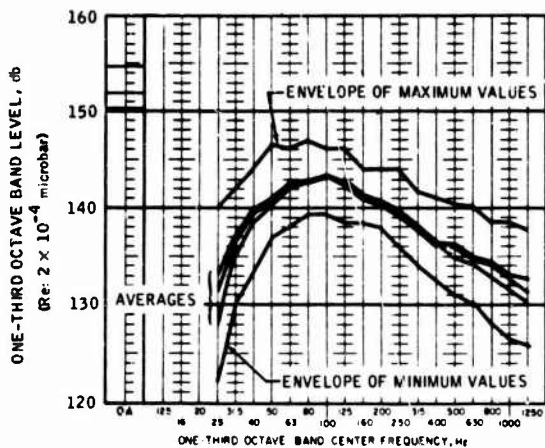
Fig. 15. Sound-pressure spectra at X_a 670 in three long-duration LTA-3 tests (average of 16 ducts in each test and maximum and minimum values for all three tests are shown)

Fig. 16. Average LTA-3 sound-pressure spectra at forward end and aft end of SLA relative to spectra at the mid-SLA location

was measured at station X_a 670, which is midway along the length of the SLA. The spectral consistency along the length of the SLA is indicated in Fig. 16; the average SPL spectrum is plotted at station X_a 778 (near the forward end of the SLA) relative to X_a 670 and at station X_a 552 (near the aft end of the SLA) relative to

X_a 670. If the field were the same at all three locations, both curves would converge to 0 db. The major deviation is in the low-frequency bands near the cutoff frequency of the horn. However, this deviation is not considered to be serious since the SLA has relatively low excitation and acceptance. The SPL in the 31-Hz bandwidth is 7 db below the bandwidth of highest SPL (at 100 Hz), and the typical SLA response (in the 31-Hz bandwidth) is 22 db below the bandwidth of maximum response (at 250 Hz). Except for an undesirable peak at 400 Hz, the

149

deviation is an average of 3 db or less between 50 and 1000 Hz.

The acoustic field inside the SLA (but external to the LM) was measured with 18 microphones placed around the LM in a configuration roughly approximating a sphere. The results of these measurements and the sound spectrum measured inside the LM ascent-stage crew compartment with a single microphone are shown in Fig. 17. (Data from this microphone are not entirely applicable for extrapolating flight conditions since LTA-3 lacked certain interior furnishings which will be installed on flight articles; in addition, the LTA-3 cabin walls had several open penetrations which will be sealed in the flight articles.) Figure 18 is a plot of the SLA noise reduction (that is, the average SLA external spectrum minus the SLA average internal spectrum) and the LM noise reduction (that is, the SLA average internal spectrum minus the LM internal spectrum). Finally, Fig. 19 is a plot of the SLA external spectrum, a predicted S-IB liftoff spectrum on the SLA exterior, and an SLA external transonic spectrum, as contained in the Apollo certification test requirement (CTR). The comparison with the transonic spectrum is of interest since this predicted spectrum had been used to derive vibration specifications for the qualification of LM components and equipment [5].
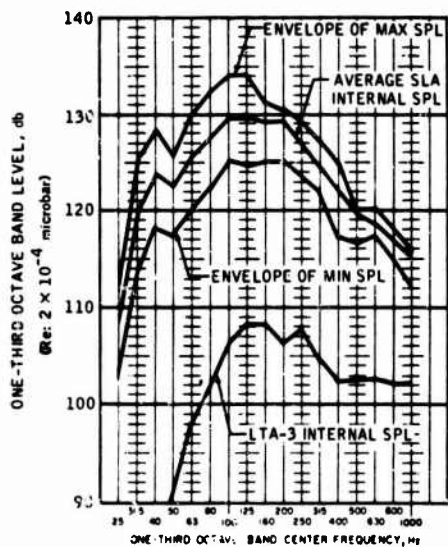

Fig. 18. Noise reduction through SLA and LTA-3
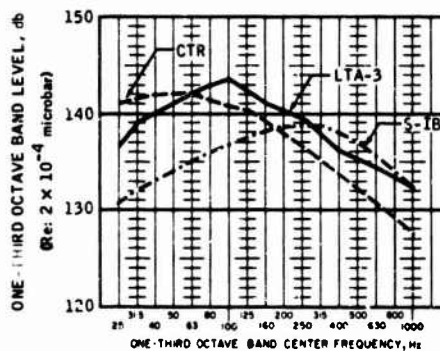
Fig. 19. Comparison of LTA-3 and predicted spectra on SLA exterior

Test Results: Structural Response

The response spectra for locations SLA-0, SLA-1, and SLA-2 are presented in Figs. 20, 21, and 22, respectively. In each figure, curves indicating the response during the calibration run (identified as "empty SLA") and the LTA-3 test are plotted with the flight envelope or response-control spectrum. The SLA responses at locations SLA-1 and SLA-2 during the calibration test provided an excellent fit to the flight envelope, but the response of SLA-0 generally exceeded the flight envelope. It should be noted, however, that the flight response of SLA-0 was not consistent with the flight responses of SLA-1 and SLA-2. This inconsistency may be artificial in that the telemetry bandwidth of SLA-0 was narrower than for either SLA-1 or SLA-2; consequently, the negative slope above 160 Hz is attributed to the

Fig. 17. Sound-pressure spectra measured inside the SLA (and external to LTA-3) and inside the LTA-3 ascent-stage crew compartment
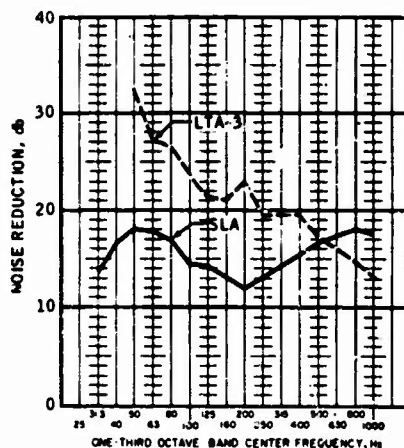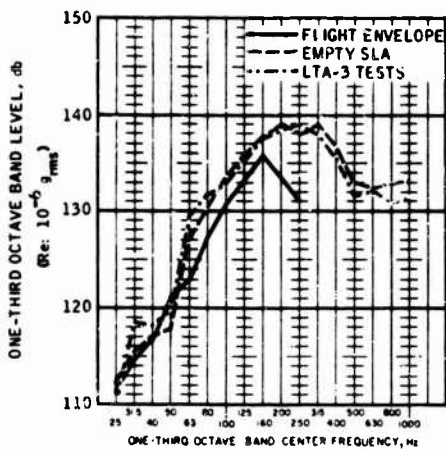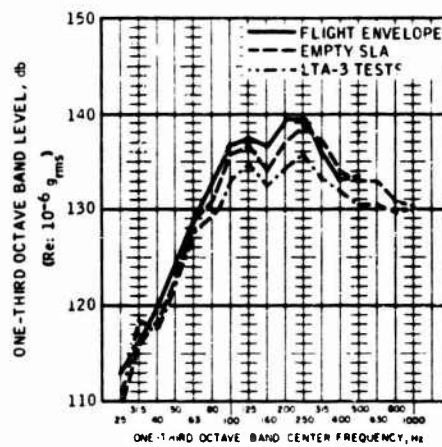
150

Fig. 20. SLA-0 response
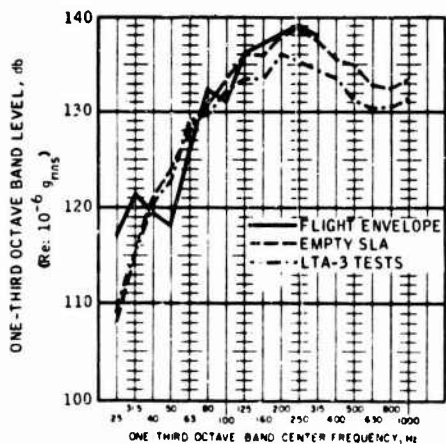spectrogram

Fig. 22. SLA-2 response
spectrogram

Fig. 21. SLA-1 response
spectrogram

limited response of the measurement equipment used in flight. If the response up to 160 Hz is extrapolated with a response characteristic, as shown in the other two measurements, a peak of approximately the same amplitude as the laboratory-induced response could be expected at 250 Hz. On this basis, the slightly poorer fit of laboratory-induced response to flight response is acceptable.

The response of the SLA during the LTA-3 test was lower in the frequency range from 80 to 800 Hz at locations SLA-1 and SLA-2 than was measured in the calibration test in which the SLA was empty. The aft-section response (as indicated by SLA-0) was almost identical for the calibration and LTA-3 tests. The small

changes in response could be attributed to the effect on the SLA structural dynamics of supporting an additional 30,000 lb, or the internal sound levels could be lower as a result of the absorption of acoustic energy by the LM. Since SLA internal sound pressures were not measured during the calibration test (empty SLA), the absorption of the LM is not known. In any case, an explanation of the causes of the SLA response variations is not forthcoming from the data obtained in this program.

CONCLUDING REMARKS

Flight certification of the LM required an acoustic test to verify the structural integrity of the LM to the high-frequency dynamic pressure environment encountered in launch and to define or verify equipment-qualification vibration-test requirements. This test was performed using a structural demonstrator vehicle designated LTA-3. The test environment was evolved from a facility calibration program which culminated in a preparatory run and which produced the best possible match of laboratory response to launch response in the empty SLA. The SLA response was a key factor in obtaining a faithful simulation of the flight environment since the SLA shrouds the LM during the portion of launch when the dynamic pressure environment exists, and the LM environment is, therefore, a unique function of the SLA response. Knowledge of the SLA response has been obtained at three locations during the launch of Apollo flights AS-201 and AS-202. Enveloping the maximum spectral values obtained from these flights produced the spectrum used for the test requirements. Close

151

adherence to this spectrum was obtained in both the calibration and the LTA-3 tests, indicating a highly realistic test of the LM in its flight environment.

In this testing, the high degree of similarity between the SLA structural vibration responses measured in the acoustic laboratory and in flight demonstrates that successful simulation of environmental excitation can be obtained without complete definition of the environmental criteria. Such a demonstration marks a forward step in the application of ground test facilities in achieving more realistic flight simulations.

REFERENCES

1. R. E. Barrett, "Techniques for Predicting Localized Vibratory Environments of Rocket Vehicles," NASA TN D-1836, Oct. 1963

2. R. E. Barret "Statistical Techniques for Describing Localized Vibratory Environments of Rocket Vehicles," NASA TN D-2158, July 1964

3. R. J. Wren, W. D. Dorland, and K. McK. Eldred, "Concept, Design, and Performance of the Spacecraft Acoustic Laboratory," Shock and Vibration Bull. No. 37, Part 5, 1968

4. R. W. White, "Predicted Vibration Responses of Apollo Structure and Effects of Pressure Correlation Lengths on Response," Wyle Laboratories, El Segundo, Calif., Rept. WR 67-4, Mar. 1967

5. Anon., "The LTA-3 Ascent Stage and Descent Stage Thermal Shielding and Support Structure," Lunar Module Certification Test Requirement LCQ-650-373, July 1966

DISCUSSION

Mr. Manning (Bolt Beranek & Newman): Were you concerned about slight changes in the excitation causing a variation of the vibration pattern on the shell? I would expect that the overall average level would not change, but perhaps the spatial pattern would.

Mr. Dorland: Yes, we considered that and we ran a series of tests to investigate that point. We found that there were some deviations in the data. We finally adopted the configuration used in this test and the data on that configuration are shown here.

Mr. Manning: Would it be better to get flight data averaged over many accelerometer locations and to control from the average?

Mr. Dorland: Yes, and we will probably do that next time.

*   *   *

VIBROACOUSTIC TEST METHODS FOR VIBRATION
QUALIFICATION OF APOLLO FLIGHT HARDWARE

Richard W. Peverley
General Electric Company
Houston, Texas

Vibroacoustic test methods were used to perform vibration qualification
tests on a majority of the components located in the Apollo service
module. The test subjects were attached to a structural segment, and
realistic reproduction of vibration environments was provided by acous-
tic excitation. Tests were conducted with both large segments, which
simulated a half segment of the Block 1 and Block 1i service modules,
and small segments, which simulated a radial beam and a fairing. This
approach was used to provide a means of duplicating accurately com-
ponent mounting conditions and thus improving the simulation that
would otherwise have been furnished by an electromechanical shaker
test. The success of the Apollo tests verified that the concept of vibro-
acoustic testing can, in many circumstances, result in a significant
improvement in vibration simulation. This paper describes vibro-
acoustic tests pertaining to the Apollo program and presents a com-
parison of vibroacoustic data with flight data and vibration test criteria
levels. Also presented is a discussion of some of the advantages and
limitations of vibroacoustic testing.

Spacecraft hardware is generally subjected
to vibration testing as a normal part of the com-
ponent qualification program. It has become an
accepted practice to conduct such tests on elec-
tromechanical shakers. Vibration test spectra
are often derived by enveloping a number of
data samples that have been acquired during
ground or flight tests. Data peaks are occa-
sionally clipped, but notches in the data are
more often filled in to provide smooth test cri-
teria. The test specimen is attached to the
shaker and vibration energy is then applied.
One of the inherent shortcomings of this ap-
proach is that spacecraft mounting conditions
are not accurately duplicated. Since the me-
chanical impedance of the shaker head is gen-
erally much greater than the impedance of the
structure, the component is not allowed to re-
spond in its natural manner. In addition, elec-
tromechanical shakers can be controlled in only
one direction at a time and three tests are often
specified to assure that adequate excitation has
been applied to each major axis. The short-
comings described above generally produce an
overtest. If the vibration test levels are mod-
erate, the overtest condition can be tolerated.
If the component is located in an area where
the vibration environments are high, however,
this overtest condition can produce unnecessary
test failures.

Many of these overtest conditions can be
avoided by conducting acoustically induced vi-
bration tests (also called vibroacoustic tests*).
Such tests are conducted by acoustical excita-
tion of a representative segment of spacecraft
structure to which the test specimen is attached.
The acoustic spectrum is shaped to produce vi-
bration responses that satisfy the test criteria.
Vibroacoustic tests can be conducted on a full-
scale structure or on structural segments.
There is a distinct advantage in using a full-
scale structure. The ability to simulate acous-
tic and aerodynamic flight environments should
produce accurate reproduction of vibration re-
sponses throughout the spacecraft. This ap-
proach does, however, require the availability
of large acoustic test facilities. Two acous-
tic test facilities which have the capability to
test full-scale spacecraft have been developed
by NASA. The NASA/MSC Spacecraft Acous-
tic Laboratory [1] has the capacity to sub-
ject an entire Apollo command, service, and
lunar module to an acoustic excitation which
closely simulates the flight environment. The

---

*The term "vibroacoustic" designates an acous-
tic test used to conduct a component vibration
test and distinguishes this acoustic test from
other types.

NASA/GSFC Combined Environmental Test Facility [2] goes one step further and combines the launch acoustic, acceleration, temperature, pressure, and mechanical vibration environments. Vibroacoustic tests can also be conducted on smaller structural segments, however, if the vibration environments are known and can accurately be reproduced.

Vibroacoustic tests have been conducted in support of the Apollo program. These tests were conducted on structural segments of various configurations and demonstrated that under many conditions, structural segments could be used to provide accurate vibration simulation. The author discussed some of the results of these tests during the 36th Shock and Vibration Symposium [3]. At that time, testing had been completed only on Block I Apollo hardware. Additional tests have subsequently been conducted on Apollo Block II service module hardware and have provided additional information for use in the evaluation of the vibroacoustic test concept. The purpose of this paper is to describe the total Apollo vibroacoustic test experience and to evaluate the advantages and limitations of the vibroacoustic approach to vibration testing.

APOLLO VIBRATION TEST PROGRAM

The Apollo spacecraft is made up of three basic spacecraft modules and an adapter, as shown in Fig. 1. The command module is composed of an inner and an outer shell, which are partially isolated from one another. This structure is reasonably stiff and well damped and, as a result, has moderate vibration response characteristics. The service module is made up of a honeycomb skin with radial beams whose shear web thickness is only 0.018 in. Equipment is located on brackets attached to the stringers of these beams, on bulkheads, and on shelves between the beams. During the launch and boost phase of a flight, the outer skin is exposed to intense aerodynamic pressure levels which produce high vibration responses. The lunar module is an extremely complex structure which contains two stages, each with its own propulsion system. The descent stage structure is a cruciform consisting of four tank compartments and one engine compartment. The ascent stage is constructed of two cylindrical sections and houses the crew during the lunar ascent and descent. During the launch and boost phase of the mission, the lunar module is housed within the service module-lunar module adapter (SLA),
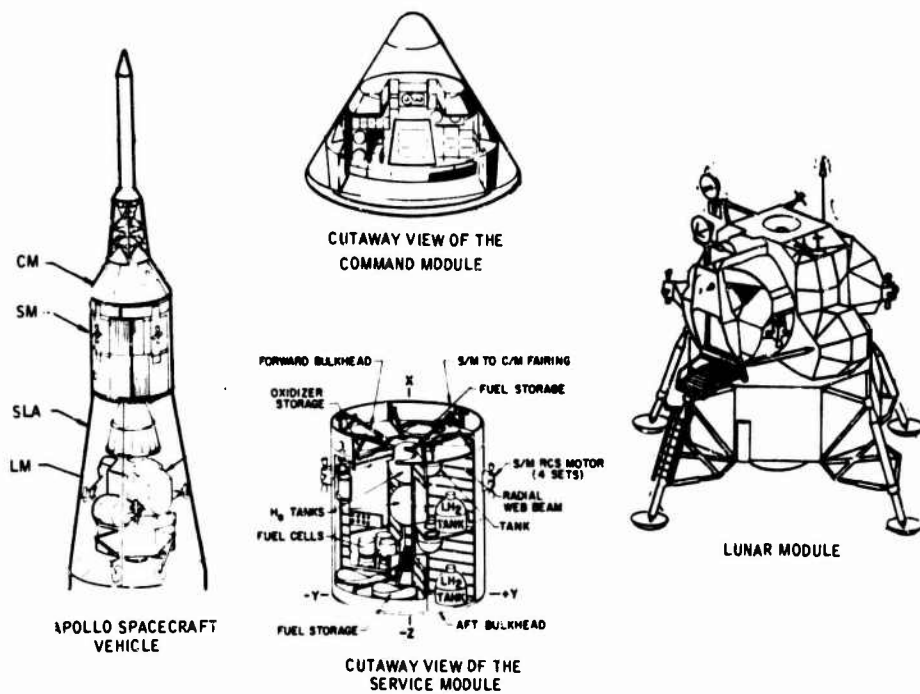

Fig. 1. Apollo command module, service module, and lunar module

154

and all of its systems are in a passive mode. Although the Lunar Module is a highly responsive structure, the exterior noise levels are sufficiently attenuated by the adapter so that the vibration levels are moderate. Thus, only the service module is exposed to high vibration environments.

Early in the Apollo program, a number of boilerplate Apollo spacecraft were flown. Thus, it was possible to acquire a significant quantity of acoustic and fluctuating pressure measurements which provided a concise picture of the excitation environments [4]. Because of the irregular aerodynamic geometry presented by the escape tower, reaction control engines, and shoulders, these environments were relatively high. Sound-pressure levels as high as 160 db were measured at the shoulder of the service module and 145 db at its base. The measured spatial average sound-pressure level of the service module versus time is shown in Fig. 2. The initial exposure to acoustic energy occurs

at lift-off. A fluctuating pressure transient occurs near Mach 1 and is probably the result of a momentary flow separation from the shoulder. The longest exposure occurs near max Q. One-third octave sound-pressure levels at max Q of the service module are also shown in Fig. 2. It was not possible to obtain accurate definition of the spectral characteristics of the Mach 1 transient because of its short time duration.

A limited quantity of vibration data were also taken during some of the early boilerplate flights. Because of the extensive differences between the boilerplate and the spacecraft structure, however, these vibration data were of little use. Thus, the initial vibration qualification test levels were based entirely on analytical methods. Later, acoustic tests were conducted on each of the three individual modules for the purpose of verifying the adequacy of the analytical predictions. An Apollo Block I command module and service module were subjected to acoustic testing at the North American
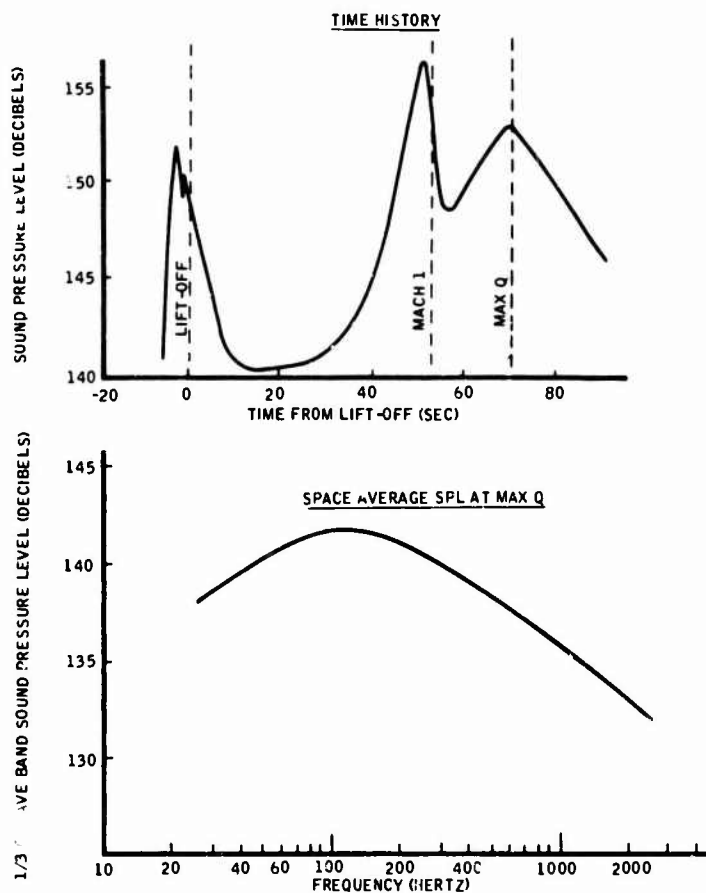

Fig. 2. Inflight acoustic and aerodynamic sound pressure levels of the Apollo service

155

Rockwell (Los Angeles Division) Acoustic Test Facility. Vibration data were obtained from spacecraft structure which contained a limited number of mass simulated components. These data were analyzed and provided vibration criteria for electromechanical shaker tests [5]. The acoustic field in the North American Rockwell facility was determined to be quasi-reverberant. Thus, the spatial correlation coefficient and the resulting vibration levels were expected to be higher than would be encountered during a flight [6]. There was, however, no way to compensate for these differences and the vibration levels measured during these tests were assumed to be valid until flight data became available. Acoustic tests were conducted on the lunar module at the NASA Spacecraft Acoustic Laboratory [7]. The lunar module was tested in its launch configuration, i.e., the lunar module inside of the adapter. The excitation, including the spatial correlation, was controlled to duplicate measured flight responses. Again, vibration data from these tests were used to provide electromechanical shaker test criteria [8].

The vibration levels measured during the command module and lunar module acoustic tests were moderate. The subsequent vibration tests, which were conducted on electromechanical shakers, did not produce an excessive number of problems. During the service module acoustic tests, however, the measured vibration levels were extremely high and exceeded the analytically derived test criteria. A typical example of the test criteria derived from these data is shown in Fig. 3. It was feared that the inability to simulate mechanical impedance properly during an electromechanical shaker test of such high amplitudes could produce an excessive number of failures. A decision was then made to utilize vibroacoustic segment testing to requalify the service module hardware to the revised levels. Acoustically induced vibration testing had been successfully used on a very limited basis in the past [9, 10, 11]. From this experience, it was felt that the vibroacoustic test approach would provide an accurate simulation of vibration responses and mechanical impedance and would, therefore, limit the amount of overtesting.
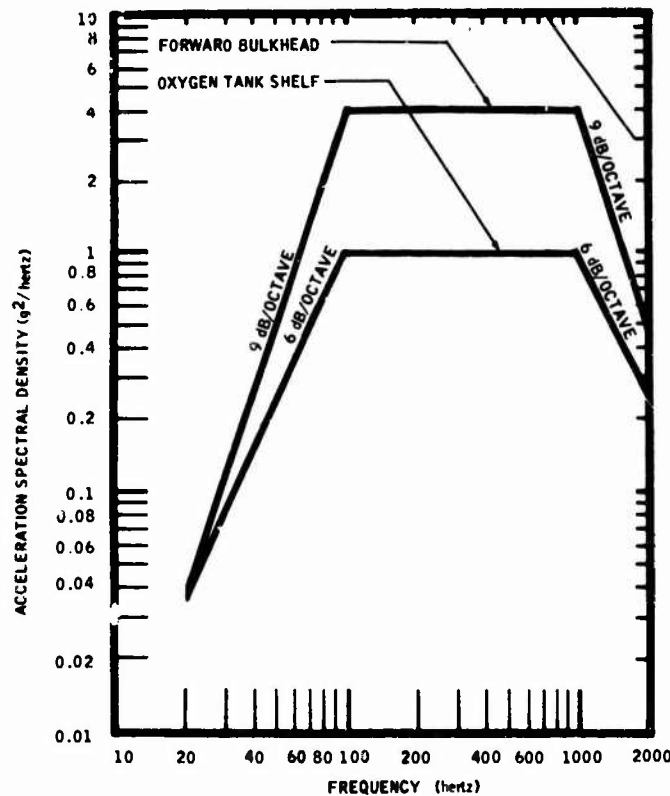

Fig. 3. Typical vibration test criteria for the
Apollo service module

156

VIBROACOUSTIC TESTS

Three different test segments were used for the vibroacoustic test. The majority of the tests were conducted on a half segment of the Apollo service module; (this test fixture was referred to as the 180-deg SM segment). A smaller number of components were tested on a segment which simulated a service module radial beam. Finally, a set of flyaway umbilicals was tested on a section of the command module-service module fairing.

180-Deg SM Segment

The 180-deg SM segment was specially fabricated using spacecraft materials. A photograph of the segment is shown in Fig. 4, and a drawing is shown in Fig. 5. The basic structure consisted of the outer shell, forward and aft bulkheads, shelves, and two (there are normally six) radial beams. The top sector was used for testing equipment mounted to bulkheads or shelves. Thus, the shelves could be moved so that the top sector of the segment might duplicate one sector on one test and a different sector on the next test. The segment was isolated from the floor with Isomode pads.

The 180-deg SM segment was oriented in the test facility as shown in Fig. 5. A fiber glass model of the command module was employed to provide the proper fairing attachment. The total test duration was 150 sec. The overall sound-pressure level was varied during the test as shown in Fig. 6. This profile was established to simulate the flight time history, and the spectral shape was chosen to simulate the space average sound pressure levels of Fig. 2. The level A portion of the test simulated the flight level at max Q while the level B part (which was 4 db higher) simulated the peak near the transonic region. The duplication of flight sound-pressure levels was good above 100 Hz. Below 100 Hz, however, the sound-pressure levels were lower in the facility. These differences did not degrade the test, however, since the quasi-reverberant field in the facility produced higher vibration levels in this frequency region; (this point is discussed in more detail later on).

The original vibration test criteria were derived from an acoustic test of a full-scale spacecraft which contained a limited number of mass simulated components. Thus, it was necessary to calibrate the 180-deg SM segment by subjecting it to essentially the same sound pressure levels, while in the same mass loading condition as the full-scale test structure. This test was conducted to assure that responses were comparable. The test subjects were attached to the segment and the same sound pressure levels were then applied. A comparison of the vibration response, measured at comparable locations on an empty equipment shelf of the original full-scale test and the 180-deg SM segment test, with and without a component attached, is shown in Fig. 7. The responses on the two unloaded structures, shown in the left-hand part of the figure, compare favorably. On the right-hand side of the figure, the vibration response at the same location on the 180-deg SM segment, but with a 17 lb component attached, shows a significant reduction of vibration levels

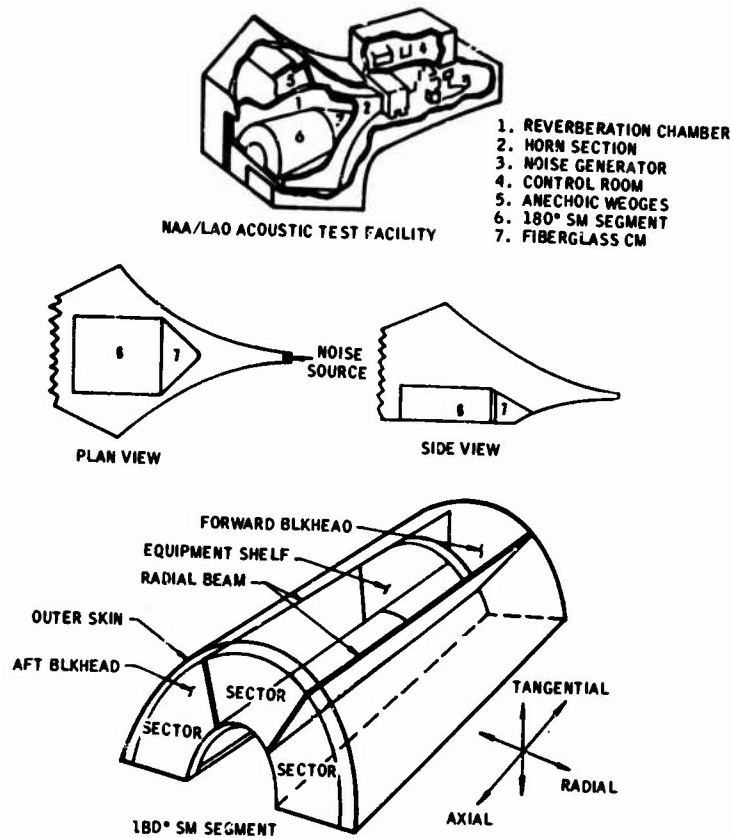Fig. 4. A photograph of the 180-deg SM segment

157

Fig. 5. Sketch of the NAR/LAD acoustic test facility
used for the 180-deg SM segment

in the higher frequency bands. Had this component been tested on an electromechanical shaker using the test levels derived from the unloaded structure, it would obviously have been overtested. The effect of mass loading, as shown in Fig. 6, was the largest that was observed. At a few locations, in fact, no loading effect could be detected. Thus, the specification of common test criteria for this bulkhead would have been unfair in some cases and quite justified in others.

A total of 56 components were tested during 13 test runs. As many as 13 components were tested simultaneously. Once the adequacy of the segment to reproduce the desired vibration levels had been established, the test criteria for each of the 13 separate tests then became the acoustic levels of Fig. 6. Vibration measurements, acquired at various locations, including the base of each component, were examined for abnormalities after each test and to detect possible degradation of the test fixture.

Component performance was monitored during each test, as required.

A significant number of changes had been made to the Block II service module structure and are listed in Table 1. Analysis of these changes indicated that the vibration characteristics of the Block II service module would be different from those measured on the Block I service module. In addition, there were a number of component changes. Thus, a similar 180-deg SM segment vibroacoustic test was planned to qualify Block II hardware. Since the external geometry and acoustic test levels had not changed, the criteria once again became the acoustic levels of Fig. 6. An initial test was also made on the Block II segment to provide a calibration of the structure.

Data acquired at comparable locations on the unloaded forward bulkhead of the Block I and Block II 180-deg SM segment are shown on the left-hand side of Fig. 8. The vibration

158

TABLE 1
Major Differences in the Block I and Block II Apollo Service Module Structure

| Area	Block I	Block II
Outer skin	No. of panels: 6 Honeycomb inner facesheet: 0.016 in. Longitudinal radiator tubes	No. of panels: 4 (Two large panels replace 4 smaller panels) Honeycomb inner facesheet: 0.010 in. Horizontal radiator tubes
Forward bulkhead	4 large tank holes Few components Facesheet 0.016 in.	No tank holes Many components Facesheet 0.010 in.

Aft bulkhead	4 large tank holes
	    2 at 45.3 in. diam
	    2 at 39.0 in. diam
		4 large tank holes
		    2 at 51.0 in. diam
		    2 at 45.0 in. diam

Fairing	1 in. honeycomb No radiators	0.5 in. honeycomb Radiators
Tanks	Length: 164 in.	Length: 154 in.
Shelves	Thickness: 1 in. Constrained 2 sides	Thickness: 1.5 and 2 in. Constrained 4 sides (Attached to outer skin)
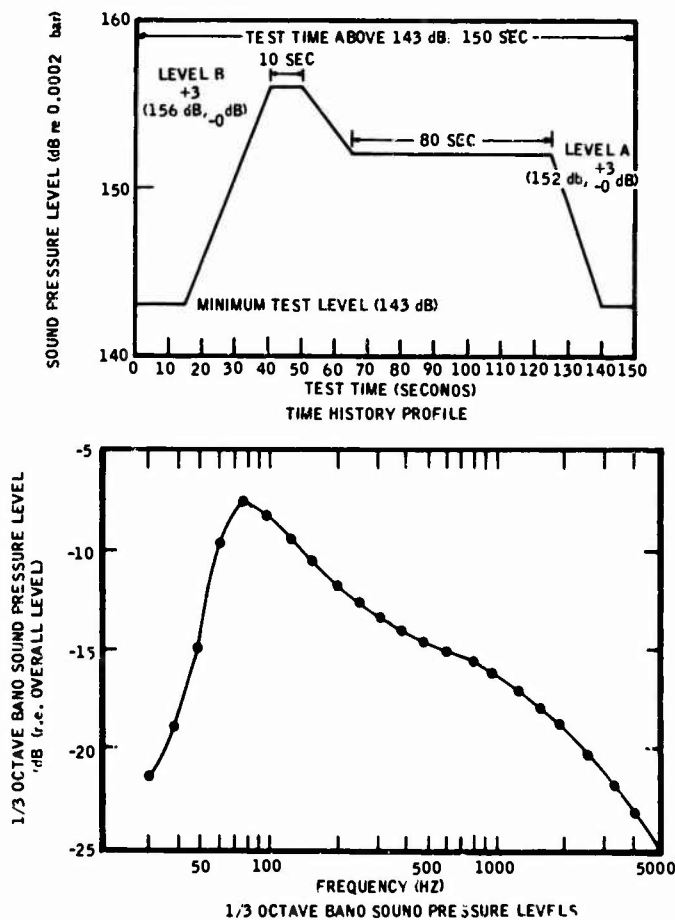
Fig. 6. Acoustic test criteria for the 180-deg SM segment vibroacoustic test
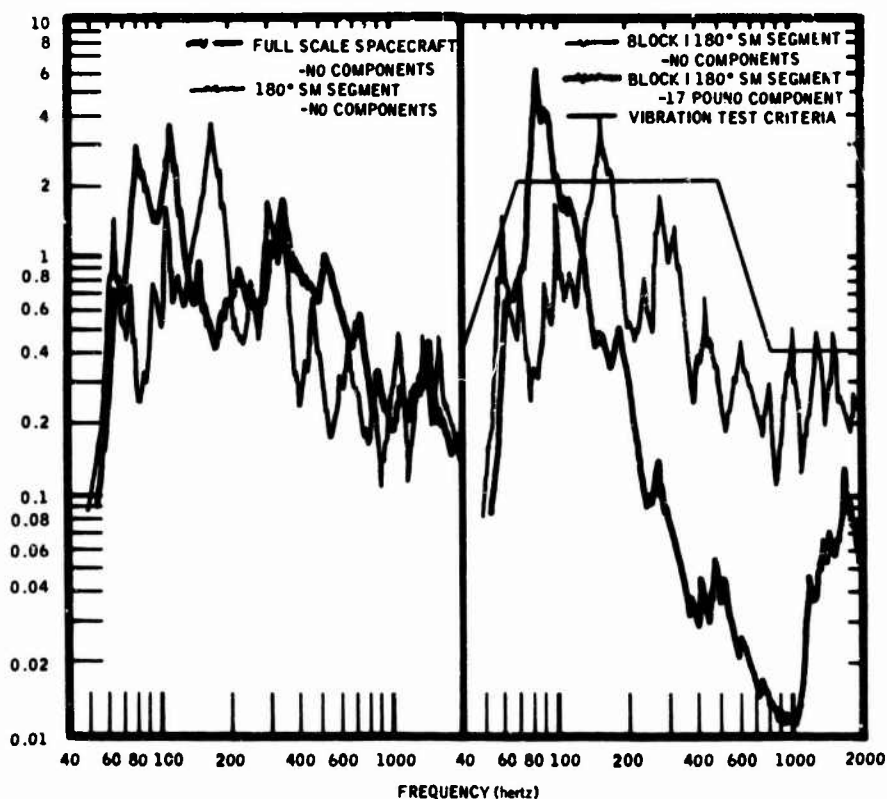
159

Fig. 7. Vibration levels measured at a common point on the service module forward bulkhead during three different tests: a full-scale spacecraft with no equipment; the 180-deg SM segment with no equipment: and the 180-deg SM segment with a 17-lb component attached (equivalent sound pressure levels applied)

responses above 80 Hz are similar. Below 80 Hz, the lighter Block II bulkhead shows higher responses. The effect of adding a 42 pound component is shown on the right-hand side of Fig. 8. Significant reduction of vibration levels was also noted, but in this case, the largest reductions occurred in the lower frequency regions. Again, the example shown in Fig. 8 exhibited the largest mass loading effect.

A total of 20 individual components were tested during four test runs. The most significant problem occurred at bracket-structural interfaces. Following the test, the face sheet of the honeycomb forward bulkhead was found to have failed at several locations. A discrepancy of this type could have been detected only when primary structure, the bulkhead, brackets, and equipment were included in the test.

A small quantity of vibration data had been acquired on the service module outer shell during one of the later Block I Apollo flights. The quantity of these data was too limited to allow for a total statistical analysis. No Block II flight vibration data have yet been acquired. Thus, only qualitative comparisons can be made to assess the relative adequacy of the 180-deg SM segment tests. A comparison of measurements acquired at a similar location during a Block I flight and the Block I and Block II 180-deg SM segment tests is shown in Fig. 9. The flight data have been scaled up 2 db to compensate for flight trajectory parameters. The Block I data agree, and the Block I-Block II comparison shows a reasonable similarity. Similar comparison of the vibration data acquired at other locations shows the 180-deg SM levels to be higher than the flight levels. A comparison of all available flight vibration data and corresponding ground test data, in fact, showed the envelope of the ground test data to be higher than the envelope of the flight data, particularly in the lower frequency regions. Thus, the vibroacoustic test exposed the equipment to higher acceleration-spectral-density
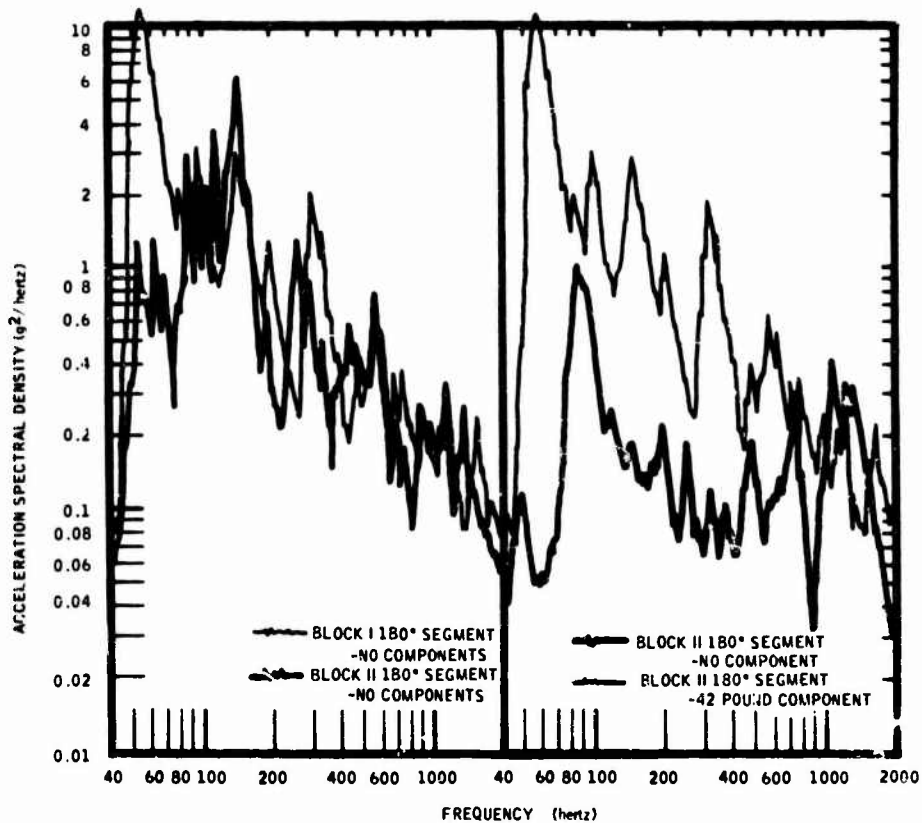
160

Fig. 8. Vibration levels measured at a common point on the service
module forward bulkhead for the Block I and Block II 180-deg SM
segment vibroacoustic test

levels than the equipment would encounter in
flight. In spite of the higher levels, a minimum
number of hardware test failures occurred.

Radial-Beam Segment Tests

The service module radial beam consists
of eight 0.018 in. panels that are bounded by
vertical and horizontal stringers. There are
six beams in each service module. The pri-
mary function of the radial beams is to carry
shear loads. Some components are located on
brackets which are attached to the horizontal
stringers. These components were vibroacous-
tically tested on a small segment that consisted
of three complete beam panels. A diagram of
the radial beam segment is shown in Fig. 10.
Since all beam panels are structurally similar,
only one test fixture was required. During each
test, the center panel of the segment was con-
figured to represent a different service module
beam panel. A typical test setup is also shown
in Fig. 10. Prior to each test, the segment

alone was placed in the chamber. An acoustic
spectrum was then found that would produce a
response equivalent to the criteria. This pro-
cedure was necessary because the criteria had
been developed from test data acquired on a
panel that was not mass loaded with hardware.
The test subject and its bracket were attached,
and the panel was again excited with the same
acoustic spectrum. No attempt was made to
duplicate flight acoustic environments, but in-
stead the acoustic spectrum was shaped to con-
trol the response. A comparison of the bare
panel response and the test criteria is shown in
Fig. 11. The test criteria were deliberately ex-
ceeded to assure that adequate excitation was
applied. A total of 29 components and their as-
sociated bracketry was tested in this manner.
Again, a minimum number of component prob-
lems was encountered.

Fairing Segment Test

A vibroacoustic test was also performed to
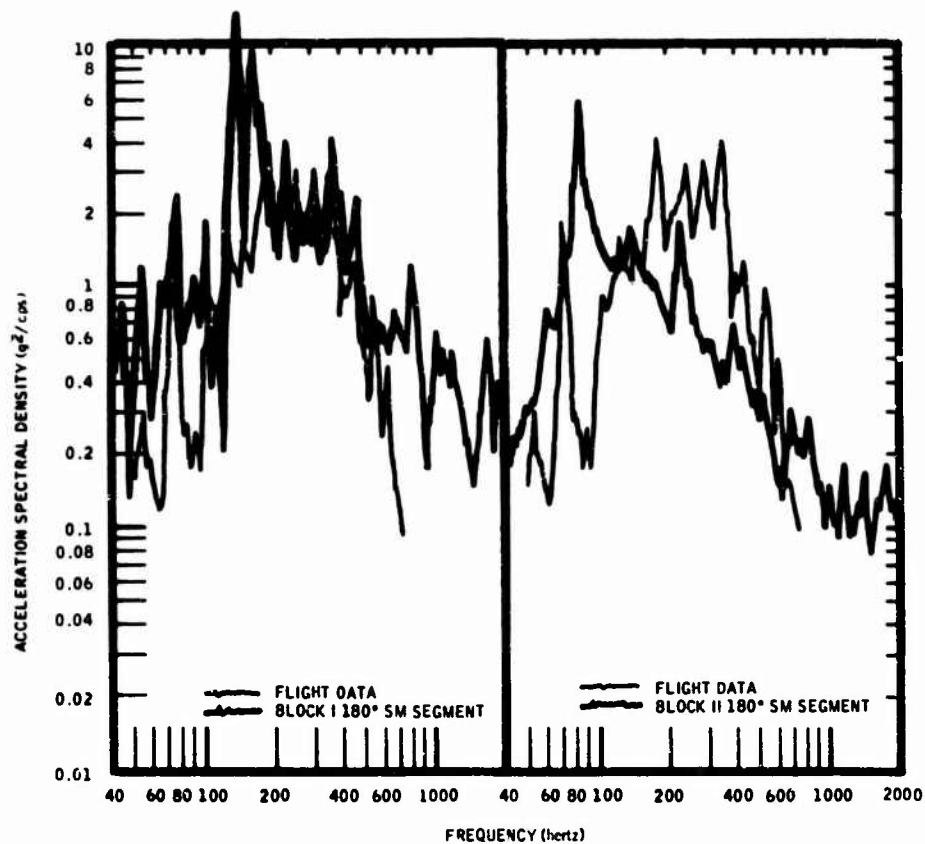qualify a flyaway umbilical; (this test has been

161

Fig. 9. Comparison of vibration data measured at a common point on
the Apollo service module outer skin during flight, Block I 180-deg SM
segment and Block II 180-deg SM segment

previously described by Stevens et al. [12]).
This component had previously failed to function
properly during an electromechanical shaker
test. The vibroacoustic test, which utilized a
segment of the command module-service mod-
ule fairing, was performed in a manner similar
to the radial beam tests. The acoustic spec-
trum was shaped to excite the panel before the
component was attached. Again, the vibration
test criteria had been derived from an unloaded
panel. Once the proper acoustic spectrum had
been determined, the component was attached,
and this acoustic spectrum was reapplied. The
flyaway umbilical functioned properly during
the vibroacoustic test. This was only one of
several examples where an extensive redesign
effort was avoided by achieving better test
simulation.

ADVANTAGES AND LIMITATIONS
OF VIBROACOUSTIC TESTING

The vibroacoustic tests had been initiated
under the Apollo program as an interim measure

to requalify service module hardware. These
tests had been designed to provide a better
simulation of flight vibration environments than
could have been obtained during electromechan-
ical shaker testing. The results indicated that
this objective had been satisfied. These vibro-
acoustic tests also provided an opportunity to
evaluate some advantages not always found in
an electromechanical-shaker vibration test
program. Some of these advantages are listed
below:

1. The improvement in the simulation of
mechanical impedance and the capability to ex-
cite equipment simultaneously in all axes are
the two most obvious advantages and require no
further discussion.

2. Vibroacoustic tests can provide a con-
venient means of testing component interfaces.
If the segment is sufficiently large, it may be
possible to conduct a test on an entire subsys-
tem. For example, the service module reaction
control subsystem (there are four per spacecraft)

162

PLAN VIEW OF THE RADIAL BEAM SEGMENT TEST UP
IN THE NORTH AMERICAN AVIATION SMALL
ACOUSTIC TEST FACILITY

SIDE VIEW OF TEST PANEL WITH A TYPICAL
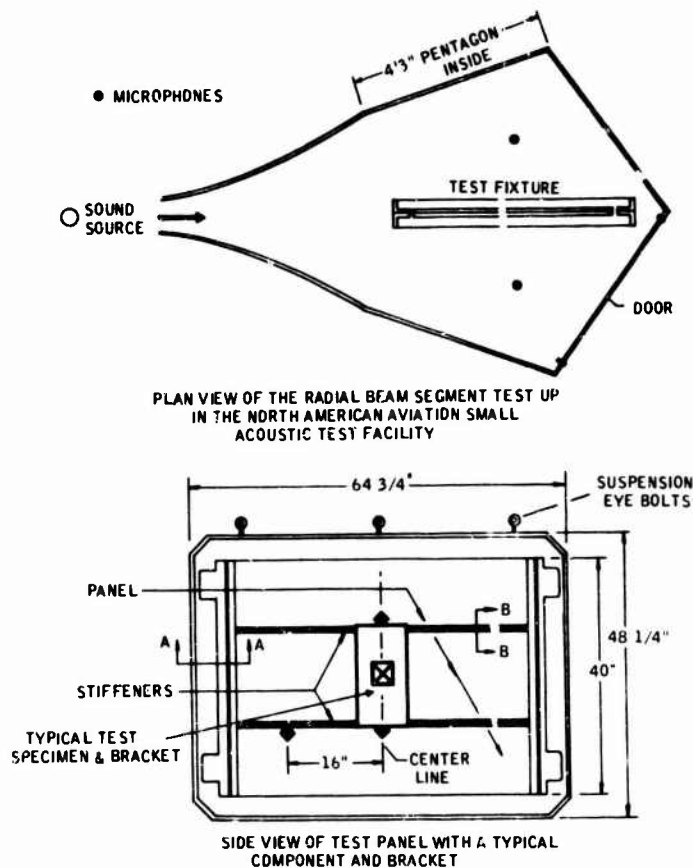COMPONENT AND BRACKET

Fig. 10.   The radial beam vibroacoustic test setup

was tested during the 180-deg SM segment vibroacoustic test. A photograph of the reaction control subsystem test article is shown in Fig. 12. Test specimens this large can also be tested on electromechanical shakers, but such tests are more complex.

3. Vibroacoustic tests can provide a convenient means of testing many components at one time, depending on the size of the segment. For example, 13 components were tested simultaneously during one of the 180-deg SM segment tests.

4. Bracket-secondary-structure-primary-structure interface integrity can often be verified.

5. Plumbing and wiring installations can be tested with the components. If these installations are long, vibration tests on electromechanical shakers often become unwieldy.

6. The effect of minor structural modifications or component relocation on structural response can be determined without acquiring flight data or conducting full-scale spacecraft tests.

7. A reasonable assessment of testing margins can be obtained. It is often difficult or impossible to determine how much overtesting has occurred during an electromechanical shaker test unless impedance measurements have been acquired.

8. Problems associated with the magnetic fields often generated by electromechanical shakers are greatly reduced.

9. Components can be exposed to vibration environments peculiar to their individual location. Often vibration data are available at only a few general locations, and test levels are specified by structural zones. By forcing the
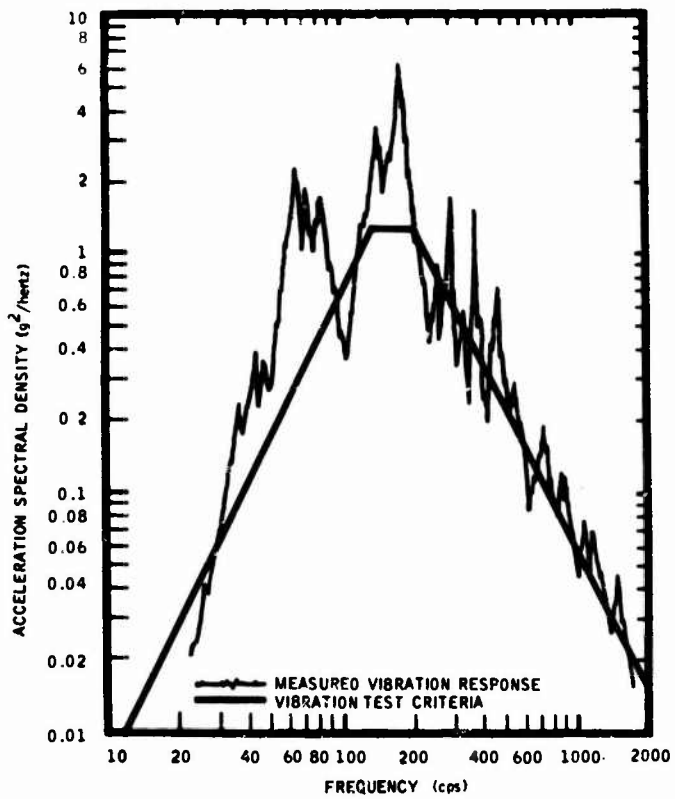
163

Fig. 11. Comparison of the vibration response of the
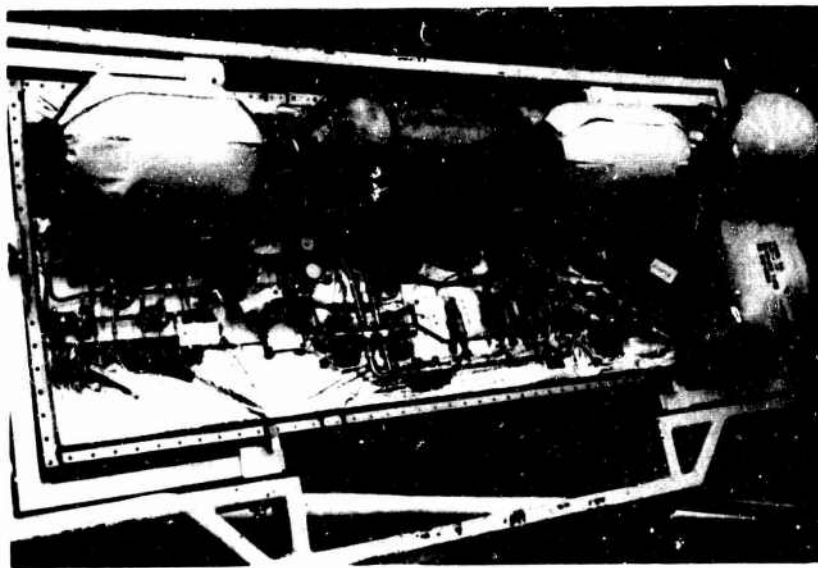radial beam segment and the test criteria

Fig. 12. The Apollo service module reaction control subsystem
which was vibroacoustically tested on the 180-deg SM segment

segment response to be equivalent to the test criteria at the specific location where the data were originally acquired, one can be assured that the vibration responses at other locations on the segment are correct.

There are a number of limitations that one should consider before planning a vibroacoustic test program. Some of these are listed below:

1. The vibration responses should obviously be induced by rocket engine or aerodynamic noise. It is not impossible to simulate mechanically induced vibration by acoustical excitation, but it would probably be extremely difficult.

2. An adequate acoustic test facility must be available. Most prime contractors do have acoustic facilities, but many vendors do not. Thus, many of the vibroacoustic tests would have to be conducted at the prime contractor's facility. The limited availability of structural segments would also require that the majority of the tests be conducted by the prime contractor.

3. The spacecraft structure should be amenable to vibroacoustic testing. If the structure is not somewhat symmetrical, a large number of segments would be required. During the service module vibroacoustic tests, for example, both the radial beam and the 180-deg SM segment could be used for a number of different installations because of their symmetry. An entire command module would have been required to test all of its components, however, because of its nonsymmetry.

4. If the vibration levels are moderate, vibroacoustic testing may not be advantageous. Unless the levels are high, the overtesting that normally accompanies an electromechanical shaker test generally can be accepted. Also, there is less concern over wiring, plumbing, and structural interfaces. However, some programs require that components be subjected to a minimum vibration test level, regardless of the environments. Such minimum test levels might be difficult to obtain during an electromechanical shaker test.

5. The specification of test tolerances will require a great deal of flexibility. Most vibration specifications require that the test spectrum be reproduced within very narrow tolerance bands. Such requirements are necessary to assure that an adequate test is conducted. The inconsistency in this approach is that the vibration responses in the spacecraft are not as repeatable and can vary from spacecraft to spacecraft or from place to place within a single spacecraft. Thus, one could not expect a vibroacoustic-segment vibration response to repeat itself within a narrow tolerance band. For example, the vibration responses of the 180-deg SM segment were very similar to the vibration responses of the full-scale spacecraft, in spite of some large differences in narrow frequency bands. Obviously, some experienced engineering judgment is required in assessing the adequacy of a vibroacoustic test.

CONCLUSIONS

The concept of vibroacoustic testing has been verified during the Apollo service module vibration qualification program. The ability to reproduce vibration responses on both large and small segments was also confirmed. This approach offers an improvement of the simulation of vibration environments over the simulation normally found in electromechanical shaker testing. Instead of forcing the component to respond to an artificial input, the structure is excited and the component is free to respond in a natural manner. In the Apollo program, acoustic energy was used as the form of excitation since it was thought to be more realistic. Mechanical excitation of the structure could have been used as well. Regardless of the manner in which the structure is excited, the principle is not changed. The vibroacoustic approach is obviously not the ultimate in vibration simulation. Its use, however, can in many circumstances result in a significant improvement in vibration simulation.

165

REFERENCES

1. R. Wren and W. Dorland, "Concept, Design, and Performance of the Spacecraft Acoustic Laboratory," Shock and Vibration Bull., No. 37, Jan. 1968

2. E. Kirchman, "Launch Phase Simulator," 1963 Proc. Institute of Environmental Sci., pp. 251-256, 1963

3. R. Peverley, "Acoustically Induced Vibration Testing of Spacecraft Components," Shock and Vibration Bull., No. 36, Part 3, pp. 39-46, 1967

4. R. Peverley and D. Newbrough, "The Derivation of Vibration Test Criteria for the Apollo Command Module, Service Module and SLA," GE/ASD Internal Publication

5. D. Newbrough et al., "Development and Verification of the Apollo Command and Service Module Vibration Test Requirements," Shock and Vibration Bull., 37, Part 5, Jan. 1968

6. R. W. White, "Theoretical Study of Acoustic Simulation of In-Flight Environments," Shock and Vibration Bull., No. 37, Part 5, Jan. 1968

7. W. Dorland et al., "Development of Test Conditions For Apollo Lunar Module Flight Qualification," Shock and Vibration Bull., No. 37, Part 5, Jan. 1968

8. D. Newbrough et al., "Development and Verification of the Apollo Lunar Module Vibration Test Requirements," Shock and Vibration Bull., No. 37, Part 5, Jan. 1968

9. H. N. McGregor, "Acoustic Problems Associated with the Underground Launching of a Large Missile," Shock and Vibration Bull., No. 29, Part 4, June 1961

10. M. C. Trummel, "Ground Test Simulation of Lift-off and Transonic Vibration Bull., No. 35, Part 2, pp. 75-84, Jan. 1966

11. R. Peverley and H. McGregor, "Missile Component and Vibration Environmental Prediction and Test Methods," IAS Paper 62-48, Jan. 1962

12. R. Stevens et al., "Vibration Qualification of Fly-Away Umbilical By Acoustic Test Method," 1967 Proc. Institute of Environmental Sci., Vol. I, 1967

DISCUSSION

Mr. Scharton (Bolt, Beranek & Newman): Why do you call these vibroacoustic tests instead of just acoustic tests?

Mr. Peverley: We talked about acoustic testing as being a means of deriving qualification levels, and we distinguished the vibroacoustic test as a means of using acoustic energy to conduct a vibration test.

Mr. Angelopulos (Lockheed Missiles & Space Co.): I noticed that your sound-pressure level profile curve differed quite markedly from a curve in an earlier paper, at the speed of sound and max Q. What criteria did you use that were markedly different from that curve?

Mr. Peverley: What we had shown was a sound-pressure level time history on the service module and adapter. The main difference was that the service module exhibited a very short duration peak at Mach 1. We reasoned that this difference was due to flow separation

and did not occur on the SLA. As far as our criteria went, we basically used the sound-pressure levels at max Q. When we conducted the test we generally just raised the levels 4 db. That was the difference between them. Because this transient peak was of such a short duration and looked more like a pulse, it was difficult to get an accurate idea of what the spectrum looked like. The best we could surmise was that it resembled the spectrum at max Q, so we used it.

Mr. Brunnemer (Hughes Aircraft Co.): Did you say that during Block I testing you have seen response levels higher than you did during the actual test in flight?

Mr. Peverley: No, the flight levels were much lower. The result was that we had a very conservative test, just looking at pure power spectral density. However, because we felt we had a better impedance match, it would not have been such an overtest had we used mechanical shakers.

* * *

166

ACOUSTICAL QUALIFICATION OF S-IC FIN STRUCTURES*

Clark J. Beck, Jr.
The Boeing Company
Huntsville, Alabama

and

David R. Kennedy
Brown Engineering Company
Huntsville, Alabama

Results of acoustic qualification testing on four aerodynamic fins are presented. The fin test specimens were portions of the aerodynamic fins used on the S-IC stage of the Saturn V vehicle. The objective was to determine if the fin could withstand the acoustic qualification test level of 163 db without structural failure. Two fins failed, while the other two fins did not fail under similar test conditions. The difference in test results is attributed to the presence of fiber-glass tape between the skin and ribs of the two fins which did not fail. Strain instrumentation shows a significant reduction in dynamic strain levels because of the presence of fiber-glass tape. The reduction in strain level resulted in the S-IC fin's passing the qualification test.

INTRODUCTION

The S-IC stage of the Saturn V space vehicle has four aerodynamic fins located close to the F-1 engines. During the launch and flight of the vehicle, the fins are subjected to a very high acoustic environment. High-level acoustic energy is recognized as a potential source of structural failure; therefore, acoustic qualification tests were performed on four fin specimens in a progressive wave chamber. Under similar acoustic qualification test conditions, two fin specimens failed while the other two fin specimens did not.

This paper describes the acoustic qualification test and presents test data which explain the failures.

TEST SPECIMENS

Four fin specimens were tested during this program. Each specimen consisted of the outboard 66 in. of the S-IC aerodynamic fin. Figure 1 shows the fin installed on the S-IC stage. The test specimen is indicated by the cross-hatched area. Fins 1* and 2* (asterisks indicate fins that failed during test) were built

Fig. 1. S-IC fin installation

especially for the acoustic tests. Fin 3 was subjected to static testing before the acoustic test. Fin 4 was built for the facilities checkout vehicle and subsequently used for acoustic testing.
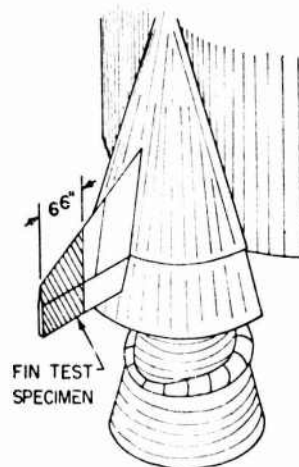
---

*Testing was conducted under a National Aeronautics and Space Administration contract.

The fins are of semimonocoque construction as illustrated in Fig. 2. The skins are 0.056-in.-thick 6% Al = 4% V titanium. The ribs and intercostals are 0.075-in. aluminum alloy, 7075-0 heat treated to the T-6 condition. The main spar consists of two machined aluminum T-caps and an aluminum web. The rear spar consists of two titanium caps and a titanium web. The leading edge is machined from a titanium bar. All joints were made with fasteners capable of taking high shear loads.

The only significant difference between the fins was the presence of a 0.015-in.-thick layer of fiber-glass tape between all aluminum and titanium mating surfaces. The purpose of the tape is to prevent corrosion between the aluminum and titanium surfaces. Figure 3 shows a portion of the fin with skin removed to reveal the fiber-glass tape. Fins 3 and 4 had the tape installed. Fins 1* and 2* did not have the tape installed, since they were built before the tape had been included in the design.
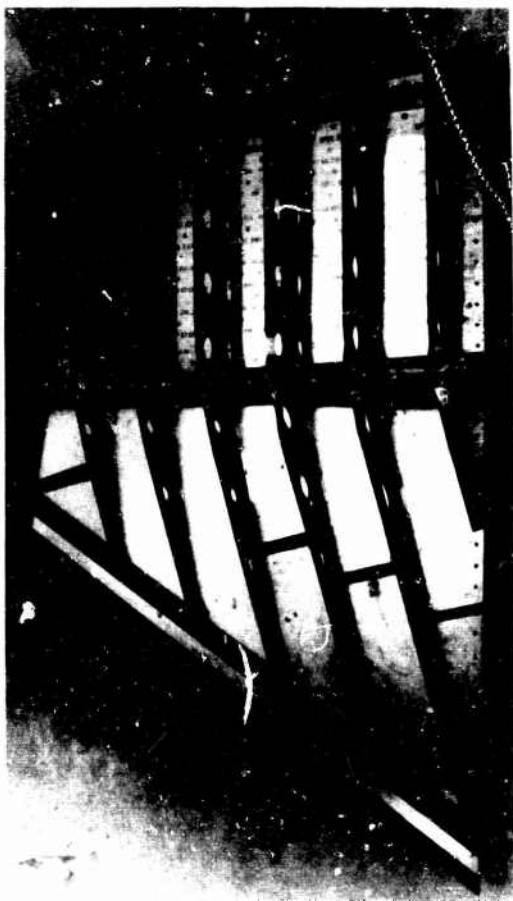

Fig. 2. S-IC fin construction (skin removed)

TEST FACILITY

All four specimens were tested in the progressive wave chamber of the 1500-cu-ft acoustic facility of Wyle Laboratories, Huntsville, Alabama. A Wyle acoustic source, WAS 3000, was used to drive the horn leading to the progressive wave chamber. The access panels in the progressive wave chamber were 6.5 ft by 8 ft, which is large enough to allow all of one side of the specimen to be subjected to the acoustic field. Each specimen was attached to a massive concrete fixture by angled brackets between the fin skin and fixture and also by a special fitting on the end of the main spar at the base of the specimen. The specimen mounted on the fixture is shown in Fig. 4. The minimum distance between the test chamber wall and the test specimen was 7 in., as shown in Fig. 5. All openings around the specimen were sealed.

INSTRUMENTATION

All of the test specimens were instrumented with strain gages and accelerometers. Five microphones were suspended inside the progressive wave chamber to measure the sound pressure levels generated over the surface of the specimens. Figure 6 shows the location of the strain gages, accelerometers, and microphones.

Data from fins 1* and 4 were recorded on magnetic tape for playback and analysis. Fin 2* and 3 data were acquired by the Wyle computer system (Control Data Corp. 3200). The test data were reduced into either 1/3-octave spectra or power density spectra, depending on the acquisition system used.

TEST PROCEDURE

Testing began on fin 1* with a sinusoidal sweep to investigate test specimen response characteristics. The sweep rate was 1 octave/min at a sound pressure level of 140 db (re 2×10^{-5} N/m^2). Tests were then run at various levels using a random noise input to shape the test spectrum. After the desired spectrum shape was obtained, four short runs were made at sound pressure levels of 154, 157, 160, and 163 db to obtain information regarding the linearity of the specimen's response. The qualification test was then started.

The qualification test spectrum was a shaped random noise spectrum from 20 to 10,000 Hz with an overall sound pressure level

168

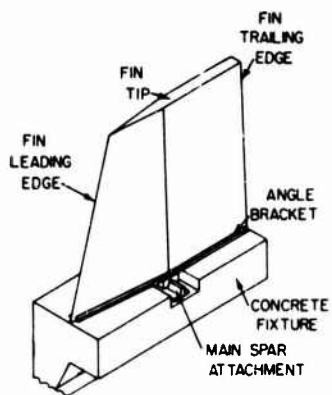Fig. 3. Fiber-glass-tape installation
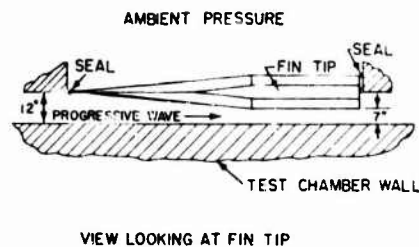(skin removed)

Fig. 4. Fin mounted on
test fixture

VIEW LOOKING AT FIN TIP

Fig. 5. Diagram of fin in pro-
gressive wave test chamber

fin specimens. The qualification test level was applied to fin 1* for a total of 54 min with an inspection every 5 min. Testing was stopped when internal failures were noted.

The test procedure for fins 2*, 3, and 4 was modified because of the failures noted in fin 1*. The procedure consisted of four short duration tests at overall sound pressure levels of 154, 157, 160, and 163 db for data acquisition purposes. The qualification test was then
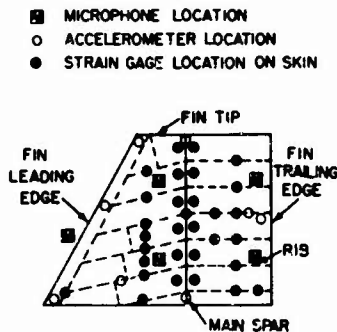
of 163 db. The microphone located at the lead-ing edge of the fin was used to establish the test spectrum. The overall sound pressure level from this microphone was maintained at 163 ± 1 db throughout the qualification test of all four

169

MICROPHONE LOCATION
ACCELEROMETER LOCATION
STRAIN GAGE LOCATION ON SKIN

Fig. 6. Instrumentation locations

Fig. 7. Failure areas, fin 1*

started at an overall sound pressure level of 163 db. The test specimens were examined internally and externally during the test to determine if failure had occurred.

TEST RESULTS

Initially, it was assumed that any failure would first occur in the fin skin; therefore, fin 1* was subjected to only external examinations during qualification testing. However, after 54 min of testing at 163 db, an internal examination was made, revealing extens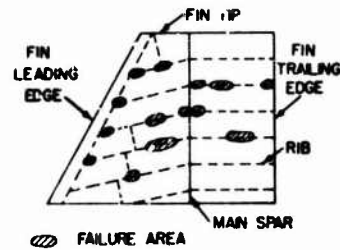ive failures of the internal ribs. Figure 7 shows the areas where failures occurred on fin 1*. The majority of the failures were cracks in the rib radii. However, enlarged rivet holes and cracks into rivet holes were also noted. Although failures occurred forward and aft of the main spar, approximately 65 percent of the failures were forward of the main spar. Figure 8 shows a typical failure forward of the main spar; note the rib radii cracks adjacent to both upper and lower skins. Figure 9 shows another failure area forward of the main spar and near the rib-leading edge juncture. A rib radius crack aft of the main spar and near the rib-aft spar juncture is shown in Fig. 10.

One-inch-diameter holes were cut through the skin of fin 2* to facilitate inspection of the internal structure. The holes were in the skin
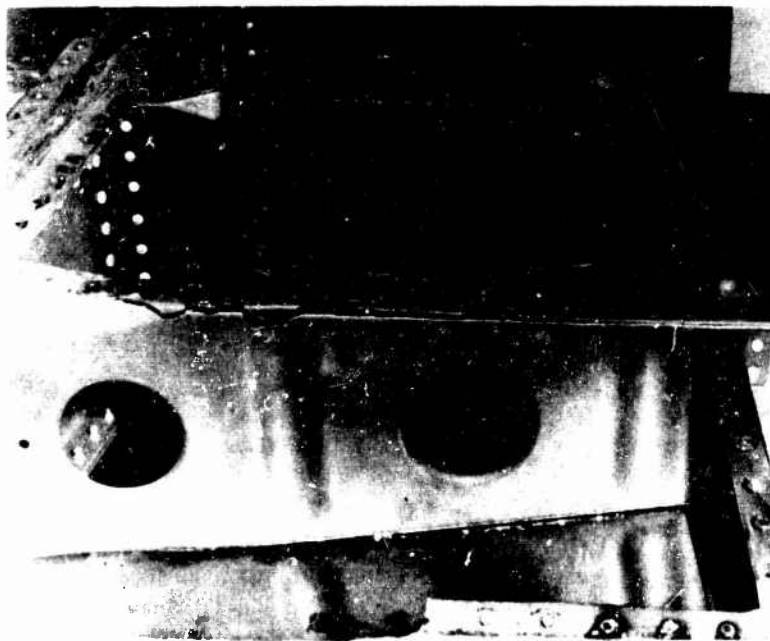
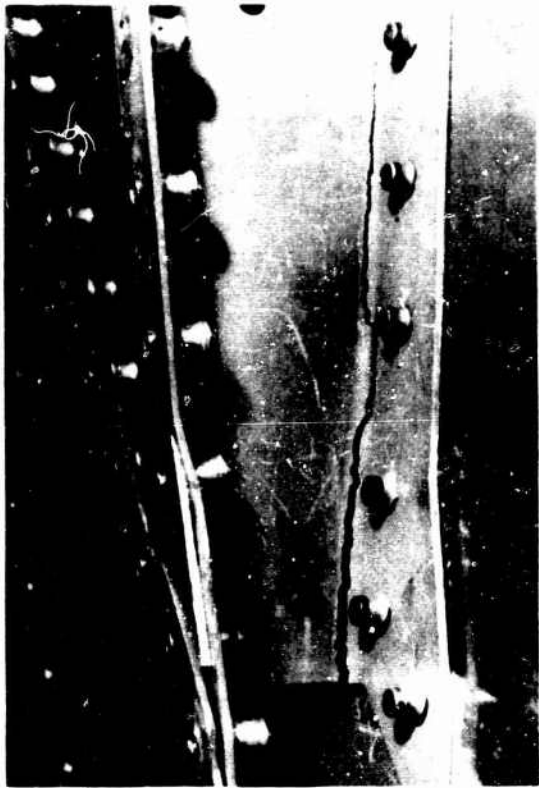

Fig. 8. Failure of rib forward of main spar, fin 1*

170

Fig. 9. Failure of rib near
leading edge, fin 1*

external to the progressive wave chamber and
were covered during testing. A crack in one of
the fin 2* ribs was noted after 5 min of testing
at 163 db. Testing was continued at a level of
163 db; after 20 min, three cracks were noted
in the rib radil. The cracks were up to 3 in. in
length. Figure 11 shows a typical failure on
fin 2*. This failure is located on a rib forward
of the main spar.

Because of the failures, the decision was
made to perform additional tests on production
line hardware. A fin which had undergone static
test (fin 3) and a fin which was built for the fa-
cilities test vehicle (fin 4) were chosen for the
additional tests. The only significant difference
between the fin test specimens was the presence
of fiber-glass tape between all rib-skin joints.
Fins 3 and 4 had the tape installed, and fins 1*
and 2* did not.

Fins 3 and 4 were subjected to the same
test as fins 1* and 2*. However, no failures
were noted after 24 and 20 min of testing at 163
db on fins 3 and 4, respectively. Testing was
discontinued at this time since the fins were
considered to be qualified for withstanding
launch and flight acoustic environment.

A comparison of the strain gage data from
fins 1* and 2* (fins without tape) and fins 3 and
4 (fins with tape) explained the difference in
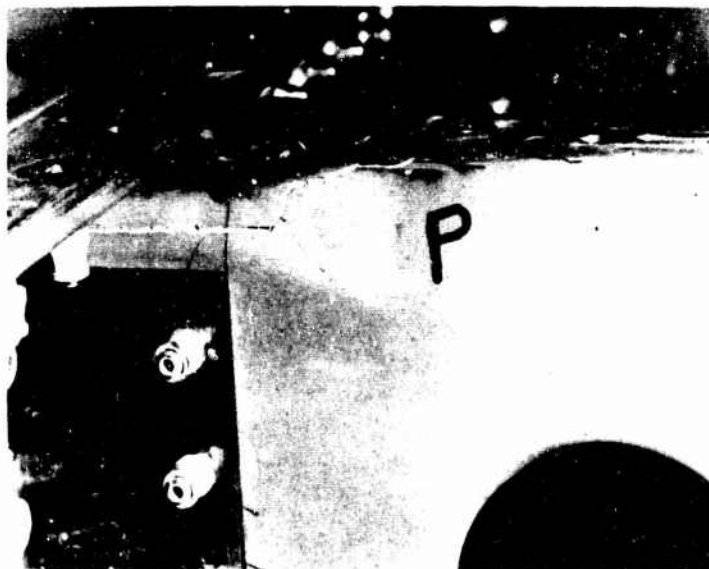test results. The average of overall strain
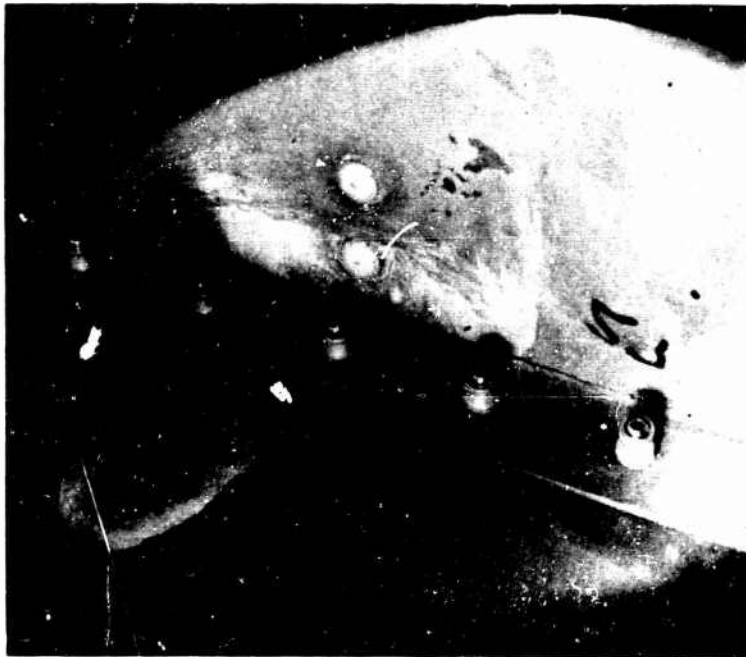

Fig. 10. Failure of rib aft of main spar, fin 1*

171

Fig. 11. Failure of rib forward of main spar, fin 2*

levels from fins 1* and 2* was approximately twice the average level from fins 3 and 4. Individual gage comparisons indicated overall strain levels differing up to a factor of 4. The difference in overall strain level was apparent in data from all strain gages. Figures 12 through 14 illustrate the change in strain level experienced between fin 1* and fin 4 (comparable results were obtained between fin 2* and fin 3). Note both the change in spectrum level of up to 15 db and the 7.5- to 10-db change in overall level. The data shown in Fig. 12 are from a gage forward of the main spar on the fin

skin over a rib. Figure 13 shows similar data trends for a gage on the skin midway between ribs. Figure 14 contains data from a gage aft of the main spar. Again the data trends are similar. The lower strain levels on fins 3 and 4 are attributed to an increase in damping caused by the presence of fiber-glass tape between the skin and ribs.

CONCLUSIONS

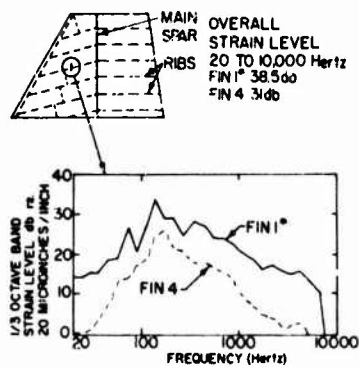These acoustic tests on the S-IC fin have shown that a seemingly small construction

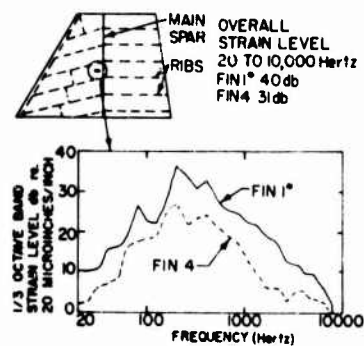Fig. 12. Strain spectra comparisons between fin 1* and fin 4

Fig. 13. Strain spectra comparisons between fin 1* and fin 4

172

difference, consisting of a thin layer of fiber-glass tape between the skin and ribs, has significantly changed the dynamic strain levels in the fin. The presence of the fiber-glass tape resulted in the S-IC fin passing the acoustic qualification test.

The test results suggest the use of fiber-glass tape or a similar material to reduce dynamic strain levels in semimonocoque structures which are subjected to high vibration and acoustic environments. However, more extensive testing is required in order to realize fully the benefits of this type of construction.

Fig. 14. Strain spectra comparisons between fin 1* and fin 4

BIBLIOGRAPHY

1. Wyle Laboratory Staff, "Acoustic Qualification Testing of Four Saturn V S-IC Full Scale Fins," Wyle Laboratories Report, Vols. I and II, Mar. 1967
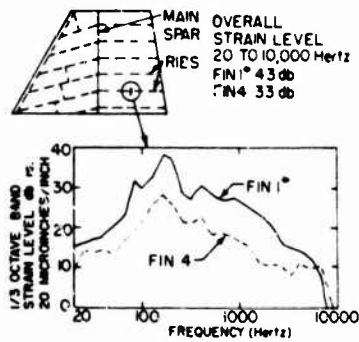
*   *   *

173

REAL-TIME COMBINED ACOUSTIC-VACUUM
TESTING OF SPACECRAFT*

Louis J. Demas
NASA Goddard Space Flight Center
Greenbelt, Maryland

During the launch phase of flight, a spacecraft is subjected to a variety of loads.
To establish confidence that a spacecraft will survive the launch environment,
practice has been to subject a spacecraft and/or components to single environment
tests in series, for which specifications included conservatisms in an attempt to
cover the unknowns arising from the combination of these single tests. However,
a more realistic test philosophy which permits real-time simulation of the com-
bined launch environments has recently been implemented at Goddard Space Flight
Center using the launch phase simulator (LPS) test facility. The LPS can repro-
duce the combined launch environments of vacuum, acoustics, acceleration, and
vibration on large spacecraft structures, all in real time.

The first combined environmental flight program test performed on the LPS facility
is described. This test was the real-time combined acoustic-pressure profile test
of the Application Technology Satellite (ATS-A) prototype spacecraft performed on
March 16, 1967.

The characteristics of the LPS acoustic and vacuum systems, pretest preparation,
test philosophy and procedures, and results of the test program are discussed.
Also included are a cursory treatment of contamination control of the facility and a
brief discussion of other combined environmental tests of this type performed on
the LPS.

INTRODUCTION

The launch phase simulator (LPS) [1], a
new combined environmental test facility at the
Goddard Space Flight Center, is being used to
perform a more realistic test on spacecraft
and/or components. The facility is capable of
exposing a spacecraft to the major environ-
ments encountered during launch.

Practice in environmental testing has been
to subject a spacecraft to a series of single
environment tests to determine if the spacecraft
will survive the launch environment. These
tests are conservative in an attempt to cover
the unknowns which arise when the launch envi-
ronments are combined. The combined effect
of several or all of the launch environments
acting simultaneously may be greater than the
measurable effect of any one of them: in some
cases, it may even exceed the combination of
these. Conversely, the effects in some cases
may neutralize one another. The real-time
combined environment capability of the LPS

enables a more realistic test to be performed
and a more thorough evaluation of spacecraft
design characteristics necessary to insure
reliability during launch. Better evaluation
will aid in reducing the need for overdesigning
a spacecraft structure at the expense of effec-
tive spacecraft weight, without increasing the
risk of underdesign and failure.

The test described here is the combined
acoustic-pressure profile (vacuum) test of the
Application Technology Satellite (ATS-A) which
was launched on April 4, 1967. The test was
the first combined-environment real-time test
to be performed on the LPS.

LAUNCH PHASE SIMULATOR

The LPS [2] consists of a large centrifuge
(approximately 117 ft in length and 500,000 lb
in weight) with a test chamber mounted on the
outboard end. The test chamber can accom-
modate a spacecraft (including adapter) up to

---

*This paper was not presented at the Symposium.

5000 lb in weight, 10 ft in diameter, and 15 ft in length. In the test chamber, a spacecraft may be subjected to the combined environments of steady-state acceleration, mechanical and acoustical vibration, and decrease in atmospheric pressure, i.e., all the environments encountered by a spacecraft during launch phase (except for temperature gradients). A brief summary of the facility's environmental capability is:

1. Steady-state acceleration: 30 g at 60-ft radius

2. Mechanical vibration: three degrees of freedom (longitudinal, lateral, and pitch) from 5 to 100 Hz, sine and random

3. Acoustic noise: 150 db rms (all decibel notations are referenced to 0.0002 μbars)

4. Vacuum: programmed to follow the launch profile.

These environments can be simulated in real time, and the systems may be operated in either a manual or automatic mode. This real-time capability insures proper sequencing of events during a combined-environment test.

Acoustic System

The acoustic system consists of a NorAir-coustic Mark V generator which operates through an exponential horn (cutoff frequency 75 Hz) at the inboard end of the test chamber, and a tubular liner which surrounds the spacecraft within the test chamber. Compressed air tanks located on the LPS arm structure supply air for the hydraulically operated noise generator. Sufficient controls and instrumentation are provided with the system to insure proper programming of acoustic testing.

The system is capable of producing an overall sound pressure level (SPL) of 150 db rms at 760 torr and 140 db rms at 100 torr, providing Gaussian random noise in any one-third-octave band with a continuous spectrum from 100 to 12,000 Hz. The spectrum is flat from 100 to 700 Hz, and from 700 to 12,000 Hz has a 6 db/octave roll-off.

Vacuum System

The LPS vacuum system consists of a four-stage steam-driven air ejector evacuation system, servo-controlled bleed valves, and a mechanical vacuum pump for holding vacuum

over long test runs. The estimated steam flow during a vacuum test is 60,000 lb/hr. The vacuum system is capable of reducing the chamber pressure from 760 to 0.3 torr (equivalent to an altitude of approximately 200,000 ft) and reproducing the dp/dt slopes of those occurring during the actual launch. Test chamber pressure is controlled to the proper level by admitting air through the bleed valves.

TEST ITEM

The ATS-A prototype spacecraft is approximately 56 in. in diameter, 73 in. in length, and 800 lb in weight. The ATS spacecraft is a relatively large, adaptable payload spacecraft designed to achieve long life in circular, medium-altitude orbits or synchronous, equatorial orbit. The ATS-A prototype spacecraft had to resemble the flight spacecraft as closely as possible. Approximately 38 in. from the base of spacecraft is the "belly band," which was considered the area of the spacecraft most sensitive to acoustic excitation and most liable to damage through improper venting because of the large volume of air that it contained.

TEST SPECIFICATIONS

The objectives of the test were to evaluate the structural response of the prototype spacecraft when exposed to the simulated launch acoustic-vacuum environments. Acoustic and vacuum tests specification levels were generated from an analysis of Atlas-Agena launch data. Design qualification exposure levels are normally derived by applying appropriate factors to flight acceptance levels. The acoustic noise flight levels were increased, but the philosophy of increasing the levels and time does not apply to pressure venting tests. For example, to increase the severity of the vacuum test, which depends on the slope (dp/dt) of the pressure vs time curve, would be to shorten the test time. To resolve this incompatibility, it was decided to maintain flight levels for the vacuum test, increase the levels of acoustic noise, increase the time duration of the maximum liftoff noise levels at the start of the test, and synchronize the time occurrence of the combined environments to reflect liftoff transonic regions.

TEST PREPARATION

To meet the required test specification levels (see Fig. 1), a modification of the vacuum control system and a change in the normal
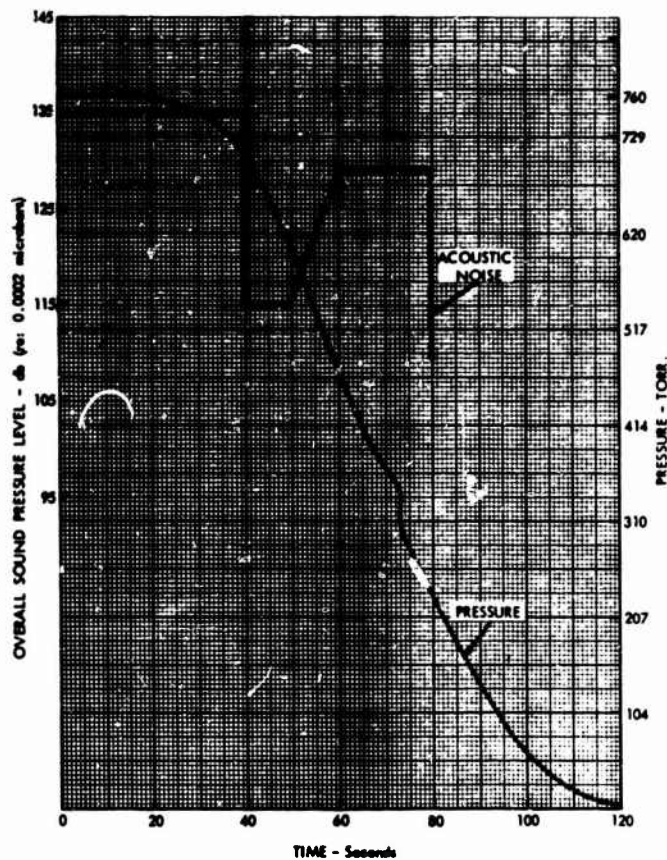
176

Fig. 1. ATS-A prototype acoustic-
vacuum test profiles

operating procedure of the acoustic system to
be made.

The critical parameter in controlling the
upper end of the simulated launch pressure pro-
file is the time required for the main vacuum
valve to open. Initially, approximately 4 sec
was required for the valve to open. The test
chamber pressure decreased from 760 to 600
torr in this time; however, this pressure slope
was too steep for the ATS-A test. Therefore,
a nitrogen system was incorporated to control
the opening and closing of the main vacuum
valve. To meet this requirement, a needle
valve was installed in the nitrogen line be-
tween the regulator and piston to decrease the
nitrogen flow rate to the piston and slow down
the opening speed of the valve. The time re-
quired for the valve to open was controlled with
this modification, and it was preset at 15 sec.
This, plus an alteration in the profile pro-
grammed for the automatic mode operation,
permitted the vacuum system to follow the

pressure profile within the required accuracy
of the test specification levels.

A mockup of the ATS-A prototype (Fig. 2)
was assembled and mounted in the test cham-
ber to aid in shaping the octave-band spectral
distribution properly. Two cylindrical fixtures
used in previous acoustic tests were used to
simulate the ATS-A geometry. The acoustic
test specification required a maximum value of
the overall SPL of 135 db rms. This required
an adjustment in the acoustic system, since it
was set up to operate at an SPL of 150 db rms.
There were two possible methods that could be
used to prepare the system for operation at this
lower level. One was to decrease the size of
the orifice between the modulator of the noise
generator and the exponential horn. This
method would have required a detailed investi-
gation of the sizing of the orifice. The other
method was to reduce the nitrogen pressure
being supplied to the generator from 140 to 40
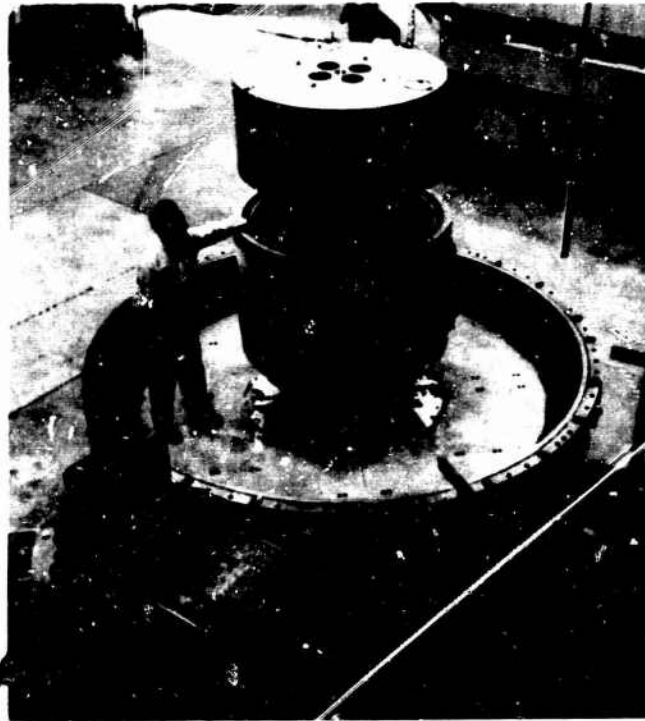psi, which would make the servo controller

177

Fig. 2. ATS-A acoustic mockup

operate more efficiently. The latter method was used because of the time element involved, and it proved to be very successful.

Several trial runs were made prior to the actual test to evaluate the performance of both the acoustic and vacuum systems and the modifications and adjustments made to these systems. During these checkouts, the test chamber was vented back to atmosphere, using air. This air was brought into the chamber from the pedestal pit area of the LPS and was not considered clean enough to keep the contamination level inside the chamber to a minimum. Consequently, to insure that the optical experiments onboard the spacecraft and the spacecraft itself did not become contaminated, the test chamber was thoroughly cleaned and a contamination study was performed. Results from these investigations indicated that the chamber contamination level was acceptable for sensitive optical experiments, and a decision was made to vent the chamber with gaseous nitrogen instead of air.

INSTRUMENTATION

The required instrumentation for the test included two pressure transducers for

monitoring test chamber pressure, one pressure transducer for monitoring internal pressure of the Agena adapter, four microphones located 90 degrees apart around the belly band of the spacecraft (see Fig. 3), nine accelerometers for monitoring structural response, and one thermocouple located inside the cavity at the forward end of the spacecraft.

TEST PROCEDURE

The spacecraft plus Agena adapter was mounted on the end cap, and the end-cap-spacecraft assembly was attached to the test chamber. Figure 4 illustrates the operation of loading the end-cap-spacecraft system onto the test chamber.

The test was performed in the automatic mode, and both the acoustic and vacuum systems operated satisfactorily. At the conclusion of the test, the chamber was brought back to atmospheric pressure using gaseous nitrogen. The end-cap-spacecraft assembly was then removed and the spacecraft given a cursory inspection. No significant damage was observed.
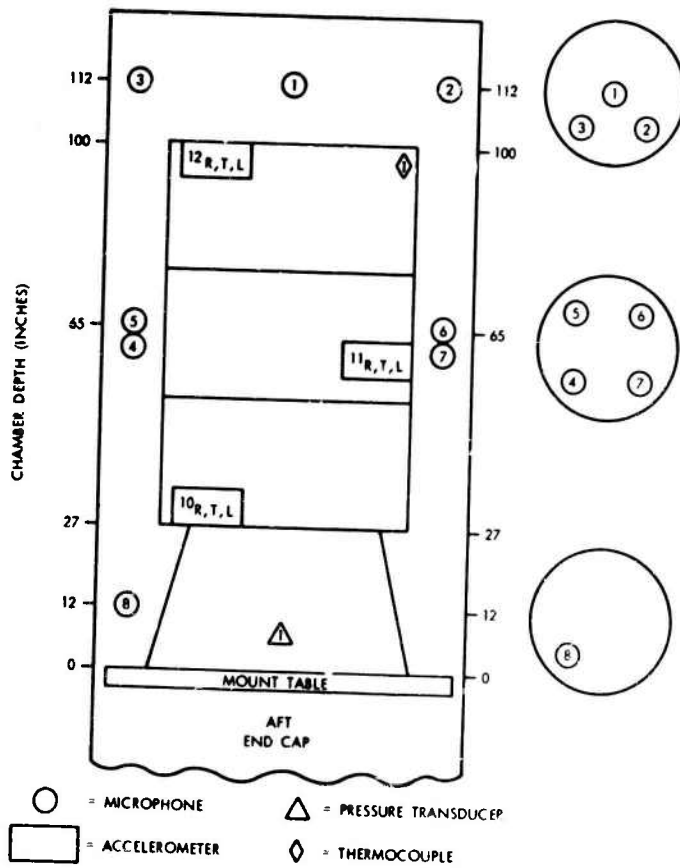
178

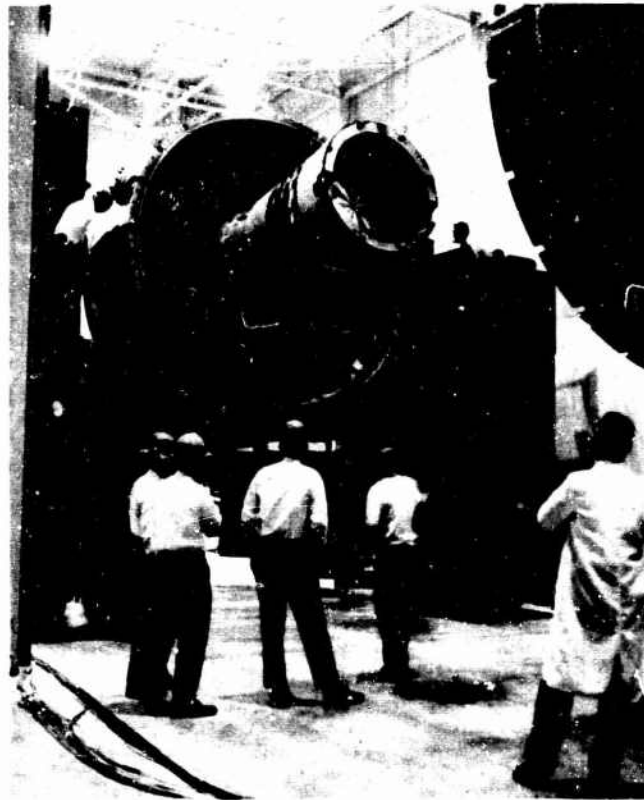Fig. 3. Transducer locations

179

Fig. 4. ATS-A prototype spacecraft, attached to LPS end cap, being tilted into horizontal position by LPS loading vehicle

RESULTS AND DISCUSSION

The acoustic-vacuum profiles achieved during the test are compared with the specification levels in Fig. 5, where the specification levels are followed very closely by the test profiles. It should be noted that the measured value is offset from the specification with respect to time; however, only a slight variation exists in the slopes of the curves. Figure 6 illustrates the octave-band spectral distribution of the acoustic noise recorded around the belly band of the spacecraft. As can be seen, this distribution falls within the ±3 db allowed for the acoustic noise specification levels.

Accelerometers mounted on the spacecraft structure sensed the acoustically induced vibrations, which were analyzed as random. An analysis of the acoustic excitations indicates that large exposed areas of the ATS-A are susceptible to random vibrations which exceeded those measured during previous vibration (mechanical) tests of the ATS-A structural model. Frequency bands in the

100- to 1200-Hz area induced response in the solar arrays which exceeded those from mechanically induced random vibration; to a lesser degree, frequency bands in the 400- to 900-Hz area induced response on the spacecraft outer frame which exceeded mechanically induced vibration inputs.

A thorough investigation of the spacecraft showed no significant damage to the belly band and forward cavity vent areas. The belly band did not appear to be damaged, indicating that the spacecraft region containing the greatest air volume was vented with no apparent difficulty. There was no apparent damage to the spacecraft due to acoustic excitation.

CONCLUSION

The combined acoustic-vacuum test of the ATS-A prototype spacecraft performed on the LPS was conducted in accordance with the test specifications. The test profiles normally met test specification levels, except for low-frequency
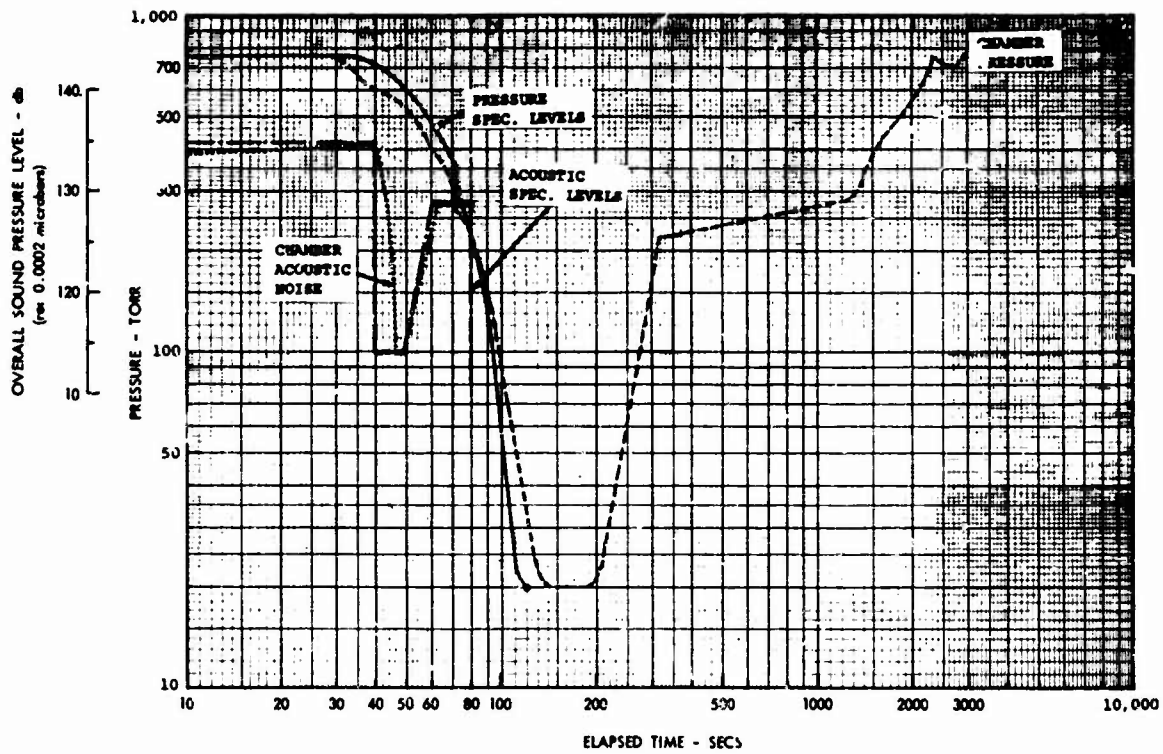
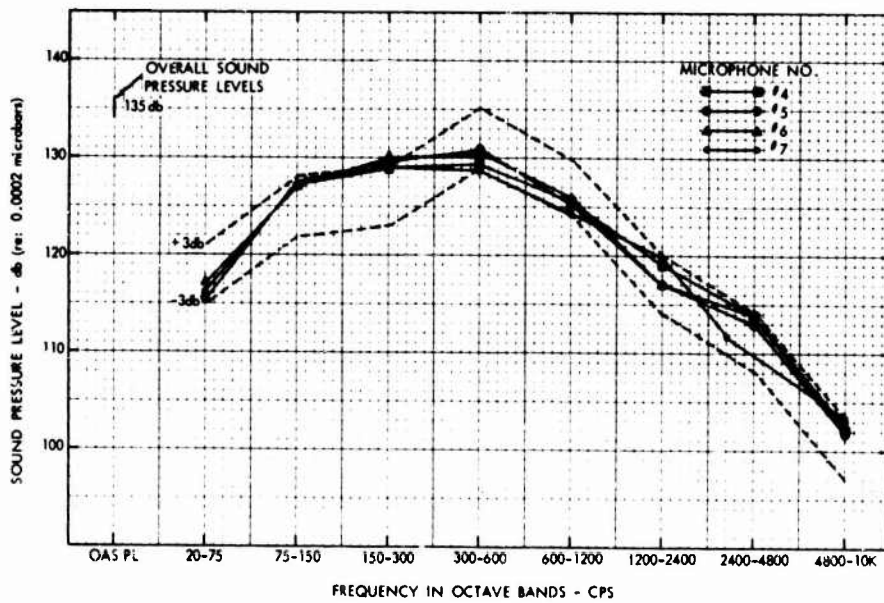Fig. 5. ATS-A prototype acoustic-vacuum test profiles

Fig. 6. ATS-A prototype octave-band spectral distribution

181

roll-off in the acoustic spectrum which was not reproduced to within-accuracy requirements.

The ATS-A combined environmental real-time test, the first to be performed on the LPS, was a complete success. As a result, a combined acoustic-vacuum test was later performed on the Radio Astronomical Explorer (RAE) Engineering test unit. Combined real-time acoustic-vacuum tests on ATS-D prototype model, RAE proto-flight model, and Orbiting Astronomical Observatory (OAO) thermal model are scheduled for the very near future.

REFERENCES

1. E. J. Kirchman, "Launch Phase Simulator," AIAA Publ. CP-11, Nov. 1964

2. E. J. Kirchman and C. J. Arcilesi, "Advanced Combined Environmental Test Facility," Shock and Vibration Bull. No. 37, Part 3, 1968

* * *

182